Empirical Analysis of Localized Casing Wear with Variations in Contact Pressure and Drilling Conditions

Dissertation

Zur Erlangung des Doktorgrades
der Ingenieurwissenschaften

Vorgelegt von

M.Sc. Tanveer Yaqoob

aus Karachi, Pakistan

Genehmigt von der

Fakultät für Energie- und Wirtschaftswissenschaften

der Technischen Universität Clausthal

Tag der mündlichen Prüfung

09.12.2021

Dekan:	Prof. Dr. mont. Leonhard Ganzer
Vorsitzender der Promotionskommission:	Prof. Dr. mont. Leonhard Ganzer
Betreuer:	Prof. Dr.-Ing. Joachim Oppelt (Clausthal University of Technology, Germany)
Gutachter:	Prof. Dr.-Ing. Hubert Schwarze (Clausthal University of Technology, Germany)

Dissertation Clausthal 2021

Declaration

I hereby declare that the content of this work has been prepared and written by myself, using the quoted references.

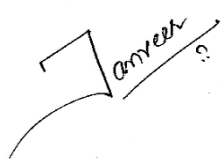

M.Sc. Tanveer Yaqoob

Clausthal-Zellerfeld, 02.01.2022

Abstract

In the race to push the limits of hydrocarbon and geothermal production (and storage), deep inclined, horizontal, and ERD wells have become the drilling norm. In building such well trajectories, processes such as drilling, reaming, rotation off-bottom and tripping always affect casing wall thickness due to its interaction with the drillstring (particularly at the tool joints) under high contact forces. This results in either an uneven circumferential thickness reduction or, in case of long continuous contact of a tense drillstring pressed against the casing inner wall, a localized deep wear-groove.

Localized dynamic casing wear is a complex phenomenon to simulate due to the number of control variables influencing the non-linear wear behavior. Wear intensity is influenced by individual combinations of service loads (changing force-area distributions), metallurgical properties (material hardness and yield strength) and prevailing tribological mechanisms (surface roughness, friction factors and wear type). For wear simulation models to be accurate, the required friction- and wear factors must be experimentally determined by full-scale tests. To fulfill this requisite, the first step of this research is to analyze existing mathematical models and conventional well planning software to establish parameters for a full-scale wear test method in terms of variable side force, drillstring RPM, axial reciprocation, and fluid type.

The design, construction, and application of a full-scale wear frame to reproduce friction- and wear factors under field conditions is the second step, and the core focus of this study. The wear frame is designed to incorporate different casing materials under a range of operational loads and lubrication conditions, and wear scenarios under similar service loads have been compared for steel, fibered glass and fibered carbon casings. A total of 14 wear tests have been carried out in the study time-frame for the casing materials under water and mud lubrication conditions.

A comparison of test results shows good consistency and agreement with previous experimental studies in terms of friction and wear factors. After the initial peak values, the wear factor is observed to decline drastically to a steady-drop range upon contact pressure reduction. For all tested materials, this steady range of values can provide a good estimate of field wear volume over time under particular service loads and drilling scenarios. Also, the measured steady values of friction factors help determine close ranges on contact pressure threshold for the casings. A proposed wear volume equation based on the experimental results is presented as a part of test results.

It has been observed from the detected trends in the test results that repeated wear tests can make casing wear predictable. With the inclusion of more steel grades, diameters and new casing materials into the experimental scope, the wear frame can be used to develop a comprehensive record of wear performance under different field scenarios for casing and tool joint manufacturing industry. Attribution of wear factors and contact pressure thresholds to specific field conditions via a wear test database, and its integration into a software solution, can fill gaps to help reduce casing wear while retaining flexibility on operational loads.

Kurzfassung

Im Wettkampf die Grenzen der Kohlenwasserstoff- und Geothermie Förderung sowie Speicherung stetig zu übertreffen und optimieren, wurden horizontale Bohrungen, tiefe Ablenkungsbohrungen und Bohrungen mit großem Neigungswinkel (ERD Bohrungen) zum heutigen Standard. Bei der Planung solcher Projekte sowie Ablenkungen, wirken sich Vorgänge wie Räumen (reaming), Bohren (drilling), Rotation off-bottom und das Ein- und Ausfahren der Bohrgestänge enorm auf die Futterrohr Beschaffenheit aus. Durch das Aufeinandertreffen und dem herrschenden Kontakt zwischen dem Bohrstrang und der Innenwand des Futterrohrs, tritt eine stärkere Abnutzung des Materials auf seitens des Futterrohrs, besonders an den Verbindungsstellen des Bohrstrangs, auf. Dies führt entweder zu einem ungleichmäßigen kreisförmigen Schwund der Futterrohr-Stärke, oder bei längerem kontinuierlichem Kontakt gegen die Innenwand des Futterrohrs, zu einer punktuellen tiefen Verschleißrille.

Ein dynamischer Futterrohr-Verschleiß ist aufgrund der Vielzahl von Variablen, ein komplexes, zu simulierendes Phänomen, da die Variablen das nicht-lineare Verschleißverhalten beeinflussen. Die Verschleißintensität wird durch individuelle Kombinationen von Betriebsbelastungen (verändernde Kraft-Flächen-Verteilungen) beeinflusst. Metallurgische Eigenschaften (Werkstoffhärte und Streckgrenze) und vorherrschende tribologische Mechanismen (Oberflächenrauheit, Reibungsfaktoren und Verschleißart) kommen zum Tragen. Damit Verschleißsimulationsgleichungen möglichst genau sind, müssen die erforderlichen Reibungs- und Verschleißfaktoren experimentell durch umfangreiche Versuche bestimmt werden. Um diese Anforderung zu erfüllen, besteht der erste Schritt dieser Forschung darin, vorhandene mathematische Modelle und konventionelle Bohrlochplanungssoftwares zu analysieren. Daraus folgt die Bestimmung von Parametern, die für ein umfassendes Verschleißtestverfahren in Bezug auf variable Seitenkraft, Bohrstrangdrehzahl, axiale Bewegung und Fluidtyp, notwendig sind.

Der zweite Schritt und somit der Fokus dieser Studie ist die Planung, Konstruktion und Anwendung eines vollwertigen Verschleißmodels zur Reproduktion von Reibungs- und Verschleißfaktoren unter Feldbedingungen. Die entwickelte Verschleißanlage ermöglicht Abrieb verschiedener Futterrohr-Materialien unter diversen Betriebslasten und verschieden Arten von Schmiermitteln zu simulieren. Unter Anwendung nahezu gleicher Betriebslasten, wurden die Verschleißprozesse für Stahl-, Glasfaser- und Kohlefaser-Futterrohrs untereinander verglichen. Der Umfang der Testreihe beinhaltete bislang 14 Tests unter Anwendung eines Schlammbasierenden Schmiermittels oder Wasser.

Vergleiche zwischen den erbrachten Ergebnissen, in Bezug auf Reibungs- und Verschleißfaktoren, zeigen eine starke Ähnlichkeit und stehen somit im Einklang mit früheren experimentellen Studien. Nachdem der höchste Verschleißfaktor binnen kurzer Testdauer erreicht wurde, ist zu beobachten, dass dieser nach einer Verringerung des Druckkontaktes drastisch und stetig sinkt. Dieses Phänomen ist bei allen getesteten Materialien unter bestimmten Betriebslasten und Bohrszenarien zu

verzeichnen und kann als einen genaueren Richtwert für Feld Ereignisse genutzt werden. Des Weiteren können mithilfe der gemessenen Werte des Reibungsfaktors, die Spanne der Belastungsdruckgrenze (Contact Pressure Threshold) an den Futterrohren genauer bestimmt werden. Eine Verschleißvolumengleichung, basierend auf den experimentellen Ergebnissen, wird als Teil der Testergebnisse präsentiert.

Anhand der ermittelten Werte sowie Trends der Versuchsergebnisse, können Vorhersagen, bezüglich des Verschleißes, getroffen werden. Indem weiterer Stahlsorten, Durchmesser und neue Futterrohr-Materialien in den experimentellen Umfang einbezogen werden, kann die Anlage unter praxisnahen Bedingungen Verschleißverhalten darstellen. Hersteller für Futterrohre und Verbindungen profitieren von diesen Simulationen, um genauere Werte bei ihrer Herstellungsweise integrieren zu können. Durch die Anlage simulierten Feld Bedingungen, können die Werte der Belastungsdruckgrenzen (Contact Pressure Threshold) und Verschleißfaktoren erlangt werden. Diese Werte werden benötigt, um eine empirische Daten Gliederung zu erstellen, welche daraufhin in eine Software integriert werden. Dies vermag den Futterrohr-Verschleiß im Voraus abzuwägen und zu reduzieren, aber ermöglicht gleichzeitig die Flexibilität bei Betriebslasten beizubehalten.

Acknowledgements

Behind this technical effort are a bunch of people, without whom this would never have been possible. Heartiest gratitude to Prof. Joachim Oppelt and Dr. Javier Holzmann for the ever-available support and valuable inputs. I count myself lucky to have them both as supervisors.

I also want to thank Prof. Hubert Schwarze for his support as a reviewer.

Special appreciation for the colleagues at ITE (Institute of Subsurface Energy Systems) workshop for tolerating the broken equipment and extra hours at the wear frame during the test phase.

A number of results in this study were possible due to consent and data support from the colleagues from Future Pipe Industries, involved in a joint industry research project.

I also want to thank my colleagues Dr. Nelson Perozo and Dr. Carlos Paz for their help and support during the work that saved me a lot of time.

To Agnes. Thank you for being there and standing by me in happy and less-happy times.

Finally, to my parents. Though not here in person, they have always been an invisible force behind me that helps me push forward.

Table of Contents

List of Figures

List of Tables

Abbreviations

API	American Petroleum Institute
BHA	Bottomhole assembly
BOP	Blowout preventer
CBL	Cement bond log
CCWD	Circumferential casing wear model
CPT	Contact pressure threshold
CWGD	Casing wear groove model
DP	Drillpipe
DS	Drillstring
DLS	Dogleg severity
ECD	Equivalent circulating density
ERD	Extended reach drilling
FF	Friction factor
FST	Full scale testing
HPHT	High pressure-high temperature
HWDP	Heavy weight drillpipe
ID	Internal diameter
KCl	Potassium chloride
KOP	Kick-off point
MD	Measured depth
MFC	Multi finger caliper
MFCT	Multi finger caliper tool
MPD	Managed pressure drilling
NRDPRP	Non-rotating drillpipe rubber protector
OBM	Oil-based mud
OCTG	Oil country tubular goods

POOH	Pulling out of hole
RIH	Running in hole
RPM	Revolutions per minute
RSS	Rotary steerable systems
SG	Strain Gauge
SST	Small Scale test
TJ	Tool joint
TC	Tungsten carbide
VME	Von-Mises envelope
WBM	Water-based mud
WOB	Weight on bit
WF	Wear factor
$(WF)_{lab}$	Wear factor based on lab experiments
WT	Wall thickness

Nomenclature

D_{TJ}	Diameter of the tooljoint, mm
D_i	Inner diameter of casing, mm
μ	Friction factor (dimensionless)
$WF(\psi)$	Conventional wear factor
$\delta WF(\psi)$	Differential wear factor
Y_P	Yield strength, lbf/in^2
P_{tw}	Collapse pressure of worn casing, MPa
P_{yw}	Yield onset pressure of worn tube, MPa
k	Ratio of unworn and worn casing
P_t	Collapse strength of actual casing, MPa
P_e	Elastic pressure factor, MPa
f	Pipe imperfections factor
δ	Reduction in pipe thickness, mm

1. Introduction

1.1. Casing wear estimation: Necessity

The drilling industry today has evolved from the conventional vertical drilling practices towards complex (S-shaped, L-shaped) trajectories, ultra-deep sea explorations, multilateral wells and extended reach drilling (ERD) projects.

Drilling-induced casing wear is a normal phenomenon in all directional wells as drilling a section imparts drillstring contacts in the build, inclined and tighter cased sections. With minor presence in slightly deviated and vertical wells (chiefly due to DS vibrations), casing wear due to contact with a rotating tooljoint is severe in high-dogleg sections. A bent drillstring incurs significant contact forces as it is “pressed” against the casing inner wall, normally at tooljoints or increased diameter sections.

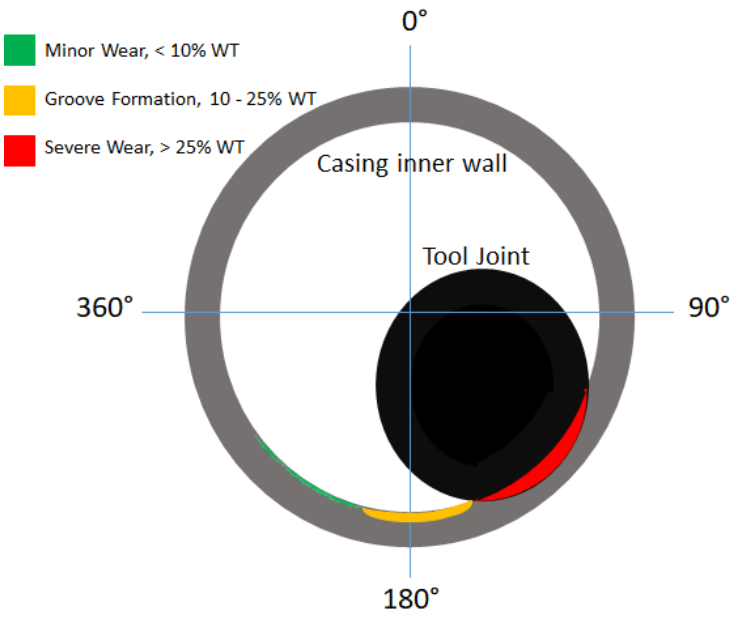

Figure 1. 1 - Crescent wear induction from the tooljoint

In terms of well stability, retaining the integrity of casing pipe against drill pipe wear is of critical importance. The issue is often encountered in deviated wells with moderate (3°-6°/100ft) to high doglegs (7°-15°/100ft). The long, continuous contact between the outer surface of a tense drill pipe/tool joint (during drilling or rotating off-bottom) or a compressed drill pipe/tool joint (in lower sections with high WOB) with the inner wall of the casing is the key element in reducing its wall thickness locally and thermally deteriorating (friction heating) the worn region. Tolerating minor casing wear (less than 5% WT) and short contacts between casing and drillpipe, wells with high doglegs generally cause the drillpipe to be firmly pressed against the casing for long periods,

causing severe wear and diminishing its yield, burst and collapse strength. This, then, becomes a stability concern in case of a deformed, bent or leaked casing. Since cemented and worn casings can't be removed, the outcome involves costly repairs to patch the damaged casing joints.

Figure 1. 2 - Sections of worn casing pipes (with percentage of wall thickness removed) [51]

1.2. Potential nature of the problem

Casing wear problems have increased significantly as the depth envelope of ERD projects have widened. The long inclined drilling sections incur continuous contact between the casing and the TJ in lower cased sections of the well. High and varying friction forces acting on the casing lead to excessive wear, making the casing susceptible to accidents such as leaks or casing collapse. To account for such issues during well-planning, well budgets undergo a significant increase in the drilling costs based on:

- Selection of thicker casings as contingency against wear
- Putting higher carbon steel grades to resist wear at deeper doglegs
- Compromising on maximum allowable doglegs for horizontal wells to prevent severe casing-drillstring contact
- Selecting casing-friendly BHAs/ tooljoints and using non-rotating drillpipe protectors around TJs
- Logging after section depth with multi-finger calipers, gyro surveys and ditch magnets on previous casings to detect wear

A 2D layout of detected crescent wear grooves in the casing from a multi-finger caliper log is presented in Figure 1.3.

In addition to the doglegs, higher depths are often associated with increased temperatures (3°C/100m) and added vibrations (lateral or torsional), both of which promote rapid casing wear. Thinned out casings are also less capable to bear axial load on the threaded connections at high temperatures, which is critical when drilling for gas reservoirs.

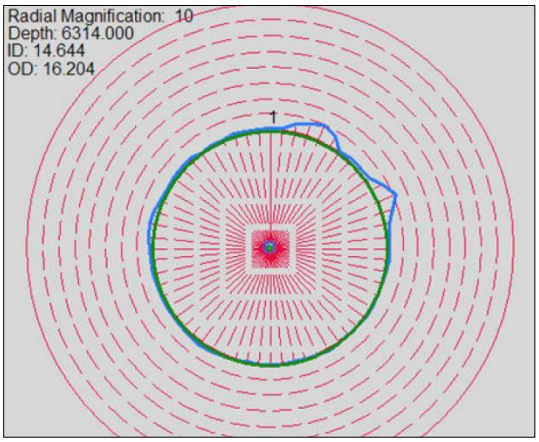

Figure 1. 3 - A view of casing caliper log at a specific well depth [21]

Issues related with worn casing may not surface immediately after drilling the section. While setting the well on completion or during the course of production, the problems may surface due to pressure surges and lead to a total or partial abandonment of the well, causing the operator economic burden if the casing wear is severe (≥40% WT) [11].

Accurate estimation of worn volume and remaining wall thickness based on a study of dynamic casing wear propagation can enable drilling engineers to improve well designs in slanted, extended-reach and horizontal scenarios, and avoid using unnecessary thick and over-priced casing grades, while minimizing the probability of wear incidents [1]. Experimental wear simulations between tooljoint and casing under field representative contact forces, rotating speeds and drilling fluid settings is a means to calibrate wear models, and to develop a refined wear database for reference wear factor and friction factor values.

1.3. Conventional approaches in industry and associated issues

The conventional approach in the industry to tackle casing wear is to run soft-string or stiff-string simulations (see section 2.2.1) on well-designing softwares (e.g., Landmark™, Sysdrill™ etc.) to have estimates on wear in advance. The wear volume and wear depth are measured as a direct function of the contact force, and fixed wear factor values from literature and general drilling situations are utilized. As will be discussed in Chapters 2 and 3, this method has limited field application to estimate wear intensity because for dynamic casing wear, parameters such as friction co-efficient, contact pressure and wear factor keep on changing continuously with changing drilling conditions such as contact area. As will be highlighted in Chapter 4, 7 and 8, the time-dependent depth and shape of the wear grove increases non-linearly and a single tool joint at a particular well depth and side force can take multiple wear factors on the casing section. The highest or “worst-case” wear factor taken by most well-plan softwares for wear calculation does not accurately represent this dynamic behavior.

In terms of field methods to measure and mitigate casing wear, the conventional way is to drill (and slide) with low tension in the doglegs, and keeping low to moderate drillstring RPM. Another way is to use non-rotating drillpipe protectors to slide down the casing and eliminate direct drillstring contact with the casing for particular sections.

A third approach is to filter and monitor the amount of metal dust received with the drill mud in the shale shakers at the surface. This is then compared to the results obtained by a casing sonic-log or a multi-finger caliper (MFC) log to have a rough idea on how much casing thickness could have been removed. In addition to the metal collected at the mud shakers, ditch magnets are also sometimes used directly in the well to gather metal shavings and estimate the amount of casing material removed.

Though the mentioned techniques provide a coarse estimate on worn mass on the casing, there are issues associated with them:

- **For wear softwares:** The friction factors are mostly assumed based on literature values for metal-metal contact instead of being calibrated against experimental/actual drilling practices with mud lubrication. The resultant wear estimates are, thereby, for worst case scenarios and result in over-estimation of casing wear.
- **For soft-string model simulations:** The soft string model assumes the entire drillstring as a long, elastic string and assumes constant force on casing string overall the drill string contact length, which is not the actual case (shown in Chapter 4). The contact force is mostly predominant at the harder tool joints and BHA sections and this is an important parameter for precise wear estimation.
- **For Caliper logs:** MFC logs are typically run through the same casing strings after setting and at the end of drilling next section. As it usually undergoes a lot of undesired noise while being run in the hole, tool calibration and compensations against the measured values are a necessity. Due to orientation errors, comparison of caliper logs may also give wrong location of wear grooves.

1.4. Outline of chapters

A summary of the structure of this thesis is presented below:

Chapter 1 encompasses an introduction to the research study, focusing on the state-of-the-art, technological gap and the necessity of the work as a part of the bigger drilling optimization context. General and specific objectives have been laid down and the scope of work has been presented to achieve these goals.

Chapter 2 highlights basic wear mechanisms important for drillpipe-tooljoint interaction and then proceeds on to an account of previous experimental studies on casing wear. Wear models

conventionally used in the industry for wear estimation are also presented in the chapter. Towards the end, a brief account of on-site casing wear monitoring techniques has been provided with a mention of applied effects of wear on burst and collapse strength of casing pipes.

Chapter 3 provides a deeper understanding on the influence of critical well parameters that influence wear intensity during drilling operations. Casing pipes are subjected to a combined effect of the mentioned parameters, and outcomes can incur minor to severe wear. This chapter also forms the basis of determining the range of parameters selected to be used for simulations in Chapter 4 and the design of the experimental setup in Chapters 5 and 6. A brief account of conventional wear mitigation techniques has also been presented at the end.

Chapter 4 presents simulation case studies taking base drilling parameters from literature review and using proprietary softwares to simulate side force values and wear volumes. These side force values are then used in the wear models presented in Chapter 2 to predict wear volume and WT reduction for a case study well. Critical side force values are then highlighted for “best” to “worst” wear factor values. The chapter also incorporates an account of recent case histories reporting wear on horizontal and s-shaped wells.

Chapter 5 takes the critical values and parameters from Chapters 3 and 4 to highlight the design process and components of the wear frame used to experimentally replicate the wear process. The individual systems, their components, along with their operational mechanisms and limits have been discussed.

Chapter 6 takes the anticipated side force and drilling parameters values from Chapter 4 to calibrate the systems of the wear frame to obtain reliable results. Sensitivity of the parameters such as axial reciprocation, side force in static and moving conditions, and tool joint rotation is analyzed on the results. A brief load distribution analysis to anticipate stress propagations upon casing contact is carried out towards the end using ANSYS. The simulated results on ANSYS for frictional stress and contact behavior have been experimentally verified later by the wear tests.

Chapter 7 presents the results gathered from 14 full scale wear tests representing field scenarios on sideforce, casing materials (steel, glass fiber and carbon fiber) and fluid lubrication. The results have been compared in the later part of the chapter.

Chapter 8 delivers a discussion on some observed characteristics during the wear propagation on casing materials. Analysis of the contact pressure thresholds, steady wear factor values and roughness profiles of casing specimens after wear are compiled in this chapter.

Chapter 9 presents conclusions on the research work and future developments to continue the study using an experimental approach to ultimately develop a wear databank.

1.5. State of the art

The puzzle of casing wear prediction has been a research topics for around 40 years in the oil and gas industry. **Bradley and Fontenot (1975)** used experimental data and wear figures acquired from Shell oil company's wells to analyze the relation between casing wear and parameters like drilling speed (ROP), drilling mud properties, drillstring type and the sliding distance of the DS contact on the casing [1]. Wear rate was declared independent of rate of penetration (ROP), and a direct (non-linear) function of the contact force and drillstring rotation. Additionally, drilling was termed as the major process inducing casing wear [7] in comparison to running wireline.

Williamson (1981) analyzed the geometrical aspect of casing wear depth with groove width and used contact pressure instead of contact force for wear calculations [1]. He proposed that the critical factor causing casing wear was the loading between the casing and TJ and derived a base relation between casing wear rate and contact pressure based on an experimental study [20].

Best (1986) extended Williamson's work by highlighting the contact force at tool joint (TJ) and surface revolutions (RPM) as critical parameters for casing wear prediction.

The linear casing wear efficiency model was presented by **White and Dawson (1987)**, asserting the amount of casing wear removed as a function of frictional energy infused at the contact. The model was used for early field wear predictions. Their experimental analysis established that high yield strength material actually wear out faster than low yield grades like K55. They also proposed that the wear rate is higher in oil-based fluid lubrication compared to water-based.

The evaluation of casing safety factor due to the reduced rupture strength after casing wear was provided by **Song (1992)**. He presented a methodology to determine the remaining strength of worn casing based on the crescent shaped groove dimensions.

The popular casing wear volume equation by **Hall (1994)** serves as the basis for many current casing wear prediction models and wear factor values for softwares. The static wear efficiency model highlighted the relation between drilling parameters such as casing wear factor, sliding distance, side (contact) force, surface RPM and drilling speed with the wear volume on the casing.

The improved casing prediction model presented by **Hall and Malloy (2005)** established the concept of contact pressure threshold leading to reduced casing wear and very low wear factors.

The effect of variable TJ sizes and varying contact pressures on casing wear was highlighted by the **Gao Equation (2010) and the Gao and Sun Models (2012)**. The non-linearity in the Hall equation, and in its relation between wear depth and rotating hours was also proposed. The models implied a non-linear casing wear propagation during drilling and tripping, and a steady-state wear during pipe rotation [11]. The models were validated by their experimental data.

Based on a field database for wells deeper than 13,000 feet, **Mitchell and Xiang (2012)** proposed an improved statistical casing wear model.

Shen and Beck (2012) proposed a finite element model for stress concentration in the worn casing based on boundary superposition principle [11].

A 3D finite element model to simulate the effects of uniform and non-uniform wear on the pipe residual strength was presented by **Wang (2013)**. Parameters such as length of wear, wear percentage, DS diameter, and casing WT were considered for modeling.

A model for calculating the remaining collapse strength of worn-out casings was presented by **Lin and Deng (2013**) incorporating the effects of pipe geometrical defects and non-uniform wear. The equation was reported to be successfully applied in field casing design process [11].

An experimental study to simulate the casing wear was carried out by **Yu and Lian (2016).** Friction co-efficient and wear factor was experimentally determined at low contact forces and was used as a numerical input for simulations carried out at higher contact forces. The results were then used to predict the reduction in collapse and burst strength of the casing pipes.

The effects of increased DS angular velocity and bit whirl on casing wear were presented by **Tan and Gao (2018)** where a composite model, comprising of circumferential wear model and localized groove wear model, was presented for more accurate casing wear predictions. Factors such as coefficients of rolling and sliding friction, TJ geometry, weight of DS were included in the model. Subsequently, a theoretical case scenario was presented to demonstrate that the model offered improved wear prediction accuracy.

1.6. Research gap

It has been established from the state-of-the-art that there is no accurate way to model casing wear for particular drilling scenarios without an experimental basis. A model can be field representative only after the inclusion of friction factors and wear factors derived from full scale wear testing. As very little comprehensive test data is available for modeling specific situations (much of it is proprietary), development of purpose-oriented test frames is the most accurate and operationally flexible way to analyze the wear behavior of the different casing materials.

Though much literature is available on general wear behavior of casings, less experimental data is available on quantification of wear propagation in terms of variable friction and wear factors, and even lesser information is available on how to experimentally determine steady wear and friction factors for field calculations/calibrations. Hall's experimental database provides the most comprehensive description of limit wear over time and contact pressure thresholds on casings under particular service conditions. Though concrete experimental inferences have been derived in the work, the data points are limited to particular materials and conditions. [6]

Recent advances in casing materials have also proposed utilization of novel materials such as fibered glass or fibered carbon for use in moderately deep well sections, and for observation wells. Over conventional steel casings, these novel materials provide much higher resistance to sour conditions and corrosion, possess a high strength-to-weight ratio, offer adequate damage tolerance, and have less installation costs. Both casing material types undergo significant decrease in strength upon wall thickness reduction and little experimental wear data is present to establish any reference on their performance upon contact with tool joint. Also, their properties deteriorate significantly over higher temperatures (90°C for glass resin-layer, 162°C for fibered graphite-layers) and no data is available to anticipate the outcome temperatures due to added friction heating upon tool joint contact.

In regard to these aspects, the research focus of this study is to investigate the variability in friction factor and wear factor for long contact intervals for different materials under field service conditions. Analyzing such variations can define a “steady wear factor” for long contact intervals that is proposed to be used for projected wear volume calculations. The design of a wear frame that can measure both the above parameters as output (along with wear quantification), while being flexible to incorporate new materials, lubrication conditions and well scenarios is also a core strength of this study. This presents a new and comprehensive experimental approach to determine representative wear factors used for field wear determination.

1.7. Objectives of the study

The primary objective of this study is to analyze timely friction behavior between casing and tool joint for different materials during drilling operations. Variable friction and wear factors are the deliverable that is to be compared with existing experimental approaches. This new methodology is aimed to improve predictions for casing wear for existing and upcoming models by determining a steady wear factor in real time and using it to predict wear rate and wear volume. Friction factor has been the key element in categorizing wear as minor, mild or severe. The specific objectives for this study involve:

- Highlighting the parameters influencing wear behavior and friction factor
- Identifying existing models that are frequently used for predicting wear intensity in the industry
- Determination of operational parameters and side force range to serve as input for wear frame design
- Design and construction of a wear frame where the corresponding force and wear will be experimentally observed
- Determination of friction factor and wear factor under operation scenarios and identify steady wear factor values to utilize for wear models for field wear projections
- Comparison of the wear behavior with previous experimental studies

1.8. Study Approach

Many previous experimental studies either test samples at very low contact forces and extrapolate the wear behavior using the same friction factor, or determine friction factor based on cumulative volume of casing removed after long time intervals.

The novel experimental approach for this study involves implementing experimental conditions that can represent field parameters, and defining wear parameters like worn volume, frictional work and friction factor as a measured output. A real-time friction moment on the tool joint is used as an input for determining friction factor, and then combined with worn volume for the wear factor.

The first phase of the thesis involves highlighting the predominant forms of wear during casing tooljoint contact and critical parameters that influence the wear behavior.

Casing wear involves dynamic and simultaneous action of various elements such as normal force, friction force, axial movements, ever-changing contact pressure due to wear area, temperature due to friction heating and it's quenching due to fluid circulation, and lubrication effects upon rotation and sliding. Designing a wear frame with an operational balance for these elements while keeping them close to field conditions is the second phase of the study.

The calibration runs and sensitivity tests of the wear frame with the aim of determining reliable, real-time friction factors and wear factors under test conditions is the next phase. This involves confining the number of factors and keeping some known parameters constant to observe the effect of single factors on the friction behavior.

The final phase then involves analysis and comparison of observed wear behavior under different conditions.

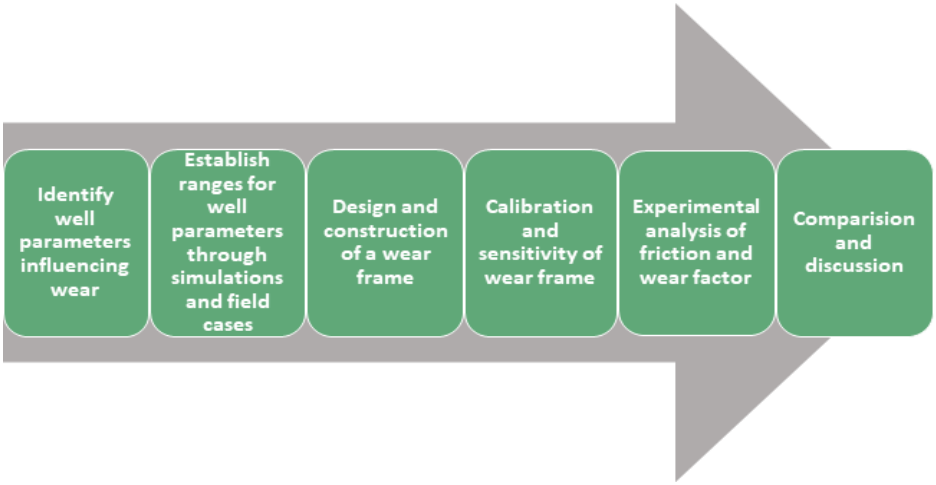

Figure 1. 4 - Work flow for phases of this study

2. Casing wear: Mechanisms, estimation and consequences

2.1. Casing wear mechanisms

Friction between the rough surfaces under high contact pressure leads to progressive wear on the casing. A metallurgical understanding of casing wear is needed to relate different forms of casing wear mechanisms to different wear rates.

For extruded (single material), seamless steel casings, the inner wall consists of atom grids and has properties such as malleability, heat conductivity and ductility. The attraction between opposing charges (protons and free-floating electrons) keeps the metal layer together. The number of free-floating electrons imparts toughness and ductility in the metal structure where it is able to deform without breaking due to shift in atoms.

Wear acceleration takes place in a heated system where the contact surface volume expands due to hysteresis heat. The metal atoms begin to vibrate at a higher frequency and tend to restructure or break-free from the contact layer as it expands. Such allotropic phase transformation results in the reduction of metal yield strength, ductility and solidity. As more heat is transferred in the metal surface, the atom removal process is accelerated. This speed of this process is dependent upon the metal composition, residing temperature, applied pressure at the contact surface and roughness of the abrasive material. For extensive wear, the process requires long time intervals and consistency in contact and relative motion of surfaces to one another.

With this aspect in background, some common types of wear mechanisms relevant for casing wear are included in the study such as adhesive, abrasive, fatigue and polish wear.

2.1.1. Adhesive wear

Adhesive wear (such as galling) can be defined as plastic deformation of very fine fragments on the casing surface. This mechanism is identified by local solid phase welding which exists when two metal bodies are in dry contact, normally for smooth steel tool joint and casing at high contact pressures. The welds are sheared off by rotation of the mating surfaces and metal is moved from casing (with low strength) to tool joint (with high strength). The effect is further enhanced by aggressive hardfacing to impart durability in TJ against wear.

A preventive measure against adhesive wear is to increase material hardness and preventing micro-plastic distortions of the surface. [10]

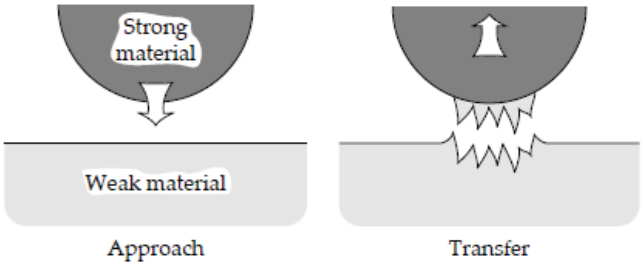

Figure 2. 1 - Material removal during adhesive wear [10]

2.1.2. Abrasive wear

Abrasive wear takes place due to direct contact between a particle or grit with a material surface when the particle is either equally hard as the surface or harder, ultimately reducing the surface thickness at the contact area. The shape of the particle or the body influences the nature of the wear occurring. Round and non-fractured bodies generally cause lesser abrasive wear then fractured and sharp-edged particles. Abrasive wear may be difficult to prevent or mitigate as it involves several mechanisms, and these mechanisms play a major role in the abrasion rate. [10].

Cutting wear occurs when a sharp edge of a material cuts into another material surface and the cut particles are removed as "wear debris". If the abraded surface is brittle, fractures might initiate on the worn surface and wear debris is a result of crack convergence. If the surface is metallic or ductile, the abraded surface is continuously deformed but no cracks take place. The wear debris in this case accumulates due to metal fatigue. The study of cutting wear under an electron microscope shows two possible mechanisms: micro-cutting and ploughing.

Micro-cutting is a phenomenon commonly encountered with the usage of tungsten carbide hardfaced joints as they come in contact with the casing. The scratching and cutting wear increases with higher contact force and higher RPM with random shaped, plate-structured wear debris. The presence of drilling fluid can also be a contributing factor to micro-cutting due to the accumulation of abrasive particles.

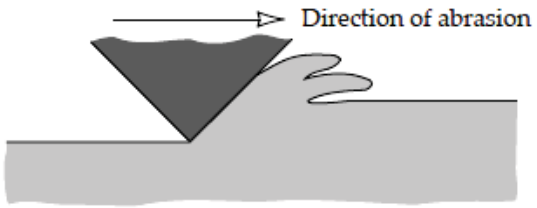

Figure 2. 2 - Scanning Electron Microscope (SEM) view of micro-cutting structure [10]

Ploughing is a cutting mechanism more common in OCTG connection threads, particularly the ones with metal-to-metal seals. Ploughing typically involves plastic deformation of the abraded

surface without actual removal of particles from it and occurs if the hardness difference between the materials is higher than 0.2. At moderate penetration depths, plastic deformation takes place whereas wear flakes may be created in the surface at increased cutting depths. The plastic deformation while ploughing mainly increases the strain hardness in the material and reduces the tendency for further ploughing on the surface [10].

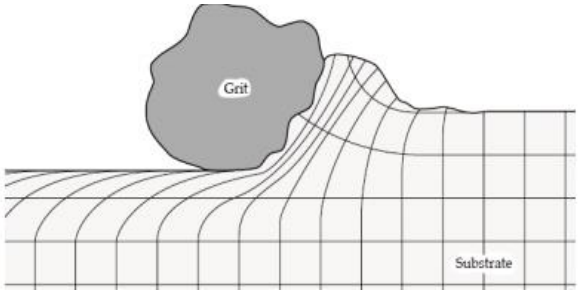

Figure 2. 3 - Plastic deformation during material ploughing [10]

Fracture wear is a form of abrasive wear that is relatively uncommon for casing wear and takes place when the abraded surface is brittle and fragile. The wear debris is formed by propagation of cracks accumulation and merging and large chunks of material are removed. Hardened metals are more prone to this kind of wear as increase of hardness reduces the yield strength and toughness. This is a contributing factor to some field observations where harder casing grades wear off more rapidly on high DP contact loads as the abrasion mechanism changes from cutting to fracture wear.

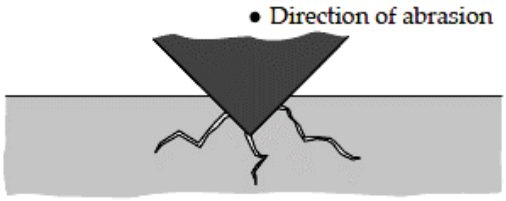

Figure 2. 4 - Fracture wear initiation and propagation on brittle metal surfaces [10]

Fatigue wear, along with micro cutting, is a more frequent mechanism for TJ-casing wear and occurs due to repeated contact of a dull edged hard particle or grit (TJ) with plastic material (casing). The resulting fatigue strain causes the material surface to be deformed (ploughed) and displaced sideward, away from the wear groove.

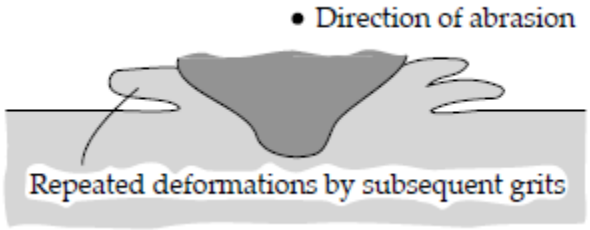

Figure 2. 5 - Fatigue wear due to repeated abrasive contact [10]

Grain removal is also an abrasive wear mechanism not typical for plastic metals but for brittle surfaces such as glass fiber casings and ceramics. Upon high load point contact, the inter-grain bonds are loosened and large grains on the surface are detached. The resulting geometrical irregularities make room for further rapid abrasion on material if the point contact forces persist.

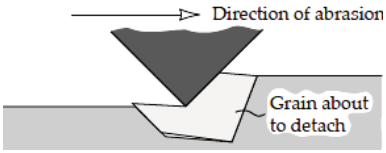

Figure 2. 6 - Grain removal mechanism in brittle surfaces [10]

Abrasive wear is the most common and rapid form of wear and the most practical method to suppress it is the application of internal coatings or hardfacing the surface to the point that the hardness at the surface is at least 0.8 of the particle hardness. The layers of tungsten carbide can be coated on to the surface in comparison to choosing expensive wear-resistant materials. The use of tungsten carbide, however, makes the surface more prone to brittle cracks and may shatter on repeated impact.

Two-body abrasion takes place when two solid surfaces come in contact with each other and one of the surfaces is harder than other owing to aggressive coatings or particles mounted on it. This is an important consideration for hardfaced tooljoints on casings as they cause rapid cutting and grooving, depending upon the force of contact and duration.

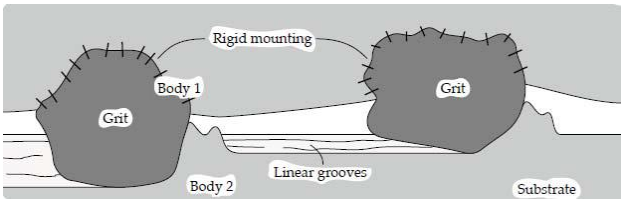

Figure 2. 7 - Two body cutting mechanism in metals [10]

Three-body abrasion is similar to two-body abrasion except for that the particles are not fixed in place, but can slide and move around the contact. Three-body wear is less intensive than two-

body abrasive wear and normally takes place when a lubricating mud particle layer is present at the contact between tool joint and casing.

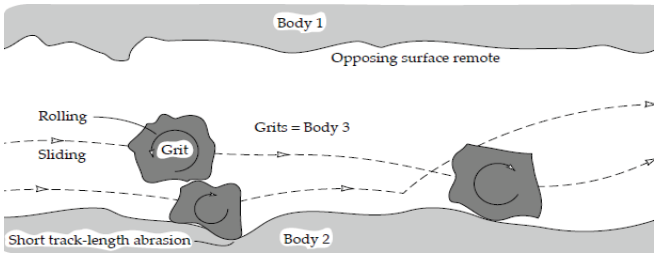

Figure 2. 8 - Three-body cutting mechanism in metals [10]

2.1.3. Polishing wear

Polishing wear results in very smooth and fine particles of steel powder created during the rolling between casing and the tool joint. The particles blend inside the soft material (casing) with the friction heat and produce a highly polished surface. The polishing wear rate is very low and it happens over longer periods of time.

Figure 2. 9 - Shiny polished layer on a failed tool joint pin section [16]

2.2. Existing models for casing wear determination

2.2.1. Soft-string model vs stiff string model for casing wear

Soft string model is a conventional wear estimation method employed in many known well design software programs. It represents the drillstring behavior neglecting the bending stiffness of the individual string components. The drillstring, therefore, performs as a thick cylindrical metal cable that is assumed to move along the well trajectory. In other words, the drillstring trajectory is the same as the wellbore trajectory and this makes it difficult to pinpoint the actual contact locations as the model assumes a long, continuous contact of the drillpipe and casing wall. The assumptions work well for conventional torque and drag analysis, yet they are unsuccessful in accurately modeling casing wear. For long drillstring contacts above and in dogleg section, soft-string model results in over predicting the wear when compared with field wear logs. The resulting wear grooves are longer (assuming longer DS contact) and focused on fixed well locations, contrary to field observations where multiple grooves occur above, inside and below the high dogleg section as stiff hardbanded tooljoints define the bending behavior of the DS.

The stiff string model provides a more accurate means for wear prediction as more variables such as the bending stiffness of the string, the shape of the wellbore and DS clearance are considered. The positions of higher bending stiffness in DS (namely at TJs and BHA) in doglegs are mostly the locations of higher contact forces. The shape of the drillpipe and its Brinell hardness can also influence the stiffness effect. Logically, a thicker drillpipe tends to stay straight and a thinner one tends to follow the curved shape of the wellbore. The shape of the wellbore is defined as a boundary and extra side force caused by the stiffness of the tool joint is applied at points where the bent shape of the drillpipe touches the boundaries.

Well tortuosity in spiral wells, also a factor not considered in soft-string model, plays a role in increasing side force as per well inclination. The deflection of the drillpipe and the value of the extra side force due to tortuosity cannot be ignored as the drillpipe presses against the spiral wellbore wall under existing forces and its own weight. Such tortuosity effects are difficult to identify as it signifies no big change in well inclination. The tortuous “wave” pattern can only be promptly identified and rectified using RSS directly above the bit, as MWD tools are placed at least a couple of joints (15m-30m) above the bit and cannot rectify the issue, if identifying the spiral waves at all. Such “support” locations where the spiral wellbore comes in contact with the DS undergo high contact forces even though the DS is not considerably bent. To incorporate this compounded side force, stiff string model serves as the better option (also for torque and drag analysis). Figure 2.10 shows drillstring defection for tortuous wellbore and added sideforce locations.

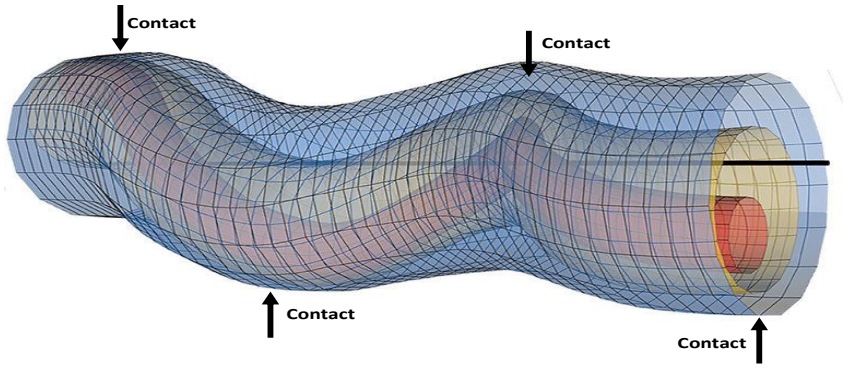

Figure 2. 10 - Side-force locations on a tortuous wellbore [48]

2.2.2. Experimental contact pressure and wear volume estimation (Williamson, 1981)

In his experimental study, Williamson estimated the ever-changing contact area between the casing and the TJ (due to increase in wear depth) as the arc of the same radius as the tool joint times the length of contact (in his experiment, 3 inches). With the aim of determining the relation between wear rate and contact pressure, his wear test involved a contact between casing and TJ at 150 rpm with slight back and forth lateral movements in the casing specimen corresponding

to a drilling rate of 20ft/hr. The casing specimens used were 9 5/8", N-80 pipes and the TJs were non-hardbanded AISA 4135. The mud used was Milgel 515 with 6% Clementex and water (80-120 mesh). The test yielded following results for wear rate under varying contact pressures (Figure 2.11).

A transition in the wear pattern occurs first around 120psi as the contact pressure pushes the solid particles into the casing wall and increases wear rate (ploughing and polishing). The next transition occurs at 250 psi when the wear mechanism changes to adhesion due to inability of the fluid to form a protective layer between the moving components.

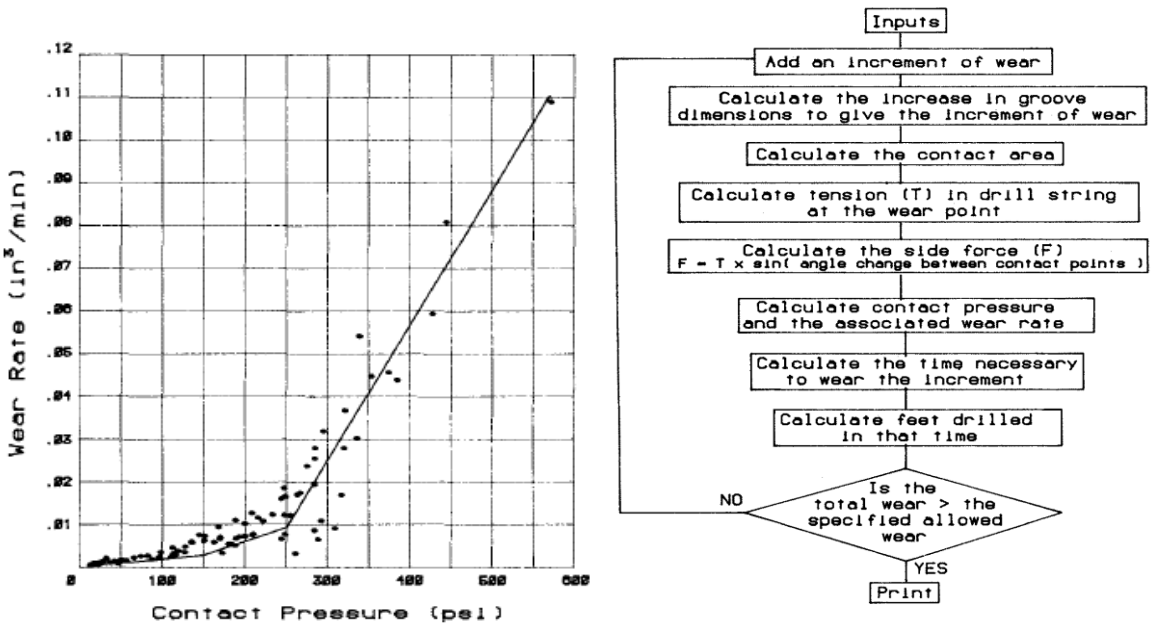

Figure 2. 11 - Casing wear test results at varying contact pressures and flowchart for the empirical model used to predict safe drilling depths [20]

Wear volume was determined using the timely variating depth and width of the groove and by using the TJ diameter and casing ID. Contact pressure values were recorded at different test intervals by stopping the test and dividing the lateral load with the effective contact area. Since the pressure declined with time (higher contact area), some tests were conducted with increasing lateral force to hold the contact pressure (results in the Figure above). Williamson also highlighted that at low contact pressure, the key wear mechanism is abrasion whereas for higher contact pressures, adhesion is the major wear phenomenon.

Based on the test results, Williamson presented an empirical model to predict the additional depths (after casing-TJ contact) that can be safely drilled at different dogleg severities. Taking RPM, ROP, TJ size, drill mud weight and number of contact points as input, he used the methodology presented in Figure 2.11 to predict drilling depths.

Based on the model, it was also estimated that the wear rate will be more rapid for smaller tool joint diameters and that use of different TJ diameters will increase the wear rate. The model, however, assumes only rotational wear on the casing at different points which is not the field case and, therefore, recommends against the application of direct experimental results in the field.

2.2.3. Wear track length model (Best, 1986)

The wear track length model by Best established an empirical linear relationship between length of wear groove and experimental drilling conditions. He also gave preliminary analysis on influence of weight of drilling fluid and TJ hardfacing on the wear speed. The wear length was defined as:

$$L_{wt} = 60 \times \pi \times d_{tj} \times \nu_f \times t_f \times \frac{L_{tjf}}{L_s} \quad (1)$$

Here,

L_{wt} is the wear track length, m

L_{tjf} is the tool joint length, m

L_s is the length of drillpipe, m

d_{tj} is the tool joint diameter in the field, m

ν_f is the drillstring RPM, rev/min

t_f is the number of rotating hours, hr

2.2.4. Experimental setup for casing wear (Bol, 1986)

G.M. Bol demonstrated the influence of various mud types and additives on the friction and wear factors in terms of formation of wear protection film and lubrication. He initially conducted small scale lubricity tests, followed later by full scale wear tests (FST) on a customized wear machine using casing C-sections and TJ specimens. The small scale test (SST) results were declared non-representative for field calculations as actual TJ/casing specimens were not utilized for the apparatus. In addition, the results obtained for some additives did not agree with the results for the same additives with full scale tests. For example, the friction factors obtained with API bentonite were between 0.09 and 0.15 whereas in FST the factors were 0.2 to 0.5, which are in agreement with field values.

The experimental setup involved contact between fixed diameters of 6.5” TJ and 9 5/8” casing (L80, N80). The side force was ranged for different runs between 4KN to 8KN. The average test RPM was 112rev/min with axial movement of around 4.8m/hr. Friction factor was calculated as

a function of wear volume and total energy supplied to the casing. The tests were performed with pure steel TJs with no hardfacing.

The full scale test results established friction factors for casing wear using several mud type and additives. The author also stated that stabilized friction factors for all mud cases are dependent upon contact time as the initial contact are is always higher and results in larger contact pressures and more FF.

The full scale test results established formation of a thin protective layer from mud additives between TJ-casing contact. This was in concordance with results from Best (1986) and Bradley and Fontenot (1975). It was also mentioned, however, that use of hardfacing may hinder the formation of this layer. Some results obtained on the lesser wear with weighted muds disagreed with the results from White and Dawson (1987). A simplified layout of the FST machine is presented below:

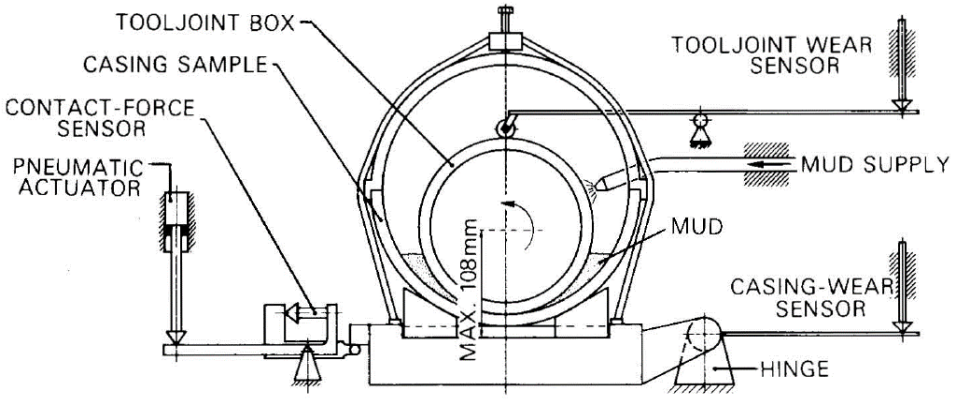

Figure 2. 12 - Simplified sketch of the testing frame from Bol et.al. [39]

2.2.5. Experimental measurements for friction coefficient (White and Dawson, 1987)

White and Dawson (1987) set up an experimental study to measure and estimate casing wear using a test frame, operating between 15 to 120 RPM and up to 13.5KN side force through the tool joint. There was no axial motion in the TJ string and the wear was focused on one short section of the casing sample. The experiments used 9 5/8" casing samples of grades K55, N80 and P110, against 6 ¾" TJ (without hardbanding). The assembly was immersed in a fluid tank and four different mud settings were used in the experimentation (weighted, unweighted water-based muds and weighted, unweighted oil-based muds). The sand content in the muds was between 0 to 2%.

At lower speeds (15 RPM), the friction coefficients were measured to be between 0.25 to 0.3 for WBMs and 0.10 to 0.15 for OBMs. The authors stated that hydrodynamic lubrication (fluid layer between the TJ and casing) was an undesirable effect during the experiments but was unavoidable during the study. A simplified layout of the test machine is presented in figure 2.13:

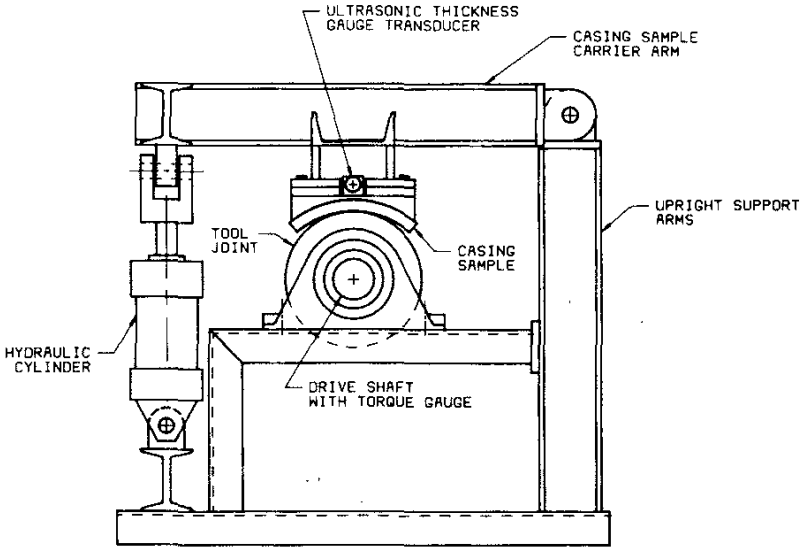

Figure 2. 13 - Simplified sketch of the testing frame by White and Dawson [3]

2.2.6. Wear efficiency model (Hall and Garkasi, 1994)

Hall came up with an empirical mathematical model based on experimental results and field observations to evaluate casing wear rate from casing-TJ grade and material, drill fluid properties, measured depth at wear locations and drill settings. With the objective of predicting, quantifying and mitigating casing wear, more than 300 casing wear tests were conducted to determine the wear factors to be used in numerical calculations for different drilling conditions. For proprietary reasons (BP and Shell were involved in the project), many casing grades TJ materials were kept confidential. A computer program (CWEAR) was developed to incorporate the model and corresponding experimental and numerical values.

An important consideration here was the determination of DLS from the directional surveys where the measurement stations were more than 100ft away from one another. The DLS measurements from short build wells for such surveys were highly unsatisfactory.

The model assumed that the wear volume is a measure of the frictional work done on the casing by the TJ. Following linear equations were given to determine the wear volume:

$$\textit{Wear volume/ foot} = \textit{frictional work per foot / specific energy provided} \quad (2)$$

Here the specific energy is value needed to wear one cubic inch of steel. The frictional work mentioned above was defined as:

$$\textit{Frictional work per foot} = \textit{Applied normal force x friction factor (experimental) x sliding distance} \quad (3)$$

A “wear factor” was the defined, incorporating the friction factor as:

$$Wear\ factor = friction\ factor\ /\ specific\ energy \tag{4}$$

And the combined wear equation became:

$$Wear\ volume\ /\ foot = wear\ factor\ x\ applied\ normal\ force\ x\ sliding\ distance$$

From the above equations, the factors “*wear volume /foot*”, “sliding *distance*” and “*applied normal force*” are determined experimentally to calculate the “*wear factor”* (in E-10 in^2/lbf). For the calculations of normal force on the casing in the model, parameters such as well trajectory, DS components, mud density and surface parameters (RPM, MD etc.) are taken as input and the “frictional work / foot” is determined based on values. This, when combined with the wear factor determined experimentally, provides the wear volume. The accurate calculation of “applied normal force” is, therefore, the major factor in casing wear estimation through the model. The normal force was taken as:

$$Applied\ normal\ force = 2\ x\ DS\ Tension\ x\ sin(DLS/2) \tag{5}$$

Here the DLS is in radians/foot

The apparent DLS measured from directional surveys between two stations *i* and *j* (in comparison to the real DLS) was given as:

$$(DLS)ij\ ,\ a = (100/Lij)\ x\ \Delta\varphi ij \tag{6}$$

Here,

$\Delta\varphi_{ij}$ is the change in direction between stations i and j in degrees

$(DLS)_{ij\ ,\ a}$ is the apparent DLS , °/100ft

L_{ij} is the MD from station i to j

Apparent DLS was presented as the safest way to make casing wear calculations apart from the directional survey values, which in many cases was not available.

For accuracy on wear factors, Hall took three possible WF values: 0.05 in case of TJ with pipe protectors, $(WF)_{lab}$ as the normal value and 2 x $(WF)_{lab}$ for worst case scenarios. For extreme cases, the third value was taken for model simulations to avoid under predictions on casing wear for field applications.

From lab experiments, the friction factor (or correspondingly the wear factor) was determined for different conditions:

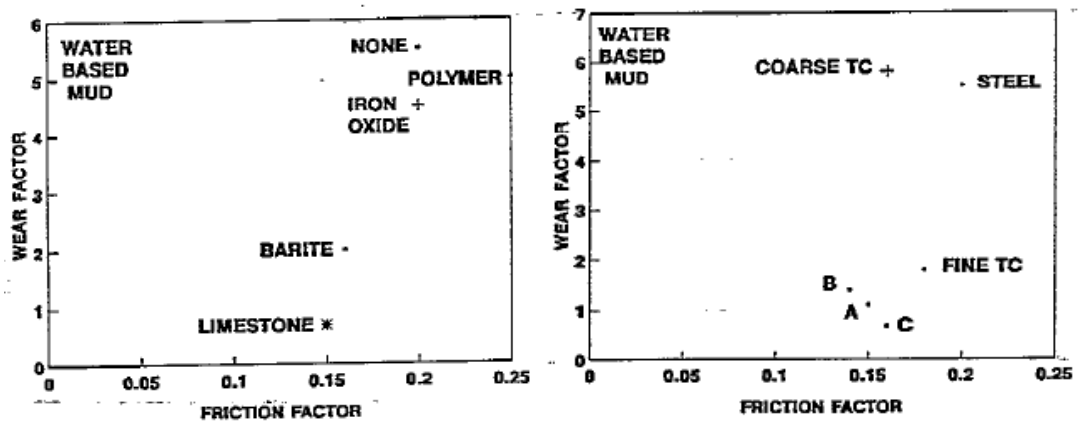

Figure 2. 14 - Wear factor for various mud additives and TJ hardfacings [5]

The mud additives lowered the wear factor by reducing the friction factor by around a quarter value. Polymer additives increased the friction factor slightly. Pipe protectors on DS also reduced friction factor. However, friction was reduced even further when run on a polished inner surface of casing compared to the rusted inner surface.

Fine TC material was experimentally found to be more casing friendly compared to coarse TC hardbanding. Other materials A, B and C reduced the friction even lower, but were not named for proprietary purposes.

From experiments, none of the inner wall casing coatings appeared to reduce the casing wear by a huge margin. Also, no casing material was declared as specifically "wear resistant" compared to the others. Even though no casing grades were specifically mentioned, it was mentioned that all casing grades were tested to be found "disappointing" from wear resistance perspective.

2.2.7. Contact pressure threshold model (Hall and Malloy, 2005)

In an extension of his previous work, Hall presented an empirical concept of contact pressure threshold by conducting more than 475 casing and riser wear tests. The tests were run for 8 hours duration and wear groove depths were measured at 0.25, 0.5, 2, 4, 6 and 8 hours. Using the previous concept of wear volume as a function of frictional work, the equation for wear volume was presented as:

$$V = \frac{\mu \times \varphi \times SD}{\varepsilon} \tag{7}$$

$$WF = \frac{\mu}{\varepsilon} \tag{8}$$

Here

V is the wear volume per foot, in³/ft

μ is the friction factor

φ is the applied lateral force, lbf/ft

ε is the specific energy (to remove 1 in^3 of casing), lbf. in/in^3

WF is the wear factor, E-10/psi

SD is the sliding distance, ft

$$SD = \pi \times D_{TJ} \times 60 \times N \times t \times f \quad (9)$$

f is the ratio of DP to TJ length, taken as 0.039 (considering L_{dp} = 30ft and L_{TJ} = 14 inches)

N is the number of revolutions

The wear volume was then defined as a combined value:

$$V = WF \times \varphi \times \pi \times D_{TJ} \times 60 \times N \times t \times f \quad (10)$$

Defining fixed experimental parameters as "Work function":

$$\psi = \varphi \times SD \quad (11)$$

The wear volume now becomes:

$$V = WF \times \psi \quad (12)$$

Wear groove depth was recorded over time, which was then converted to work function:

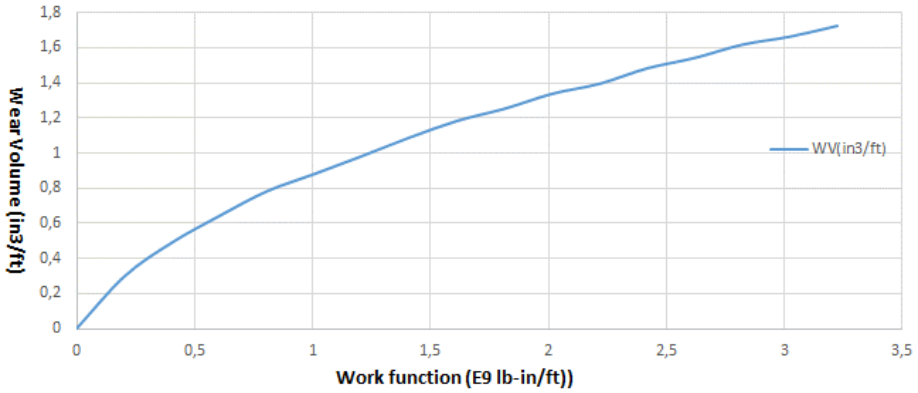

Figure 2. 15 - Conversion into work function vs. wear volume, plotted after Hall (2005)

The work-function plot is obtained by curve fitting using the following function:

$$V = A \times (1 - e^{(-B \times \psi^C)}) \quad (13)$$

Parameters A, B, and C are curve-fitting parameters. A is the constant for maximum wear volume (limiting value) for the test conditions as the groove depth will not increase after the limiting wear volume. This limiting wear volume is independent of tool joint and casing diameters but is

used to convert the wear volume to groove depth. The test conditions are defined in the table below:

Table 2. 1 - Experimental conditions applied in Hall's test setup [6]

Casing	N-80		TJ	AISI 4145 Steel			field units		Mud	field units	
OD	9,625	in	OD	6,25	in	Side force	3000	lbf/ft	Density	10	lb/gal
ID	8,681	in	length	3,25	in	RPM	158	RPM	Bentonite	26	lb/bbl
Wall	0,472	in				Axial speed	20	ft/hr	Barite	41	lb/bbl
length	4	in				length reciprocation	2	in	Sand	30	lb/bbl
weight	47	lb/ft				test time	480	min	Viscosity	50	sec

To define the concept of contact pressure threshold, parameters such as "conventional wear factor" and "differential wear factor" were defined. Conventional wear factor is defined as the slope of the line connecting the beginning to the end of the wear volume curve against work function for the 8-hour wear experiment. Differential wear factor, on the other hand, is the slope of the tangent to the wear volume curve and corresponds to an earlier beginning of wear and more wear volume removed per work function. The definitions and relations for both the functions are provided in the equations and figure below.

Conventional wear factor:

$$WF(\psi) = \frac{V(\psi)}{\psi} = \frac{A \times (1 - e^{(-B \times \psi^C)})}{\psi} \tag{14}$$

Differential wear factor:

$$\delta WF(\psi) = \frac{dV}{d\psi} = A \times B \times C \times e^{(-B \times \psi^C)} \times \psi^{(C-1)} \tag{15}$$

And the corresponding definitions from experimental conditions:

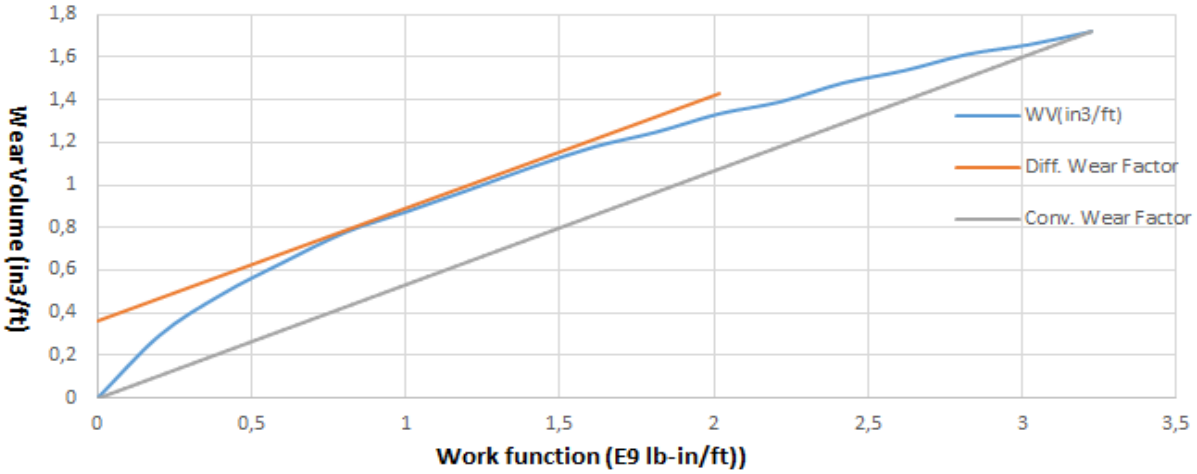

Figure 2. 16 - Definition of differential and conventional wear factor, plotted after Hall (2005)

Finally, the contact pressure threshold is defined as the contact pressure where both conventional and differential wear factors coincide on the x-axis and highlights the maximum groove depth for a given lateral force. As an example, it was provided that for 9 5/8", N-80 specimen worn by a 6 5/8" non-hardbanded tooljoint, the contact pressure threshold under 3000lbf/ft will be 73 psi.

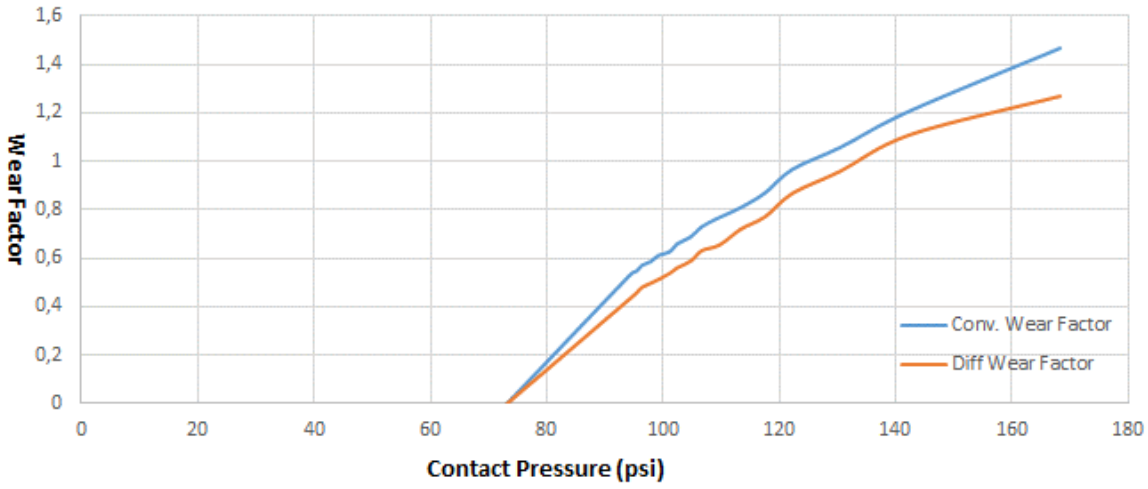

Figure 2. 17 - Example for contact pressure threshold for the specimen, plotted after Hall (2005)

At contact pressure threshold, the maximum wear width (inches) is given with the following formula:

$$W = \frac{\varphi}{12 \times CPT} \tag{16}$$

Geometrically, the corresponding maximum groove depth is given as:

$$h = r - R + 0.5 \times (\sqrt{(4 \times R^2 - W^2)} - \sqrt{(4 \times r^2 - W^2)}) \tag{17}$$

From the relations, it can be derived that if the width of the groove remains less or equal to the diameter of the tooljoint, higher pressure of contact force (lower contact area) is feasible for a lower maximum groove depth value. If the groove width is higher the TJ diameter, CPT will never be reached and the groove will keep on deepening.

From the experiments, the contact pressure threshold for the specimen was determined as the specimen reached a maximum groove depth of 0.020 inches in the first 4 hours and did not wear further in the remaining time period.

Using the maximum groove depth D, the increase in the groove depth at different time intervals can be determined using the following empirically determined equation (based on experimental data and curve fitting):

$$h = D \times (1 - e^{(-E \times t^F)}) \quad (18)$$

D, E and F are primary curve-fitting parameters. Most wear tests couldn't reach the maximum groove depth within the test time period and the test data was extrapolated to achieve parameters at maximum depth. It was also stated that wear factor as well as contact pressure thresholds for the casing wear must be estimated experimentally as there is no theoretical way to estimate these parameters.

2.2.8. Prediction of casing wear in extended-reach drilling (Gao and Sun, 2010)

Gao and sun proposed a mechanical model to estimate the location and depth of wear based on well depth, trajectory and rotational/sliding properties. Data from drilled wells was utilized for calculations on wear factor and the model accuracy was compared and improved in comparison with the field values.

Gao also used the classic wear efficiency model by Archard (1980) as basis and termed the total work done on metal removal per energy dissipated in the casing during casing-TJ contact as the wear efficiency η, defined as:

$$V = \frac{\eta}{H_b} \int \mu N L \, dl = f_w \int \mu N L \, dl \quad (19)$$

Here,

V is the Wear volume, m^3

H_b is the Brinell Hardness, N/m^2

f_w is the wear factor, $pascal^{-1}$

N is the contact force, N/m

L is the total rotational distance, meters

μ is the friction coefficient

Based on the wear geometry, he also proposed the formula for wear area estimation:

$$S = 60 \times \pi \times f_w \times \mu \times n \times D_{TJ} \times N \times \frac{L_M}{ROP} \quad (20)$$

Here,

S is the Wear area, m^2

n is the RPM, r/min

D_{TJ} is the TJ Diameter, m

L_M is the drilled depth, meters

The above formula was cumulated to estimate the total wear of all the tooljoints passing through the same position for a depth drilled:

$$S = 60\pi f_{\mathrm{W}} \mu L_{\mathrm{s}} \sin\alpha \sum_{i=1}^{m} \frac{q_i D_{\mathrm{tji}} n_i}{ROP_i} \tag{21}$$

Here,

Ls is the drillpipe length, m

$m = L_m/L_S$

α is tangent section angle, degrees

q_i is the weight of the ith drillpipe per unit length, N/m

For sign convention, he took radius of curvature as positive in the build sections and negative in the drop sections, the axial load was taken as positive in compression and negative in tension, and the contact force was taken as positive when applied on the lower side of the wellbore compared to the high side, where it is taken as negative.

He also provided relations for area and maximum depth of the casing wear groove for three scenarios based on diameters of TJ and casing, weight of DP and TJ eccentricity.

For single crescent groove, the wear area was expressed as:

$$S = {R_{tj}}^2 arcsin\frac{d}{R_{tj}} - {R_{ci}}^2 arcsin\frac{d}{R_{ci}} + d.a_{tj} \tag{22}$$

For a blunt crescent groove formed by another tool joint with a higher diameter, the wear area was expressed as:

$$S = {R_{tj2}}^2 arcsin\frac{d_2}{R_{tj2}} - {R_{ci}}^2 arcsin\frac{d_2}{R_{ci}} + d_2 a_c \tag{23}$$

Here the depth of the groove does not increase as worn area from the second tool joint does not exceed the worn area of the first joint. It rather “blunts” it on the edges, increasing the width of the groove.

For sharp crescent wear groove formed by a second TJ with smaller diameter consequently, the wear depth is increased and the wear area is expressed as:

$$S = {r_{tj}}^2 arcsin\frac{d_2}{r_{tj}} - {R_{tj}}^2 arcsin\frac{d_2}{tj} + d_3(a_1 - a_2) \tag{24}$$

Here,

R_{tj} is the radius of bigger TJ, m

r_{tj} is the radius of smaller TJ, m

d is the half with of the groove formed by respective TJ, m

R_{ci} is the inner radius of casing, m

a_{tj} is the eccentricity of respective TJ, m

a_c is the casing eccentricity, m

2.2.9. Model for Impact force distribution during DS vibrations (Samuel and Kumar, 2014)

The model examined the impact of varying rotary speeds of the bit, leading to dynamic downhole whirl and impacts between drillstring and inner wall of the casing. A linear relationship between the rotational speed, excitation factor and bit frequency was presented as the initial step:

$$f = {}^{(N \text{ x } EF)}/_{60} \tag{25}$$

Here,

f is the bit frequency, cycles/ sec

EF is the excitation factor (3 for tri-cone bits, 8- 12 for PDC bits)

Using Hall equation as the basis, the abrasive wear as a result of DS whirl impacts was modeled. The impact wear volume of the inner casing wall by each impact of the tool joint in integral form of this model is presented in Eq. X.

$$V_{impact} = \int_0^{t_i} \frac{k}{H} \text{ x } \frac{N}{60} \text{ x } \pi \text{ x } D_{ds} \text{x } F(t) dt \tag{26}$$

Here,

V_{impact} is the impact wear volume, in³

k is the abrasive wear coefficient of the casing

H is the hardness of the casing, Pa

D_{ds} is the outer diameter of the drillstring, in

These excitations result in dynamic transverse displacement that is different from the static position of drillstring without vibration. The second step was to determine the impact forces to be used in the wear equation. A mathematical analysis incorporating four different force distribution models was made and it was established that the impact force distribution varies

over the time of impact. The actual downhole impact force $F(t)$ can be a random combination of all the four models:

Parabolic Pattern:

$$F(t) = F_{max}\left[1 - 4\left(\frac{t}{t_i} - 0.5\right)^2\right] \quad (27)$$

Elliptical Pattern:

$$F(t) = F_{max}\sqrt{1 - 4\left(\frac{t}{t_i} - 0.5\right)^2} \quad (28)$$

Cosine (linear direction) Pattern:

$$F(t) = F_{max}\left[1 + cos\left(\frac{2\pi t}{t_i} - \pi\right)\right] \quad (29)$$

Skewed (changing direction) Pattern:

$$F(t) = \frac{F_{max}}{y_{max}}\left[\frac{2}{\omega}\phi\left(\frac{x(t) - \xi}{\omega}\right)\Phi\left(\alpha\left(\frac{x(t) - \xi}{\omega}\right)\right)\right] \quad (30)$$

Here,

F_{max} is the maximum impact force, approximated by DS weight and well trajectory, kips

t_i is the impact time, min

$x(t) = x_{max}\frac{t}{t_i}$ is the displacement on x-axis

y_{max} is the displacement along y-axis

x_{max} is the maximum x-axis value for the chosen skewed function

$\phi(x) = \frac{1}{\sqrt{2\pi}}e^{-\frac{x^2}{2}}$

$\Phi(x) = \frac{1}{2}\left[1 + erf\left(\frac{x}{\sqrt{2}}\right)\right]$

ξ is the location parameter

ω is the scale parameter

α is the shape parameter

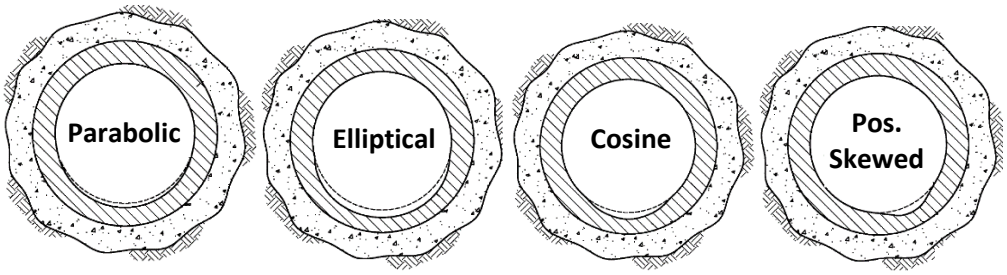

Figure 2. 18 - Impact force distribution patterns [45]

The patterns were then simulated using a case study to estimate the wear volume and depth of groove on a 7", N-80, 226 lb/ft casing string. The results highlighted the elliptical force distribution to induce the largest wear volume and groove depth. In comparison to the static model which showed 2.5% reduction in wall thickness, the elliptical force distribution showed a maximum depth of groove to be 14% of WT. This implied that the remaining casing wall thickness may be overestimated using static models for casing design without considering the impact forces and their patterns.

2.2.10. Case-specific casing wear prediction using stiff-string model (Samuel and Kumar, 2016)

This model from Samuel and Kumar investigated that in real operating scenarios, the overall casing wear is affected by all operations where the DS is passing through the casing, instead of just drilling phase. This model used the casing wear model presented by Hall et al. (1994) as basis and slightly modified it to adapt to five well operations - drilling, back-reaming, off-bottom rotation, sliding and reciprocating.

For drilling or back-reaming, the drill bit operates downwards (drilling) or upwards (back-reaming) the hole from a given measured depth. Therefore, contact points between the TJ and the inner casing wall continuously change as the DS moves along the casing wall. The equation of casing wear volume performed by Hall is modified in this model with the assumption that the inner casing wall is only contacted with the TJ, and there is no pipe-body contact. As a result, the side force and the ratio of Length of TJ and length of DP is calculated to consider this contact solely caused by TJ.

$$WV = W_f \times SF_{tj} \times \pi \times D_{tj} \times RPM \times 60 \times t \times \frac{L_{tj}}{L_p} \tag{31}$$

$$SF_{tj} = SF_{ft} \times \frac{L_p}{L_{tj}} \tag{32}$$

Here,

WV is the wear volume, in³ /ft

W_f is the wear factor, E-10/psi

$D_{tj}$is the tool-joint OD, in.

RPM is the rotary speed of drillstring, rpm

t is the operating time, hrs

$L_{tj}$is the length of TJ, ft

L_p is the length of drillpipe, ft

$SF_{tj}$is the side force acting on the TJ, lbf

$SF_{ft}$is the side force per ft of drillpipe, lbf/ft

Furthermore, the contact point on the inner casing wall as well as the side force varies with the movement of the drillstring. In order to simulate the movement of the drill string, the entire casing string was divided in steps of 30ft and the position of the drill bit is altered every 30ft during the movement from the start depth to the target end depth. As a result, the entire number of the drilling steps is shown as Equation

$$S_{op} = |(MD_{end} - MD_{srt})|/30ft \quad (33)$$

Here,

S_{op} is the number of operation steps

MD_{srt} is the start depth, ft

$MD_{end}$is the end depth, ft

The cumulative wear volume from each drilling step for the whole casing was calculated by equation 34 to acquire total depth of wear groove and the remaining wall. The whole casing string can be further divided into small portions of 10ft in order to increase the precision of casing wear simulation to take into account any tiny wear contact between drillstring and inner casing wall, and to reduce the over prediction of average casing wear.

The drillstring does not move axially during rotating off-bottom operations. The variation in contact position between the TJ and inner casing wall is not considered in this operation, and the ratio of lengths of TJ and drillpipe in Equation X is 1. The modified equation X becomes:

$$WV = W_f \times SF_{tj} \times \pi \times D_{tj} \times RPM \times 60 \times t \quad (34)$$

For sliding case, the drillstring do not rotate so RPM is not taken into the equation. To accurately estimate casing wear, the sliding distance can also be divided to many operational steps 30ft each as in drilling scenario.

$$WV = W_f \times SF_{tj} \times d_{sld} \times 12 \times \frac{L_{tj}}{L_p} \quad (35)$$

$$d_{sld} = MD_{end} - MD_{srt} \quad (36)$$

Here,

d_{sld} is the total sliding distance, ft

The wear caused by drillstring reciprocation is closely related with the reciprocation distance, mentioned in equations 38 and 40. When the distance of reciprocation operation is longer than 30ft, the operational distance can also be segmented into different steps. The wear volume is given by:

$$WV = W_f \times SF_{tj} \times d_{rcp} \times 12 \times \frac{L_{tj}}{L_p} \quad (37)$$

$$d_{rcp} = \sqrt{d_{ax}^2 + d_{rot}^2} \quad (38)$$

$$d_{ax} = L_{stk} \times 12 \quad (39)$$

$$d_{rot} = \pi \times D_{tj} \times RPM \times t_{stk} \quad (40)$$

Here,

$d_{rcp}$is the total reciprocation distance, ft

d_{ax} is the axial distance while reciprocating, in

$d_{rot}$is the rotational distance while reciprocating, in

$L_{stk}$is the stroke length, ft

$t_{stk}$is the stroke time, min

The scenarios were then used to estimate downhole wear for inclined field well trajectories and the results were compared with field wear log measurements. The results predicted slightly higher wear compared to the well logs, which was attributed to ambiguities in model input wear factor parameters and field log calibration. The model, however, provided accurate estimations on wear locations and was able to predict minor wears during non-drilling operations that are normally not-planned in well design phase.

2.2.11. Experimental study on casing wear in highly deviated drilling (Yu and Lian, 2016)

An experimental study to simulate the casing wear was carried out by **Yu and Lian (2016).** The previous researches generally employ the concept of using average contact pressure values and total sliding distance during the drilling period. Since the contact pressure is an inverse function of the contact area, these assumptions on average contact pressure may not be fully accurate. Therefore, a numerical study was made using experimental results and their usage in finite element models. The experimental study involved two stages:

(a) In the first stage, a P110 casing ring specimen (OD= 54mm, ID = 38 mm) was worn by a tool joint "pin" (OD of 4.7mm). The normal force between the surfaces was varied and the change in friction moment was recorded. The objective was to determine a validated friction coefficient to use in the numerical simulations for accurate results.

The correlation used to determine the co-efficient of friction is given below.

$$\mu = {}^{M}/_{(F \times r_M)} \tag{41}$$

Here,

M is the friction moment (N-m)

F is the normal force and (N)

r_M is the mean TJ pin radius (m)

From the experimental data, following force and friction moment points were observed and friction moment was calculated to be 0.2087 (from the figures).

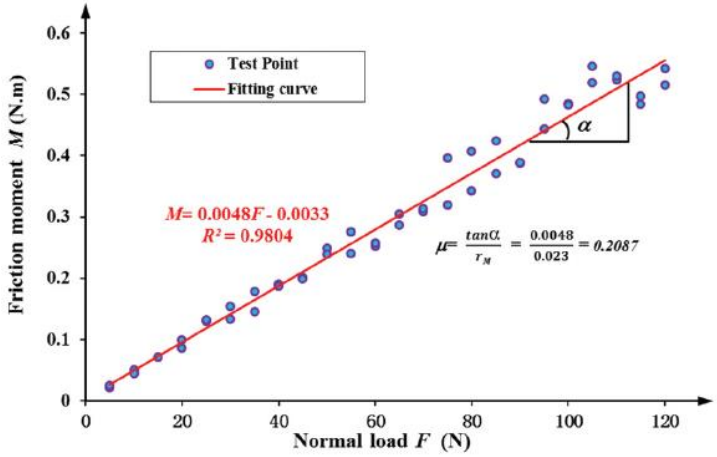

Figure 2. 19 - Determined friction coefficient between the TJ pin and P110 ring [11]

(b) The second stage involved an experimental casing wear to check the validity of numerical simulation results and to estimate casing wear coefficients for calculations. The TJ specimen used

is a S135 ring (OD=168mm, width=5mm) that is pressed and rotated against a square casing plate of 13mm width. A KCl based fluid with 1.02 g/cm³ density is flowing at contact and the contact forces varies from 60N to 120N at a rotational speed of 60rev per minute. The test setup is shown in the figure below.

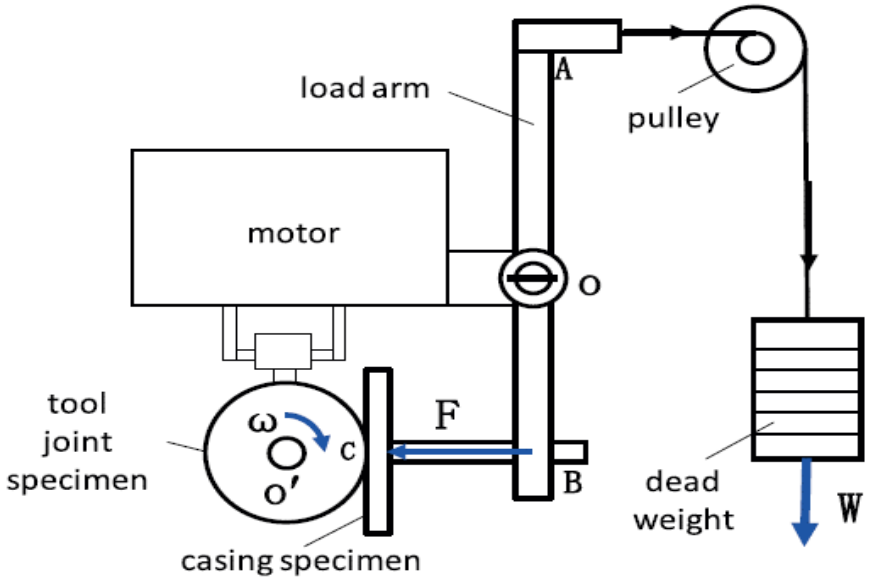

Figure 2. 20 - Casing wear experimental setup after Yu et al. [11]

The base idea is that the work done by friction is divided primarily into the heat consumed by process and the wear in the casing. This defines the wear efficiency as

$$\eta = \frac{U}{W} = \frac{V_w H}{\mu F_N L_S} \tag{42}$$

And the wear coefficient is defined as

$$f = \frac{\eta}{H} = \frac{V_w}{\mu F_N L_S} = \frac{V_w}{W} \tag{43}$$

Here,

V_W is the wear volume (m³)

F_N is the contact force (N)

L_S is the sliding distance (drilling rpm × rotating time) (m)

U is the heat energy consumed by wear process (J)

H is the Brinell hardness of casing (N/m²)

W is the friction work (J)

The wear coefficient f, determined from the above equations and test setup, was found to be 4.4566 x 10^{-7} MPa^{-1} and was applied in the numerical simulations.

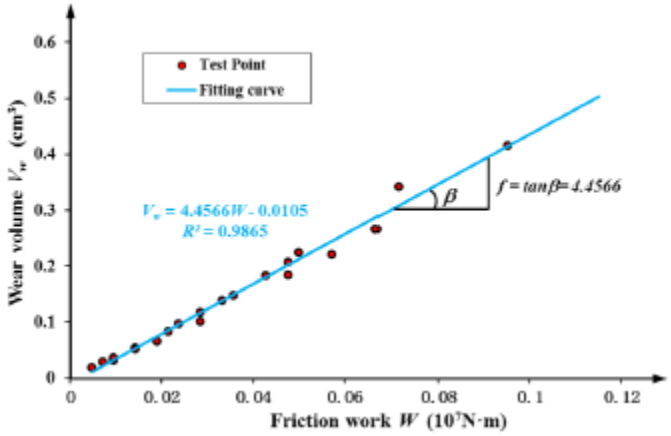

Figure 2. 21 - Wear coefficient based on experimental test values [11]

Since the experimental process involves continuous changes in contact force, time and sliding distance, the contact pressure also changes instantaneously. To simulate the process, the wear process was divided into three processes to be simulated separately and repeated over large number of cycles:

- Determination of contact pressure and sliding distance
- Estimation of wear depth and volume
- Changes in surface geometry at contact points to determine the new contact pressure

Finite element simulations of the above equations with constant μ and f yielded good agreement with test results for V_W for different rotating time values.

2.2.12. Prediction of combined casing wear due to eccentric and drillstring whirl (Gao and Zhou, 2018)

Gao and Zhou presented a composite wear model by combining the circumferential casing wear model (CCWD) and the groove casing wear model (CWGD) for DS whirl scenarios. Since rolling and sliding friction both take place during DS whirl and downward movement, the model assumes total energy dissipated in the casing due to circumferential wear and groove wear, to enhance wear prediction accuracy. The sliding velocity between casing and TJ was simplified to be:

$$v = \left(R_{ci} - R_{tj}\right)\Omega + R_{tj}\omega \tag{44}$$

Here,

Ω is the whirling motion angular velocity, rad/s

Ω is the angular velocity of the rotary table, rad/s

They defined the whirling motion based on the value of Ω, where a positive value was taken as forward whirl, and negative value as backward whirl and zero as no whirl.

They assumed that during vertical drilling, the whirl induces uniform circumferential wear with depth of wear given as:

$$d_w = a + R_{tj} - R_{ci} \tag{45}$$

Here,

d_w is the wear depth, m

a is the TJ eccentricity, m

A is the worn area, m^2

$$\mathrm{a} = -R_{tj} \pm \sqrt{{R_{ci}}^2 + \frac{A}{\pi}} \tag{46}$$

For directional drilling wells, the depths of maximum and minimum wear were defined as per phase angle, as the drillstring rotates and side force is unequally divided due to gravity pull.

$$d_w(\theta) = \mathrm{a} + R_{tj} + \varepsilon.cos\theta - \sqrt{{R_{ci}}^2 - (\varepsilon.sin\theta)^2} \tag{47}$$

Here,

ε is the eccentricity of the whirling motion, m

θ phase angle, deg

The maximum wear is at the bottom with θ equal to 0° and the minimum being at the upper end where θ is 180°.

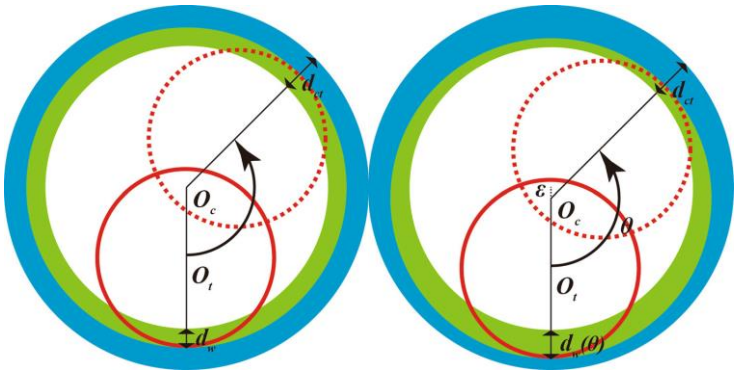

Figure 2. 22 - Whirl wear patterns in vertical and directional drilling [1]

As per the models discussed before, this model also termed the friction factor as the key component defining the wear volume and rate of wear. The equation for total wear was derived by the Hall equation as:

$$V = f_w \int (\mu_s N_d L_s + \delta_r N_d L_r) dl \quad (48)$$

Here,

f_w is the casing wear factor, dimensionless

μ_s is the coefficient for sliding friction

δ_r is the coefficient for rolling friction

L_s is the sliding distance, m

$L_r$is the rolling distance, m

N_d is the contact side force, N

A case study was made to simulate the equations over the entire well depth and wear depths were compared for groove and circumferential wear through a sensitivity analysis by changing parameters such as whirl direction (Ω), speed of rotation, TJ radius, DS weight, sliding coefficient and rolling coefficient.

It was established that whirling angular velocities and friction factors were key to accurate prediction of circumferential and groove wear.

2.3. Casing wear monitoring

2.3.1. Ditch magnets

Ditch magnets are tools specifically designed to catch and remove metal components that are removed as a result of casing-DS interaction and are mixed along with the drilling fluid. The base concept is to trap the metal particles accumulated in the mud that aren't filtered by the surface shakers. The tool is especially viable during milling operations where the debris can cause wear on mud pumps and surface equipment, if not removed. The magnet is normally suspended via soft line in the mud stream at the shaker and is wiped from the metal parts to be reused.

Though the tool can identify the presence of casing wear, it cannot provide any details on the location and nature of the wear. The volume on worn casing attached to the ditch magnets relies chiefly upon the borehole hydraulics such as mud axial velocity in borehole, pump rate and drillstring RPM [16].

Figure 2. 23 - Ditch magnet before and after capture of metal shavings [16]

2.3.2. Multi-finger caliper log

Originally designed to detect corrosion and wall thickness reduction on inner casing/tubing wall, a multi-finger caliper tool provides information on the casing wear such as shape and depth of wear, presence of uniform/groove wear. The tool has a number of equally and angular-oriented fingers that have tungsten carbide tips. The fingers expand until the inner wall of the tubing or casing and the variation in contact angle due to holes, corrosion pits, inner surface defects, distortions and casing wear is detected.

Table 2. 2 - Multi-finger caliper resolution and accuracy [17]

No. / Fingers		Casing Size [in]	Accuracy [in]	Resolution [in]
24	Standard	1.75 – 4.5	0.020	0.0020
	Extended	1.75 – 7.0	0.020	0.0030
40	Standard	3.0 – 7.0	0.020	0.0015
	Extended	3.0 – 10.0	0.025	0.0022
60	Standard	4.5 – 10.0	0.025	0.0030
	Extended	5.0 – 14.0	0.030	0.0050
80	Standard	8.5 – 14.0	0.030	0.0070
	Extended	8.5 – 20.0	0.030	0.0140

Wear marks with width less than the lateral gap between two adjacent expanded fingers on the caliper may go undetected. Plus, the tool does not provide information on wall-thickness reduction and is better to diagnose casing wear in presence of an ultrasonic wall thickness tool. In the absence of wall thickness data, the caliper measurements are adjusted against a baseline caliper log to account for the manufacturing tolerances and separate these from the wear areas. Calipers with different number of fingers account for different resolution and accuracy (Table 2.2). The accuracy and resolution both normally reduce with lower pipe diameter and number of arms [17]. A diagram of a typical multi-finger caliper tool is presented in Figure 2.24.

Figure 2. 24 - Multi-finger caliper tool [32]

Many operators rely on multi-finger caliper measurements for validation on model results. As the bit advances further, the collective work done along the new section is compared to the metal recovered on the surface and is then modeled to generate a groove profile on the lower side of the wellbore. The groove profile is then compared with caliper log values.

2.3.3. Magnetic thickness detector

A magnetic thickness detector provides a measure of wall thickness as information on casing wear. The transducer emits magnetic waves and the difference in velocity and amplitude is recorded. As mentioned earlier, the combination of magnetic thickness tool (MTT) and a multi-finger caliper can provide a comprehensive insight on the location of wear, an impression on if the wear is external or internal, and the shape and nature of wear. 3D images can be plotted on computer and enhanced to review depth-oriented visuals on locations and conditions of casing wear.

Figure 2. 25 - Magnetic Thickness Tool (MTT) for detection of variations in pipe thickness [18]

2.3.4. Ultrasonic imager tool

The ultrasonic imager utilizes a transducer on a rotating tool (to scan the total inner wall), which emanates ultrasonic signals (200-700 kHz) and measures the thickness of the casing as well as cement quality as disruptions in travel time of the sound waves at the signal receiving unit. Since the positioning of the log is important in wellbore for accuracy, the imager is often mounted with

centralizers in directional wells to keep the tool centrally positioned in the casing. Based on tool response, following parameters are measured:

- Signal travel time provides data for internal radius.
- Signal amplitude provides data for the condition of the cement
- Resonance frequency provides the casing thickness data.
- Resonance decay provides the cement resistance data.

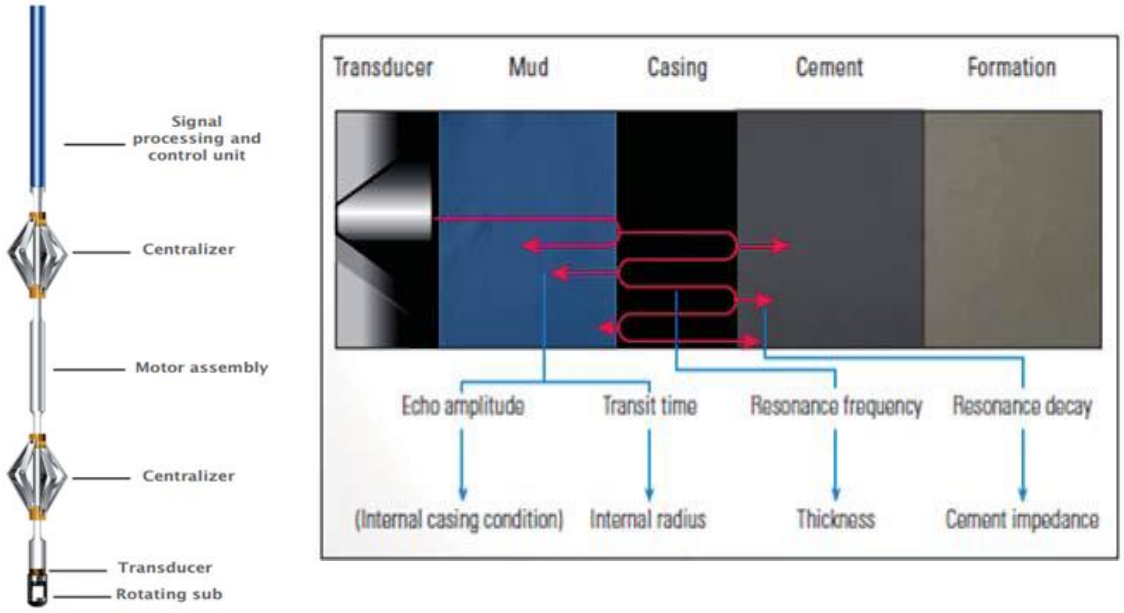

Figure 2. 26 - Ultrasonic imaging tool for measuring inner wall thickness [19]

2.4. Effect of wear on casing collapse strength reduction

Field casing collapse due to drilling-induced wear is not a frequent phenomenon but there have been reported cases where worn joints in conductor pipes have collapsed during welding operations on the wellhead. [28] Using the formulas in the API 5C3 bulletin on estimation of collapse pressure, we can roughly evaluate the collapse pressure of the casing based on its yield strength.

$$P_{YP} = 2Y_P \left[\frac{\left(\frac{D}{t}\right) - 1}{\left(\frac{D}{t}\right)^2} \right] \tag{49}$$

Y_P – yield strength, MPa

The formula is derived from the Lame Equation, based on the yield at the inner wall of the casing. It does not represent the true collapse pressure but rather the external pressure P_{YP} that reaches

the material yield strength just before the collapse instability. The plastic region of collapse is higher than the yield collapse and can be estimated by a similar formula:

$$P_P = 2Y_P \left[\frac{A}{\left(\frac{D}{t}\right)} - B\right] - C \qquad (50)$$

These equations have been derived empirically from test results test on K-55, N-80 and P-110. A, B and C are empirical coefficients depending upon material grade.

During the course of this study, test data from 30 collapse test specimens was averaged to establish a relation between collapse pressure and pipe D/T.

Table 2. 3 - Test data used for calculations

Grade	Nominal OD [mm]	Wall thickness [mm]	OD/t	Avg. Test Col. Pressure [MPa]	Nominal Collapse Pressure [MPa]	Avg. Test Residual Stress [MPa]	Avg. Test Yield [MPa]	Theoritical Yield [MPa]
110	139,7	10,54	13,3	138.4	111.83	150,5	977	830
110	273,1	20,24	13,5	126.4	97.2	60,9	906	830
110	273,1	15,11	18,1	74.0	65.8	81,0	876	830

Using equations 49 and 50, the relation is plotted in Figure 2.27.

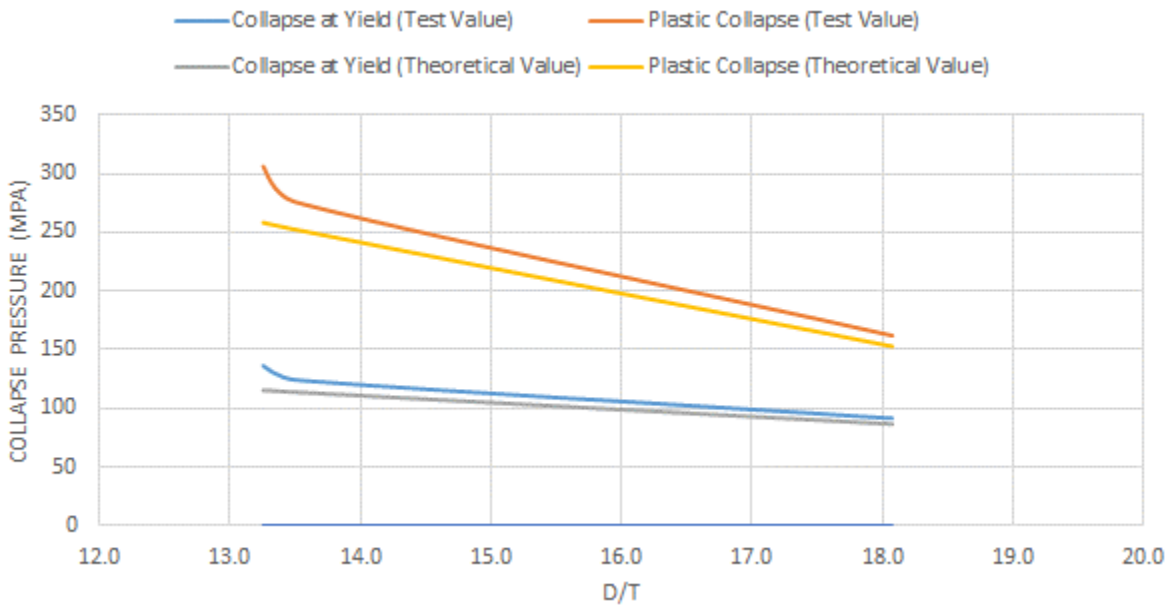

Figure 2. 27 - Collapse strength with D/T ratio of casing tubes

The collapse pressure decreases as wall thickness reduces. The parameter t/tmin is an equivalent to decreasing minimum wall thickness of the casing. The API formula and actual tested line has an approximately 8% difference.

To analyze the effect of wall reduction on collapse, Tamano's model (1983) was used on the pipe data. For unworn casings, the model provides similar results as the API formula but takes into account parameters such as pipe ovality, eccentricity and residual stress. The model can be simplified with the following equations.

$$\frac{P_{yw}}{P_{YP}} = k = \frac{P_{tw}}{P_t} \tag{51}$$

Here,

P_{tw} is the collapse pressure of worn casing, MPa

P_{yw} is the yield onset pressure of worn tube, MPa

k is the ratio of unworn and worn casing

P_t is the collapse strength of actual casing, MPa

P_t can be expressed as:

$$P_t = \frac{1}{2}\left[(P_{YP} + P_e) - \sqrt{(P_e - P_{YP}) + 4f.P_{YP}.P_e}\right] \tag{52}$$

P_e is the elastic pressure factor, MPa, given as

$$P_e = \frac{2E}{1-\nu^2}\frac{1}{\left(\frac{D}{t}\right)\left\{\left(\frac{D}{t}\right)-1\right\}^2} \tag{53}$$

f is the imperfections factor and is given as:

$$f = 0.808\upsilon(\%) + 0.00114e(\%) - 0{,}1412\frac{\sigma_r}{\sigma_y} \tag{54}$$

$$P_{yw} = \frac{\sigma_y(a^2 + b^2)[(a^2+b^2-c^2)^2 - 4a^2b^2]}{2b^2[(b^2-c^2)^2 - a^2(a-2c^2)^2]}.\left(\frac{d}{D_i+\delta}\right)^{\left(\frac{\delta}{t}\right)} \tag{55}$$

Here,

$b = D/2$, $a = b - (t_{max} + t_{min})/2$ and $c = (t_{max} - t_{min})/2$

δ is the reduction in thickness, mm

D_i is the inner diameter of casing, mm

Using equations 51 to 55, a rough estimate on the reduction on collapse is seen as:

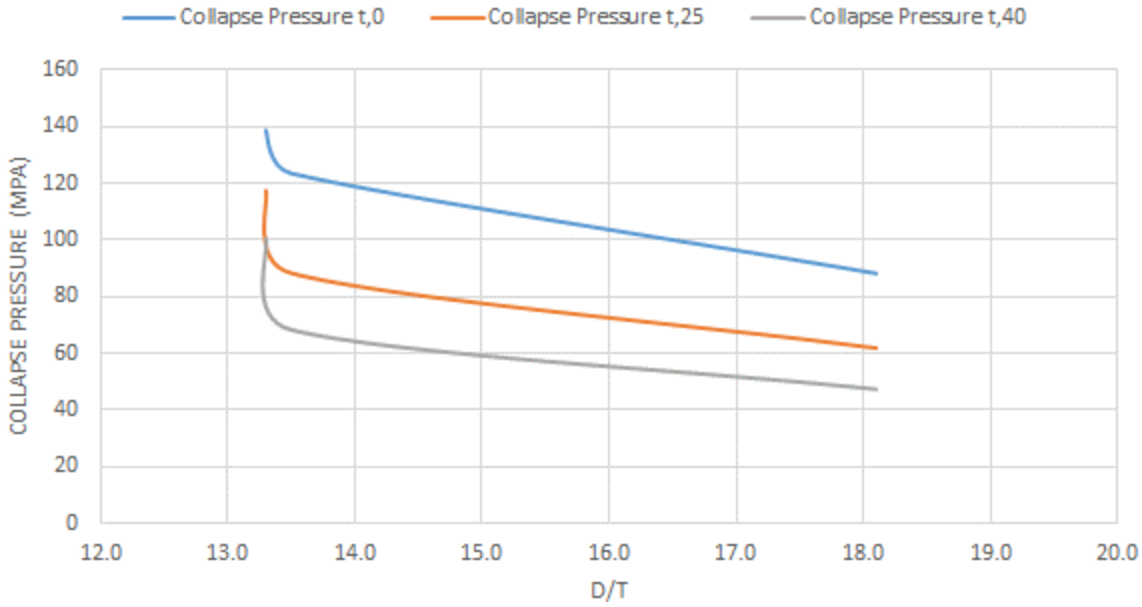

Figure 2. 28 - Collapse strength reduction with casing wear

A plot for the worn casing grade 110 under different D/T is presented with 0%, 25% and 40% WT reduction. Statistically, a 25% WT reduction causes around 16% reduction in collapse strength. The decrement goes up to 30% collapse strength reduction for 40% WT loss.

2.5. Effect of wear on casing burst strength [34]

Similar to the reduction in collapse strength of the casing, its burst strength (capacity to withstand ballooning against internal pressure from fluids) is also reduced, making it prone to expansion from within and additional axial stress (tension). Severe wear can result in leaks in connections and casing pipe failure. Since ballooning of casing is seldom observed on the field, the common approach in predicting burst strength of worn casings is to utilize correlations from API 5C3 on pipe burst strength and make a linear reduction in burst pressure by projecting groove wear as circumferential wear on the total inner wall of casing.

API 5C3 uses Barlow equation to calculate pipe internal pressure capacity (called as internal yield pressure). The formula is given as:

$$P_{burst} = 0.875.\frac{2Y_p t}{D} \tag{56}$$

Here,

D is the outer diameter of casing, mm

t is the thickness of casing, mm

The burst strength is directly dependent upon the pipe material and its thickness. The factor 0.875 is the maximum tolerance for wall thickness deviations from the nominal pipe thickness (12.5%). Compared to the more modern versions of this equation e.g., initial yield burst equation and rupture-burst equation, the API equation provides the least values for burst strength.

$$P_{burst-initial} = 0.875.\frac{2Y_p}{\sqrt{3}}.\frac{2t}{D}\left(1-\frac{t}{D}\right) \quad (57)$$

$$P_{burst-rupture} = 0.875.\frac{2Y_p t}{D-t} \quad (58)$$

Figure 2.29 shows the comparison of three equations with API equation predicting the least burst pressure.

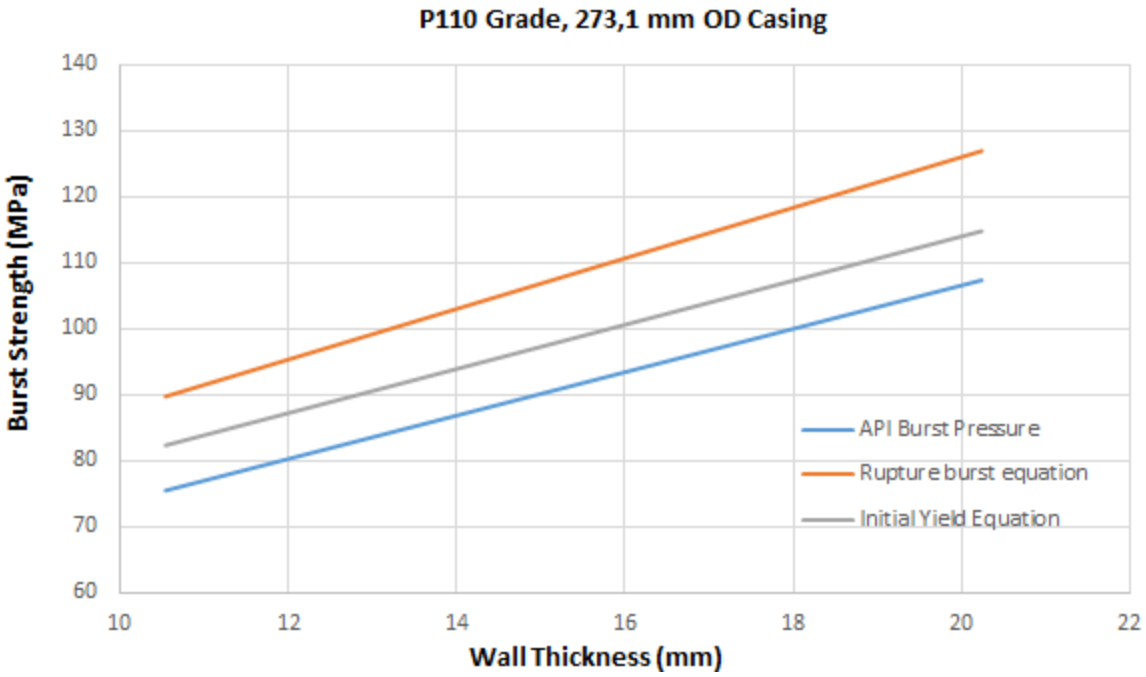

Figure 2. 29 - Burst strength with thickness of casing tubes

With reduced wall-thickness, the applied inner tensile stresses (hoop stress) acts on the remaining wall thickness and increases on the worn section.

$$\Delta\sigma_\theta = \frac{F_{hoop}}{t-w} \quad (59)$$

w is the remaining wall thickness, mm

There is also an additional bending moment that acts on the worn casing due to imbalance in force-moment symmetry, causing further bending and tensile stress. Based on the Wu and Zhang model (2005), the new changed hoop force on the worn groove is given as:

$$F = P_i W + \frac{P_i {r_i}^2 - P_o {r_o}^2}{{r_o}^2 - {r_i}^2}.w + \frac{(P_i - P_o){r_i}^2 {r_o}^2}{{r_o}^2 - {r_i}^2}\frac{w}{r_i(r_i + w)} \quad (60)$$

$$M = \frac{Ft}{2} \quad (61)$$

Here,

F is the hoop force on the worn section, N

P_i is the pipe internal pressure, MPa

r_i and r_o are the internal and external radii, mm

w is the wear thickness, mm

M is the bending moment, N-mm

For comparison purposes, the additional bending moment on the groove is ignored here and the total internal stress is calculated as per the Wu and Zhang model.

$$\sigma_{\theta,w} = \frac{P_i {r_i}^2 - P_o {r_o}^2}{{r_o}^2 - {r_i}^2} + \frac{(P_i - P_o){r_i}^2 {r_o}^2}{{r_o}^2 - {r_i}^2}.\frac{1}{r^2} + \frac{F}{t-w} + \frac{1.95.F.(2r - r_i - r_o - w)}{(t-w)^2} \quad (62)$$

For calculating the initial yield burst strength of the worn casing, the above calculated stress is taken as total internal stress, with casing radial factor taken as:

$$\sigma_{\theta,w}(r = r_i + w) = Y_p \quad (63)$$

Figure 2.30 shows the initial burst strength for worn casing and its comparison to unworn casing burst strength from API (0% tolerance and 12,5% wall tolerance) and initial yield burst equation with uniform wear. The plot shows that for wear up to 20% of thickness, the crescent-worn-burst strength follows the uniform-wear-initial-yield-burst strength equation. The gap widens slightly for higher wear but still stays under the API burst strength tolerance limits of 12.5% on the pipe wall. The API 12.5% tolerance equation with uniform wall reduction can be safely used to plan pipe burst limits without bending and under 20% WT reduction.

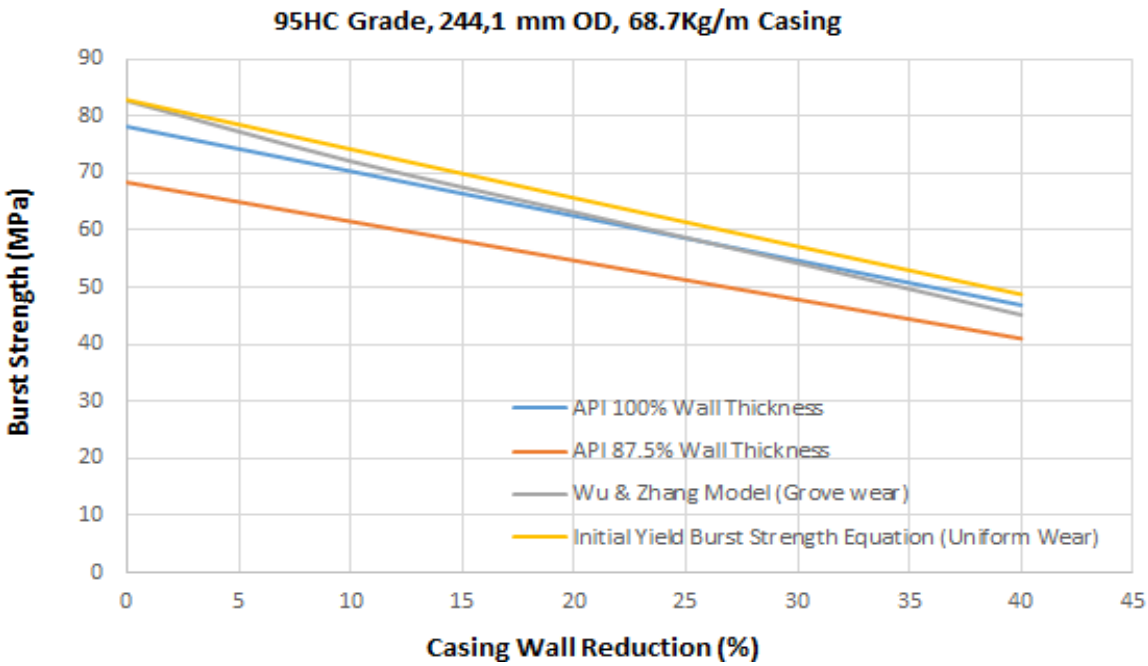

Figure 2. 30 - Burst strength with thickness of casing tubes for different burst equations

3. Critical parameters affecting casing wear and its mitigation

As discussed in Chapter 2, casing wear occurs due to a combined effect of different drilling parameters that vary significantly from well to well. Some models discussed in Chapter 2 use data from caliper log measurements, when available from the field, for validation and accuracy. However, for operations where caliper or ultrasonic log data is not available, the models then pose an inaccuracy concern as many factors influencing the wear behavior change considerably for wells. These factors include well trajectory, DS and casing configurations, operational parameters (RPM, DS tension) and drill fluid properties. Each of these factors affects friction and wear during casing-TJ contact to a major or minor extent. These parameters and their effect on wear rate is individually discussed in this chapter.

3.1. Trajectory- Abrupt dogleg severities and tortuosities

Every directional well has a series of curved arcs from the kick-off point termed as doglegs. Though doglegs are a necessity for drilling directionally, unintended doglegs are a part of every directional well. The effect of these unplanned doglegs defines parameters of apparent and actual dogleg severities expressed after Hall et al. [25] as:

$$(DLS)_{i,j,app} = {}^{30}/_{L_{i,j}}\, \Delta\phi_{i,j} \tag{64}$$

Here,

$L_{i,j}$ is the measured depth, m

$(DLS)_{i,j,app}$ is the apparent dogleg severity, °/30m

$\Delta\phi_{i,j}$ is the angle change from survey point i to j

If the change of DLS is observed over an interval length shorter than at planned MD, the ratio of planned and actual interval MD can be used to determine actual DLS.

For example, if $(DLS)_{i,j,a}$ = 4°/30m, $L_{i,j}$= 30m and the DLS changes after 15m, then:

$interval\ factor = {}^{30m}/_{15m} = 2$, and the actual DLS is

$$(DLS)_{i,j,real} = {}^{4^\circ}/_{30m}\, x\ 2 = {}^{8^\circ}/_{30m} \tag{65}$$

Since actual DLS can only be known after logging the well, the calculation of the side force and casing wear is based upon planned DLS. Based on the above calculations, the real unintended dogleg is always higher than the apparent one. Therefore, side force calculated from apparent dogleg will under predict the wear. An example of the linear relationship between DLS and wear volume is given in Figure 3.2. For comparison purposes, the wear volume is mentioned in field

units. Well parameters used for calculations can be found in Appendix.11.1. Wear volume is determined from the equations from Hall and Malloy (section 2.2.7) for a sample case study.

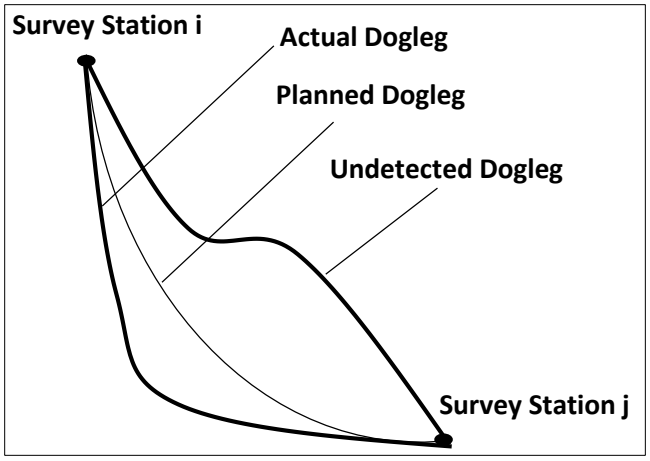

Figure 3. 1 - Apparent, actual and undetected doglegs

A problem arises when abrupt doglegs between measuring stations go undetected and cause wear as the DP is pressed on the tight spots.

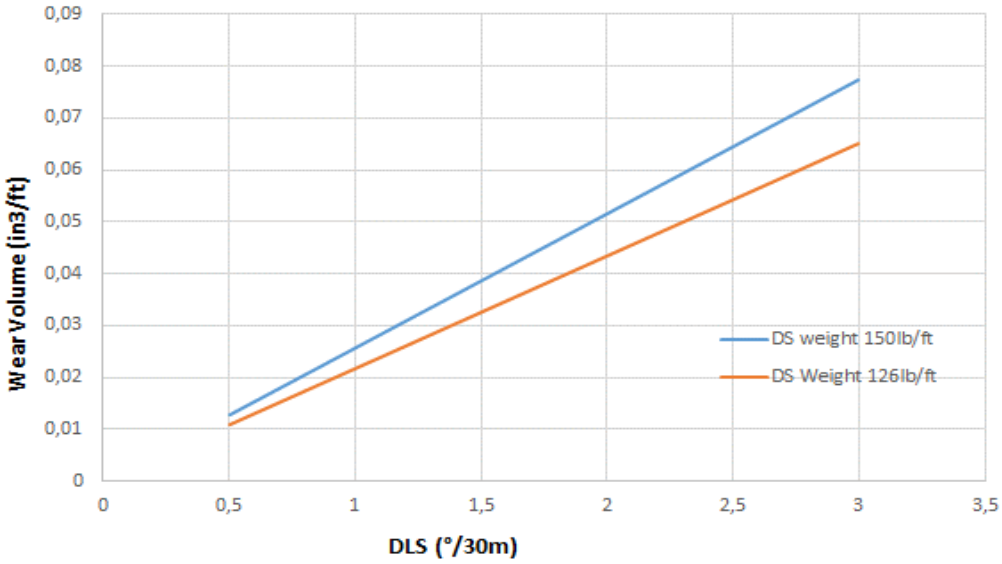

Figure 3. 2 - Casing wear volume with increasing doglegs

A tense drillstring will cause rapid wear in the undetected dogleg in Figure 3.1 on the high side on build section and on the low side for the drop section. Since soft-string models cannot simulate non-linear, multiple grooves at the same depth (e.g., combined wear from TJ and pipe body), it assumes single, deep grooves and over estimates wear in comparison to results from the MFCL afterwards. Similar to this approach, Hall (1994) also suggested using a higher wear factor (up to 4 times the experimental wear factor) to “safely” predict wear in well design with

higher or multiple doglegs. In such wells, the higher side force is also due to more sliding and longer contact between casing and DS.

Even without abrupt doglegs, minor unintended inclinations can occur in wells due to drilling tortuosity where even vertical wellbores can turn slightly spiral if minor inclinations are not immediately corrected. It is important to consider this as during well planning, collapse and burst design accounts for individual points of maximum wear and assumes least casing strength over inclined sections. Though there will be no major issues with torque & drag or running casing, casing wear will occur as the drill string “touches” the spiral casing at occasional points. This can only be corrected real time using rotary steerable systems directly at the bit.

Accumulation of tortuosity in the directional plan requires precise gyro/ MWD survey data taking measurements at short intervals (every 2-5 ft.) and identifying minor tortuous doglegs to establish a statistic back-wear model [35]. This can, in turn, be used to plan wells with similar trajectories to have a more exact orientation of DLS at shorter depths. Most wells, however, do not utilize precise gyro survey techniques, and normal drilling location surveys are taken over longer intervals that cannot identify these short sinusoidal patterns in casing strings. Therefore, the recommendations from Hall of assuming twice or four times the wear factor determined experimentally are still a well-planning practice with many operators.

3.1.1. Analyzing side force with DLS on existing wells using well-planning software

To lay a better understanding of side force and wear variations with DLS and well inclination, well data from 4 drilled wells was simulated with a software (Landmark™ by Halliburton) to predict local side force, wear volume and wall thickness remaining. The two examples mentioned here include a horizontal well and an S-shaped well, labeled as well H1 and S1. Simulations on wear volumes were carried out with a linear wear factor and using stiff-string model.

(a) Horizontal well

The horizontal well H1 was drilled vertically to 3230m and then deviated to reach an inclination of 90° at 4320m MD with an average DLS of 3°/30m. The last cased section is 9 5/8” (L80 and C95) at 2953m with open hole following until the TD. The fluid selected for the horizontal section was 11.18 ppg KCl WBM. Details on drilling parameters, cased sections, operations sequence and applied BHAs is presented in Appendix 11.1. A schematic of the S section is presented in the figure below:

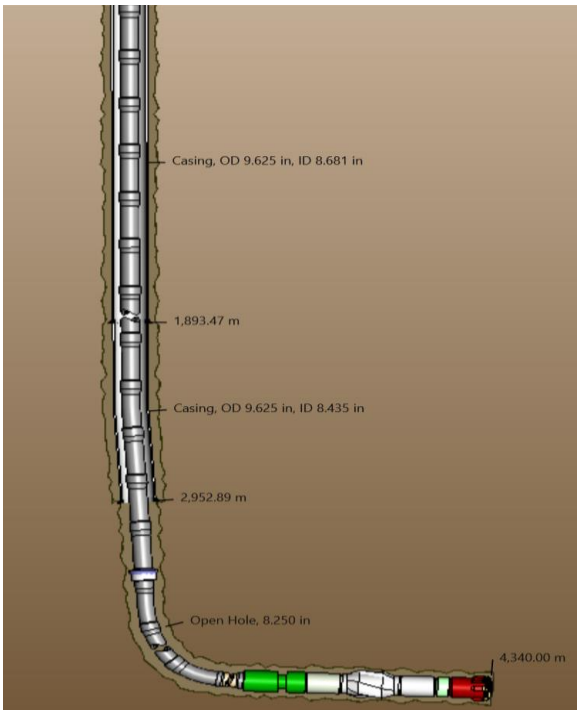

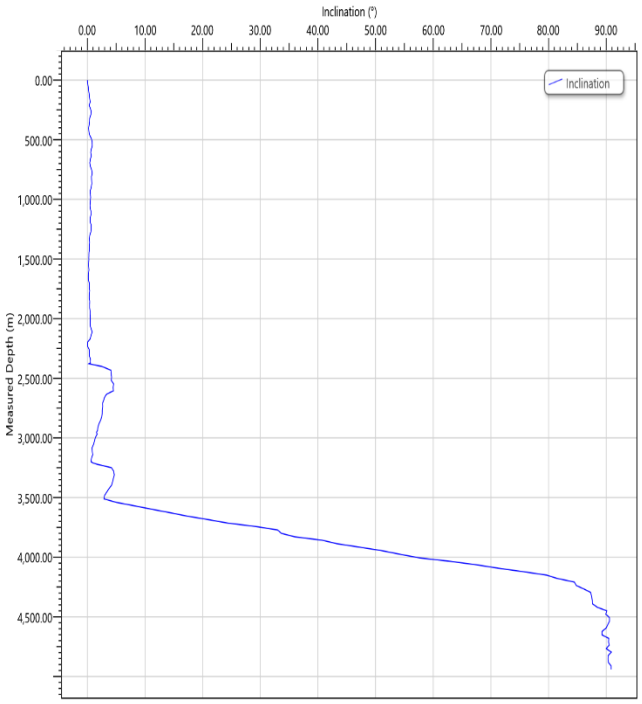

Figure 3. 3 - Horizontal section trajectory and inclination for well H1

During the final drilling phase, peaks of side force of around 4000lbf/length were detected at 2400m due to local compressions against the casing. Other significant increases in contact force can also be noticed at 2600m and 2700m.

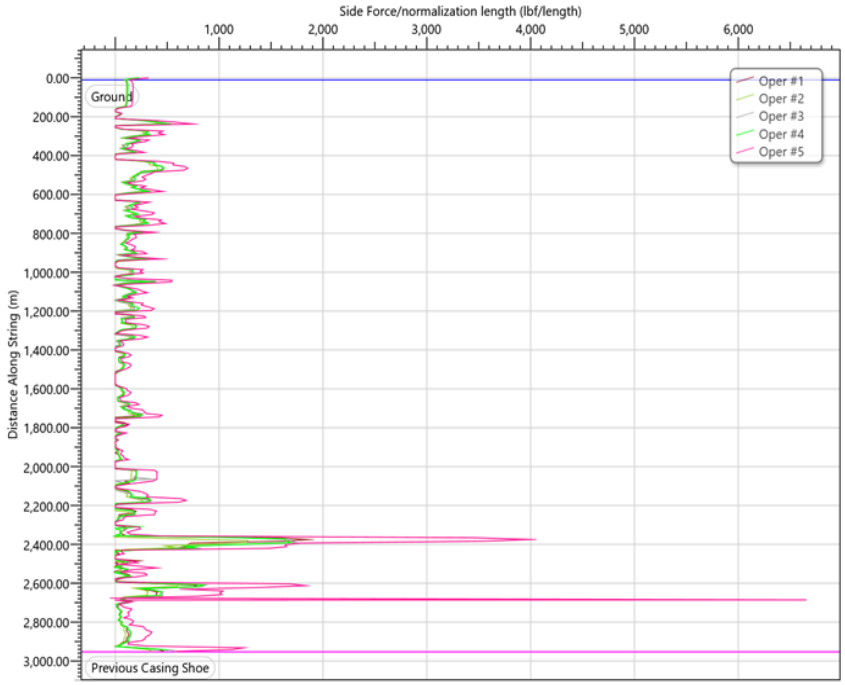

Figure 3. 4 - Side force spikes in 9 5/8" cased section for well H1

The resulting wear volume and remaining wall thickness along with depth is presented in Figure 3.5. Significant wear volume peaks were identified at the locations of high contact stresses. In agreement with the arguments in section 3.1., the wear intensity is observed to be directly and significantly dependent upon inclination and DLS.

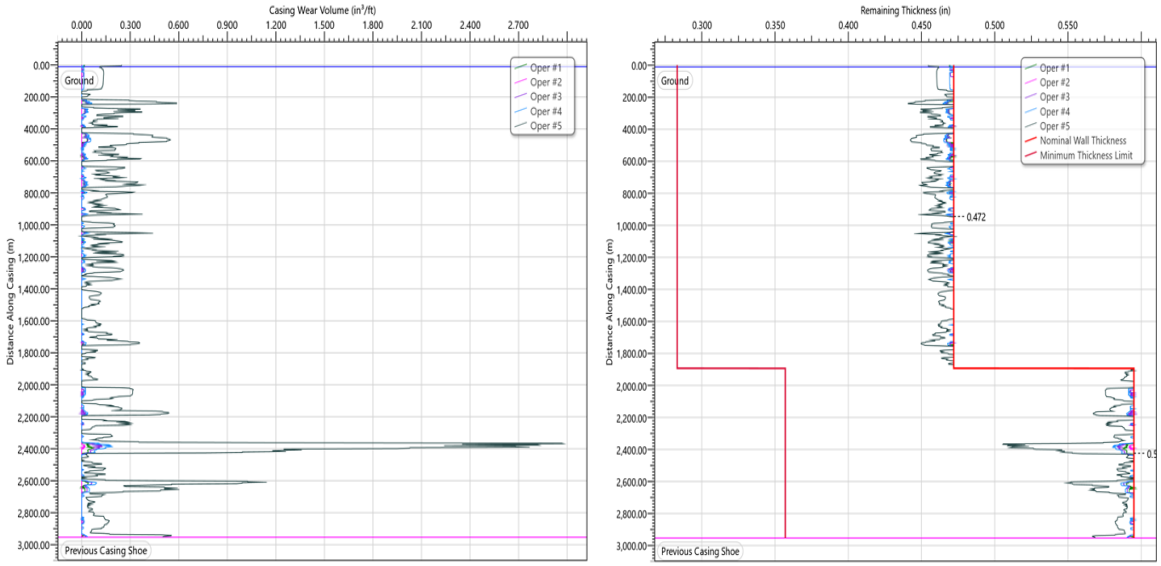

Figure 3. 5 - Wear volume and remaining thickness for the 9 5/8" cased section for well H1

Landmark™ also highlighted the corresponding decrease in collapse and burst pressure as a result of the localized wall thickness reduction. Though still within acceptable domain, pronounced collapse and burst pressure reductions were observed against high-wear sections.

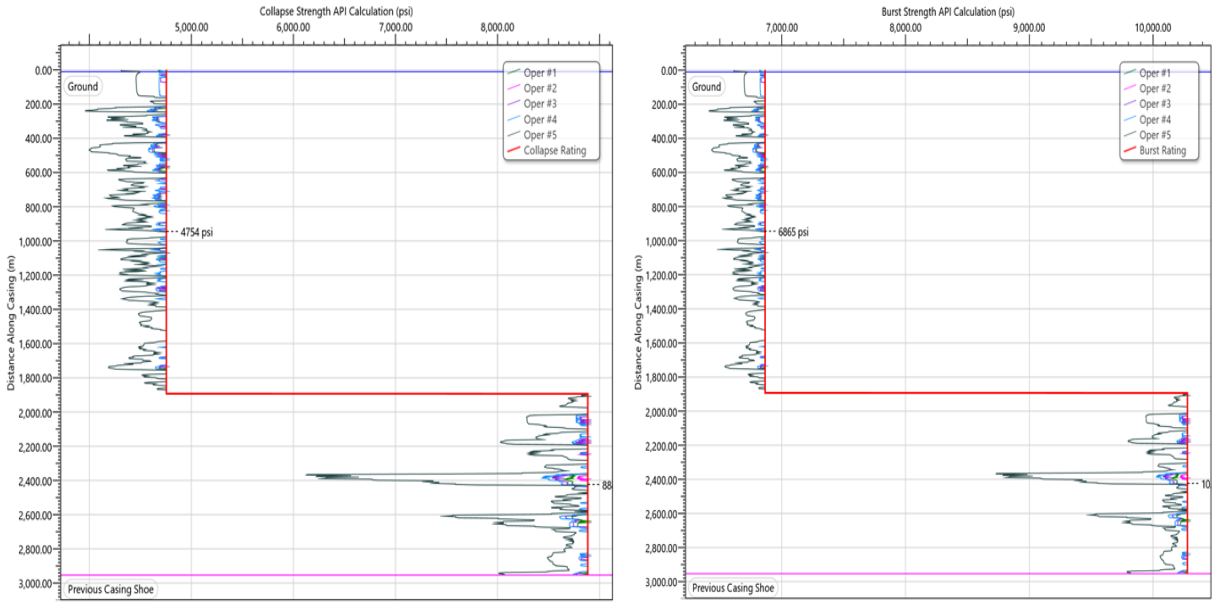

Figure 3. 6 - Reduction in burst and collapse pressures for the 9 5/8" cased section for well H1

(b) S-shaped well

The well S1 was drilled vertically initially until 400m and then directionally with a maximum DLS of 3.2°/30m until reaching an inclination of 25° at 908m. The inclination was held until 2000m following a drop section. The inclined 12 ¼" hole was cased with a 9 5/8" L80 casing until 2681m. This followed a 8 ½" openhole section with the drop back to vertical at 2645m and extending vertically further to 3151m MD. The fluid used for the last section was 10.3 ppg KCl WBM. Details on drilling parameters, cased sections and applied BHAs is presented in Appendix 11.2. The schematic of the S section and well inclination chart is presented below:

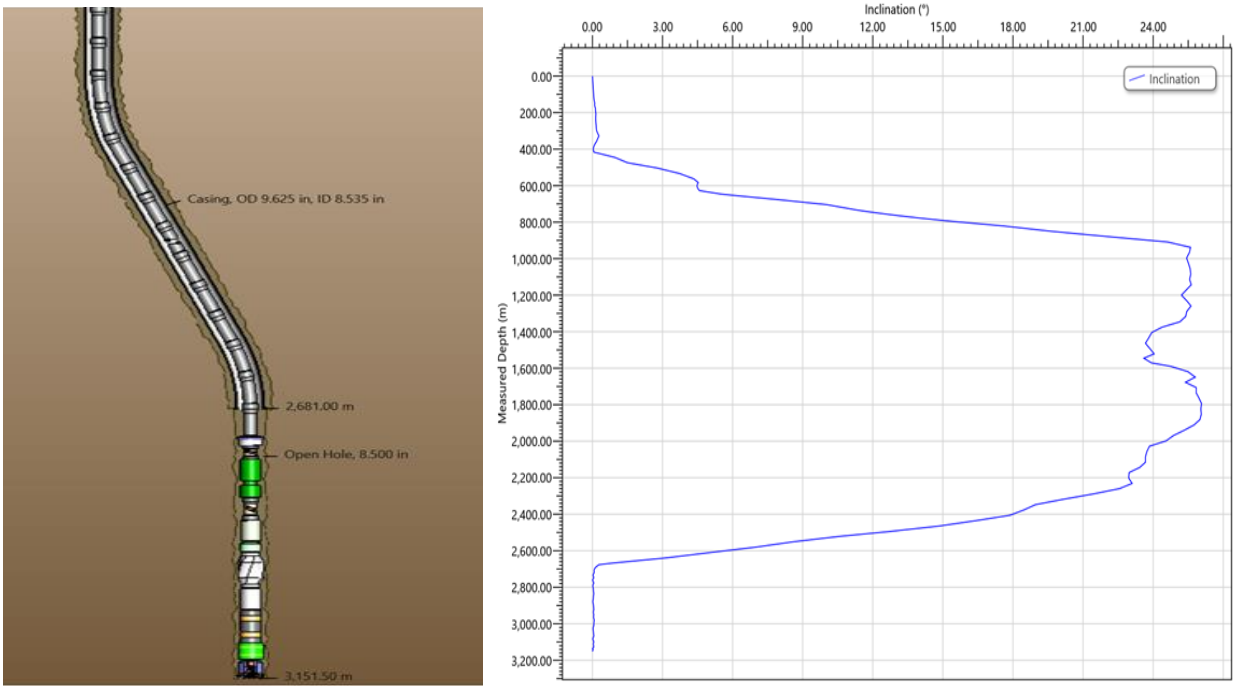

Figure 3. 7 - S section trajectory and inclination for well S1

Some contact force spikes were observed in the upper build section (between 600m and 800m) during both drilling and rotation off bottom operations, though not as high as for the horizontal well. These forces can be attributed to

(1) the DS being pressed against the build section during drilling as high WOB was applied during this phase and

(2) the DS being pulled against the same section under DS weight and additional tension due to frictional drag as the DS is lifted and rotated off the bottom.

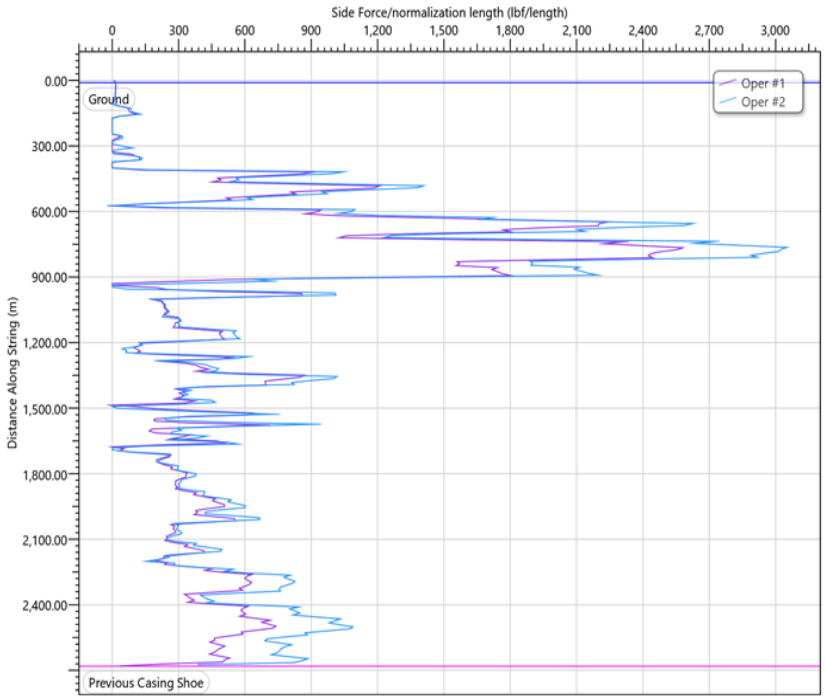

Figure 3. 8 - Side force values in 9 5/8" cased section for well S1

The accumulated wear is also not as high as for the horizontal well. The wear volume and remaining wall thickness along with depth is presented in Figure 3.9.

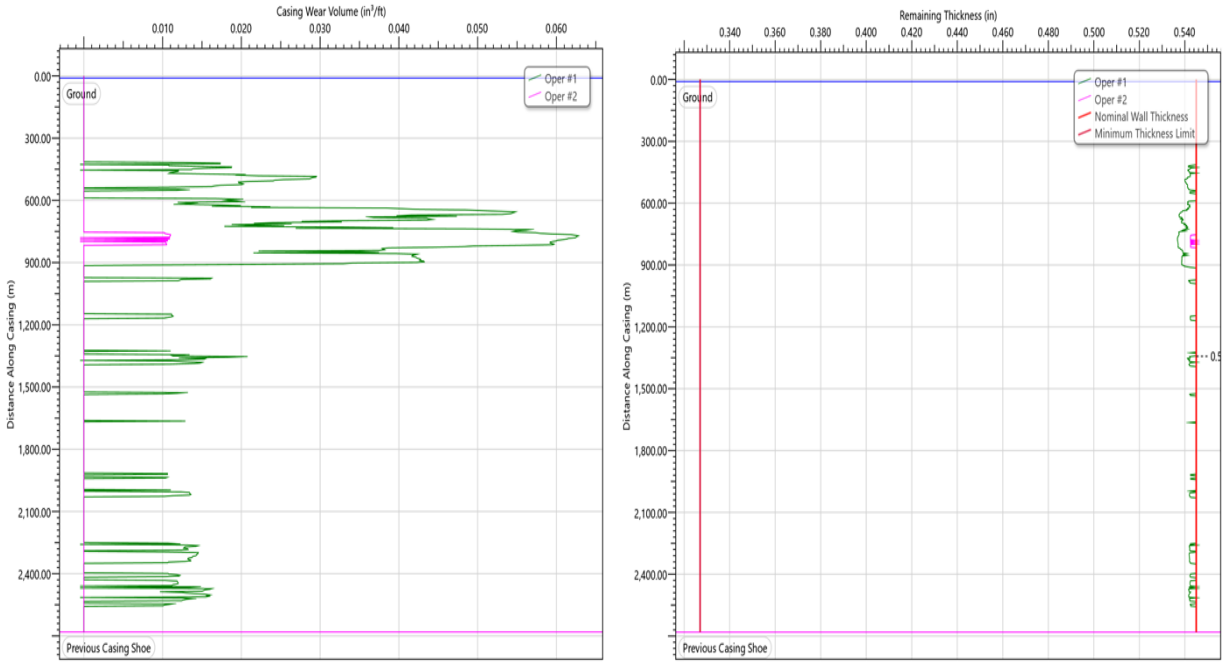

Figure 3. 9 - Wear volume and reduced wall thickness in 9 5/8" cased section for well S1

3.2. Drilling RPM, tripping and reaming

As mentioned in Chapter 2, each operation during drilling phase induces a different rate of wear due to change in surface parameters (RPM, WOB and hook load) and their side force resultant. The friction factor variates complexly from static to sliding, rolling and combined with each operation.

Modified Hall equations for the operations such as reaming, sliding and rotating off-bottom given by Samuel et al. are presented in section 2.2.10. It is important to add these minor wear episodes in the total wear count e.g., if it is a standard practice by an operator to ream the hole after every pipe stand in the inclined section. In the design of the wear frame, it is also intended to simulate a combined scenario of off-bottom rotation (TJ rotation without axial movement) and reaming (TJ rotation with axial movement) to analyze friction factor change in two cases. Also, the type and flow rate for drilling fluid will be an important part of the design of the wear frame.

Modeling of casing wear while well-planning should employ a range of friction factors for DS rotation, sliding or reaming with corresponding wear factor values. While sliding up and down, the friction factor does not change reversibly due to DS geometry, well geometry, trajectory and alteration in contact points. Also, the amount of side force calculated from DS tension in simulations and experimental tests should account for mud buoyancy effect on the DS tension [36].

Surface parameters such as RPM and rotating hours have individually a linear relation with the wear rate as shown in Figure 3.10. The chart is plotted keeping other parameters constant in Hall equation at assumed values, mentioned in Appendix 11.2. This is not the case in practice as other parameters also keep changing and so does the wear factor, affecting the wear volume non-linearly in the combined effect.

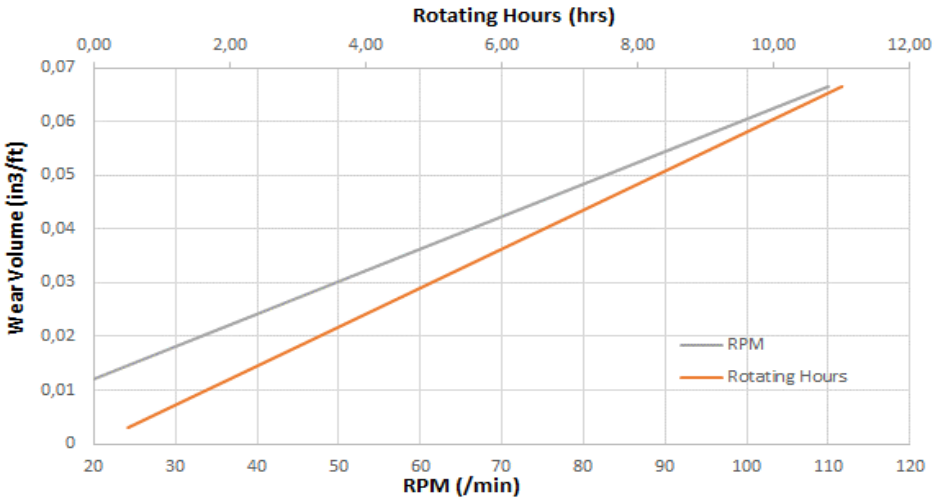

Figure 3. 10 - Casing wear volume with increasing RPM and rotation hours

3.3. Material selections

Steel grades used for casing and TJ significantly influence wear rate as the type of steel and contact surface used in both components defines their tribological behavior and the friction factor upon interaction. The key material properties defining wear resistance of the casing/TJ are the Brinell hardness and surface roughness of the components. Austenitic steels are resilient to cutting and fracture wear due to higher ductility and are also corrosion resistant but are easily deformed by ploughing. Harder martensitic grades guarantee yield strength but fail against cutting wear in abrasive contact (with TJ hardfacing). Another factor that reduces wear is the hardness contrast between the components. Figure 3.11 shows an empirical laboratory analysis on metal interaction with different and similar hardness values.

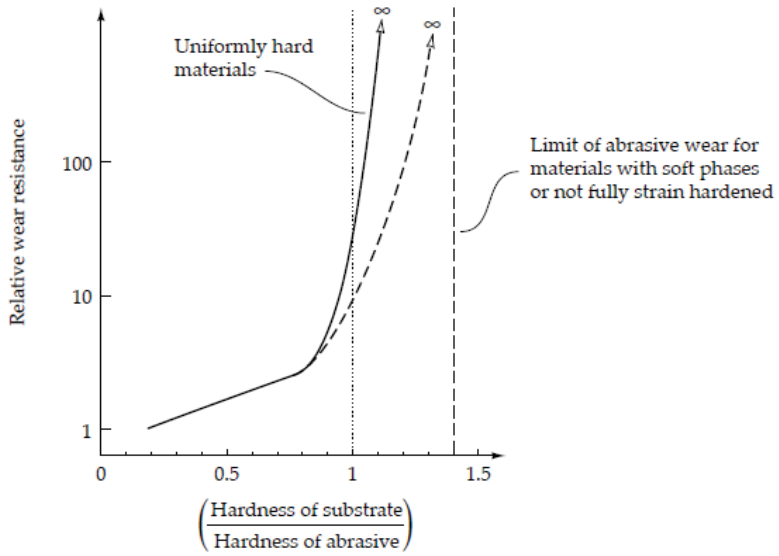

Figure 3. 11 - Metal wear resistance with hardness contrast of contact surfaces [10]

3.3.1. Casing material- Grade and inner surface treatment

Different casing grades have different resistances to TJ wear but high hardness carbon steel grades cannot be always used in wells e.g., for CO_2 environments where 13% chromium grades are used to impart durability against carbonic acids. Also, for corrosion resistance, grades with higher chromium are used that depict poor wear performance owing to their reduced yield strength and susceptibility to ploughing.

A yield strength comparison from material tests for grade Q125 with Q125SS (with 13% Cr) and Q125HY (high yield) is given in Figure 3.12. The sour service (Q125SS) grade has minimum yield strength of 908 MPa, in comparison to the Q125 grade having 986 MPa and the Q125HY grade with 1094 MPa yield strength.

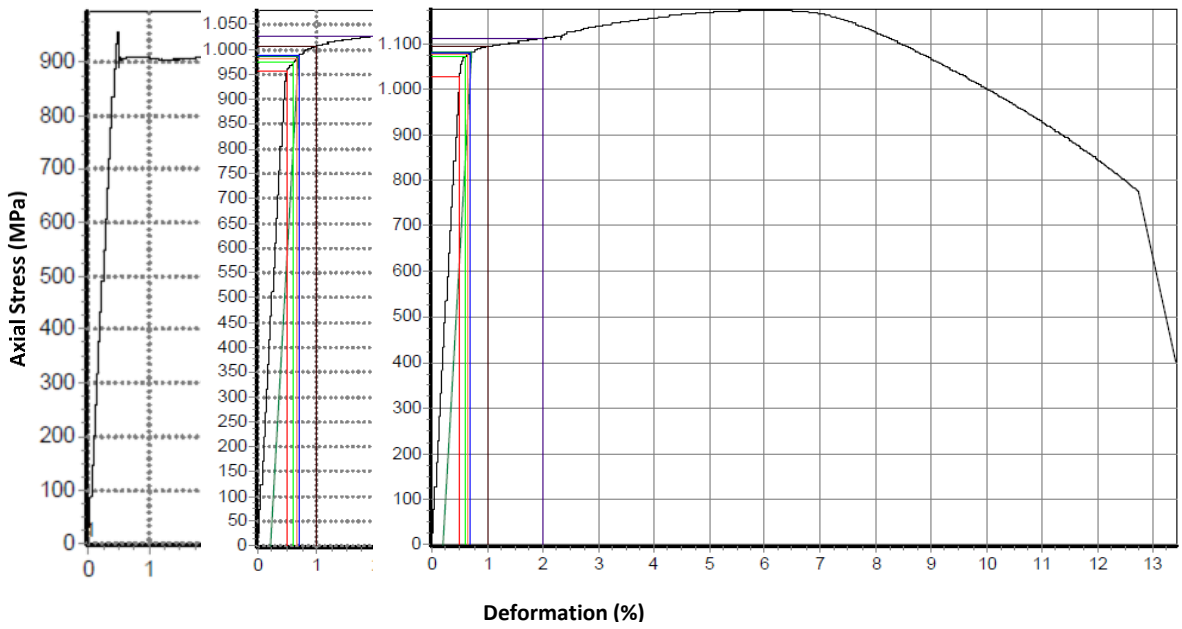

Figure 3. 12 - Yield behavior Q125HY (right), Q125 and Q125SS grades

Based on the experiments conducted by Hall et al. (1994), there is no "low wear" casing grade. High carbon grades have the maximum worn casing strength and resistance to ploughing but are very prone to abrasive cutting wear. Experimental determination of wear factor for casing material is a complex task as the efforts conducted so far haven't been able to correlate specific wear factors for particular casing grades. The same casing grades have shown a variety of wear factors depending upon the operational parameters [37]. For example, the wear factor drops up to 3 times with same casing and tool joint specimen as the inner wall of casing is polished after initial wear and the contact roughness diminished. Additionally, the worn casing strength is also a measure of the residual stress in the pipe which is individual on pipe specimens based on the extrusion process and heat treatment [34]. Experimental work, therefore, is expected to have a range of wear factors with the higher values taken as representatives for safe predictions.

$$\sigma_y = \sqrt{{\sigma_{\theta,w}}^2 + {\sigma_r}^2 + {\sigma_a}^2 - {\sigma_r}^2{\sigma_{\theta,w}}^2 - {\sigma_a}^2{\sigma_{\theta,w}}^2 - {\sigma_r}^2{\sigma_a}^2} \quad (66)$$

Here,

σ_y is the worn pipe burst strength, MPa

$\sigma_{\theta,w}$ is the worn pipe internal stress (hoop stress), MPa

σ_r is the pipe residual stress, MPa

σ_a is the applied axial stress, MPa

3.3.2. Tool joint- Geometry and hard-facing

As in selection of casing material, the wear factor is critical on selection of TJ steel material and its hardfacing. The testing standard for casing friendliness and wear resistance of a TJ is the ASTM G65-A, which recommends selection of TJ based on its own wear, friction factor with casing, stress cracking rate, re-application feasibility, nature of drilling environment and cost.

For around 60 years, tungsten carbide hardfacing has been the norm in the drilling industry. Though crushed tungsten carbide (TC) layer imparts wear resistance on the TJ, it is experimentally found to be severely aggressive to the casing due to its hardness contrast with the casing and its roughness. To avoid severe two-body wear, it is normally preferred to have a finer, rounder TC particle layer as hardfacing where surface micro-faces do not extrude outwards. The modern DPs are welded with platinum and chromium carbides that are more casing friendly and corrosion cracking resistant but require special handling on pipe elevators and more re-applications on pipe for optimum performance (e.g., in case of flaking). A comparison of their wear performances is presented in Figure 3.13.

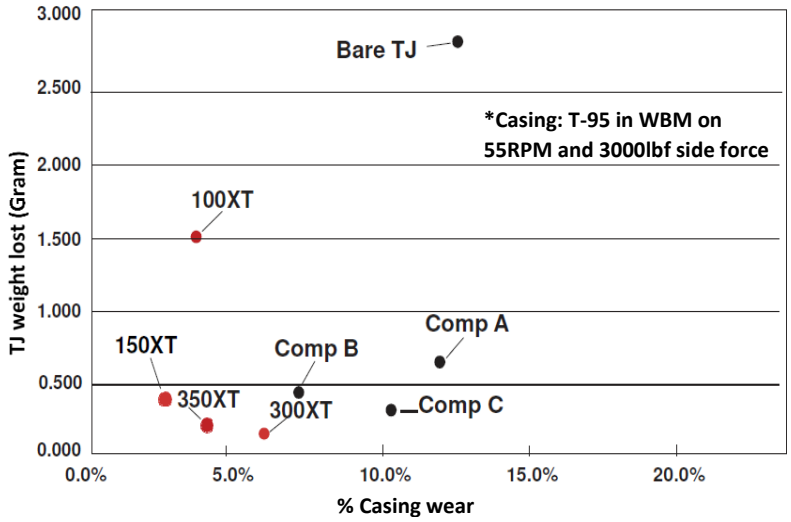

Figure 3. 13 - Wear performance of bare TJ vs. TC (Comp A/C) vs. Chromium Carbides (XT™)[39]

Treating the surface of TJ to reduce friction requires additional polishing treatments that poses an economic choice between the costs of TJ treatment vs. the possibility if the amount of expected wear will be critical to the well.

The diameter and geometry of the TJ also plays an important role as it defines the depth and width of wear, provided side force and wear factor remain constant. Initial rate of wear is always higher then later as the contact area is very low (high friction factors from 0.3 to 0.5) [39]. The friction factor stabilizes as the wear area widens and contact force is distributed. TJ hardfacings are either externally flushed or arched in geometry. Flushed designs provide uniform surface

contact with the casing to minimize wear whereas arched profiles have crescent surface and can cause more wear on casing. A larger contact surface reduces the contact pressure for a given side force, and both parameters keep changing as the wear increases.

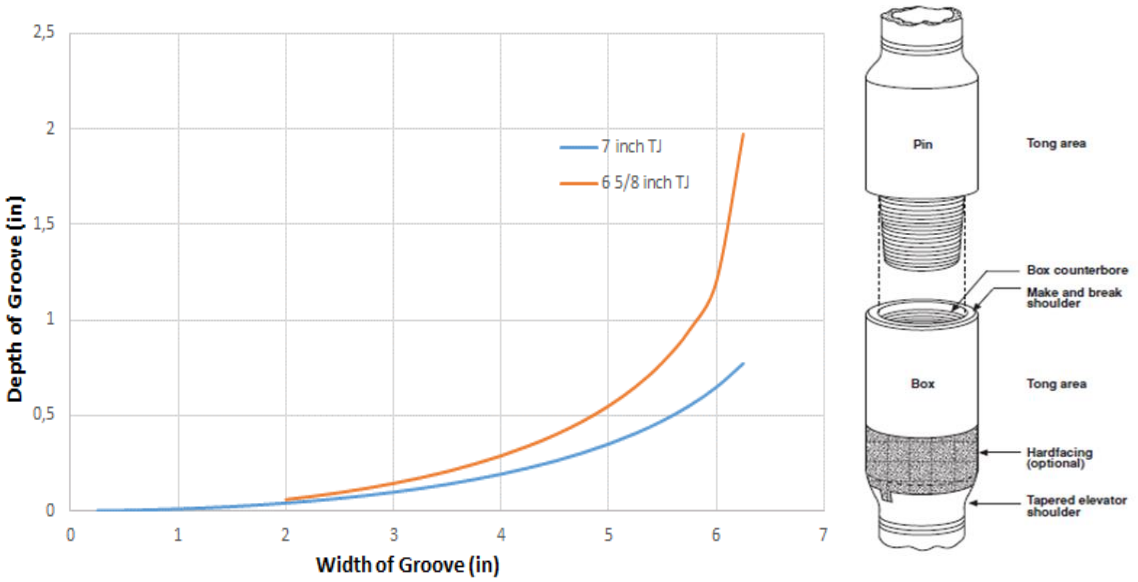

Figure 3. 14 - Increase in wear depth with TJ width and its flushed profile

It is also noticeable from field operations that casing wear is more prominent in upper sections where the ratio of casing to TJ diameter is bigger. When $D_{casing}/D_{tooljoint}$ is lower, bending and buckling tendencies tend to reduce significantly, increasing the contact surface and reducing the contact pressure. Side force calculations should, therefore, also incorporate buckling tendencies in larger OD casing sections.

3.4. Fluid selection

The type, density and solid content of drilling mud is accountable for the shift between adhesive and three-body abrasive wear mechanisms. The choice of Water-based muds (WBMs) vs oil or synthetic muds leads to very different wear factors, so do the additives for weightage, viscosity, emulsification and added lubrication. The wear factors using drill-cutting-solids and mud effluents are the most representative of the wellbore conditions.

A key property in the reduction of friction due to mud lubrication is the attachment of softer particles on the contact surface to reduce galling to three-body wear. This also depends upon the condition of the casing surface as the new mud system is introduced in the contact system. Rough surfaces (lesser initial-wear) undergo higher final-wear compared to polished worn surfaces (higher initial wear).

3.4.1. Choice of water- vs oil-based mud

Water-based muds generally induce higher wear coefficients compared to oil muds, depending upon the mud weight. Lower mud weights fail to form a lubrication layer on the contact and result in severe galling of casing (Friction factor 0.3-0.5). Weighted KCl/Polymer muds show good wear resistance with reduction in friction factor to 0.25. A distribution of FFs with mud weight for barite muds is shown in Figure 3.15.

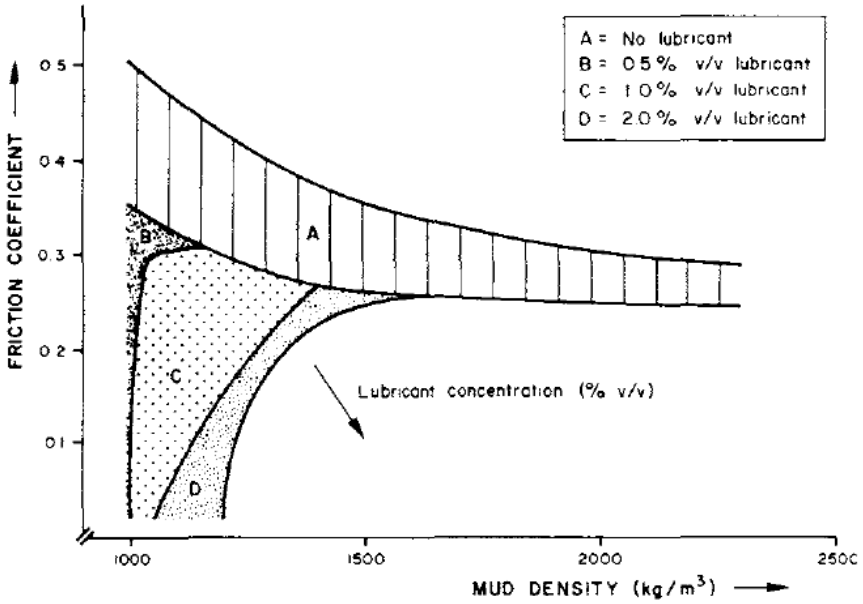

Figure 3. 15 - Friction factor for barite WBMs with increasing density and lubrication [39]

Oil and synthetic mud systems have a better lubrication effect owing to particle slippage and metal dust inhibition. As the metal particles are worn out, they are coated by oil and slipped out of the contact. This is not the case in WBMs where the particles remain smeared on the contact surface and cause further three-body abrasion. They are also more resistant to temperature degradation and retain their precipitation content on the TJ-casing surface in inclined wells. Therefore, the friction factors for OBMs are up to 10 times lower as water-based muds for same contact force and casing/TJ configuration. Invert oil emulsions also show similar results for wear as OBMs (friction factor around 0.15).

3.4.2. Additives and solid content

Increasing the solid content (2-5%) in the mud supports wear resistance as the mud layers between TJ and casing build up and shifts the wear mechanism from metal-metal galling to particle-metal abrasion (three-body). However, higher concentrations/ coarser solid particles in the mud system directly prevent adequate formation of layer and do not affect galling.

Insoluble sand content used in weighting agents has different effects in different concentrations in WBMs. In moderate concentrations (2-5%), it is shown to have a slight negative impact on the wear behavior, causing momentary wear increase on the casing due to three body abrasion. This wear, however, is not intense and is overshadowed in the severe wear influence of barite /bentonite on the mud.

Barite weightage has shown variable wear factors for different weights. Lower densities have shown higher adhesive wear whereas moderate to high densities have shown drastic reductions in wear factors. Barite, however, exhibits lesser FF at higher weights then pure bentonite, quartz and iron oxide muds.

Bentonite weightage is experimentally proven to have adverse effect on casing wear if the particle size is too big to form a lubricant layer between casing and tool joint, or if the contact force is too high to allow the lubrication film to form. Additional lubrication helps in reducing the friction and degree of metal adhesion in lighter mud weights.

Special additives for lubrication, viscosity reduction and fluid-loss decrement show minor and inconstant effects on wear. Polymeric fluid-loss reducers have very little effect on wear. Viscosity reducers (lignites and lignosulfates) show slight wear reduction due to their aggregated layered structure. Additional lubrication with emulsions shows significant reduction in friction when in lower concentrations (<5%) in lighter WBMs (FF~0.1-0.5)[39].

3.5. Formation anomalies

The effect of formation properties such as hardness and penetration strength influence the drilling practice adapted to drill through (WOB, RPM) and this fluctuation in parameters results in peaks in side force. Such peaks are also often associated with DS whirl and stick-slip, which will be discussed in section 3.7. on drillstring problems.

3.5.1. Hard-formations (high WOB)

Hood et al.(2003) discusses that in harder formations such as deep limestones, shales and cherts, the bit is forced into undesired azimuthal and inclinational changes as hookload is reduced. The inclinational changes can be detected above the bit through RSS, but the azimuthal changes create undetected horizontal doglegs that cause unexpected bending. This bending is mostly detected only when the DS starts buckling and whirling [40]. A good practice to eliminate this anomaly is to ream the hole after every stand in harder doglegs.

3.5.2. Anisotropic and Interbedded formations

Interlaying anisotropic formations with varying penetration strength results in WOB fluctuations and undesired steering of DB due to bending moments. As with harder formations, these drill beds might induce doglegs giving rise to wear passages for forthcoming directional sections.

3.6. Effect of mud motors and wirelines

Application of a Moineau motor for performance drilling reduces the number of surface RPM, and keeps the wear rates in the upper doglegs low. However, the necessity to control bending moments due to WOB still persists with motor application. Also the motor imparts a slight shift in the drill bit directions leading to small azimuthal tortuosities that may not fully resolve the micro-dogleg problem in harder formations. This argument, however, is based on a theoretical review and still lacks field validation.

The effect of multiple wireline runs on inclined cased sections is very minor compared to rotary wear by drillstring. On rough estimates, it can be considered to be around 5% of the DS wear provided the mud conditions remain the same.

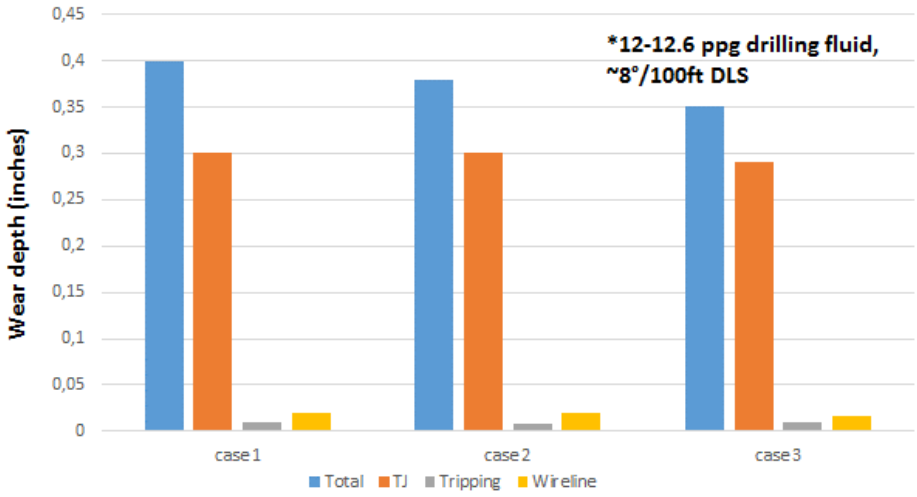

Figure 3. 16 - Wear depth for different operations for three well scenarios [2]

3.7. Drillstring problems

A high wear factor can also result from impacts due to drillstring irregularities such as unintended bending which will then cause the DS to buckle, whirl or undergo stick-slip if the speed or WOB is not reduced. During these abnormal DS movements, if the buckled/vibrating section is inside a cased segment with high $D_{casing}/D_{tooljoint}$ ratio, it will "hammer" the casing at random intervals. The main wear mechanisms in such impacts are galling and fatigue wear due to repeated DS impacts. An individual account of the problems is given below. Other problems such as DS twisting and bit chipping do not have a direct impact on casing wear and are not discussed in the study.

3.7.1. DS bending and buckling

High and sharp doglegs achieved in horizontal applications mean an immediate increase in the axial tension or compression on the convex section of the wellbore. Despite the initial bend in

the pipe in the curved section and the resulting compression, DP rotation under this axial stress results in further bending and serious fatigue and yield issues, especially on the tool joints. As mentioned before, a higher $D_{casing}/D_{tooljoint}$ room gives the DS tendency to have additional bending moment and to buckle in doglegs. The phenomenon is normally encountered in 60° to 90° inclinations due to drilling with high WOB and low RPM. The critical buckling load for a rotating drillpipe is nearly half of that for a non-rotating pipe [40]. Plausibly, DS buckles in the more ductile regions (pipe body) and the stiffer regions (tooljoint) are pressed against the casing.

3.7.2. DS Whirl

Rotation of DS around casing axis in addition to rotation around its own axis results from imbalance of surface parameters (too high WOB or surface RPM). The impact of a whirling DS on the casing wall causes momentous peaks in the side force which are time-dependent. The resulting wear is combination of groove and circumferential wear that interchanges and the impact patterns are random (elliptical, parabolic etc.). The total whirl energy is divided into rolling impact, sliding impact and heat. Based on the random behavior, it is difficult to formulate a direct relation between surface parameters during whirl and the side force on casing. A detailed layout on the dynamic impact patterns and the resulting impact force is mentioned in section 2.2.9 (Samuel) and 2.2.12 (Gao). Integrity of whirl wear in drilling plans are still an uncommon practice due to non-validation of existing models with field data.

3.7.3. Torsional Stick-Slip

The level of torsional vibrations characterized by rotational acceleration and deceleration normally occurs at the bit and impacts the motor performance, if installed. For BHAs without motor, stick-slip accumulation in DS will cause momentous, high-speed episodes on the bottom part of DS as the torsional energy stored in the bit exceeds the friction between bit-face and formation. This is a phenomenon normally encountered in openhole sections and is disastrous for bit and TJ connection integrity. However, if the impact is observed in cased-hole sections, the effect of a drastic increase in RPM will lead to the effect on the wear volume as described in Figure 3.17 (side force and wear factor assumed constant, rotating time for each phase 25 min).

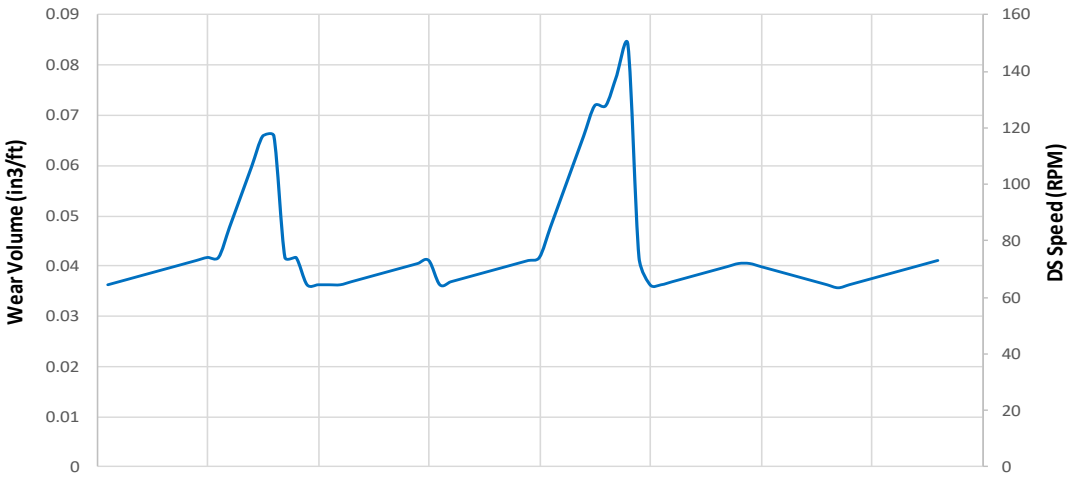

Figure 3. 17 - Linear wear volume to rotating speed relation while stick-slip

3.8. Casing wear mitigation

In addition to using multiple wear factors for DS and casing design, some effective ways to improve wear on field are discussed below.

3.8.1. Operational parameters and practices

The major operational phase causing wear is drilling and off-bottom rotation. Some advisable field practices during these phases include:

- Running new/coarse layered/rougher hardfaced TJs only in the openhole DS sections.
- Conducting a gyro survey post casing run to help efficiently plan wear factors for the next section.
- Utilizing desanders and desilters to keep coarser insoluble solids to a low concentration.

3.8.2. Casing material

For sections where severe wear is unavoidable (e.g., below build sections), hard, high yield casing materials (e.g., Q125, V140) are generally more resistant to adhesive wear in KCl/polymer mud environments for higher barite mud weights. Corrosion resistant alloys are susceptible to severe wear by fresh TJ hardfacing and also compromise more on the remaining strength of worn casing.

3.8.3. DP protectors

Many experimental studies such as DEA-42 have highlighted non-rotating DP rubber protectors (NRDPRP) to bring down the friction factor to up to $1/4^{th}$ of the value without them. Using multiple wear factors for wear estimation on the same drillstring for sections with- and without NRDPRPs is a recommended practice.

The NRDPRP is installed near the TJ and comprises of three base components: A rubber/plastic sleeve or pad with linear or spiral gaps for mud flow, and two light-metal surface bearing collars to allow DP rotation without rotating the pad. Further lubrication is allowed by the mud layer flowing between the pipe and the protector. Such configuration allows NRDPRPs to be used in a wide variety of directional trajectories and to withstand bottomhole temperatures up to 110°C.

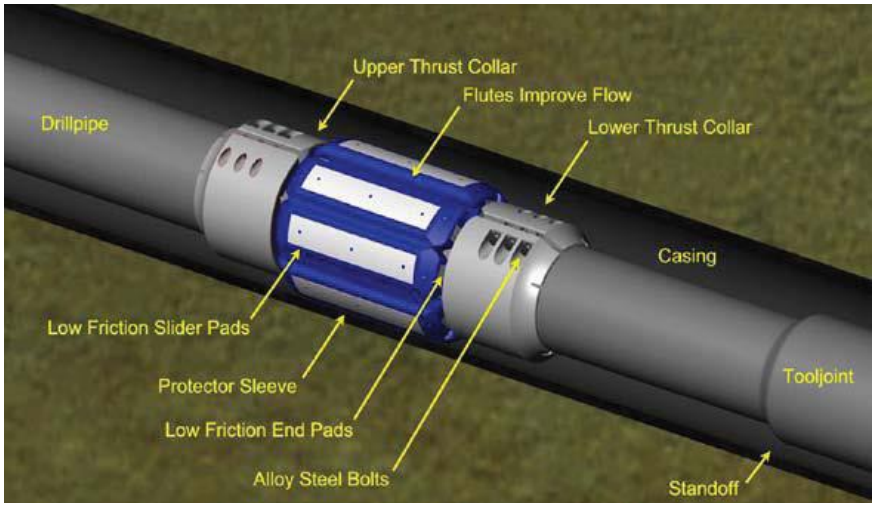

Figure 3. 18 - Schematic of Non-rotating DP protectors and its components [43]

The base mechanism involves the higher OD of the protector minimizing the interaction of TJ with the casing as the DP rotates in the protector sleeve and does not contact casing wall. In addition, it also reduces the $D_{casing}/D_{tooljoint}$ ratio so that DS has less tendency to bend. For quick doglegs, the critical part that faces most wear is the upper collar with the upper part of the pad, which can then be reversed for the next run to enhance tool life.

Excessive side force due to buckling significantly reduces NRDPRP life. Also, the axial slippage along the pipe body when impacted axially on the casing wall is a phenomenon that requires field data to support its use. For sections below sharp build and doglegs higher than 10°/30m, it is advisable to use wear factors without installation of NRDPRPs.

3.8.4. Spray coatings

In addition to NRDPRPs, thermal spray coatings are also pursued as a wear mitigation technique. The base idea is to have a harder, low-friction inner protective layer that resists wear before the tooljoint reaches the inner-laying casing material. Coatings can be characterized in to dry and wet-coatings, with wet (plasma) coatings being the popular method due to ease of coating application (shown in Figure 3.19).

The coating material is generally applied by pre-heating the material (powder or molten) and spraying it on the target surface by a spray gun. The process can be carried out at normal room

conditions and overlapping layers are sprayed to ensure minimum coat-porosity and maximum thickness (subject to required ID).

Even with the ease and low cost of application, thermal coatings provide limited protection to casing inner wall for long slanted sections. For long drilling/contact intervals, the coated material may become thinner and tool joint can still reach the casing metal. This is particular to long off bottom rotation intervals where the tooljoint is rotating at high speed about a fixed depth.

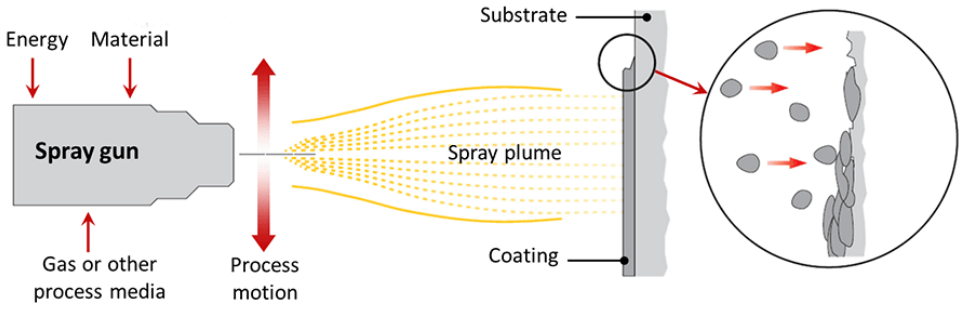

Figure 3. 19 - Plasma spray coating mechanism [58]

3.8.5. Low-friction hardbands

The application of casing-friendly hardbands is usually meant for inclined /build sections where severe wear is anticipated as per contact force. While the classical Tungsten-carbide hardbands were primarily aimed to protect the tool joint, new proprietary materials are focused more on reducing the friction upon contact with the casing. Some examples are Arnco 350XT®, Duraband®NC, Nitronic 60® and Castolin OTW®.

Due to the application of a smoother hard-face (as mentioned in Figure 3.20.), any possible thinning of hardband then follows re-application of hard-face. The process is relatively economic and simple.

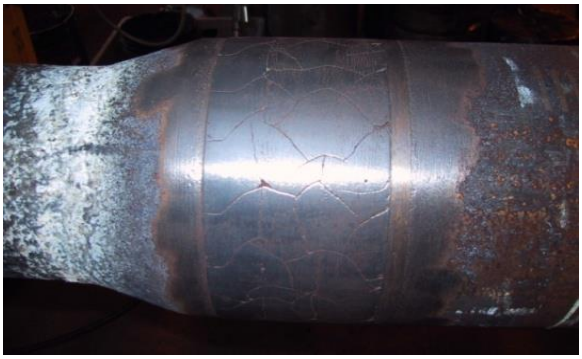

Figure 3. 20 - TJ Hardbanding Arnco 350XT® with a smooth hard-face [38]

4. Selection of wear parameters for experimental setup based on simulations and case histories

To simulate the wear parameters to be used for experimental setup design, a case study was made for a directional well for wear calculations to be compared to the experimental results. The scenario selected for this was a planned horizontal section from a shale gas well for PetroChina in the Wei field in east china. The trajectory profile of the well is provided in Figure 4.1. The target measured depth is 19,685 ft (5965m) with a TVD of 10,341 ft (3152m). The drillstring, drill fluid and casing design parameters are presented in the Appendix 11.5.

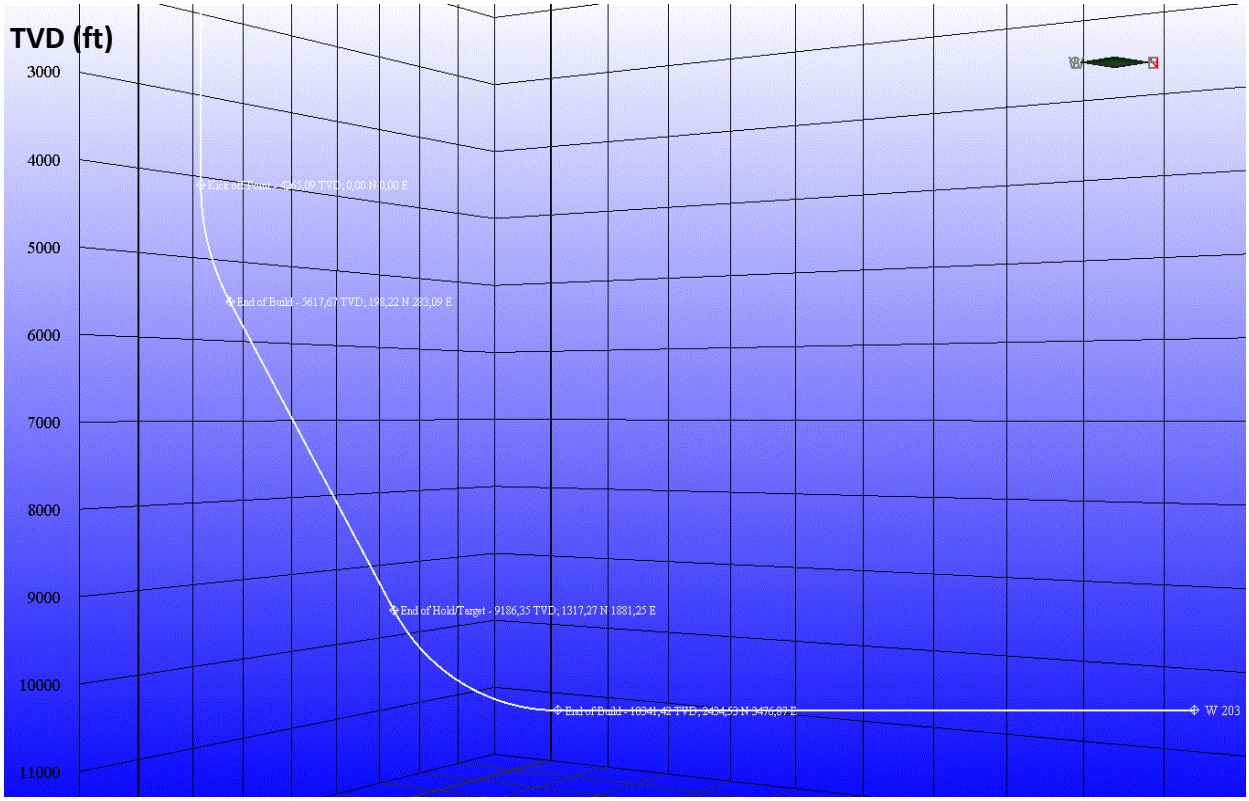

Figure 4. 1 - Well trajectory for the case study (vertical section until 4265ft)

The drilling of horizontal open hole section from casing shoe at the 10,322ft TVD included five different operations including slow surface rotation while drilling with motor, tripping in, tripping out, hole reaming and rotating off bottom. The section depths and surface parameters are presented in Appendix 11.5. The operations showed to induce considerable side force on the cased 9 5/8inch build section. Analyzing the final build until 12,119ft MD, a simulation of both soft-string model and stiff string showed soft string resulting in a higher concentration of side force in the section and on single casing locations. As per literature recommendations, stiff string model was taken as the more accurate and suited for side force determination. The side force variation for both the cases are presented in Figures 4.2. and 4.3. The forces are estimated while

beginning drilling at the next section (drill bit at 12,150 ft). The simulations for side force and well trajectory were done using Sysdrill™ (Emerson E&P).

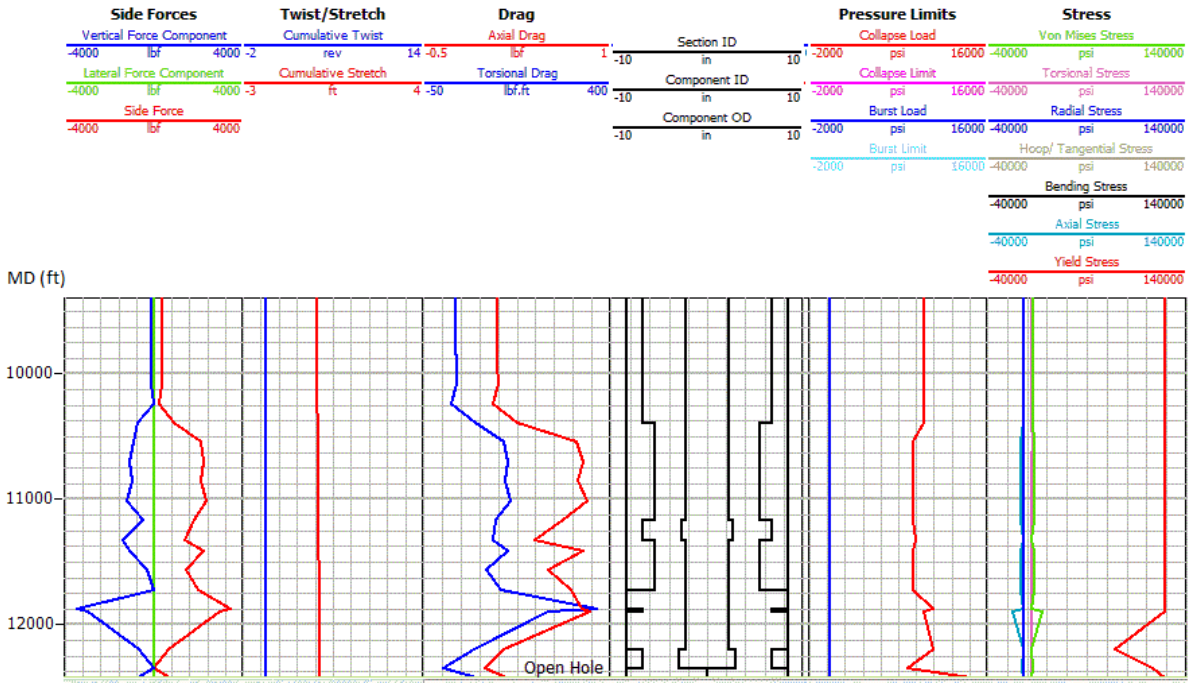

Figure 4. 2 - Side force estimation on the cased liner at 12,170ft MD (Stiff string model)

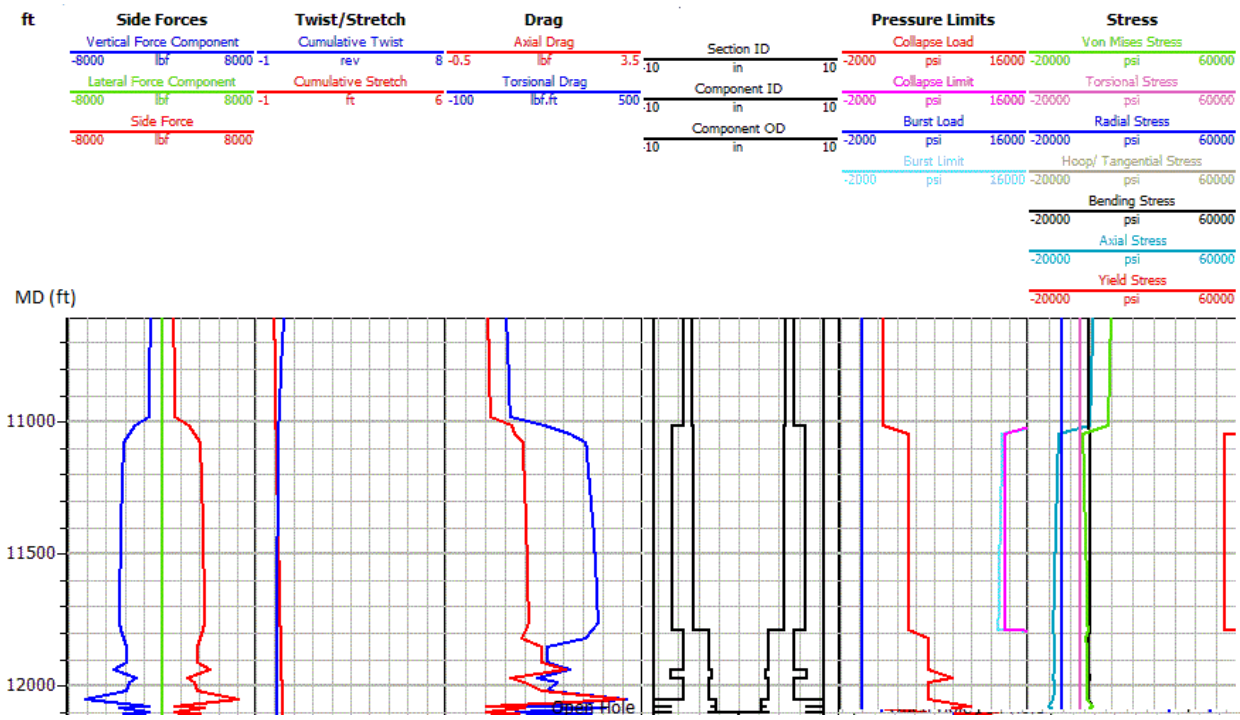

Figure 4. 3 - Side force estimation on the cased liner at 12,170ft MD (Soft string model)

As presented earlier in the Chapter 2, the soft string model approach presented an over-prediction of sideforce (Figure 4.3). High values of sideforce were observed over the entire bottom section of the drillstring, indicating a continuous DS contact with the casing. The estimated sideforce was 3375 lbf (15.5KN) on average with spikes in the BHA section. In comparison, the stiff string model provided regular spikes on side force with an average value of 1125 lbf (5KN). This side force with its occurrence at regular intervals is deemed more realistic in such a drilling scenario.

The combined load analysis (for frictional drag, buckling, tension, compression, collapse, burst) was deemed non-critical for the DP yield strength from the software. Owing to higher temperatures at the target depth (up to 110°C), the maximum tension in the DS during tripping out and rotation operations was calculated due to friction in the horizontal section and the slanted upper well trajectory. No critical values closing the reduced yield strength of the DP (due to temperature) were observed.

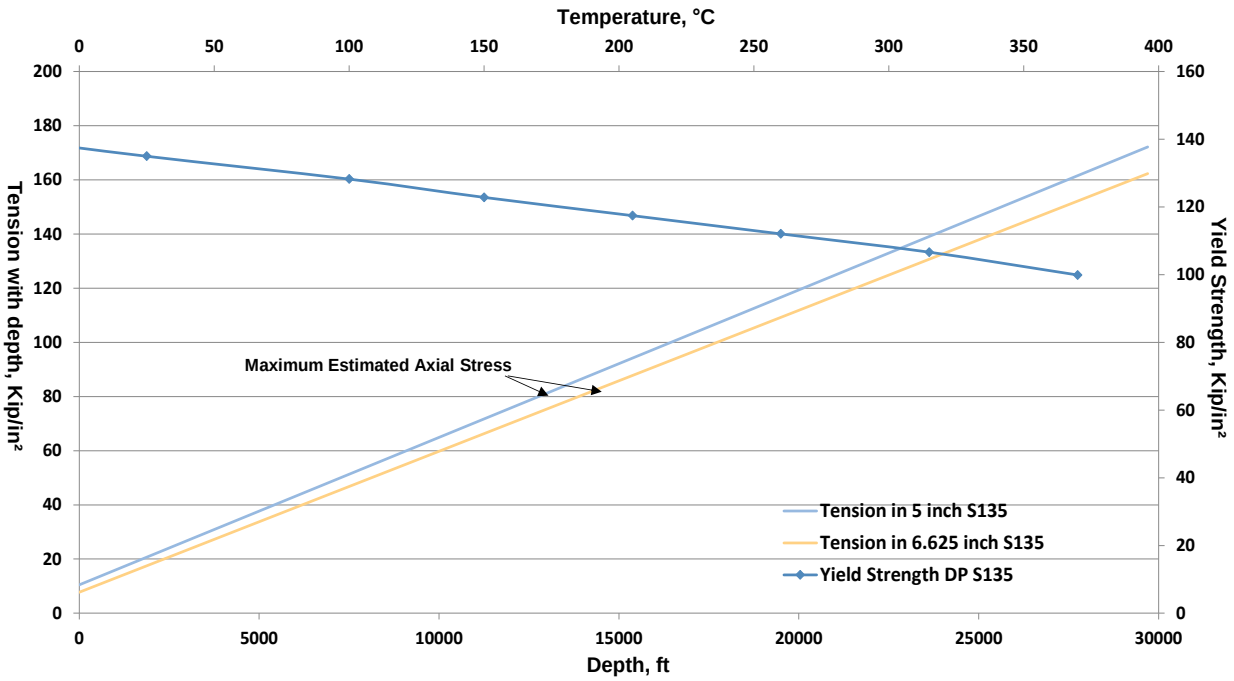

Figure 4. 4 - Maximum axial stress estimation until TD

Some buckling due to compressional push was expected time to time above the BHA in the horizontal section while drilling beyond 16,819 ft but those are ignored in the calculations since the contact points were in openhole. To avoid any critical buckling values, the WOB was kept for all operations to a maximum value of 5klbf.

Based on application of WBM polymer mud and contact between single TJ material of fine TC material with N80 casing, a single wear factor of **1.7E-10**/psi was selected. The selection was

based on experimental values from Hall et al. (1994 and 2005). The maximum experimental conventional wear factor for N80 grade and fine TC tooljoint was found to be 1.7E-10/psi and based on the recommendations from Hall et al. (1994), a conservative $(WF)_{field}$value of three folds $(WF)_{lab}$ value (section 2.2.6) was taken. Lesser values of $(WF)_{field}$ are expected during the actual drilling scenarios.

For determination of wear volume and wall thickness reduction, equations from Hall et al. (2005) and Samuel et al. (2016) from Chapter 2 were used. The wear volume is estimated for the intermediate liner near the casing shoe at 12,119 ft. A breakdown of wear volume as per drilling processes for the production section is provided in Figure 4.5.

In the course of above calculations, the following assumptions have been made:

- The casing wear is calculated as a proportional resultant of the varying side force (mud, drillstring and casing material remains same). The reduction in wear factor after initial rapid wear and the concept of contact pressure threshold have not been applied to this calculation.
- Conversion of friction work into heat and material alteration is not considered.
- A single high $(WF)_{field}$ = 3 x $(WF)_{lab}$ is taken for calculations. Deviations observed at locations of lower side forces while drilling were adjusted with the same wear factor.

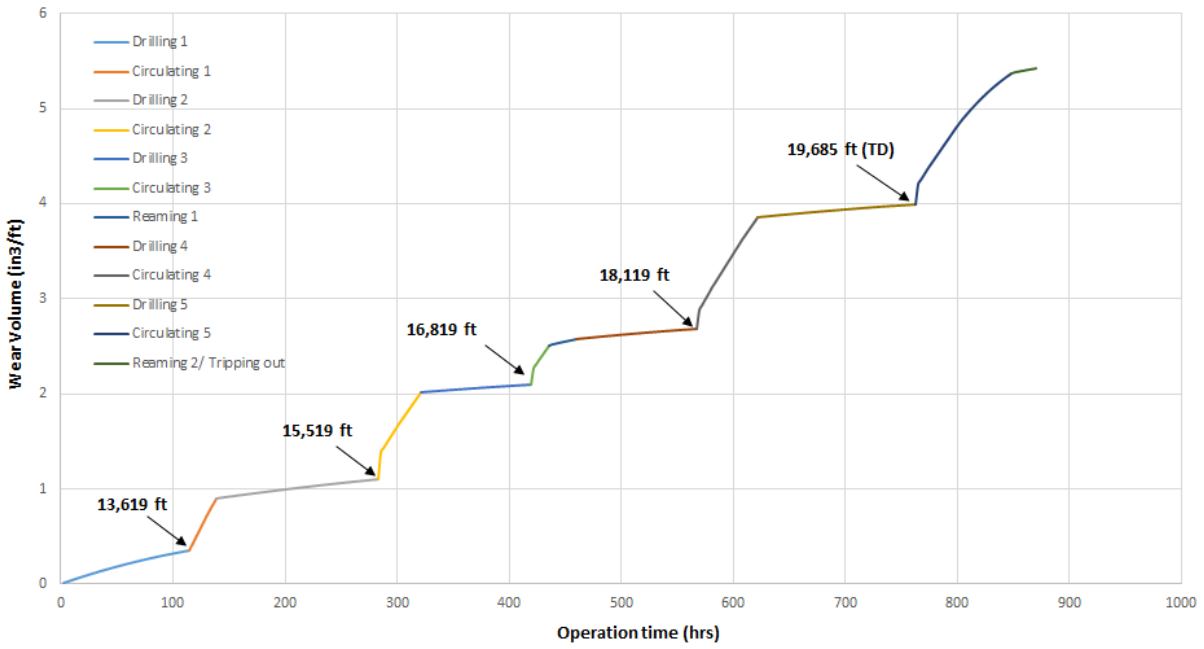

Figure 4. 5 - Wear volume during individual drilling steps

The distribution showed that in addition to the moderate wear during drilling and reaming steps, extreme casing wear is induced during all rotating-off-bottom steps. The wear increases linearly while drilling/reaming due to moving TJ-casing contact. This is not the case while rotating off-

bottom when the DS lays at a single point on the casing and the side forces are maximum due to high tension in the drillstring in pulling the bit off-bottom and overcoming the frictional drag with the formation in openhole. The maximum casing volume (and wall thickness) is lost during the operation "Circulating 5" due to the long rotational contact of 84 hours between casing and TJ. The lost volume for this operation was estimated at 3.96 in³/ft for 705,600 revolutions, with the wall thickness reduction of 0.37 inch from original WT of 0.55 inch (67%).

The wear volume determined for each process was back-calculated to determine the wall thickness lost during each operation. The contact points during different operations were taken to be different from each other but it was assumed that during each step, the TJ passes through the same point on the casing for the entire step. For example, for the operation "Drilling 5", it was assumed that all TJs pass through the same casing grove during the entire drilling interval and the cumulative lost volume is the volume of one deep crescent grove formed at the end of the interval. The formulas to convert wear volume to wall thickness, along with a graphical illustration, are presented below:

$$WV = 12(\beta r^2 + 2\sqrt{P(P-R)(P-r)(P-S)} - \alpha R^2) \quad (67)$$

$$cos\alpha = \frac{(\boldsymbol{R^2 + S^2 - r^2})}{2RS} \quad (68)$$

$$\beta = arctan\frac{(\boldsymbol{R.sin\alpha})}{((R.cos\alpha) - S)} \quad (69)$$

Here,

$S = R - r + h$

$P = {}^{(R+r+S)}/_{2}$

R is the casing inner radius, in

r is the TJ radius, in

h is the depth of grove, in

α is the casing contact angle at the worn arc, rad

β is the TJ contact angle at the worn arc, rad

S is the eccentricity, in

P is the radius of worn arc, in

Geometrical contact angles α and β for different values of grove depth for 6 5/8 inch TJ and 9 5/8inch casing were calculated. Some used values of α and β are presented in the table below.

Table 4. 1 - Geometrically determined contact angles for different grove depth values

h (in)	S (in)	α (rad)	β (rad)	P (in)
0.000	1.216	0.000	0.000	4.341
0.025	1.241	0.170	0.238	4.353
0.035	1.251	0.201	0.280	4.358
0.042	1.258	0.219	0.307	4.362
0.048	1.264	0.234	0.327	4.365
0.052	1.268	0.243	0.340	4.367
0.056	1.272	0.251	0.353	4.369
0.060	1.276	0.260	0.365	4.371
0.064	1.279	0.267	0.375	4.372
0.066	1.282	0.272	0.382	4.374
0.069	1.285	0.277	0.390	4.375
0.071	1.287	0.281	0.396	4.376
0.074	1.290	0.287	0.404	4.378
0.076	1.292	0.290	0.409	4.379
0.079	1.294	0.295	0.415	4.380
0.080	1.296	0.297	0.419	4.381
0.082	1.298	0.301	0.424	4.382

Corresponding wear volumes were converted into wall thickness reductions and values were cross-matched with the above α and β values.

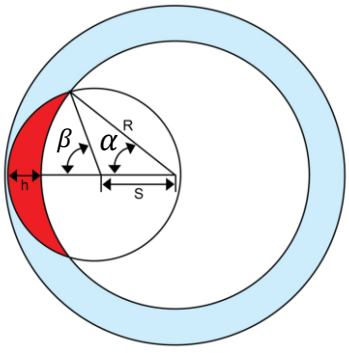

Figure 4. 6 - Wear volume illustration to calculate wear depth [46]

The remaining wall thickness was then determined from original thickness for each of the twelve drilling operations and the values showed significant more loss of wall thickness during off-

bottom rotation then for drilling phase. Considering that the entire wear during the twelve operations was focused on a single groove, the casing almost loses the entirety of its thickness at the end of the last reaming phase. The last three circulating intervals also show very similar behavior (slopes) of reduced wall thickness due to identical fluctuations in tension (or sideforce) present at the contact point with each circulation interval. The two reaming operations show steeper slopes compared to drilling slopes due to higher sideforce values while pulling the DS upwards. The actual field wear depth is expected to be lower than the plotted values as the pressure declines gradually with increase in worn area to meet the contact pressure threshold.

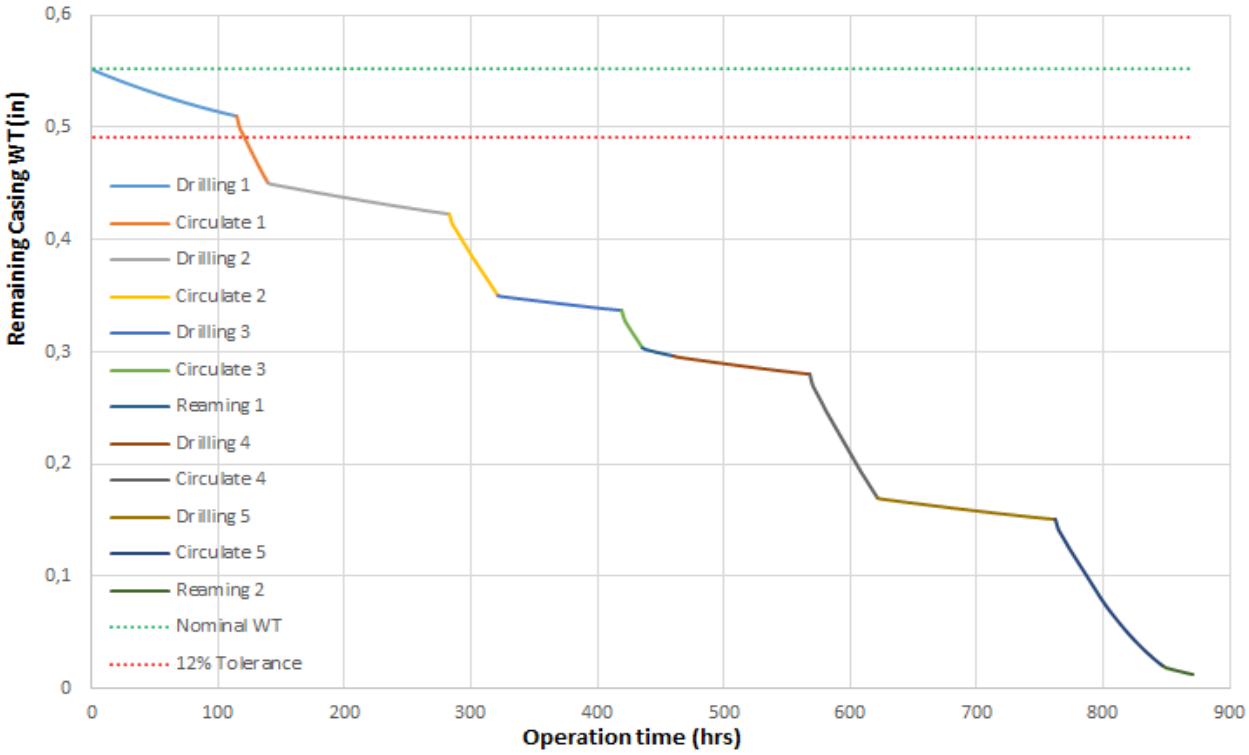

Figure 4. 7 - Remaining wall thickness during individual drilling steps

4.1. Case Histories

In order to confirm the wear parameters obtained from simulations for their use in the experimental design, some field case histories are also included in the study. When analyzing field cases, most wear results are based on reverse-modeling the measured WT reductions from the USIT /Multi-finger caliper logs to arrive at the estimated wear volume and then using the section RPM, drill-time and sideforce to deduce the frictional work done. The two quantities are then divided to get the approximation on the WF. Mitchell and Xiang presented a comparison of such back-modeled WF values based on well parameters for horizontal and S-Shaped wells. [12]

Table 4. 2 - Field based reverse-modeled wear factors [12]

Well Type	BHA Type	Location	Mud Type	WF Average E-10 psi^{-1}	WF Maximum, E-10 psi^{-1}
Horizontal	Conventional	North Dakota	Oil	60	240
Horizontal	Conventional	North Dakota	Oil	30	60
Horizontal	RSS	Texas	Oil	20	20
Horizontal	Conventional	Oklahoma	Oil	10	20
Offshore Inclined	RSS	Gulf of Mexico	Synthetic	2-5	10
Offshore Inclined	RSS	Gulf of Mexico	Synthetic	7	7
Offshore Inclined	RSS	Gulf of Mexico	Synthetic	3	10
S-Shaped	RSS	Columbia	Oil	1.5	2
S-Shaped	RSS	Columbia	Oil	1.5	2.5
S-Shaped	RSS	Columbia	Oil	1.5	3
S-Shaped	RSS	Texas	Water	5	10
S-Shaped	Conventional	Rockies	Water	10	18

An account of some recent case histories reporting noticeable casing wear is presented below:

4.1.1. Casing wear and collapse: Sajaa field, Sharjah UAE, 2003

Sajaa is an onshore condensate gas field tapping into limestone reservoirs up to 4000m (13000 ft.) depth. The reservoirs have an average initial pressure of 8000 psi, with mud densities of 14 ppg in the reservoir section. The well 39 taken as a case history is a horizontal two-lateral well from 2003. The well was initially planned to be completed horizontally with a 7inch tieback liner in a 9 5/8inch casing that collapsed above the shoe and incurred damage to the liner tieback. The casing collapsed while flow testing at 10800ft. Two laterals were then drilled in the casing for production, from which the second lateral experienced a stuck pipe and the well was put on production with the lower BHA left inside the horizontal section. The well was produced packer less through tubing.

The casing collapse in well 39 was attributed to severe casing wear WT reduction during horizontal drilling. Conservative casing wear predictions were made for well 39 during well planning phase as an addition to the torque and drag calculations. Soft string model was used for the analysis and the cumulative frictional work done on the casing was determined for each drilling phase. The total worn volume was reverse calculated to the maximum wear grove depth at the lower side of the liner. A single empirical wear factor was utilized for the initial calculations. The simulation led to impractical and inconclusive results.

The collapse at the well emphasized the need to specifically focus on accurate wear predictions and modify the wear calculation practices. Following corrections were made for calculating wear for subsequent wells:

1. Multiple wear factors for different BHA runs as per nature of TJ hardfacings (fine TC, coarse TC and rough TC)
2. Different wear behavior (factor) for sliding entries
3. Reducing wear factors with increasing grove depth
4. Adjusting parameters in sections where remaining WT reaches zero

The corrections improved the quality and execution time for the simulations. Also, casing ID measurements were carried out for subsequent wells to log both the 7 in. liner and 9-5/8" in. production casing with a single run. The chosen tool was a 60-fingers caliper with an accuracy of 0.03in.

The wear predictions were then compared with the multi-finger caliper measurements on the field for the subsequent well 32. The results showed averaged values between coarse TC (160 x 10^{-10} /psi) and rough TC predictions (1600 x 10^{-10} /psi). The caliper readings were then reverse calculated to find a general wear factor of around 500 x 10^{-10} /psi.

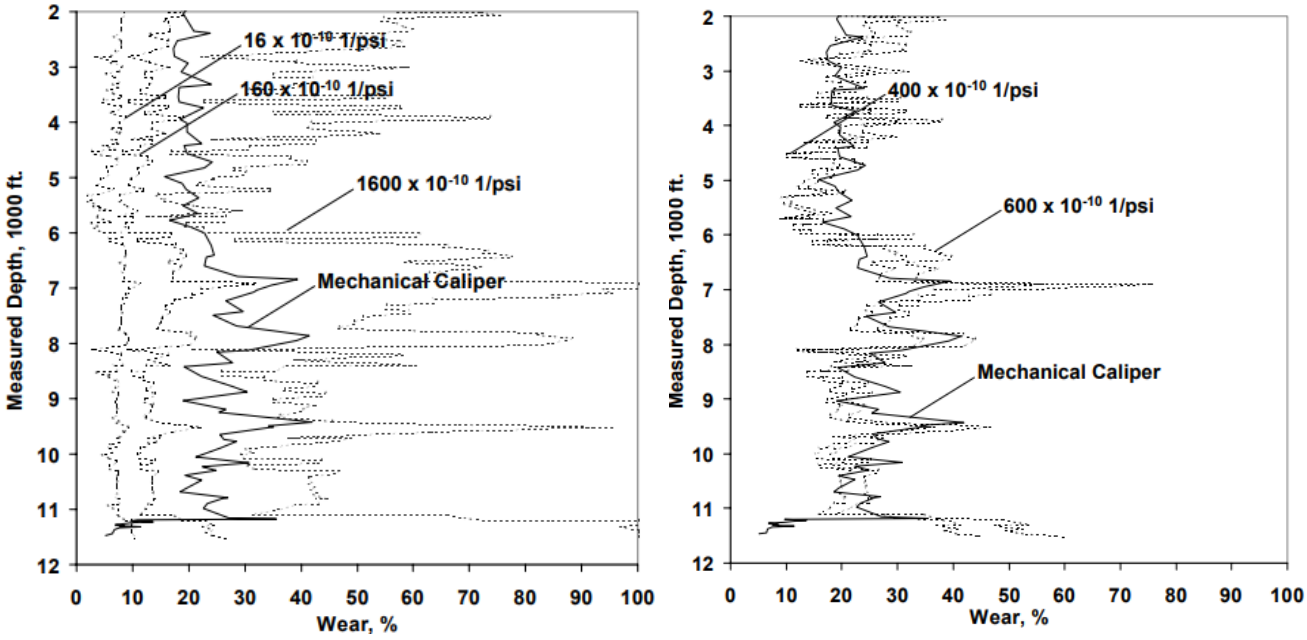

Figure 4. 8 - Comprasion of calculated and measured wear (left) and adjusted trial-and-error estimate of wear factor (right) [33]

4.1.2. Casing wear and collapse: Gulf of Mexico, 2014 [55]

The reported case history is from a horizontal over-pressured well in the Cardenas field in the Gulf of Mexico. The average TVD for the wells is around 19700ft, drilling into dolomite beds with an equivalent density (ECD) of up to 14 ppg. MPD techniques are often employed while tapping fractured dolomites where the ECD has to be changed abruptly to 4 or 5 ppg. A schematic of the well is shown in Figure 4.9. As can be seen, the 9 7/8" intermediate liner at 17740ft was tied back to the surface with a 9 5/8" casing and the entire string was cemented. Following a 8 ½" hole further, a 7" liner was then placed until 19000ft and attached to a 7 5/8" tieback up until the surface, creating two un-cemented concentric strings to be filled with N_2 injected from the surface.

The 5 7/8" openhole production section was drilled to 21000ft in the fractured zone (using MPD) with an ECD of 5.8 ppg. Rotating off-bottom, reaming and one complete trip to surface were carried out until reaching the TD. After running back in, the DS was pulled back as N_2 was injected in the concentric annulus for five hours. After the injection period, the DS was pushed back in but was found to be stuck. A fishing job was performed after several freeing attempts and over 14400ft of DS was recovered. Calculating the depth of stuck-pipe, the inner 7 5/8" casing was cut at 13100ft and pulled but was also found to be stuck. The section was plugged and a side track was drilled with a 4 1/8" hole to reach the TD.

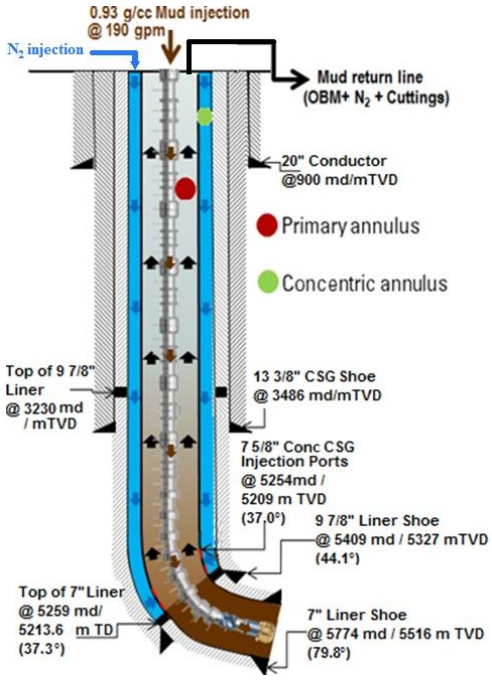

Figure 4. 9 - Schematic of the horizontal well from Cardenas field [55]

Analysis of the drilling stages ascertained a collapse in the 9 7/8", deforming in on both the DS and the 7 5/8" casing. The casing, fluid and DS plans were revisited to check if a severe pressure

drop was observed during the drilling of 5 7/8" section. Since no caliper log results were available, a combined loading analysis was carried out, including external pressure from the cement (checking CBL & cement densities), internal pressure while drilling (section fluid plan), thermal loading, high axial tension and casing wear.

The expected casing wear for the 9 7/8" section while drilling the 8 ½" hole was 1% per trip and a total of 5% loss of WT based on model. The post-collapse analysis, however, regarded casing wear as the second biggest factor responsible for the collapse of the casing. The higher sideforce due to the 78° inclination, along with long rotating hours and frequent changes in internal pressure could have led to the collapse of the joints. It was recommended to have better directional control and to employ NRDPPs for the future Cardenas wells. Also, the casing grades were planned to be selected to fulfil the design criteria even after 5% wear.

4.1.3. Casing wear: North US, 2015

A case history reported by WWT international in 2015 involved increased volumes of metal chunks recovered on the shale shaker while passing through a 9 5/8" casing at the beginning of a horizontal section to drill horizontally further. The high WOB push on the drill bit was anticipated to have pressed the DS against the casing in the upper shallow dogleg (4°/100ft) sections from 2000ft to 3100ft. Figure 4.10 shows the detected spikes in the sideforce while drilling the horizontal section, along with a sample of recovered casing metal from ditch magnets at 3100ft. On recommendations of WWT intl., the critical sections were further drilled with NRDPPs to reduce the side force. The metal recovered daily after deploying NRDPPs was reduced to 0.5lbs from a previous value of 12lbs.

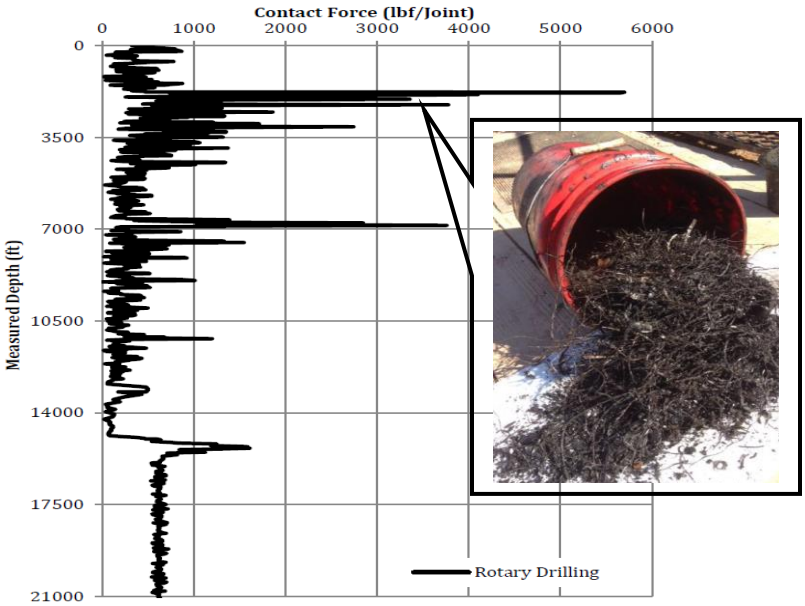

Figure 4. 10 - Calculated contact forces with metal sample recovered at 3100ft [52]

4.1.4. Casing wear in S-shaped well: Latin America, 2015

A reported case history from 2015 reported a low ROP (2 ft/hour), high RPM (150 RPM) scenario for a S-shaped well in Latin America. The sections above and below the S build-section (12 ¼" hole diameter) around 6500ft experienced significant sideforce (3800lbf/joint), posing a question on the integrity of the 11 ¾" cased pipes to be placed after reaching section TD. The issue was addressed prior to drilling the next 10 ½" section by placing NRDPPs on the entire length of the DS passing through the 11 ¾" casing. For the 8 ½" (cased with 7" liner) and 6" openhole, NRDPPs were again placed to protect the 11 ¾" casing due to higher doglegs.

The USIT caliper log results upon reaching the TD showed significant wear in the 7" liner (26% WT removed) with a back-calculated wear factor of up to $60x10^{-10}$/psi. In comparison, the protected 11 ¾" casing had only 13% loss of WT with a back-calculated WF of up to $4.5x10^{-10}$/psi. The higher wear factors from 7" liner, when applied to the 11 ¾" section in the model, showed up to 40% loss in WT. A plot of the anticipated vs. actual wear, along with the well trajectory, is shown in Figure 4.11.

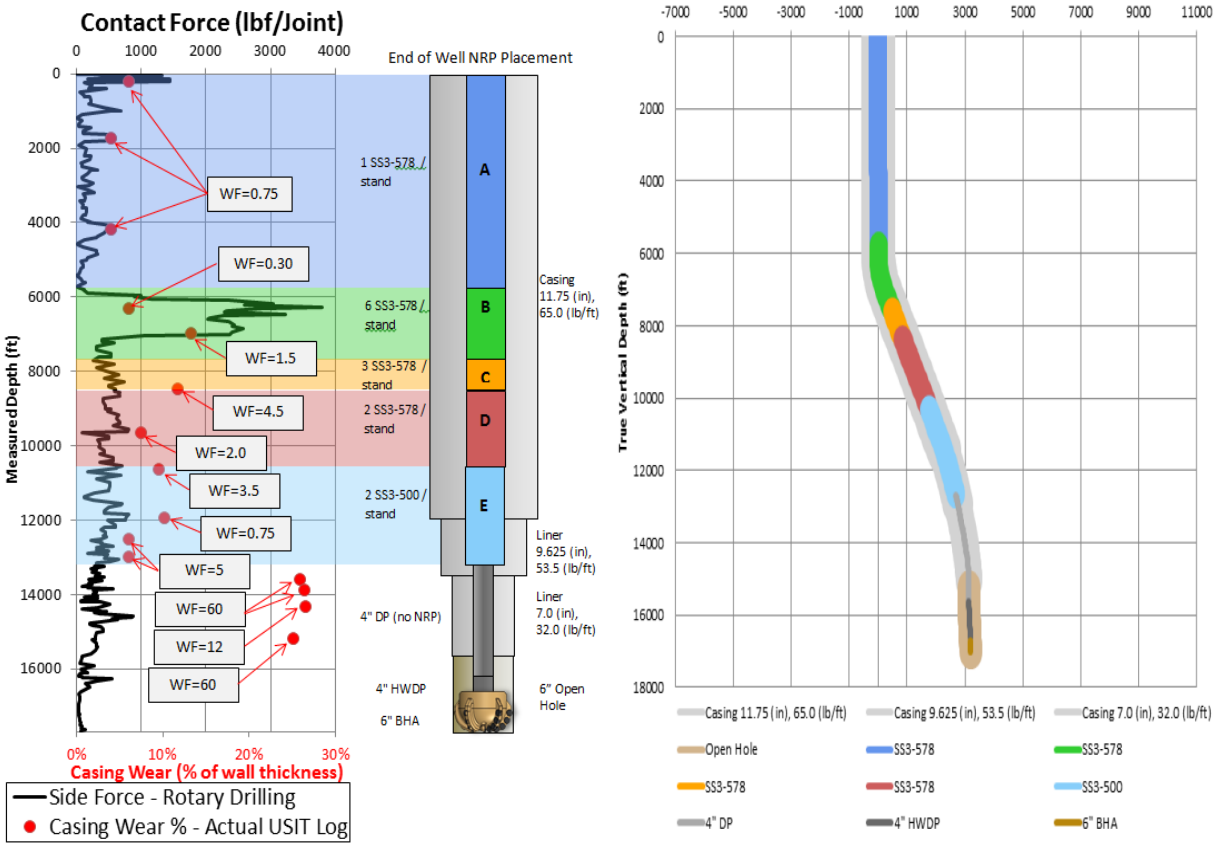

Figure 4. 11 - Observed wear factors on the s-shaped well vs the anticipated side force and well trajectory [54]

4.1.5. Casing wear: Middle East, 2015

A series of horizontal wells in the Middle East with average MD of 11000ft reported significant wear at the KOP and the cased sections above while drilling the horizontal bore. One such well showed severe wear in the 7" liner placed in the build section while drilling the subsequent 6 1/8" horizontal section. Estimated wear factors from wear models in the build region were around 10 - 50 x 10^{-10} /psi during the bit run that drilled 4000ft from the 7" liner shoe. Based on the past wear incidents, a caliper was run in the liner section while logging the openhole section. The back-modeled results showed up to 40% WT reduction in the build region and above due to high tensions while rotating off-bottom and sliding operations. A record of the observed wear values, along with the well trajectory is shown in Figure 4.12. The rest of the 6 1/8" section to TD was drilled with NRDPPs placed against the build section. The practice reduced both the casing wear and TJ wear in the openhole section, as no considerable wear was noticed on the TJs upon tripping out and no significant metal amount was observed on the shakers.

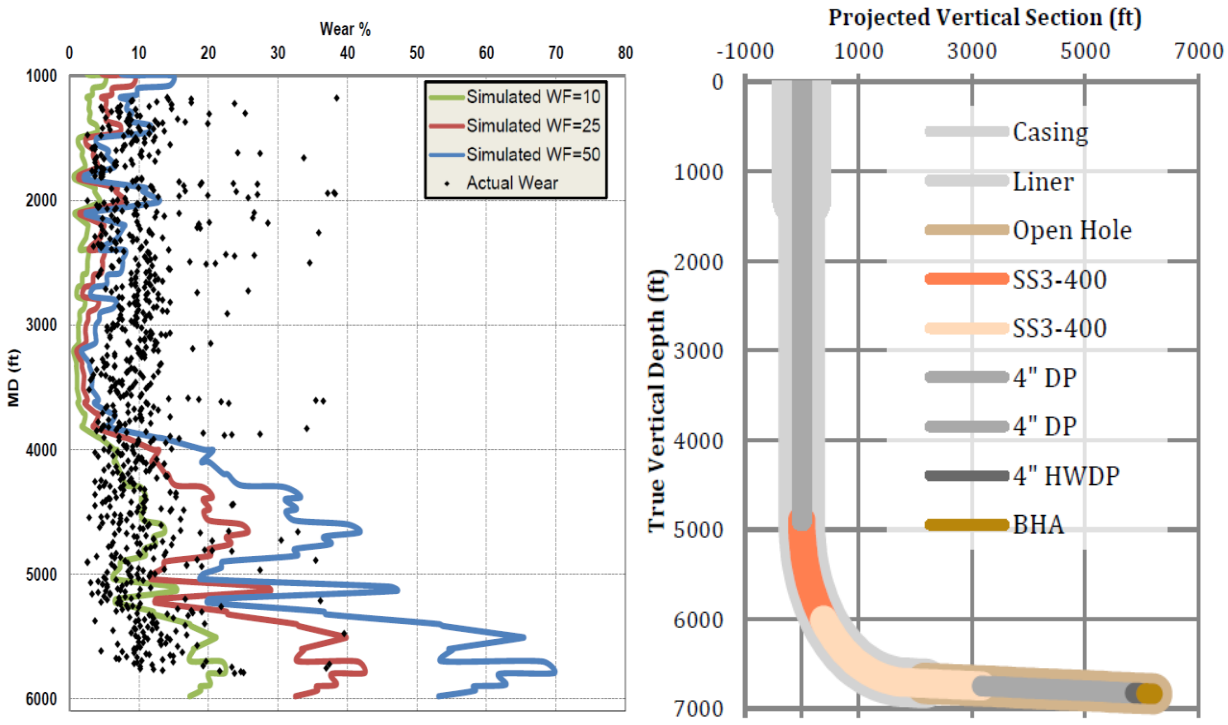

Figure 4. 12 - Observed vs. modeled wear on the 7" liner and 9 5/8" casing from USIT logs, along with the trajectory for the case well [56]

4.1.6. Casing wear: Alpine field, Alaska US, 2018

The recent cases of pronounced casing wear in the directional wells in the Alpine field, northern slope Alaska were presented in 2018 as a part of the study by ConocoPhillips to test the effectiveness of non-rotating DP protectors (NRDPP) for the wells under prevalent operational conditions, and to check the viability of a commercial casing wear prediction software. The field

has over 200 directional wells with an average MD of 22000ft and the longer ERD wells reaching up to 30000ft in 2018. Owing to anti-collision requirements and faulted reservoir lithologies, the wells (single and multi-lateral) typically have L- and S-shaped trajectories and have been increasing in lateral projections over the last 10 years with the recent multi-laterals having more than 30218ft combined lengths.

The presented well (CD-5) has a 7 5/8" intermediate casing extending into the 6.75" main-bore lateral with a 4.5" liner until the TD. The casing is then milled above the shoe with the same 6.75" second lateral and 4.5" liner. A schematic of the well is presented in Figure 4.14. The casing wear software was initially calibrated against a similar trajectory offset well that reported a 60% loss of WT at a location at 2300ft depth while drilling at 11500ft. Results from MWD tool, gyro survey and multi-finger caliper were used to determine the actual dogleg, max. depth of grove and wear volume. These were then back-calculated to determine the wear factors that were used as an input for calculations for CD-5. Soft string model with was utilized with WFs of 17 x 10^{-10} /psi (DLS of 7.25°/100ft) and 30 x 10^{-10} /psi (DLS of 11°/100ft) selected for model calibration based on gyro and MWD measurements. The wear equation used for modeling was based on the Mitchell and Xiang model [12].

The well CD-5 employed plastic NRDPPs at the TJ at critical dogleg locations inside the 9 5/8" casing. NRDPPs were accounted for by a 95% reduction in the wear factor in the model. The protectors were installed from surface until 12400ft when the bit was at the TD at 25000ft. The greater portion of the casing joints exposed to DS between the bit and the first NRDPP suffered wear. However, the wear in the areas of maximum dogleg was considerably reduced. A schematic showing the NRDPP placement with depth and resultant sideforce (from DS tension) is shown in Figure 4.13. A total of 390 protector joints were used with a density of 1 protector/drillpipe.

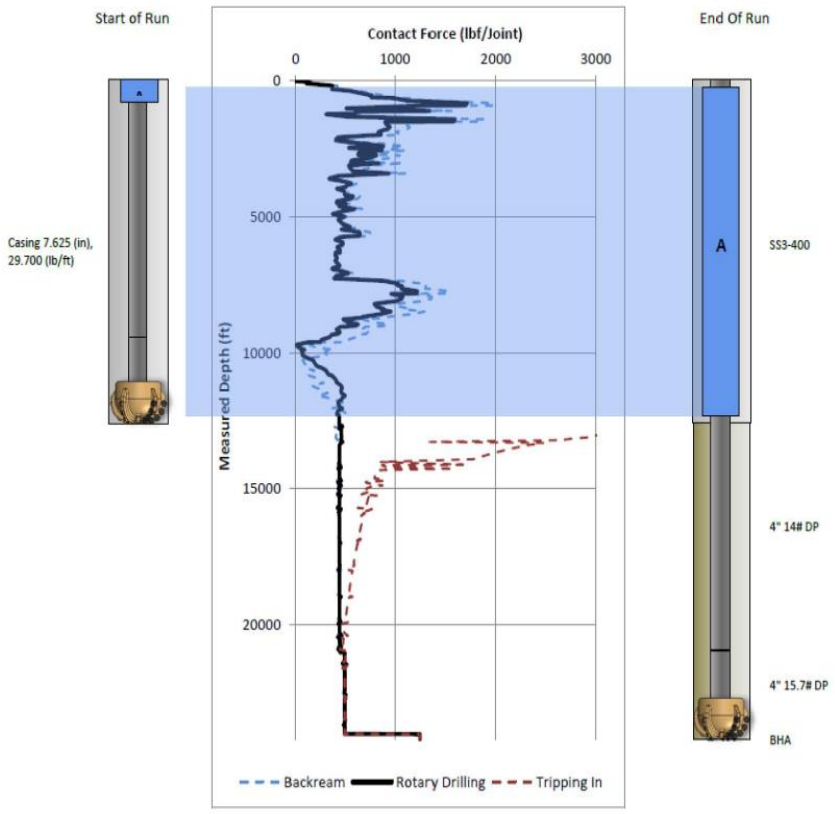

Figure 4. 13 - Sideforce distribution along with depth using NRDPP placement for well CD5 in Alpine Alaska [50]

An average of 1800lbf/joint was determined from DS tension with the NRDPPs. The installation of 1 NRDPP/pipe was based on model recommendations to minimize sideforce and WF. The NRDPPs were also occasionally replaced after reaching maximum sleeve/bearing life. Other considerations for minimizing wear included limiting rotating off-bottom and hole reaming hours (installing additional reamer above the motor for reaming while drilling). Limiting maximum DLS and using RSS to avoid drastic DLS changes was also included in the drilling plan. Contingency plans included casing patches and thick-walled casing for lower sections while drilling horizontal production section.

Based on input data, the model and software estimates were compared with the casing caliper log results for CD5 (after drilling) and were found to be in good agreement. Based on sideforce reduction due to NRDPPs (average 1800lbf/joint vs 2900lbf/joint on offset wells) allowed a wear decrease of 60% from total worn volume for offset wells. A schematic of the well trajectory and comparison between model and caliper results are presented in Figure 4.14. The future wells with longer ERD trajectories (up to 40000ft) are aimed to be drilled with similar mitigation strategies.

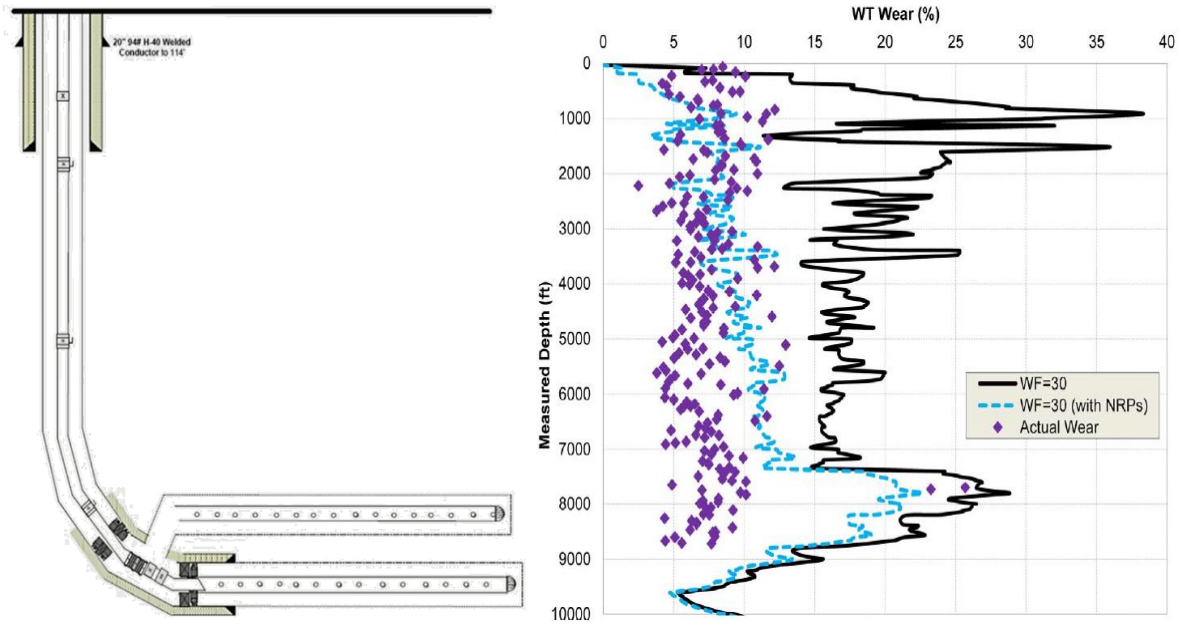

Figure 4. 14 - CD-5 well schematic with wear comparison between model and caliper log results [50]

4.1.7. DP and casing wear: Permian basin, 2020

A recent case history observed considerable wear on TJ and casing while drilling horizontally on a 3.2km long lateral section for a well in the Permian basin. The worn out TJs were rendered unfit for further drilling due to the loss of coarse hardband layers, and required re-banding. NRDPPs were utilized in the case for a better centralization effect of DP and eliminate rotating contact between TJ and casing in the higher dogleg sections. As a result, no TJ wear was further observed with only minor casing wear. A comparison on the unprotected TJ after wear vs. the TJ with NRDPP after reaching TD is shown in Figure 4.15. The major casing wear sections were located above the build for the horizontal section. Severe drillpipe wear took place, both at the build section and at the horizontal section due to weight concentration and long rotating contacts with forces exceeding 1000lbf/joint.

Figure 4. 15 - Worn TJ (in red) vs. TJ protected with NRDPPs (in green) on Permian basin [53]

4.2. Selected design and material parameters

Based on the simulated case studies and studied field scenarios, the following parameters were selected for the initial wear tests (as design parameters):

4.2.1. Material and diameter selection

In addition to simulation results and field case results, the choice of materials and diameters is also based on material availability. The selected materials are presented in the table below. For all wear tests, the tooljoint is taken as the aggressive (wear-inducing) body whereas the casing is taken as the softer (worn) body.

Table 4. 3 - Materials and diameters selected for wear tests

Selected Casing Materials	95HC carbon steel, glass fiber, carbon fiber
Selected Casing OD	244.5 mm (9 5/8”), Equivalent ODs for glass fiber and fibered carbon casings
Selected Tooljoint Material	High-yield steel
Selected Tooljoint Diameter	6.875 mm

4.2.2. Contact force, rotary speed and reciprocation speed selection

Excluding the spikes in the side force values in simulation and field cases, the average rotating contact force in built sections is in the range of 1100 lbf to 1500 lbf. This is taken as the design parameter. Rotary speed and axial reciprocation speeds are also selected based on field cases.

Table 4. 4 - Contact force, rotary speed and reciprocation speed selected for wear tests

Rotating Contact force	5 KN (1124 lbf) to 6.7 KN (1506 lbf)
Applied Rotary Speed (RPM)	100 to 120
Axial (Reciprocation) speed	Up to 100 m/hr

4.2.3. Selection of mud properties

A base water-based mud is selected for the wear tests with a low viscosity and density (no cuttings incorporated in the wear test). To analyze the effects of mud solids, the tests are planned to be run both with pure water and weighted mud.

Table 4. 5 - Mud properties selected for wear tests

Mud Weight	9.3 ppg to 9.5 ppg
Viscosity	15 centipoise
Initial Temp.	Room temperature
Components	Barite (about 25% by weight of water)
	Bentonite (about 5% by weight of water)

5. Casing wear frame: Design and test parameters

The design, simulations and construction for a wear frame to determine the friction and wear factor on full scale scenarios is the next stage of the research. For this purpose, an older wear frame from 1991 was modified to fit the study requirements with the idea to be able to measure friction factor and wear parameters in real time under rotating, sliding and combined scenarios for different side force and RPM conditions.

5.1. Older frame: Components and test procedure

The old frame was built to only qualitatively test the wear resistance (against formation) and casing friendliness of proprietary hardfacing materials. A total of 8 tool joint specimens were tested consequently against casing C-sections and abrasive material layers (representing formation). A fixed casing diameter (9 5/8inches) and material (C-90) were maintained for all casing tests. The tests involved measuring the thickness of worn casing and worn TJ for a total contact interval of six hours. Two TJ specimens were tested side by side against casings /abrasive formation material. The fluid used was clear water to see the influence of pure metal-metal adhesion without particle abrasion effect from mud particles. The measured reduced thickness was then plotted against the total number of revolutions for each of the hardbanding material. The surface parameters included a fixed side force of 4.5 KN (1011lbf), a fixed RPM of 160 min^{-1} and a fixed axial velocity of 24.5 m/hr. All tool joints were of 5.5 inch OD. A schematic of the old frame is provided in Figure 5.1.

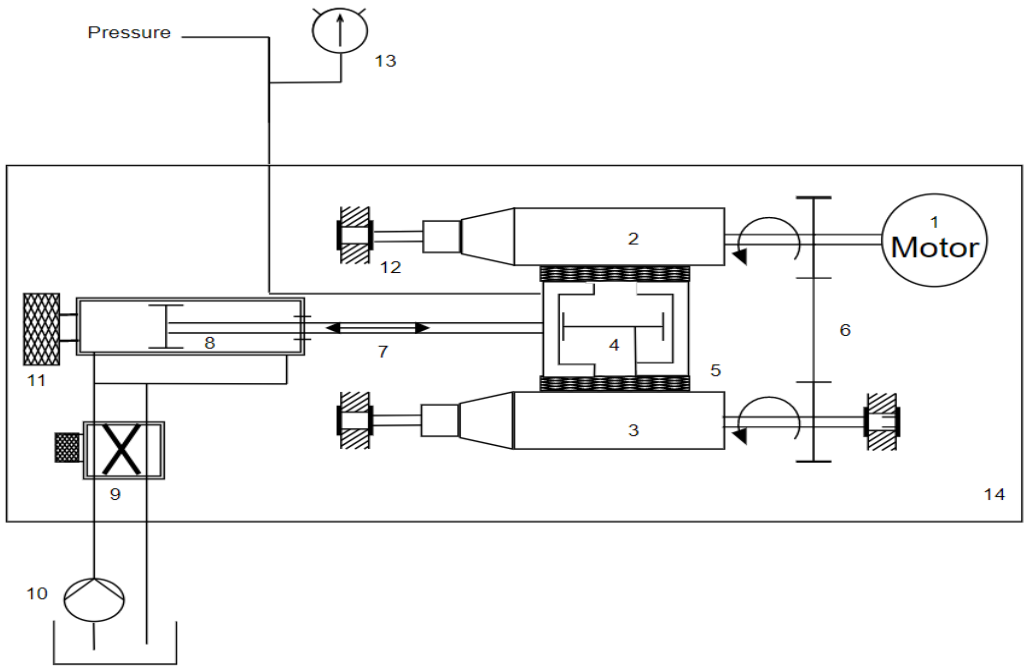

Figure 5. 1 - Schematic showing components of the old frame

The components corresponding to the labels include:

1. Motor for rotating the tool joint specimens
2. Tool joint 1
3. Tool joint 2
4. Cylinder piston to press two casing/formation samples against the TJ
5. Abrasive material attached to both sides of a cylinder piston
6. Metal chain connecting both rotating TJ shafts to the motor (motor output divided between both wear specimens)
7. Metal rod connected to the casing unit
8. Hydraulic piston to reciprocate the metal rod
9. Flow lines to distribute hydraulic pressure on both sides of the piston
10. Hydraulic pump
11. Fixation for hydraulic cylinder
12. Fixation for moving shafts
13. Hydraulic pump for pressing cylinder piston attached to casing /abrasive material
14. Work bench

5.2. Modification goals

Once the frame was selected to be modified, the calculations, construction and modifications for different components and their function mechanisms was carried out to make the wear test represent field operations. Some modifications undergone include:

- Upgrade of side-force inducing piston cylinders for side force variations
- Removal of one platform so that only one casing specimen is tested under higher side force conditions (for better dynamic control)
- Upgrade of axial reciprocation piston to variate TJ lateral movement speed
- Inclusion of strain-gauges (X-rosettes) and a wireless data transfer module through the TJ rotating shaft for friction torque measurements
- Installation of a motor panel, frequency controller and speed encoder to vary and monitor TJ rotating speed
- Installation of a new fluid circulation tank and fluid motor to circulate weighted drilling fluids in a loop through the setup
- Installation of a load sensor directly behind the casing to observe side-force in real time.
- Installation and calibration of pressure transducers and load sensors for real-time monitoring of side-force and pressures in side force (pneumatic) and reciprocation (hydraulic) systems
- Data acquisition system and operator interface for monitoring measured factors on a computer panel

A detailed description of different frame systems is presented in the next sections of the chapter. The flexibility with parameter variations, along with real-time measurements under field loads makes this frame unique in comparison to the past frames. A sketch of the modified version of the machine is presented in Figure 5.2.

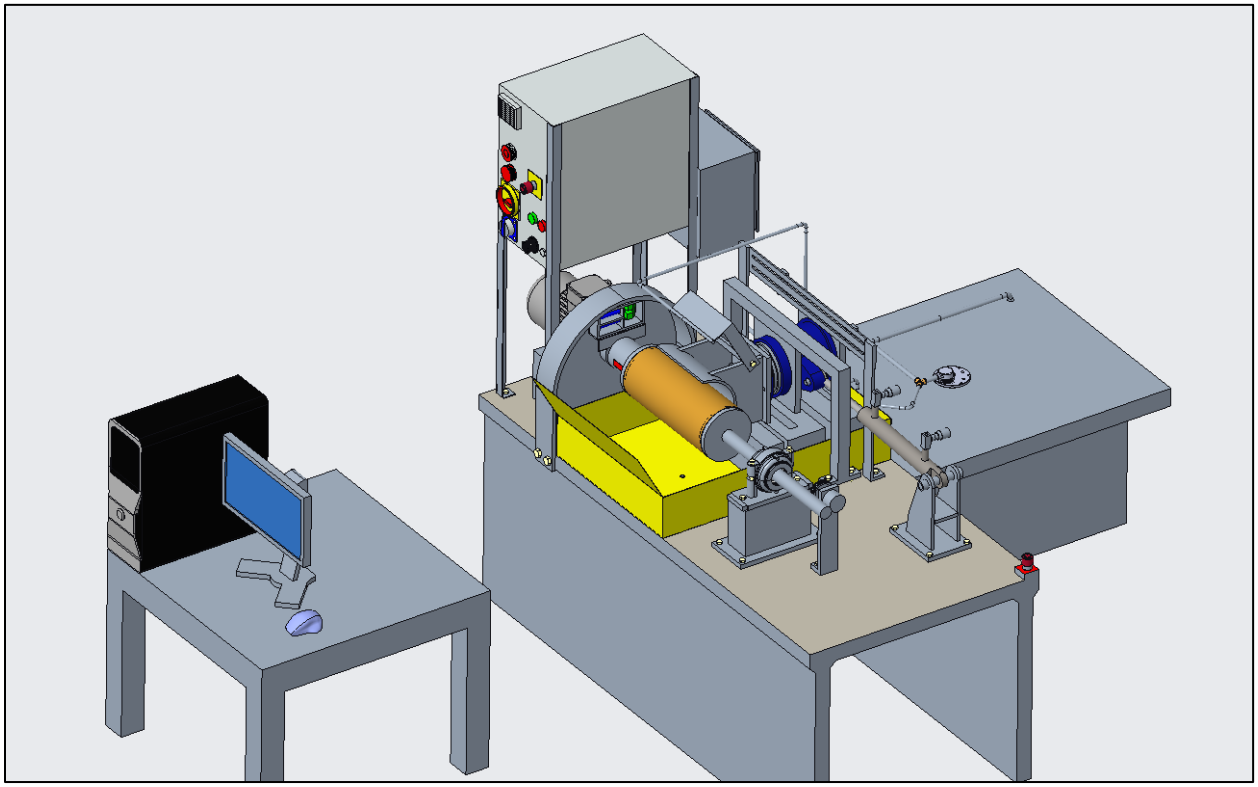

Figure 5. 2 - CAD of the modified version of the frame

5.3. Wear frame systems

The objective of the experimental setup was to measure friction and wear on a single casing specimen under high contact force and variable rotating and axial reciprocating speeds.

After modifications on the frame, the entire component structure of the frame can be divided into five systems:

1. Contact / Side force System
2. Tool joint Rotation System
3. Axial Reciprocation System
4. Mud Circulation System
5. Measurement and Data Acquisition Systems

5.3.1. Contact / side force system

The contact force system is designed to keep a steady and uniform contact between the casing inner wall and the rotating tool joint. The casing specimen to be tested is cut to a specific length (240 mm) and into a C-section (arc length 230 mm to 240 mm) and then welded on to a metal adapter. The adapter can be then attached to a pneumatic side force piston to be pressed against the rotating tool joint. A sketch of the C-section on the metal structure is presented below.

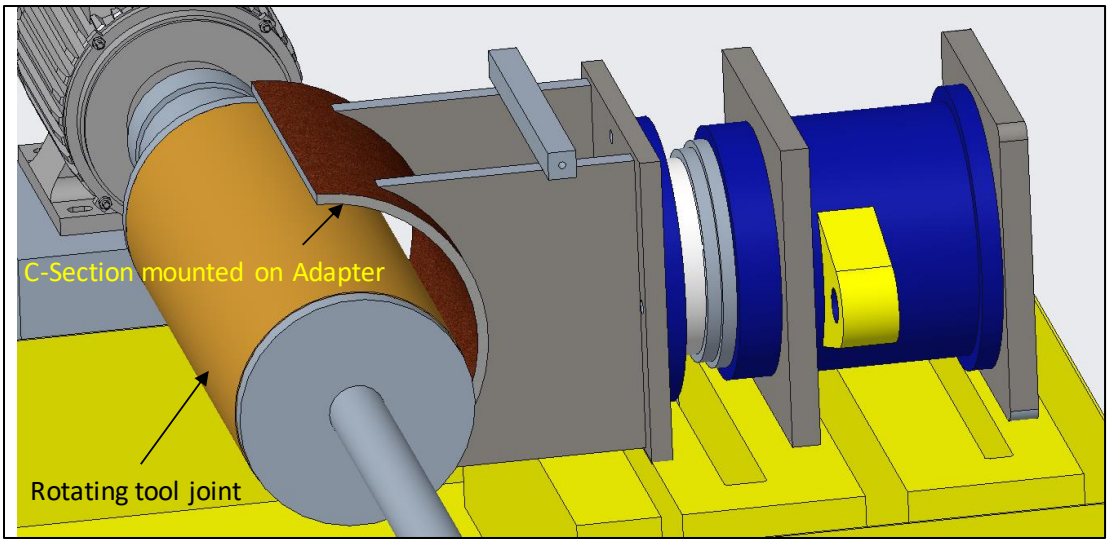

Figure 5. 3 - Fixation of casing C-section on the pneumatic piston

The metal rod welded on the top of the frame houses the sprinkler hose for the drilling fluid.

The piston applies side force to the tool joint via pneumatic pressure through a small back-hose. The extension on the side (in yellow) is connected to the metal rod for axial movement of the cylinder.

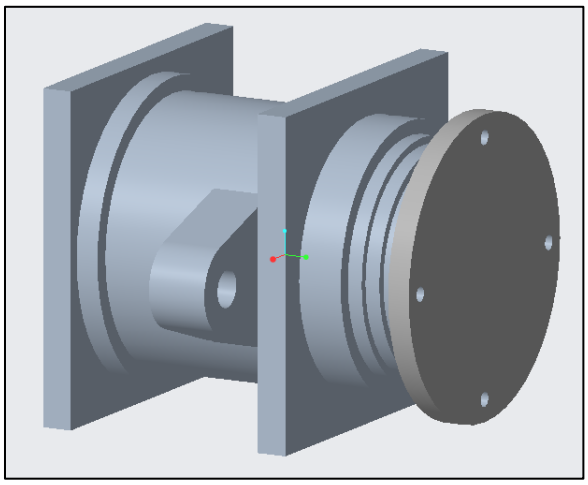

Figure 5. 4 - Pneumatic piston for application of side force

A pressure transducer connected to the pneumatic pump records the pneumatic pressure at the piston (inner) face. Knowing the piston inner diameter, the force applied by the cylinder is determined and taken as the applied press force for the casing-TJ contact.

$$F_{side} = A_{piston} \times P_{transducer} \tag{70}$$

The diameter of the inner piston face is 5.59 inches. Therefore, for a pressure reading of 126 psi on the pressure transducer, the side force acting on the casing specimen becomes:

$$F_{side} = \pi \, {(5.59)^2}/{4} \times 126$$

$$F_{side} = 3092 \; lbf$$

Side force up to 2000 lbf can be applied through the cylinder with rotation (static force can be up to 3500 lbf).

5.3.2. Tool joint fixation and rotation system

The rotation system of the frame comprises of the tool joint being mounted on a motor shaft by means of mounting discs screwed inside the tool joint to keep the tool joint and the shaft concentric. Fixed beam support is provided to the tool joint on one side by the fixed motor and by a fixed ball bearing assembly on the other side.

The motor is attached to a frequency regulator (in the box unit above the motor in Figure 5.2.) to control and variate the RPM (up to 120 RPM). The real time rotating speed can be observed on the computer panel by means of a speed encoder next to the bearing assembly (on the left side in Figure 5.5).

For added safety, emergency shut-off switches are provided on both sides on the frame.

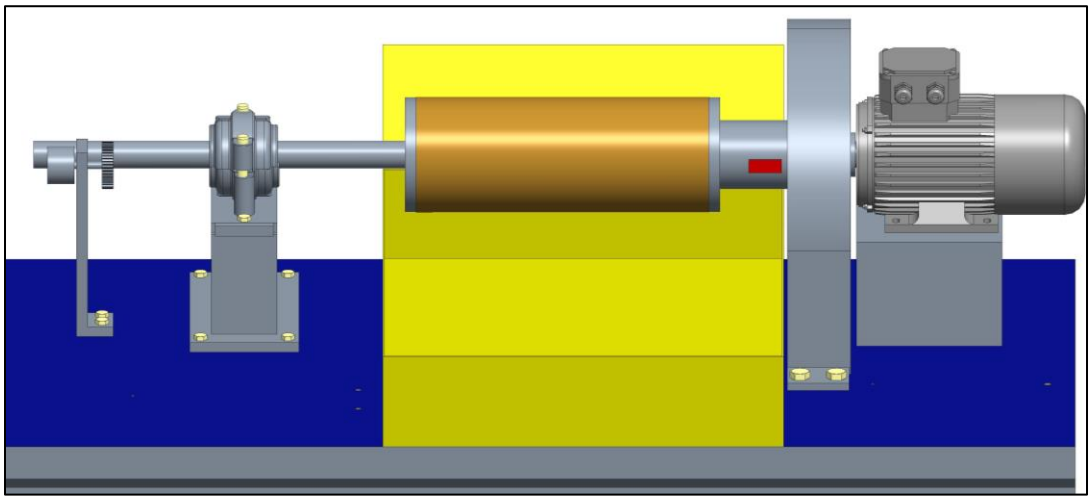

Figure 5. 5 - Rotating tool joint on an electric motor shaft

5.3.3. Axial reciprocation system

Axial reciprocation in the casing-TJ contact represents tripping/drilling operations (with rotation) and sliding operations (without rotation). The rod attached to the pneumatic piston is connected to a hydraulic piston unit that moves in alternate directions. The cylinder is linked to a hydraulic pump via two valves for forward and backward motion. The speed of axial movement in both directions can be adjusted by varying the pressures in the two valves. The pressure in the valves is observed on the computer panel via a pressure transducer connecting it to the control desk. The piston is fixed on the other end by a fixation that allows it to turn slightly about a pivot to ensure efficient axial movement and avoid getting jammed.

Two control switches (in green in Figure 5.6) installed on a frame above the movement surface can be moved and fixed about a hinge to adjust the maximum reciprocation distance. The hydraulic flow to the piston in the cylinder reverses itself to the other valve as soon as the pneumatic piston wall touches the control switch in either direction.

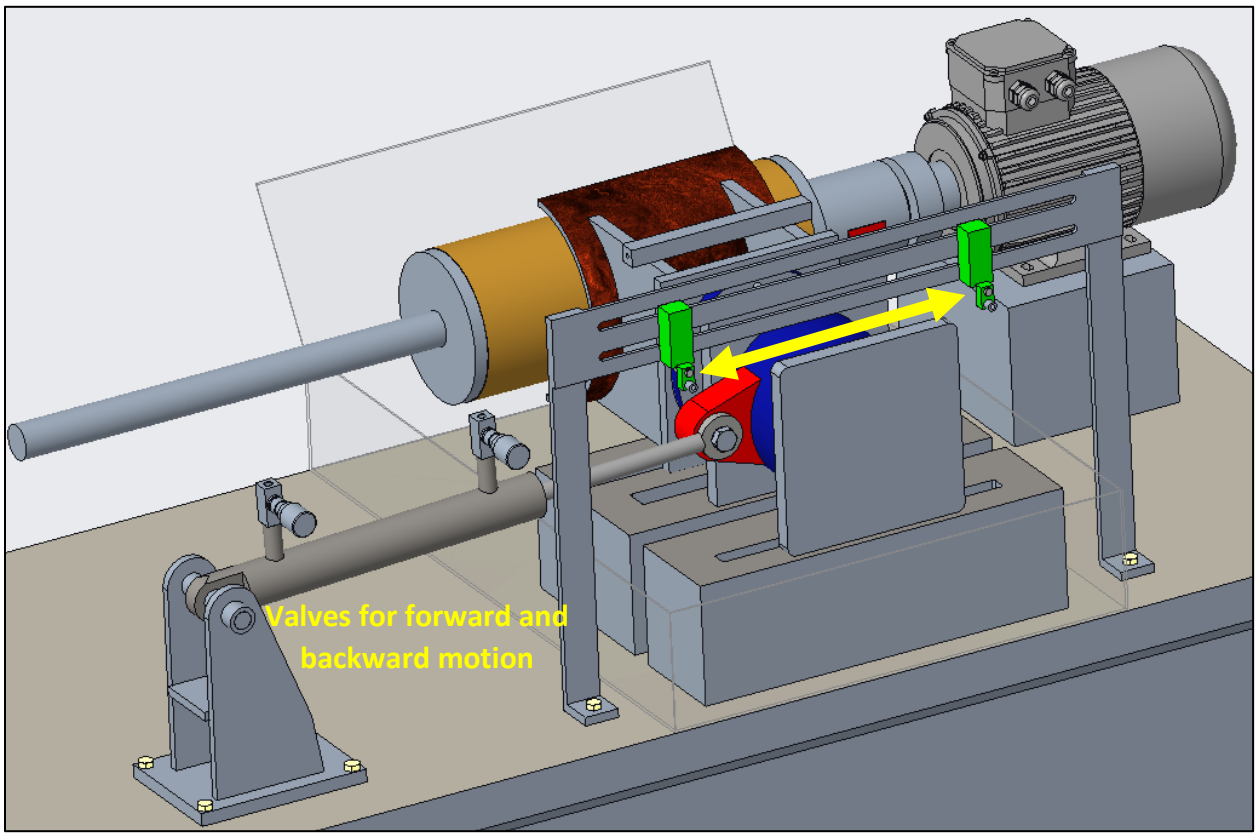

Figure 5. 6 - Hydraulic unit attached to the casing piston for axial movement

Axial movements at speeds up to 6 m/min can be achieved with the hydraulic unit. The axial displacement takes place over a greased platform (highlighted in gray in Figure 5.6) that regulates

the movement, holds the C-section assembly to avoid undesired movements (uplifting of piston upon contact) and reduces vibrations in the specimen while rotation.

5.3.4. Fluid circulation system

The mud circulation systems includes the following components (in order of numbers in Figure 5.7):

1. A Fluid Tank
2. A Motor for Fluid Circulation
3. A Diverter Valve
4. Flow lines
5. Outflow back to Tank
6. Inflow to Sprinkler

The mud to be circulated is mixed (with barite and bentonite) in the tank using an external agitator motor. The lid of the tank houses an electric fluid motor to pump the fluid into the sprinkler mounted on the casing adapter. The sprinkler has a series of outflow openings through which the fluid flows onto the casing-TJ contact.

The fluid flushes the worn particles at the contact and flows into the bowl (in yellow in Figure 6.6.). The bowl has an outlet opening with a magnet attached nearby that holds worn metal shavings. The fluid flows out of the bowl through a flow line from beneath the table and back into the tank. A fine sieve that surrounds the electric motor in the tank filters out any coarse particles/ escaped shavings accumulated in the mud.

The motor has a fixed circulating flowrate of about 9 liters per min. The flowrate ensures a continuous flow of mud from the sprinkler throughout the test duration. The temperature of the mud is monitored in the bowl/ in the tank by a laser thermometer at regular intervals (for increments due to friction heating of the specimen).

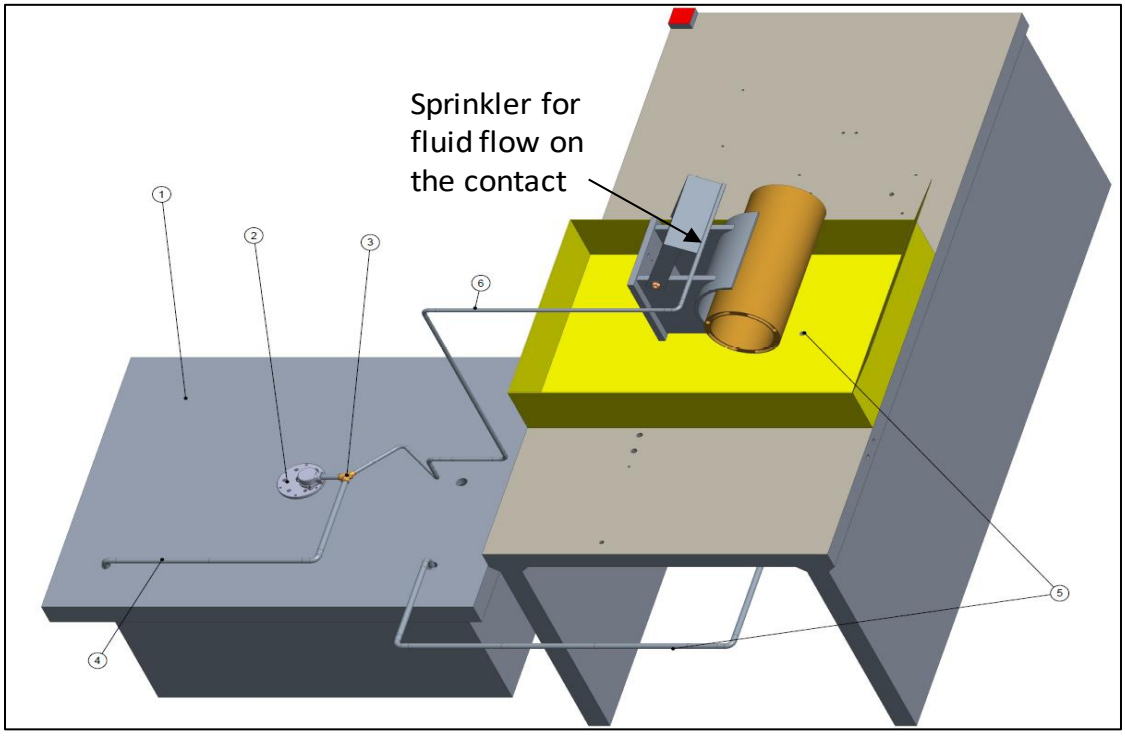

Figure 5. 7 - CAD schematic of the fluid circulation system

5.3.5. Measurement, data acquisition and control systems

The data measurement unit comprises of the load cells and strain gauges installed to obtain essential test parameters such as friction torque and contact load at the C-section.

5.3.5.1. Friction torque sensors

The friction torque generated in the shaft due to the contact between the casing and the rotating tool joint is monitored by means of glued electrical strain gauges (SG). The resistances for SGs are very small, their changes are measured through a signal amplification measurement system so that the precise change in resistivity can be measured. The amplified signal is finally displayed to a screen where it can be interpreted by an observer. A continuous change in strain is recorded as a dynamic progression, and a recorder is used to display and record continual changes in strain with time in terms of output current.

For a steel shaft, the influence of high torsion moment will twist the shaft along the force plane. These stresses are observable on the shaft surface and are detectable using the strain gauges (see Figure 5.8). The shaft, initially non-stressed with SG element parallel to the surface, is loaded with torsion moment due to friction and the SG element is deformed to an angle with the shaft axis.

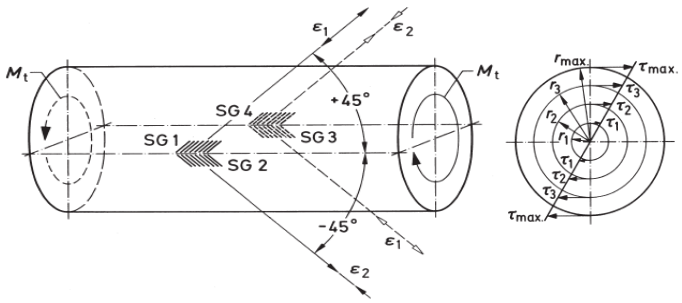

Figure 5. 8 - Strain gauge deformations on a torsion shaft [22]

The Wheatstone bridge setting used for the SGs is a full bridge circuit (two half bridges at 180° on the shaft) with transfer of signals from the SGs to the controller via a wireless data transfer module. The decision to use a wireless transfer is based on the experiences during initial test runs with slip rings. The noise in the signal from the slip ring bushes due to lateral shaft vibrations was found to be very high and noise separation from useful signal was too difficult to carry out. A wireless module, unlike slip rings, is mounted directly near the strain gauges and eliminates any noises due to shaft vibrations.

Referring to Figure 5.8, the maximum shear stress at the strain gauge is calculated by:

$$\tau_{max} = \frac{1}{2}\epsilon_{45} \,.\, G \tag{71}$$

ϵ_{45} = Measured Strain (m/m)

G = Shear Modulus (N/mm^2) = $\frac{E}{2}.\frac{1}{1+\nu} = 0.393\ E$

The corresponding torsional moment can be determined from equation 5

$$M_t = \tau_{max}.S_P \tag{72}$$

S_P is the polar section modulus,

$$S_P = \frac{\pi.d^3}{16} \tag{73}$$

With that, for a full bridge, the torsional moment becomes

$$M_t = \frac{1}{2}\epsilon_{45} \,.\, G.S_P \tag{74}$$

And the friction work in joules (also equivalent to N-m) is given below. n is the RPM

$$W_{Friction} = 2.\pi.n.M_t \tag{75}$$

A schematic of the strain gauges and the data module is presented in Figure 5.9. To protect the strain gauges from the flow of mud, an aluminum cap cylinder with sealings is placed around them. The selected wireless module is also fluid-resistant (IP67).

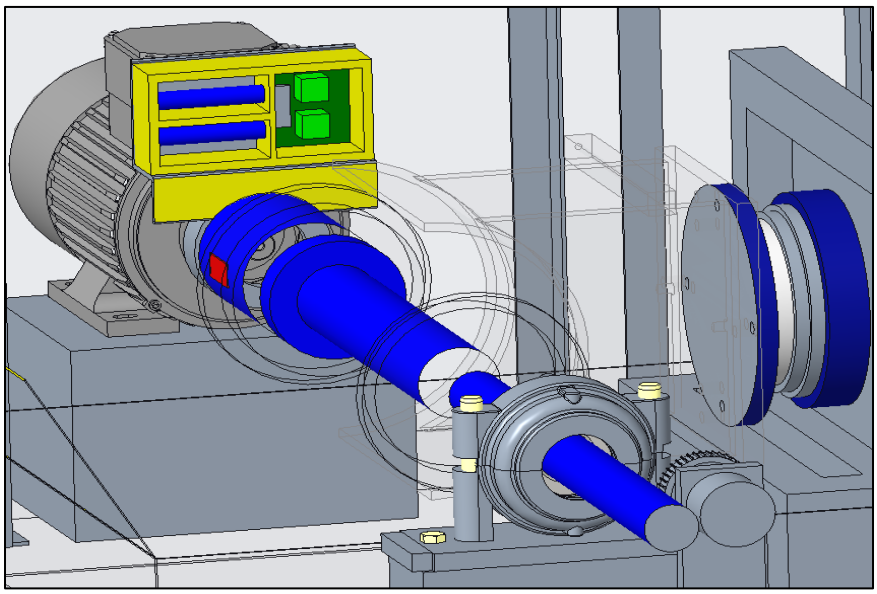

Figure 5. 9 - Friction torque strain gauges (in red) along with the data module (in yellow)

5.3.5.2. Contact load sensor

In addition to the pressure transducer at the pneumatic piston (which provides the press force), the necessity of an added load sensor just behind the c-section arises from the presence of:

1. Vibrations while rotating and reciprocating
2. Residing friction force between the tool joint and casing that adds more compression when the contact is not centralized due to rotation and reciprocating movements

Under these conditions, it is important to know the real residing contact force at the C-section to be able to accurately determine friction factor and wear factor. A load sensor, therefore, was installed directly behind the C-section by grinding a small opening in the pneumatic piston and putting the load sensor between the C-section and the piston without any threads in between. This ensured that the applied press force and the added compression from tool joint rotation is observed directly at the load sensor without hindrances from threads.

A schematic of the load cell placement is presented in Figure 5.10. Similar to the friction torque system, the load cell is also water proof against the flow of mud.

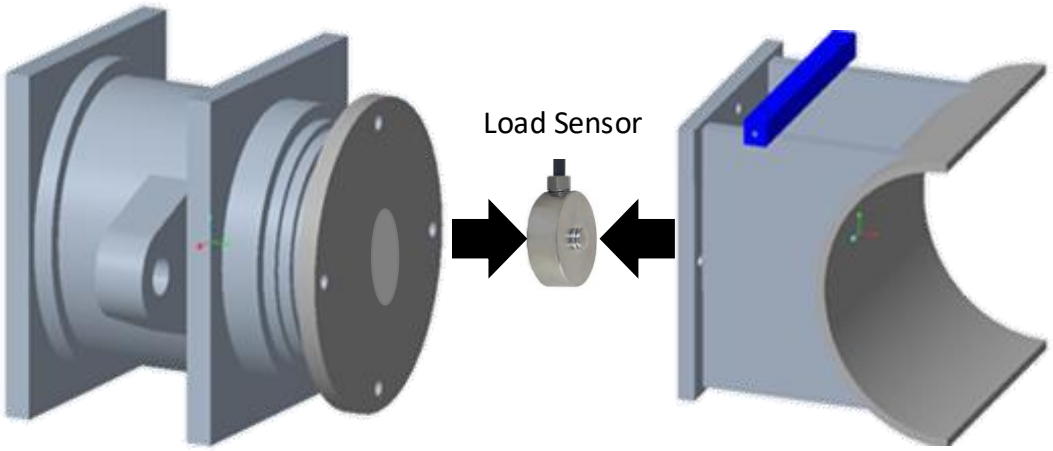

Figure 5. 10 - Placement of a load sensor between the C-section and the pneumatic piston

5.3.5.3. Operating panel and display unit

The operating panel of the frame includes a data recorder and a display of output parameters. Shaft rotating speed, pneumatic pressure in the piston, hydraulic pressure in the reciprocating piston and the total contact force at the casing C-section is displayed in real time. The signal from the strain gauges is displayed in another Tab.

A layout of both operating tabs is presented from a calibration test in Figure 5.11. The smaller darker tab (on the right) is the operating and display module from the strain gauges (Strain in mS). The bigger tab and the parameters on the right are based on output signals from the speed encoder (RPM), pneumatic pressure transducer (bar), hydraulic pump pressure (bar) and the load sensor behind the casing specimen (KN).

Figure 5. 11 - Layout of the display and operating panel

5.4. Frame assembly and safety features

Based on the wear frame design in Figure 5.2., the actual frame after modification and installment of system components is presented in Figure 5.12. Additional pictures of the frame under test conditions are provided in Appendix 11.18.

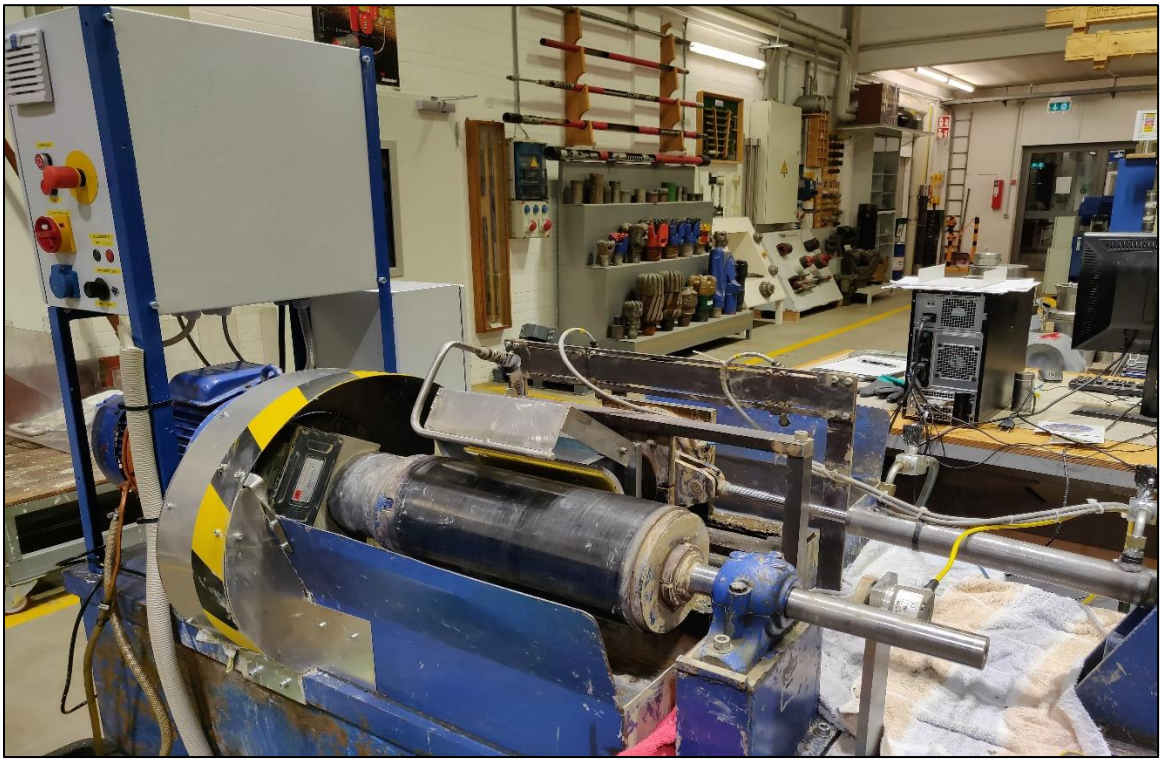

Figure 5. 12 - Final stand of the wear frame for tests

Some features were also added to ensure operator safety during tests. The entire contact area was covered with a Plexiglas lid for protection against mud spraying and to avoid any direct operator access to the contact area while the test is in process.

Emergency shut-off switches were placed on both sides of the machine and on the operating panel. For added safety, it is forbidden to operate the wear frame under dry conditions (especially in glass fiber and carbon fiber wear tests due to material dust).

5.5. Comparison of the wear frame with API casing wear standard

As per literature review, API standard 7CW is the only direct standard for full-scale wear determination due to casing-TJ contact. Available from June 2015, it provides experimental basis to determine wear factor for field wear simulations.

5.5.1. Procedure and schematic

1. The tooljoint cylinder to be tested is mounted on a shaft and rotated at a speed of 155 rpm.
2. The tooljoint is impinged against the “polished” inner wall of casing at a pre-defined side load and lateral movement speed.
3. A crescent shaped groove is worn into the inner casing wall. The test duration is 8 hours.
4. The depth of worn groove is measured at time intervals of 15, 30, 60, 120, 240, 360 and 480 minutes.
5. A prescribed side load value of 3000lbf/ft is applied based on contact length
6. Drilling fluid is sprinkled through a nozzle at the contact area.
7. Based on worn volume and frictional work done, a wear factor is determined using relations defined in the standard.

The API 7CW is based on the experimental study by R.W.Hall and Mauer Engineering in 2005 (detailed version in section 2.2.7). The test standard is laid out for TJ-casing wear as well as for TJ-formation contact wear.

A schematic of the test is provided in Figure 5.13.

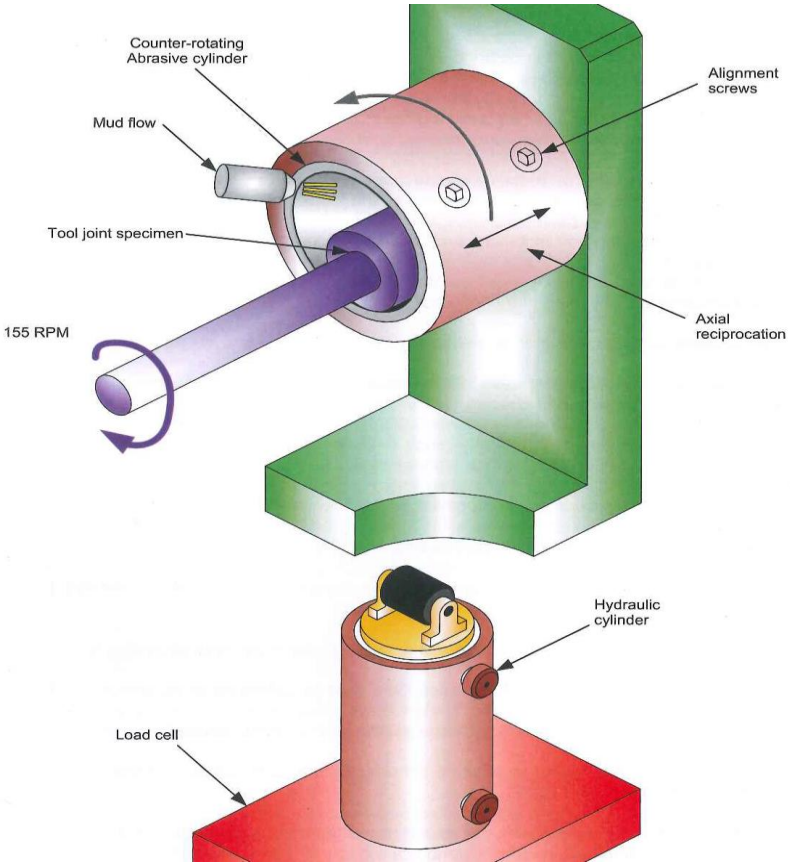

Figure 5. 13 - Operation schematic of a wear test as per API 7CW [59]

The capabilities of both wear frame designs are tabulated in a direct comparison in Table 5.1.

Table 5. 1 - Operational capabilities of API 7CW and ITE wear frame

	API standard 7CW Wear Frame	ITE wear frame
Casing specimen can be tested full scale	**X**	**X**
The contact geometry, material roughness, specimen alignment and contact conditions are designed close to field conditions.	**X**	**X**
Galling, abrasion and combined wear can be tested on the casing.	**X**	**X**
Fluid flow is applied at the contact to remove metal debris and to cool the specimens.	**X**	**X**
Method can be used for qualitative & quantitative mesurements.	**X**	**X**
Method can measure wear over longer contact intervals.	**X**	**X**
Wear factor based on worn volumes over time	**X**	**X**
Friction factor based on dry, wet and lubricated contact		**X**

6. Wear frame sensitivity and stress distribution simulation

Before the beginning of wear tests, the load, torque and speed sensors were calibrated and several test runs were made with the wear frame. The goal was to evaluate the effects of individual parameters on the combined dynamic process (rotation, side force and reciprocation altogether).

6.1. Calibration of contact load under different operating parameters

6.1.1. Analysis of contact load at a single contact location on tool joint

The load cell behind the casing C-section and the pressure transducer were both calibrated against external load and pressure sensors to obtain accurate measured values. After calibration, a summary of the measured side force corresponding to different applied pressure values is presented in Figure 6.1. The values plotted were measured at a single contact location upon the tool joint.

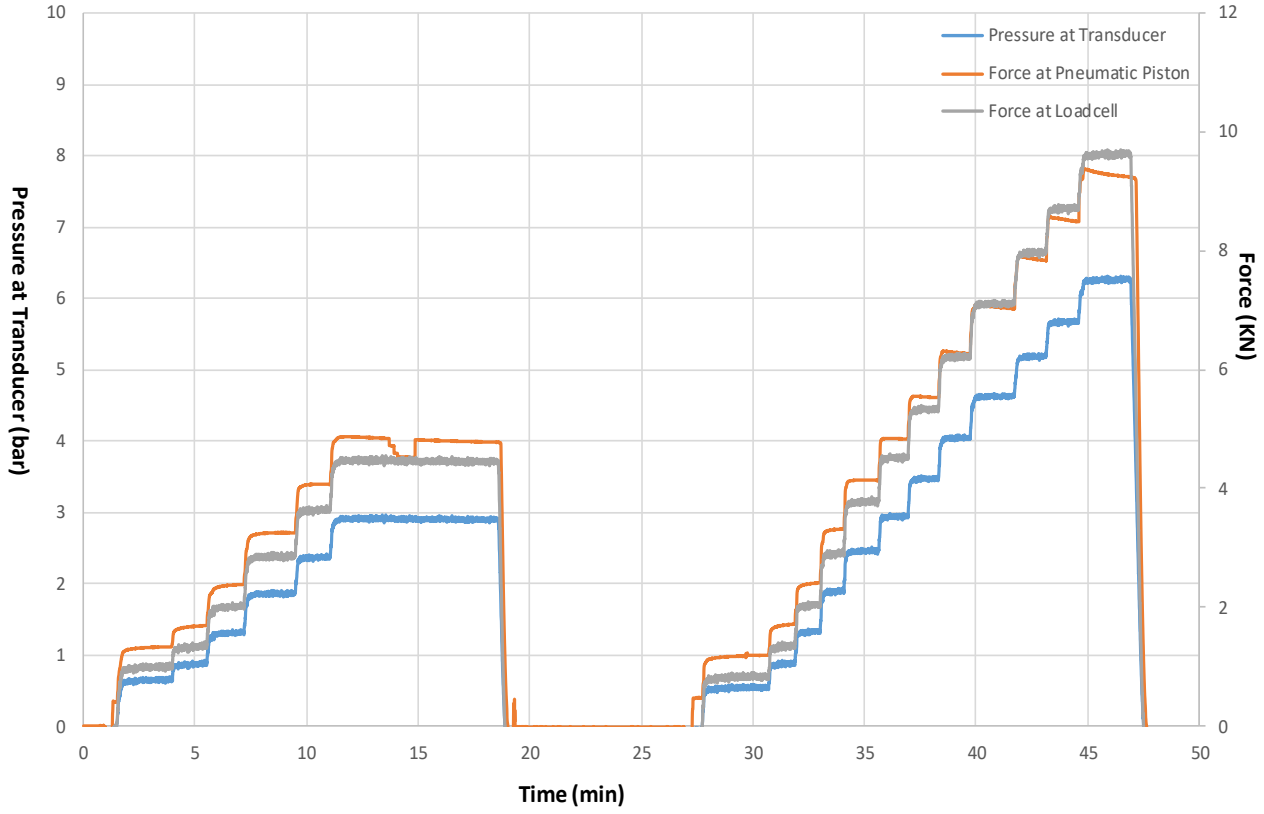

Figure 6. 1 - Measured side force at different pressure values (at a single location)

A close up of the above graph at a pressure of 3 bars is presented in Figure 6.2. This is shown in particular here because all the wear tests conducted so far have been made at the same applied pressure of 3 bars. The static force (derived from piston area and pressure at transducer) and the average force measured at the load cell are in good agreement at approx. 4.7KN.

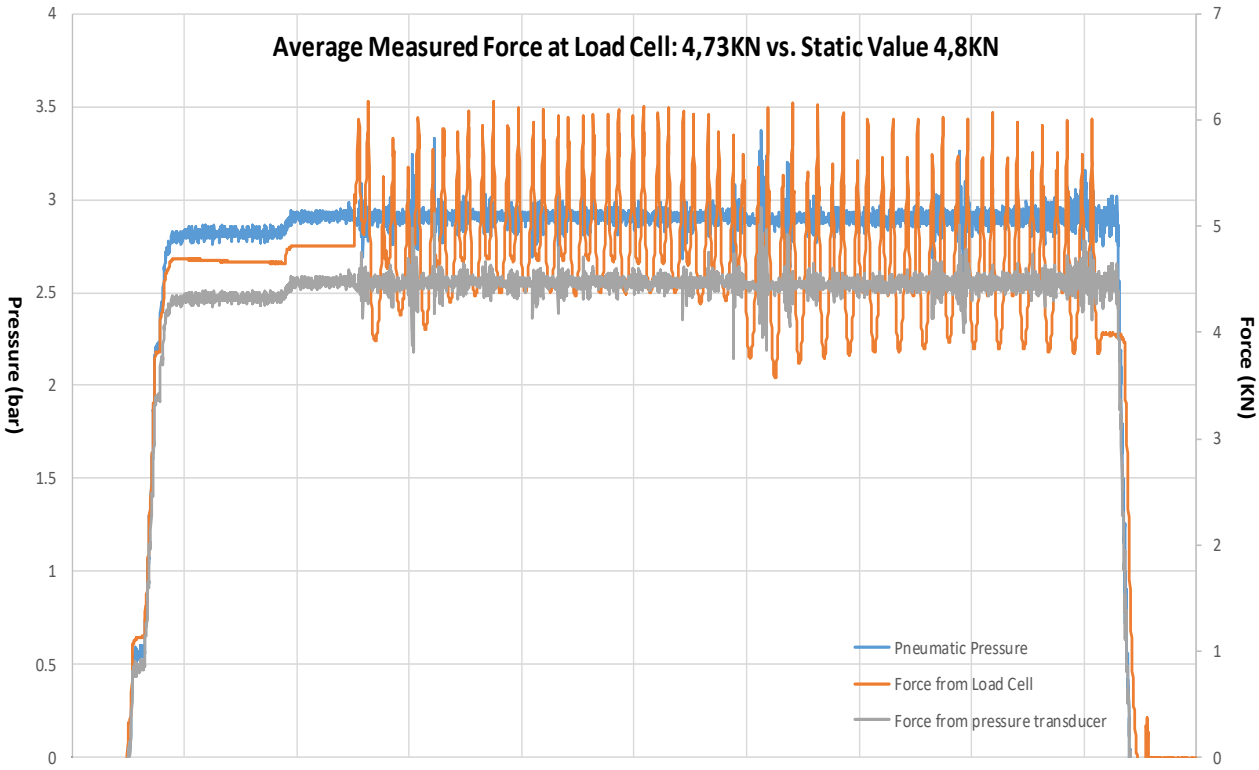

Figure 6. 2 - Measured side force at 3 bars pressure

6.1.2. Analysis of contact load at multiple contact locations on tool joint

The tool joint is a hollow elastic metal cylinder that will undergo slight bending when stressed with high lateral loads when mounted on the shaft in a concentric position. Therefore, it is important to identify any significant fluctuations and deviations due to the virtue of the location of the C-section on the tool joint. Repeated measurements on a single location are in good agreement with each other. However, changes in location caused minor fluctuations in measured force values and differences in measurements were observed in comparison to the force from the pressure transducer.

Upon repeated measurements, this is attributed to slight bending in the tool joint at the middle due to the high contact force upon it. A schematic of the tool joint fixing discs provides a better understanding of the phenomenon in Figure 6.3.

The error is slightly higher for lower pressures which are due to inaccuracies of the pressure transducer while measuring very low pressures (0.5 to 1.5 bar). For higher pressures, the error is mainly due to slight bending in tool joint and is significantly lower. At 3 bar pressure (selected test pressure), the error was about 1% with 8.4% fluctuation in reading. A summary of the static force calibration runs is presented in Table 6.1.

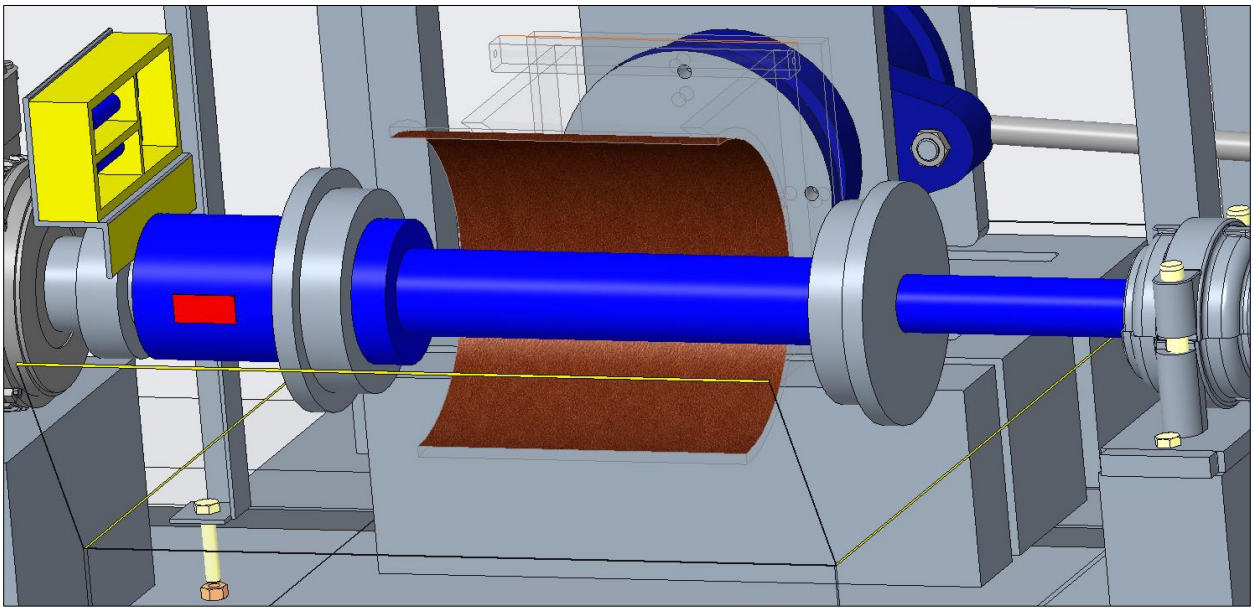

Figure 6. 3 - Fixation of tool joint resulting in slight bending in the middle

Table 6. 1 - Calibration runs at different locations with static load

Static Force								
Pressure at transducer (bar)	Force at Load Cell Run 1, Middle (KN)	Force at Load Cell Run 2, Middle (KN)	Force at Load Cell Run 3, Middle (KN)	Force at Load Cell Run 4, Left (KN)	Force at Load Cell Run 5, Right (KN)	Force from pressure Transducer (KN)	Error with Pressure Transducer (%)	Fluctuation in Value (%)
0.00	0.00	0.00	0.00	0.00	0.00	0.00	0.00	0.00
0.50	0.78	0.81	0.71	0.59	0.79	0.79	7.59	13.04
1.00	1.39	1.30	1.40	1.46	1.46	1.58	12.96	7.33
1.50	1.97	2.03	2.24	2.15	2.19	2.38	12.26	12.76
2.00	2.98	2.89	2.95	2.94	2.69	3.17	9.60	3.06
2.50	3.63	3.72	3.90	3.87	3.70	3.96	5.19	7.20
3.00	4.55	4.77	4.95	4.91	4.76	4.75	0.77	8.41
3.50	5.46	5.77	5.97	6.01	5.67	5.54	4.04	8.90
4.00	6.43	6.77	6.91	6.89	6.53	6.33	5.54	7.16
4.50	7.35	7.69	7.89	7.93	7.50	7.13	7.11	7.06

The values in Table 6.1 are plotted in Figure 6.4 for comparison ease. Slight fluctuations at lower pressures can be observed in the plot. The pressures were applied at time intervals of 10 min for each value.

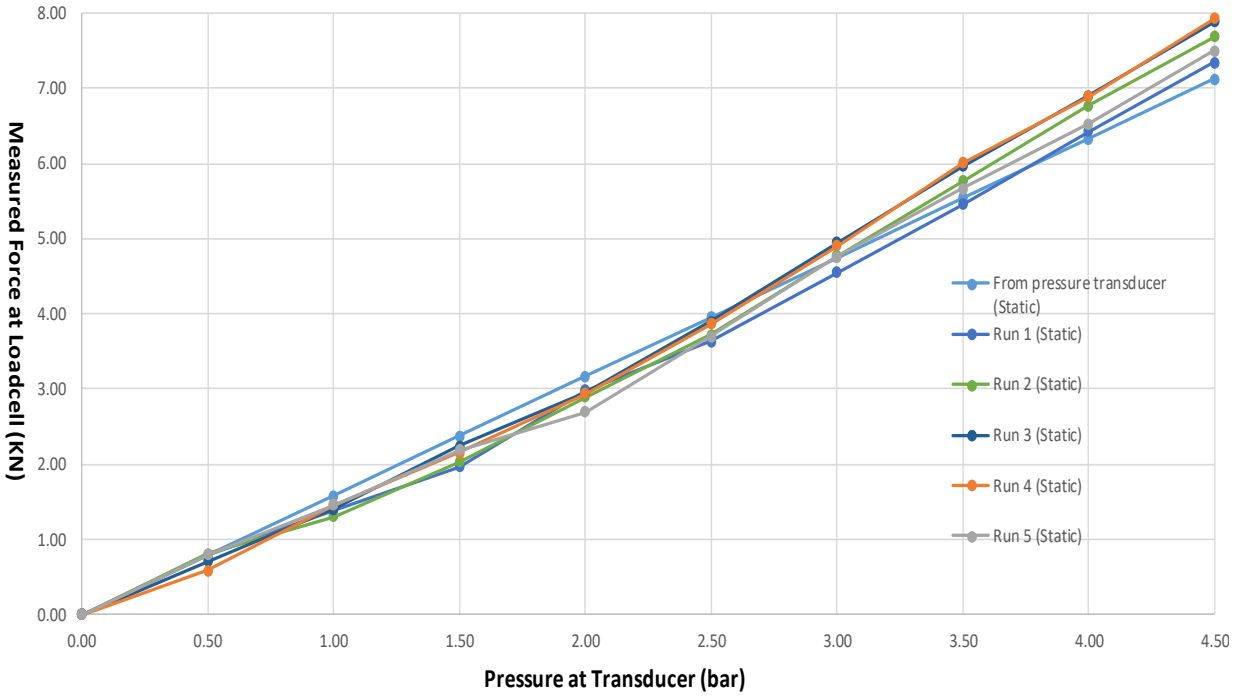

Figure 6. 4 - Plot of static load calibration runs at different locations

6.1.3. Analysis of contact load while sliding (without TJ rotation)

This calibration phase was to identify the effects on contact force solely due to reciprocation. For this purpose, the casing C-section was placed in continuous reciprocating contact with the tool joint under different pressures, but without rotation. The observed results were very similar to the ones obtained by applied static loads at individual locations. A summary of three calibration runs for reciprocating loads is presented in Table 6.2.

Table 6. 2 - Calibration runs at while reciprocating at different loads

Reciprocating Movement						
Average Pressure at Transducer (bar)	Force at Load Cell Run 1 (KN)	Force at Load Cell Run 2 (KN)	Force at Load Cell Run 3 (KN)	Force from average pressure at Transducer (KN)	Error with Pressure Transducer (%)	Fluctuation in Value (%)
0.00	0.00	0.00	0.00	0.00	0.00	0.00
0.52	0.80	0.70	0.92	0.83	2.73	26.94
1.01	1.39	1.34	1.49	1.61	14.25	10.68
1.51	2.30	1.95	2.17	2.40	11.97	16.21
1.99	3.10	2.68	2.90	3.15	8.72	14.46
2.56	3.84	3.50	3.77	4.05	9.25	9.14
2.99	4.77	4.43	4.52	4.74	3.67	7.40
3.52	5.43	5.34	5.19	5.57	4.81	4.41
3.96	6.30	5.82	5.85	6.28	4.73	7.95
4.50	6.98	6.61	6.61	7.12	5.75	5.52

The values in Table 6.2 are plotted in Figure 6.5 for comparison ease. Slight fluctuations at lower pressures can be observed in the plot. The pressures were applied at time intervals of 10 min for each value.

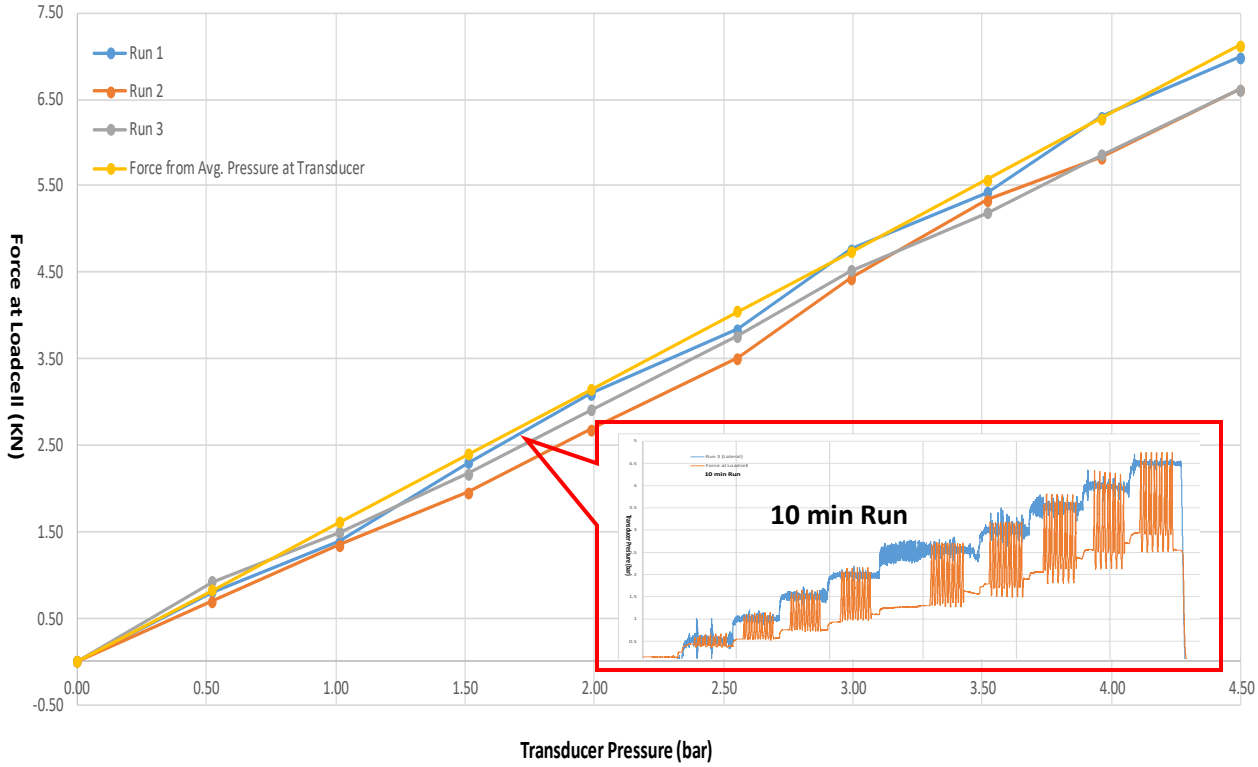

Figure 6. 5 - Plot of reciprocating calibration runs at different pressures

6.1.4. Analysis of contact load while rotating (without reciprocation)

The next phase of calibration runs was to analyze the influence of rotation upon the contact force. For this purpose, the casing specimen was set in contact with the rotating tool joint, but at a fixed location. Some elements that were anticipated to cause fluctuations and differences from the static load values were:

1. compression imparted due to friction upon rotation
2. added compression due to friction force at the contact when the centers of TJ and casing are not aligned
3. increased vibrations at higher speeds (100-120 RPM)

To reduce the errors and keep the casing specimen center close to the plane of the tool joint center, a “stabilization frame” was put over the cylinder (Figure 6.6). The sole purpose of this frame was to avoid any big jumps during high-speed vibrations and “lifting-up of the casing specimen” due to high pressure.

It is notable at this point that some of these errors arising due to vibrations and misalignments of TJ and casing centers cannot be avoided due to the required nature of wear mechanism. The freedom of movement in axial (reciprocation) and lateral (side force) directions are necessary as per design criteria. Any fixations on the casing or tool joint will deviate the wear frame design from representing field conditions.

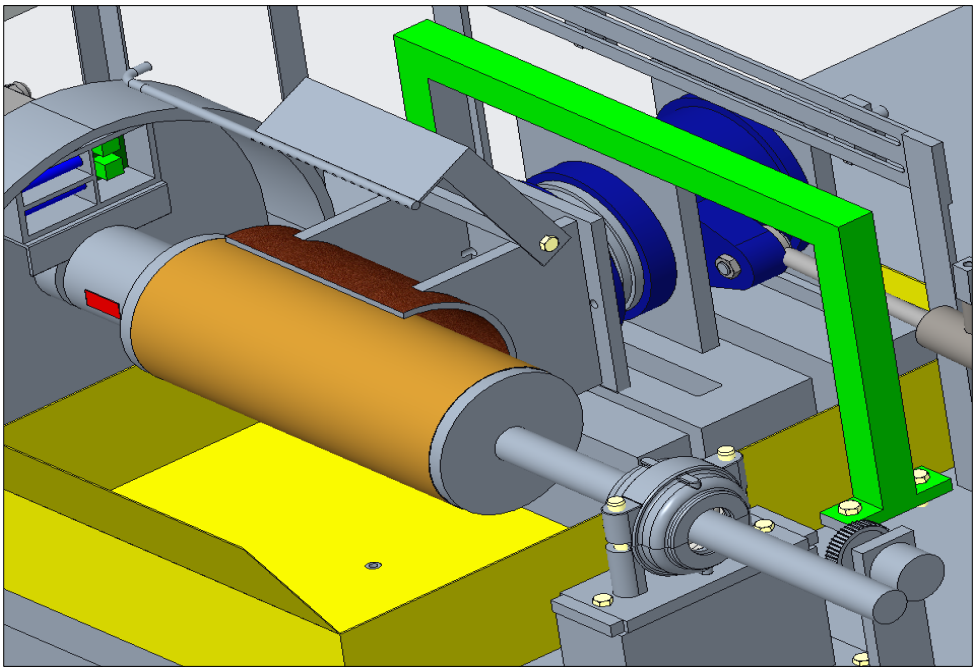

Figure 6. 6 - Stabilization frame (in green) to minimize vibrations

The measured force at the load cell upon rotation was significantly higher than the calculated force from the pressure transducer. Multiple runs were made at different pressure time intervals (0.5 min, 1 min and 10 min) and similar force values were observed after each run without high fluctuations (about 10% at higher pressures).

A table summarizing the calibration runs is presented below. All force values were taken after adjusting the zero/TARE point for pre-existing forces in the pneumatic piston.

Unlike static and sliding runs where measured forces were similar, a general 30% increase in average force from load cell was observed at 100RPM. At 3 bars (applied test pressure), the increase in contact force is 29% (6.7KN in comparison to 4.8KN from pneumatic pressure transducer).

Some calibration runs made at 75 RPM also yielded similar results. Since the planned wear tests were to be conducted at 100RPM (or higher), further calibration runs at lower speeds were not carried out. After repeated similar force readings at 100RPM (about 6.7KN), it was decided to take this value as the contact force during the actual wear tests, unless the next calibration phase (rotation with reciprocation) results in different force values.

Table 6. 3 - Calibration runs at while rotating at a single location at different pressures

Rotation Only at 100RPM									
Force App. Time	1min	1min	1min	10 min	10 min	10 min			
Average Pressure at Transducer (bar)	Force at Load Cell Run 1 (KN)	Force at Load Cell Run 2 (KN)	Force at Load Cell Run 3 (KN)	Force at Load Cell Run 4 (KN)	Force at Load Cell Run 5 (KN)	Force at Load Cell Run 6 (KN)	Force from average pressure at Transducer (KN)	Error with Pressure Transducer (%)	Fluctuation in Value (%)
0.00	0.00	0.00	0.00	0.00	0.00	0.00	0.00	0.00	0.00
0.44	1.19	1.28	1.31	1.14	1.25	1.19	0.82	33.37	13.89
1.03	2.41	2.79	2.44	2.37	2.40	2.40	1.67	32.29	16.88
1.45	3.66	3.78	3.52	3.52	3.25	3.53	2.37	33.19	15.09
2.00	4.71	4.75	4.53	4.81	4.36	4.81	3.18	31.72	9.60
2.50	5.80	5.74	5.72	5.75	5.29	5.78	3.97	30.09	8.99
3.01	6.87	6.89	6.72	6.93	6.32	6.50	4.78	28.71	9.12
3.47	8.00	7.71	7.88	8.19	7.38	7.45	5.56	28.41	10.46
4.00	8.68	8.60	8.86	8.96	8.02	8.12	6.34	25.81	10.90
4.45	9.15	9.51	9.58	-	9.53	9.59	7.06	25.52	4.70

A layout of a calibration run (Run 6 from the above table) at 100RPM is presented in Figure 6.7.

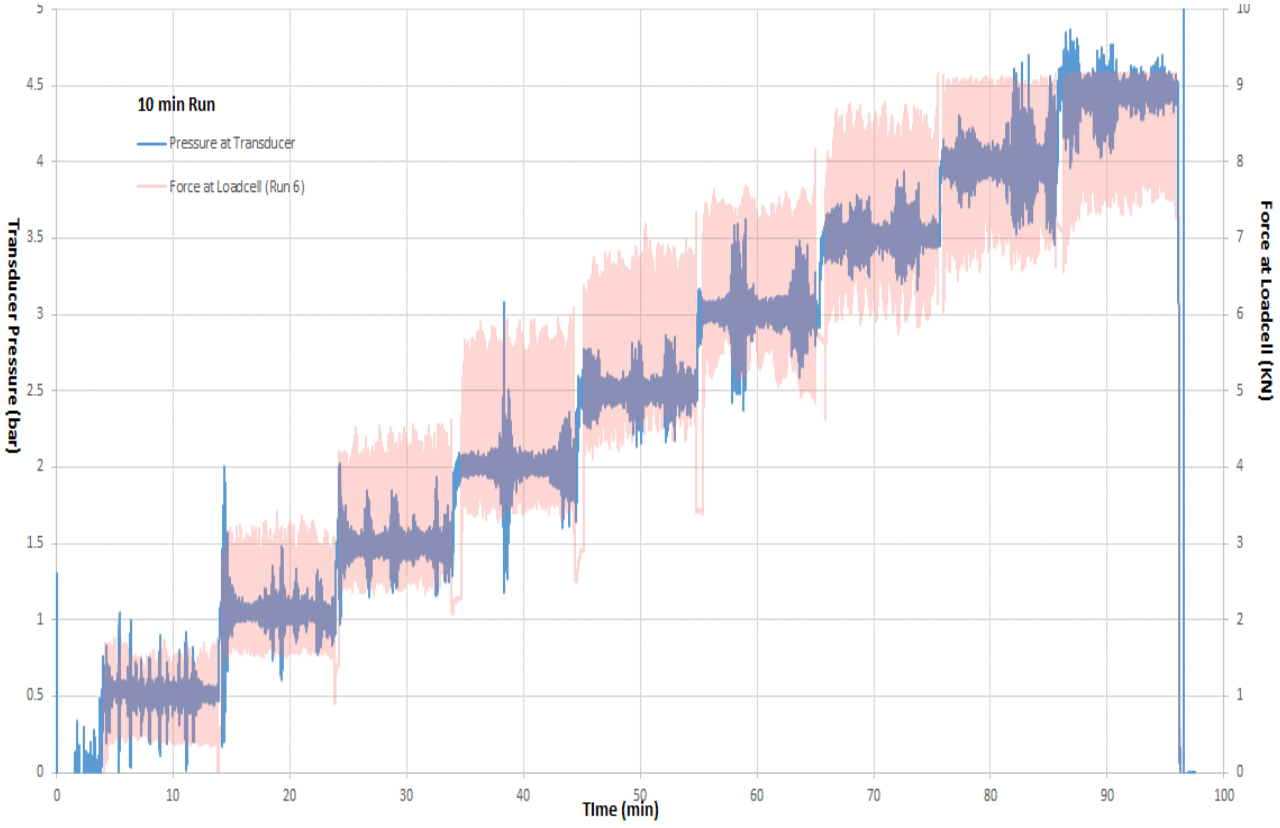

Figure 6. 7 - Plot of a calibration run at 100RPM at different pressures

6.1.5. Analysis of contact load while rotating with reciprocation

The last phase of calibration runs was carried out to identify if the contact force increments observed during the rotation phase remain the same with added reciprocation. 10 calibration runs were made to identify any additional variation due to reciprocation effects, with contact intervals of 0.5 min, 1 min and 10 min for each force value. Based on previous calibration runs with reciprocation motion only, it was expected that added reciprocation will only cause minor variations (due to tool joint cylinder bending).

Table 6.4 shows the contact force values observed during the "full test calibration". The term full test calibration is used in terms of the argument that the planned wear tests (for all materials) are to be carried out at 3 bars of applied pneumatic pressure (corresponding to 6.7KN or 1500lbf), 100RPM rotating speed and with reciprocation movement. The observed forces were very similar to those observed during the rotation phase, proving again that reciprocation only has a minor effect on side force for the wear frame.

Table 6. 4 - Full test calibration runs at different pressures

Full Test Calibration												
Force App. Time	0,5 min	0,5 min	1min	1min	1min	1min	10 min	10 min	10 min			
Average Pressure at Transducer (bar)	Force at Load Cell Run 1 (KN)	Force at Load Cell Run 2 (KN)	Force at Load Cell Run 3 (KN)	Force at Load Cell Run 4 (KN)	Force at Load Cell Run 5 (KN)	Force at Load Cell Run 6 (KN)	Force at Load Cell Run 7 (KN)	Force at Load Cell Run 8 (KN)	Force at Load Cell Run 9 (KN)	Force from average pressure at Transducer (KN)	Error with Pressure Transducer (%)	Fluctuation in Value (%)
0.00	0.00	0.00	0.00	0.00	0.00	0.00	0.00	0.00	0.00	0.00	0.00	0.00
0.49	1.03	1.16	1.14	1.16	1.26	1.08	1.15	1.20	1.29	0.78	33.13	22.35
0.98	2.35	2.55	2.27	2.32	2.39	2.56	2.45	2.45	2.58	1.56	36.08	12.71
1.48	3.61	3.47	3.68	3.79	3.75	3.66	3.68	3.59	3.47	2.34	35.54	8.82
2.01	4.94	4.75	4.99	4.76	4.76	4.79	4.64	4.67	4.54	3.18	33.13	9.48
2.44	6.09	5.63	6.01	5.82	5.86	5.74	5.62	5.58	5.26	3.87	32.49	14.49
3.03	6.79	6.90	6.93	6.94	6.82	6.68	6.45	6.50	6.70	4.80	28.81	7.21
3.43	7.92	7.55	8.00	7.80	7.94	7.59	7.36	7.25	8.15	5.43	29.73	11.73
4.02	8.64	8.39	8.62	8.51	8.60	8.55	8.09	8.31	9.08	6.37	25.38	11.57
4.46	9.45	9.09	9.15	9.20	9.27	9.20	9.10	8.46	9.31	7.07	22.63	10.86

A layout of a calibration run (Run 8 from the above Table) is presented in Figure 6.8, which looks similar to the plot in Figure 6.7. This confirms that rotation is the most critical factor affecting the contact load.

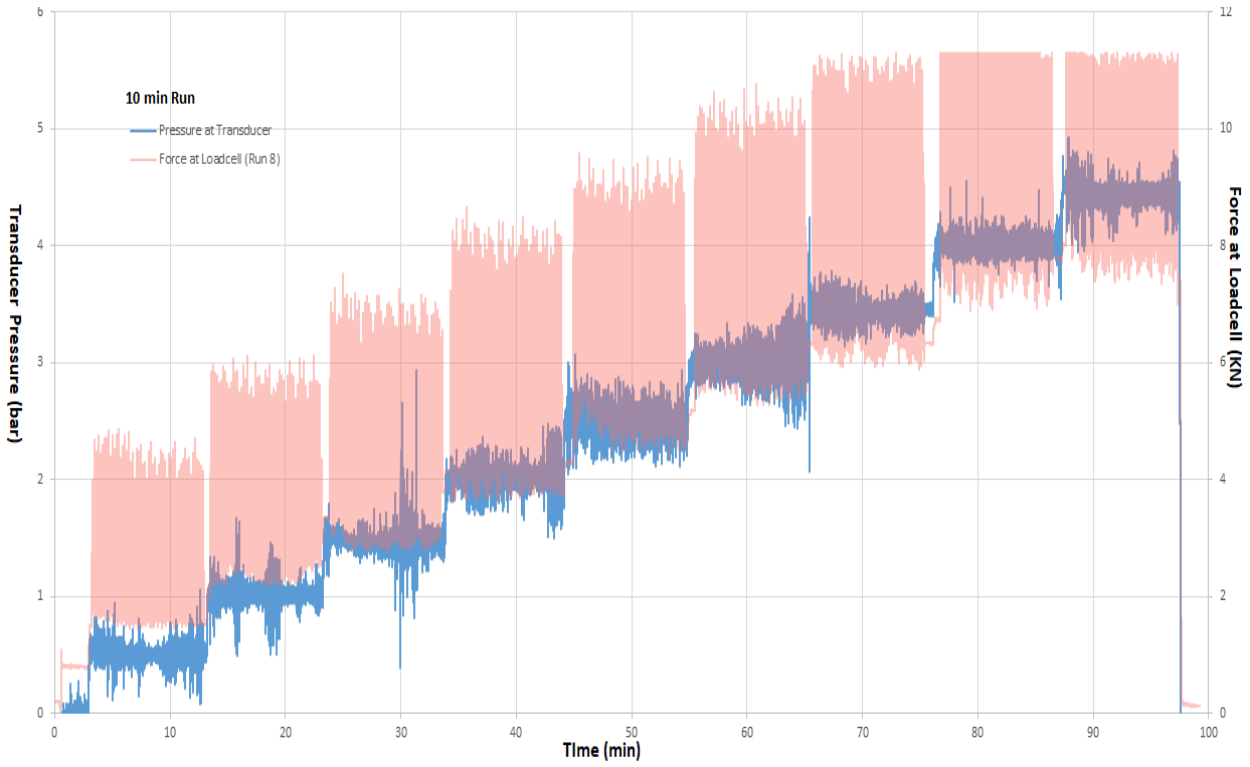

Figure 6. 8 - Plot of a full test calibration run at different pressures

The measured force values of all calibration runs provide a force envelope under different pressures for static and rotating conditions (shown in Figure 6.9). As will be seen in Chapter 7, the observed forces during wear tests remain within this force envelope. As mentioned earlier, some associated fluctuations and vibrations cannot be avoided with the wear frame as the tool joint center cannot be held parallel to casing center due to freedom of rotation and reciprocation.

The presence of an added frictional and vibrational force due to rotation also highlights the significance of experimentally determining wear behavior for casing wear. Although effects of drillstring vibrations are not an integral part of the study, it is noteworthy that even slight vibrations between the tool joint and casing can add considerably to the total side force. In this regard, the concept of measuring sideforce solely based on drillstring tension may yield inaccurate results for a drillstring rotating at high speeds.

Wear standards (such as API 7CW) directly pertaining to casing wear are relatively new and do not account for such vibrations. This points out to an advantage with the ITE wear frame that the added force due to uncontrollable discrepancies can be recognized and categorized in real time. Based on the observations during this study, it is also recommended for experimental wear studies to measure the side force directly behind the contact and use the total measured value as basis for wear calculations.

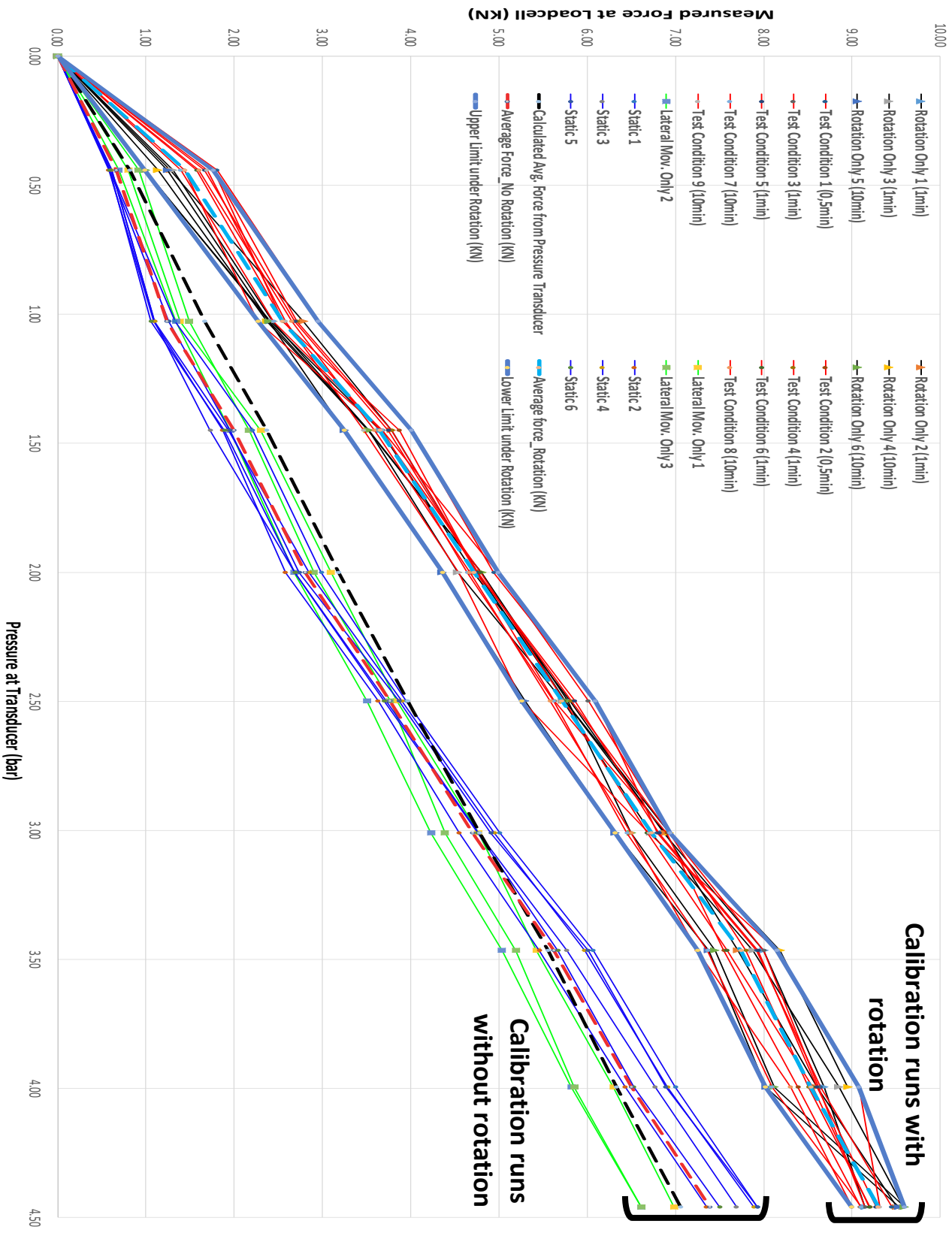

Figure 6. 9 - Plot of a full test calibration run at different pressures

6.2. Sensitivity of friction torque sensor

For measurement of friction torque, the two v-shaped X-rosettes at 180° on the shaft are subjected to bi-axial stresses. For accurate measurements, however, the strain gauge axes must correspond to the principal stress directions. A layout of the strain gauge positions on the shaft w.r.t the principal side force direction is presented in Figure 6.10.

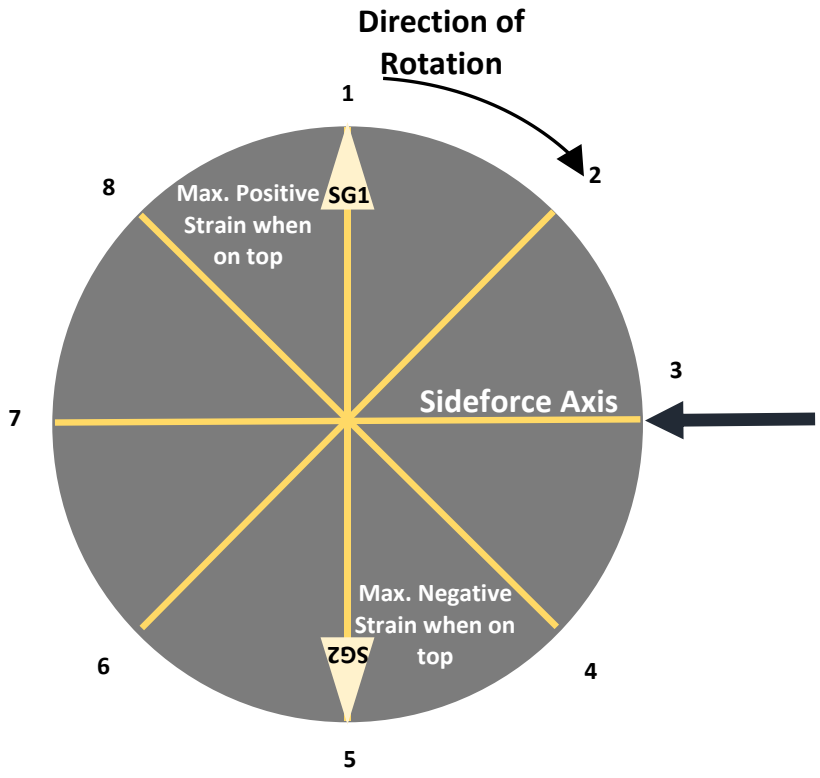

Figure 6. 10 - Location of strain gauges on the shaft

From such a configuration, there is always a shift in deformation pattern as the strain gauge axes (points 1 and 5) become parallel and then perpendicular to the side force axis. When the stain gauges are aligned perpendicular to the side force axes (the position in the Figure), a maximum positive or negative strain value is observed ($|\epsilon 1| = |\epsilon 2|$). This is the case when points 1 or 5 are on the top. On the other hand, a minimum signal (theoretically zero) is observed when the strain gauge axes are aligned parallel to the side force axis (when points 1 or 5 are aligned with contact point.

Some strain signals were still observed (about 10 µ-strain) when the strain gauges were aligned parallel to the side force axis at higher forces (beyond 6KN). Assuming no inaccuracies due to positional asymmetries and with compensation of reverse-strains (because of a full Wheatstone bridge), this inaccuracy is due to the presence of minor bending strains in the shaft. As higher loads are applied on the shaft, especially at the hollow center location, the shaft undergoes minor

bending deformations. As noted for side force increments due to rotation in the previous sections, this slight error due to bending is difficult to remove as the tool joint cannot be rigidly mounted in the middle without causing complications for wear tests (e.g., losing flexibility of mounting and unmounting the tool joint).

For this reason, the two maximum strain measurements (with SGs aligned perpendicular to force axis) are considered and an average strain of the two is taken for friction torque measurements.

Figure 6.11 shows the response from the strain gauges during a wear test. An averaged value of the strain peaks for each of the 13 test phases (highlighted by the orange line) is used for friction factor and wear factor determination.

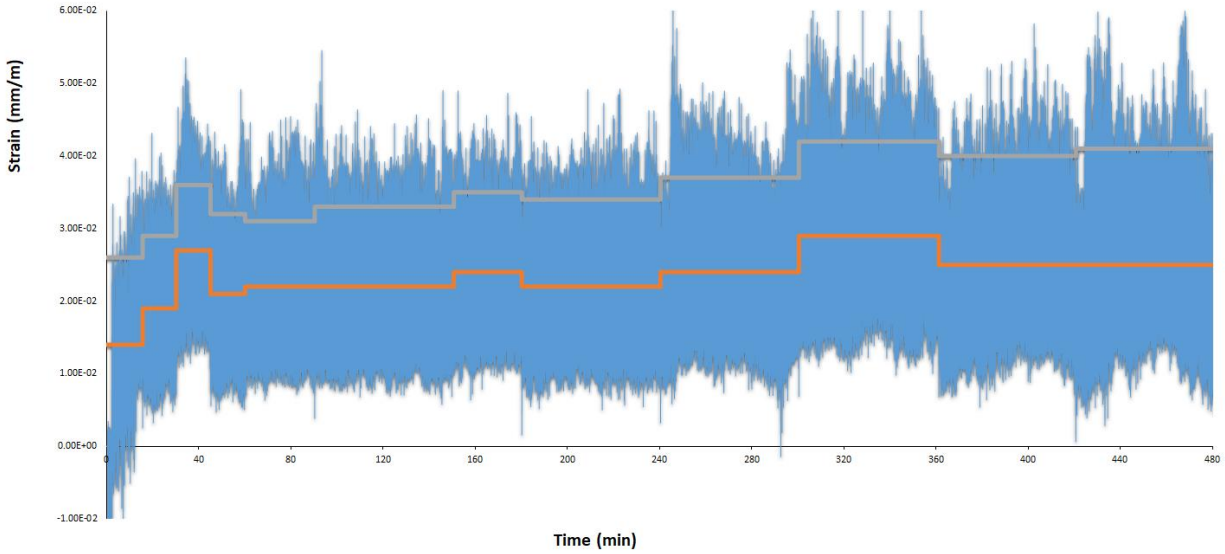

Figure 6. 11 - Strain gauge response: Average (orange) and peak values (gray)

6.3. Stress Distribution Analysis at the C-section

A basic ANSYS simulation was also carried out to anticipate the maximum friction shear stress acting on the C-section upon contact and rotation, and to track its propagation.

In order to be able to carry out the simulations in a short time interval (to simply track frictional stress), the imported geometries from Creo Parametric were simplified as much as possible. This involved importing the C-section and the tool joint, applying zero displacement to bring them in contact and allowing movement only in one axis direction (side force). A static structural analysis system was used with a coarser mesh.

Though the contact was automatically recognized upon removing displacement, some corrections had to be applied so as to create an initial “line” contact between the two elements (detection on Gauss contact) so that the materials do not move into each other upon contact.

This line contact is the area of maximum stress as after wear propagation, the increment in area results in a continuous decrease in stress.

The tool joint was selected as the “Contact Body” and the casing specimen as the “Target Body”. It was also configured to rotate the tool joint about a fixed axis (“fixed support”) with an input rotational moment (taken as the friction moment from calibration runs). The contact was defined as a frictional contact (μ = 0.3 for dry steel-on-steel contact).

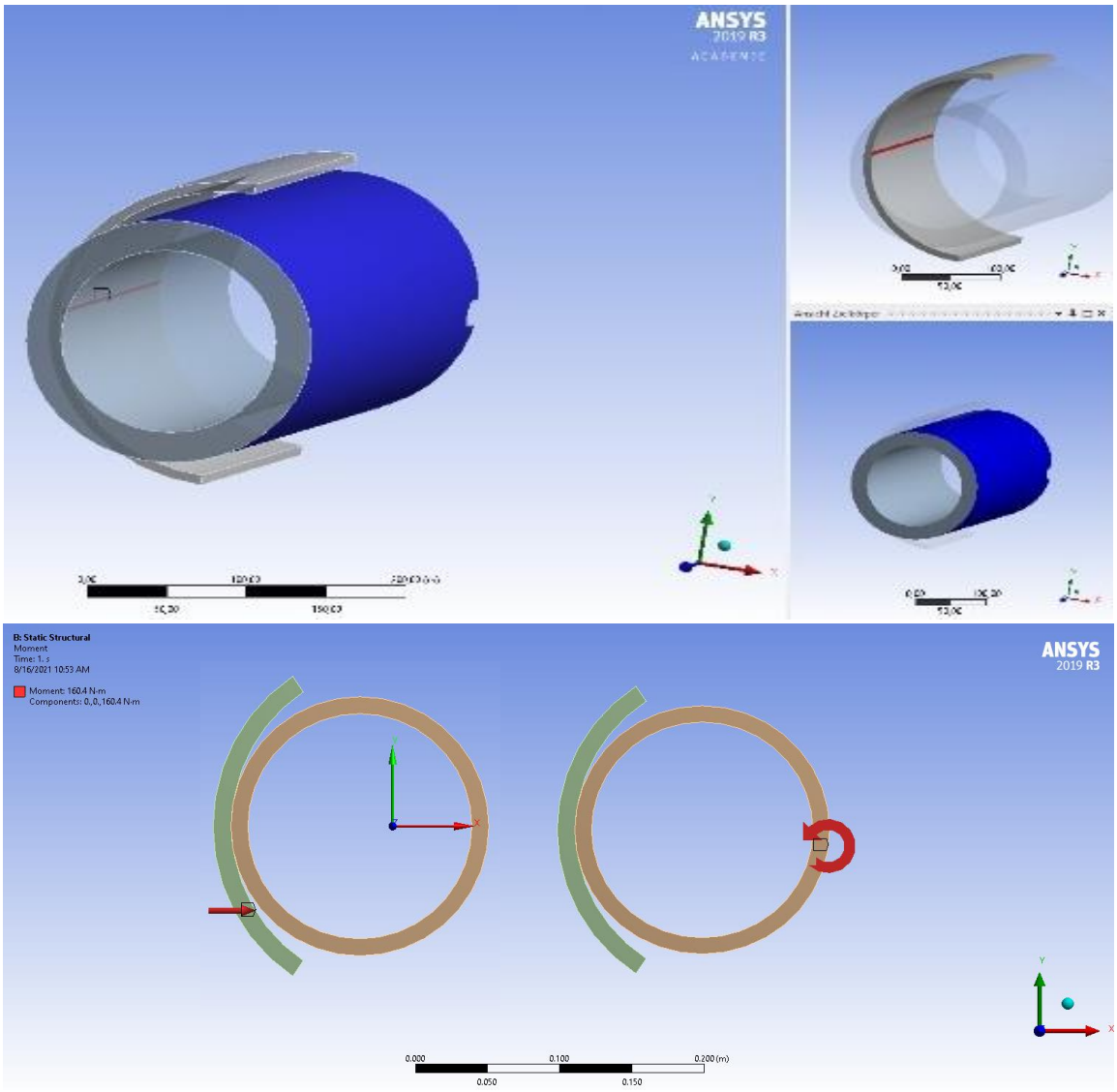

Figure 6. 12 - Defining the contact and moment between the tool joint and casing

Different pressures (corresponding to varying side forces) at different friction moments were defined into the model and resulting expected frictional stresses were noted. Thermal effects (to simulate friction heat propagation) were not included for simplicity reasons and because the fluid was expected to cool down the heating at the contact point.

Based on the configurations, the following calculated frictional stresses were noted at 6.7KN side force different friction torque values (Table 6.5). The values were then compared with actual frictional stresses calculated from the strain gauge response. Both range of values showed similarities and also provided an anticipated frictional stress range at a specific side force.

Table 6. 5 - Calculated frictional stress (ANSYS) vs frictional stress from strain gauges

Strain (µS)	Calculated Friction Moment (N-m.)	Max. Friction Stress, Strain Gauges (MPa)	Max. Friction Stress, ANSYS (MPa)
25	160	0.94	0.95
27	173	1.01	0.97
29	186	1.09	1.02
31	199	1.17	0.95
33	211	1.24	0.91
35	225	1.32	0.98

An example showing the frictional stress propagation at 160N-m frictional torque is presented in Figure 6.13. The Figure also shows stress propagation outwards from the contact line at the middle of the casing specimen. The simulations validated (with some % of error) the frictional stresses observed during the wear tests and the approach for determining friction factor using shaft torsion.

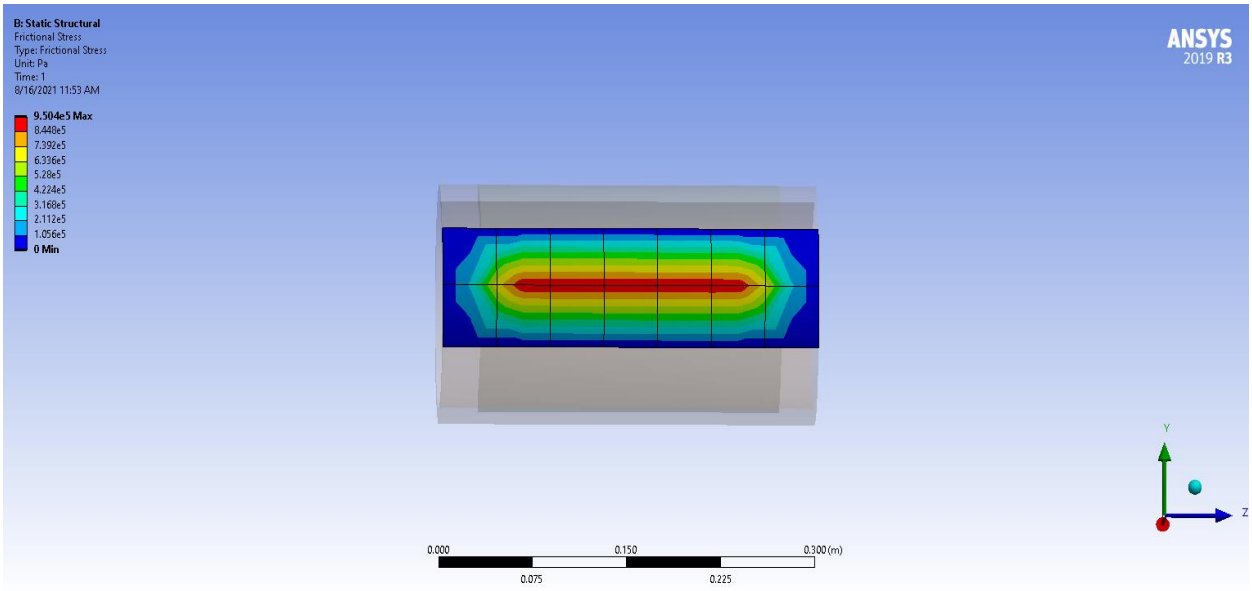

Figure 6. 13 - Frictional stress propagation between the tool joint and casing

7. Wear tests and comparisons

A total of 14 full wear tests, involving 8 hours of contact between the rotating steel tool joint and the casing specimen, were performed as a part of the experimental work. A summary of the work with the order of tests, number of tests, type of casing material and type of lubrication fluid is presented in Table 7.1.

Table 7. 1 - Base summary of the wear tests carried out

		Casing Material			Lubrication Fluid	
Order	**No. of Tests**	**Steel**	**Glass fiber**	**Carbon fiber**	**Water**	**Water-based Mud**
1	3	x			x	
2	4	x				x
3	3		x			x
4	2			x		x
5	1		x		x	
6	1			x	x	

7.1. Specimen characteristics and preparation

Based on the type of material, the C-section properties and preparation methods are presented below.

7.1.1. Steel C-section

All seven steel casing C-section specimens had the same material and geometrical properties, presented below:

Table 7. 2 - Properties of the base steel casing pipe

Parameter	Metric Units	Field Units
Outer Diameter (Average)	245.75 mm	9 5/8"
Wall Thickness (Average)	12.58 mm	1/2"
Inner Diameter (Average)	220.60 mm	8.685"
Measured Yield Strength	796 Mpa	115 ksi
Material	95HC	

The pipe specimen was selected based on the simulations and case histories reported in Chapter 4. The detailed measurements for pipe diameter, thickness, ovality and eccentricity is presented in Appendix 11.6.

The base pipe was cut to form cylindrical “rings” of pipe with a length of 240mm. From each ring, 3 C-section specimens with a circumferential length of about 257mm were cut. Since it is important to consider even minor (mm) of wear thickness, each C-section specimen was again measured for calculations (at square points shown in Figure 7.1 on the left).

The specimen was then welded at the back wall to the adapter and, after cooling, was ready to be mounted up on the wear frame. Measurements of wall thickness during the tests were performed using an ultrasonic wall thickness measurement device with an accuracy up to 1/100th of millimeter.

Figure 7. 1 - Measuring (left) and welding of the C-section on the adapter (right)

7.1.2. Glass fiber C-section

The glass fiber base pipe had the following material and geometrical properties:

Table 7. 3 - Properties of the glass fiber casing pipe

Parameter	Metric Units	Field Units
Outer Diameter (Average)	260.30 mm	10 ¼”"
Wall Thickness (Average)	4.90 mm	0.2"
Inner Diameter (Average)	250.5 mm	9.86"
Material	Fibered glass reinforced with thermoset epoxy layer	

Unlike steel casing, the glass fiber casing has a layered structure, from which the first 0.3 mm of inner wall thickness is formed of an amine-cured resin layer that will be worn first before the tool joint can reach the glass fiber. The glass fiber is impregnated with the cyclo-aliphatic resin structure. The material is brittle, with a density of around 2600 Kg/m^3. The cut length of the specimens was the same as for steel casings (240mm) with a circumferential length of about 230 mm.

Due to the brittle and non-metallic nature of the material, the cut C-sections could neither be welded upon the adapter nor could withstand the high contact force directly without any back

support. Therefore, another adapter with a “C-section support” and screw threads was used so that the glass fiber specimen could be screwed on to the adapter and would also have steel support to withstand the high contact forces.

A picture of the glass fiber specimen mounted on the adapter is shown in Figure 7.2.

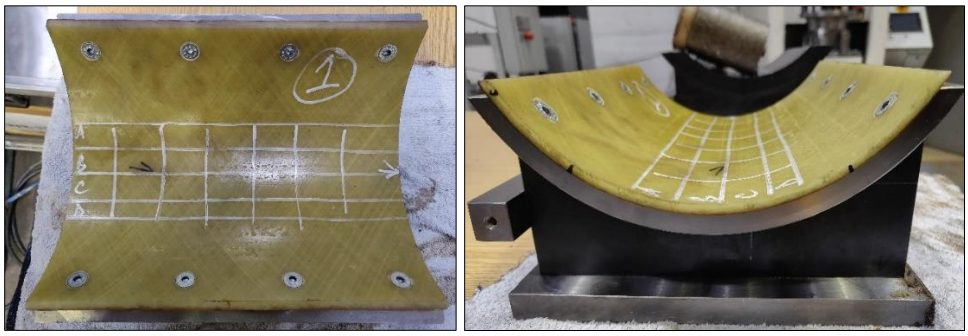

Figure 7. 2 - Measuring (left) and fastening of the glass C-section on the adapter (right)

Since the glass fiber material does not have an extruded (seamless) wall, its thickness cannot be measured accurately by the ultrasonic wall thickness device. For this reason, the C-section had to be dismantled at measurement phases of the test and the WT was measured by a thickness gauge manually to determine the maximum depth of groove after each interval.

7.1.3. Carbon fiber C-section

The carbon fiber base pipe had the following material and geometrical properties:

Table 7. 4 - Properties of the carbon fiber casing pipe

Parameter	Metric Units	Field Units
Outer Diameter (Average)	257.8 mm	10.15 ”"
Wall Thickness (Average)	25.4 mm	1"
Inner Diameter (Average)	207 mm	8.15"
Material	Carbon fiber impregnated with thermoset epoxy resin layer	

Like glass fiber casing, the carbon fiber casing has a layered structure, though without any internal resin layer. The material is softer compared to steel or glass, with a density of around 1810 Kg/m^3. The thermoset resin material for carbon fiber impregnation is the same as for glass fiber casing. The cut length of the specimens was the same as for steel casings (240mm) with a circumferential length of about 270 mm.

For the carbon fiber casing, the wall thickness was sufficient to withstand high side force values. However, the material could not be welded on to the adapter. Therefore, another adapter with screw threads was constructed so as to directly screw the casing specimen on to the adapter

(without support). Wall thickness measurements for the specimen were also made manually with the WT gauge.

The layout of the carbon fiber casing on the adapter is provided in Figure 7.3.

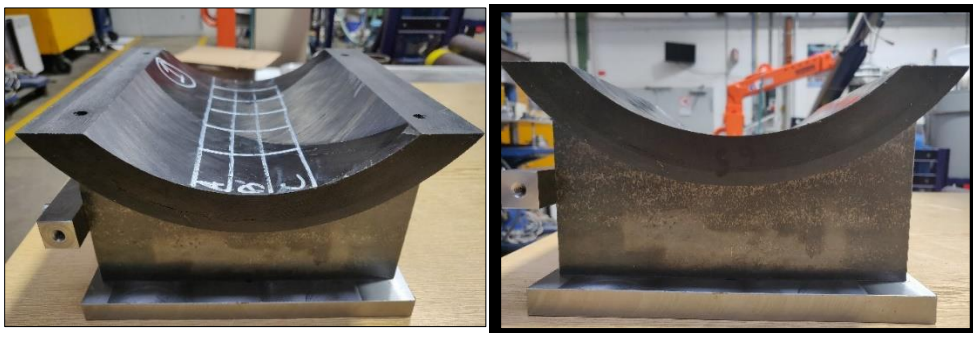

Figure 7. 3 - Measuring (left) and fastening of the carbon fiber C-section on the adapter (right)

7.2. Characteristics of water-based mud

The density and viscosity of drilling muds are primarily aimed to lift and suspend cuttings so as to avoid differential sticking and hole cleaning issues. For the wear tests, no cuttings were included in the test design and the base function of the mud was to cool and lubricate the contact. For this purpose, a simple barite-bentonite mud with low density of 9.4 to 9.5ppg (~1138kg/m^3) and a low viscosity of 14 to 15 centipoise was used for all the wear tests with mud.

One other necessity for using a low mud viscosity was the ease of flow with the sprinkler at the contact. Upon using a heavier mud (10.2 ppg), flow blockages were encountered at sprinkler holes and the fluid was not able to be sprayed effectively upon the contact.

The density of mud was measured before and during the tests using a mud balance and was adjusted accordingly if needed. Similarly, the viscosity of the mud was measured using a Fann35™ Viscometer.

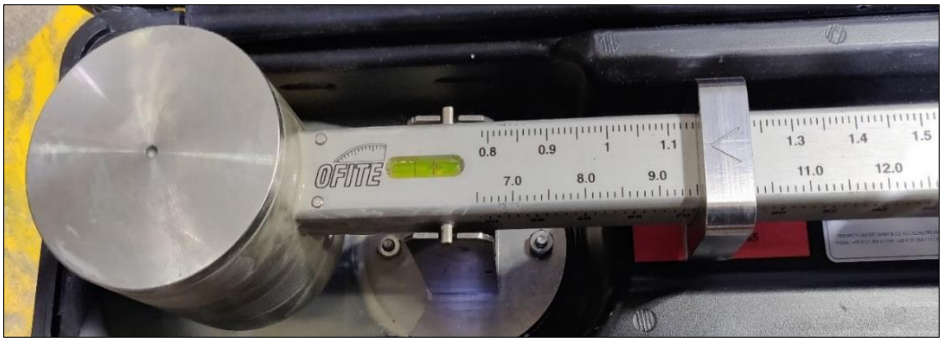

Figure 7. 4 - Measurement of mud density before and during wear tests

The density was increased using barite (1/5th by weight for about 110L water in the tank) and the viscosity by using bentonite (1/20th or up to 5% by weight for 110L water).

7.3. Test procedure and operational parameters

1. The individual casing C-sections were attached on to the adapter and mounted upon the pneumatic cylinder.
2. The tool joint shaft is rotated at 100RPM and impinged against the casing inner wall at a contact force of about 6.7KN /1500 lbf (value can fluctuate due to vibrations). A crescent groove is observed upon the length of casing section.
3. The friction torque observed due to torsion at the shaft provides a value of the friction factor.
4. During an 8-hour wear test, the worn wall thickness is measured at 13 intervals (excluded from the contact duration). These intervals are at 15, 30, 45, 60, 90, 120, 150, 180, 240, 300, 360, 420, and 480 minutes.
5. The worn wall thickness allows for determination of wear area (groove area), wear volume and wear factor over time.

7.4. Reporting

1. Friction factor is calculated based on the measured frictional torque.
2. Rotating distance is based on the TJ diameter and measured RPM over the contact time intervals.
3. Frictional work is calculated based on rotating distance, side force and measured friction factor.
4. Wear factor is calculated based on cumulative worn volume and frictional work.
5. Specific energy is calculated from the wear factor and friction factor.
6. Specimen texture/roughness (qualitatively) is analyzed before and after wear test.

7.5. Wear tests results for steel casing with water

During the 8 hours contact of wear test with steel casing, significant casing wear was observed at the operational parameters. At least 4mm of wall thickness (about 1/3rd of the total wall) was removed in all three wear tests with water. Direct metal on metal contact resulted in severe adhesion (galling) and polishing of the casing surface. The wear process incorporated a lot of metal shavings that were gathered upon the magnet (installed near outflow from the bowl) and at the sieve around the fluid motor.

The process also induced significant friction heating at the contact and some of the worn metal chippings from the casing was actually welded onto the tool joint. Temperatures over 90°C were recorded at the contact using a laser thermometer. Since there was flowing water always present at measuring points, the actual temperature at the contact is anticipated to be higher.

The layout of the test protocol for test 2 with measured and calculated values is presented in Table 7.5. The equations used for calculation of the parameters have been explained in detail in Chapter 2 (sections 2.2.6, 2.2.7, 2.2.9 and 2.2.11) and are, therefore, not repeated here.

Table 7. 5 - Test No. 2 protocol with measured and calculated parameters

Casing/TJ	Measured Side Force (kN)	Pressure on Cylinder (bar)	Contact Area (m2)	Contact Pressure (MPa)	RPM	Time (min)	Mechanism	Worn WT (mm)	Cum. Worn WT (mm)	Cum. Wear Volume (xE5) (m^3/m)	Max Strain (µS)	Friction Factor	Max Friction Stress (MPa)	Friction Moment (N.m)	Frictional Work (J)	Cum. Frictional Work (J)	Wear Factor (E-10/psi)	Specific Energy (E14 psi)
Casing 95HC (244,5x11,95) mm- Stainless Steel TJ	0.00	0	0.00000	0	0	0	Rotating & Sliding	0.00	0.00	0	0	0.00	0	0	0	0	0	0
	6.73	3	0.00837	0.804	100	15	Rotating & Sliding	0.35	0.35	0.8121	18	0.20	0.676	115.6	1089063	1089063	123	16
	6.73	3	0.01082	0.622	100	30	Rotating & Sliding	0.24	0.59	1.7688	23	0.25	0.864	147.7	1391581	2480644	114	22
	6.73	3	0.01272	0.529	100	45	Rotating & Sliding	0.23	0.82	2.8846	18	0.20	0.676	115.6	1089063	3569707	170	12
	6.73	3	0.01421	0.474	100	60	Rotating & Sliding	0.21	1.03	4.0438	16	0.17	0.601	102.7	968056	4537763	198	9
	6.73	3	0.01548	0.435	100	90	Rotating & Sliding	0.20	1.23	5.2558	26	0.28	0.976	166.9	3146183	7683946	64	44
	6.73	3	0.01787	0.377	100	120	Rotating & Sliding	0.43	1.66	8.1713	15	0.16	0.563	96.3	1815105	9499051	266	6
	6.73	3	0.01905	0.353	100	150	Rotating & Sliding	0.24	1.90	9.9596	17	0.19	0.638	109.2	2057120	11556171	144	13
	6.73	3	0.02015	0.334	100	180	Rotating & Sliding	0.24	2.14	11.85	15	0.16	0.563	96.3	1815105	13371276	172	9
	6.73	3	0.02171	0.310	100	240	Rotating & Sliding	0.37	2.51	14.948	18	0.20	0.676	115.6	4356254	17727530	118	17
	6.73	3	0.02302	0.292	100	300	Rotating & Sliding	0.34	2.85	17.971	25	0.27	0.939	160.5	6050353	23777883	83	33
	6.73	3	0.02482	0.271	100	360	Rotating & Sliding	0.51	3.36	22.79	22	0.24	0.826	141.3	5324310	29102193	150	16
	6.73	3	0.02577	0.261	100	420	Rotating & Sliding	0.29	3.65	25.667	27	0.29	1.014	173.4	6534381	35636574	73	40
	6.73	3	0.02679	0.251	100	480	Rotating & Sliding	0.33	3.98	29.053	20	0.22	0.751	128.4	4840282	40476856	116	19

The wear groove propagation on the steel casing was observed over the entire length of the specimen which indicated an even distribution of force along the C-section. Though vibrations and reciprocation of the casing was expected to cause a shift of forces, the overall wear pattern was satisfactory in comparison to previous experimental studies. Some pictures of worn casing from test 2 are presented in Figure 7.5.

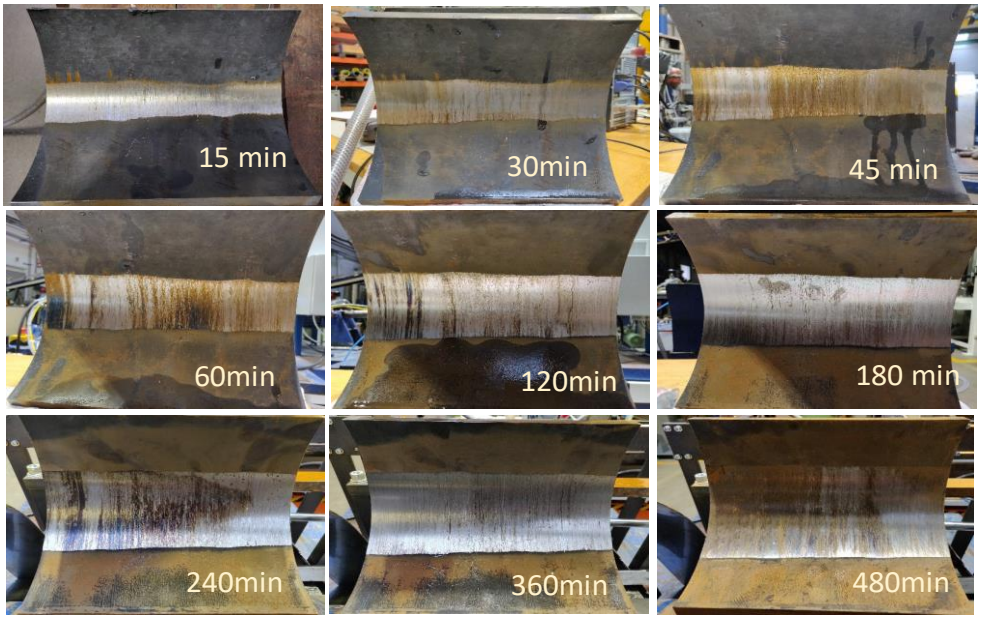

Figure 7. 5 - Wear grooves observed at different time intervals for Test No. 2

A closer look at the wear grooves under a micro-imager showed clear galling and polishing spots. A view of a micro image for test 2 at 480 minutes is shown in Figure 7.6.

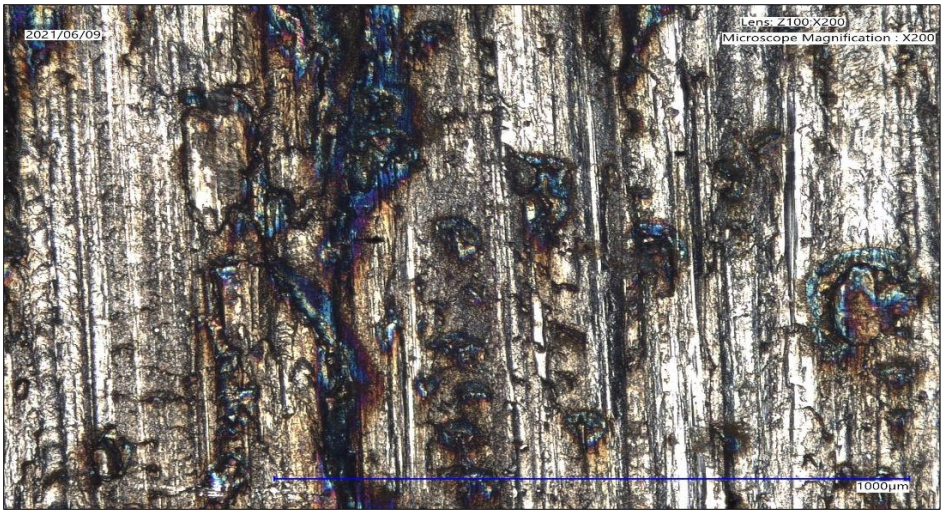

Figure 7. 6 - Wear mechanism and pattern observed under a micro-imager (Test 2: 480 min at 200X Zoom)

A measure of worn depth over time is shown in Figure 7.7. The graph shows a clear reduction in rate of wear but does not reach the contact pressure threshold (limit wear) in the 8 hours of test duration.

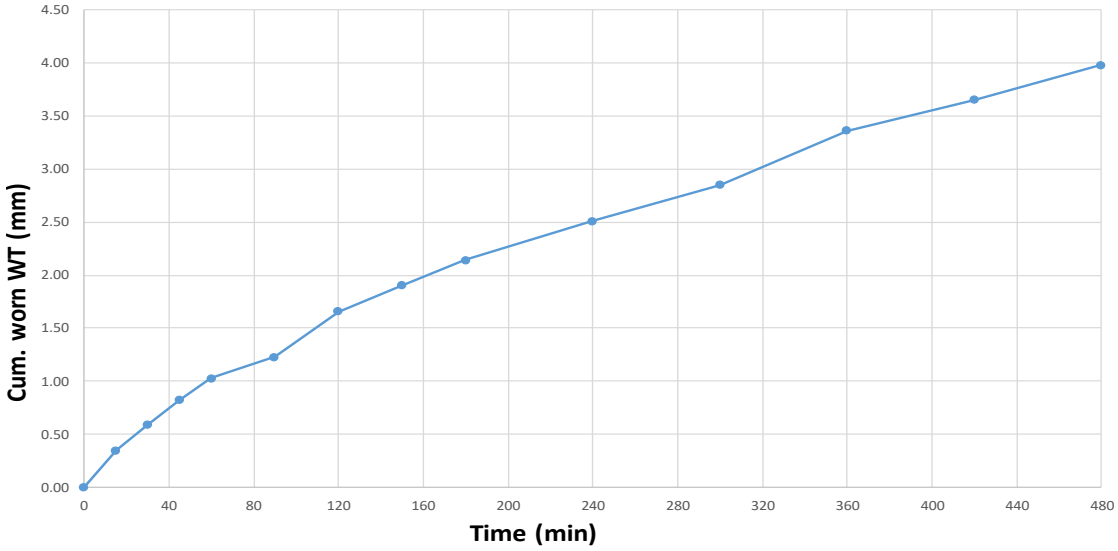

Figure 7. 7 - Cumulative worn WT observed over time for Test No. 2

Based on the strain gauge response (leading to frictional moment), the propagation of friction factor with time for test 2 is presented in Figure 7.8. The friction factor for the metal-metal contact was observed in the range of 0.16 to 0.29, which is very realistic for dynamic contact between polished steel layers.

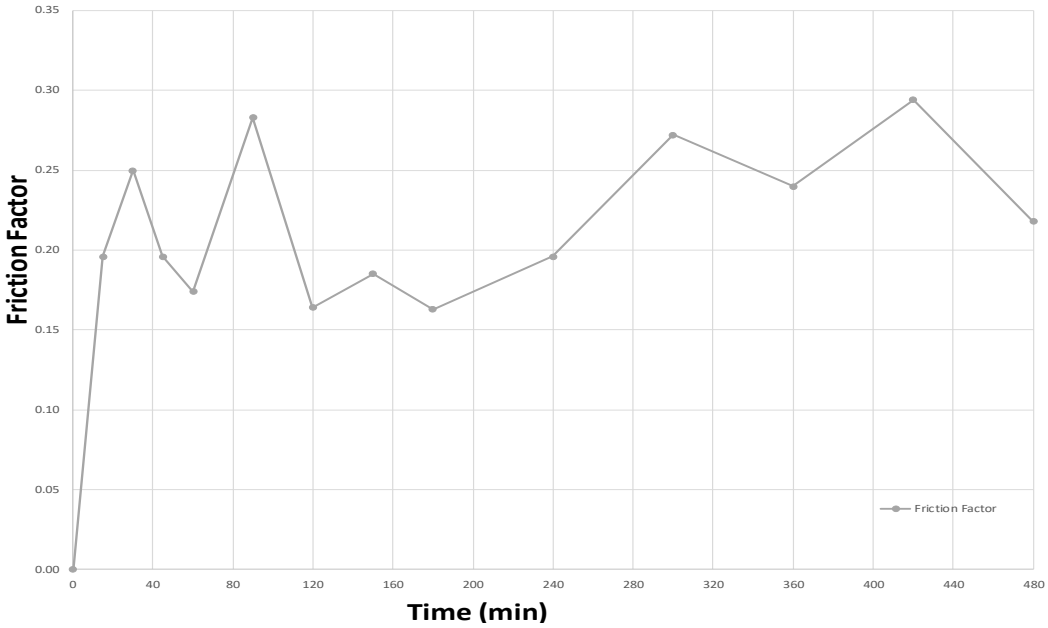

Figure 7. 8 - Friction factor values observed over time for Test No. 2

The wear factor, calculated as wear volume per amount of frictional work, was observed to follow a slight declining pattern following an initial spike as the contact pressure reduces with increments in worn area. As most authors have used field units (E-10/psi) for the wear factor, the values here are shown in the same units for comparison purpose.

The calculation of wear factor and worn volumes over time also enabled calculation of contact pressure thresholds for the casing materials under different lubrication conditions. The plots for CPT for the materials are shown in Chapter 8 along with the discussion on test results.

The same test procedure and calculations were performed for the other two tests for steel casing wear with water. The test protocols for test 1 and 3 are presented in Appendix 11.7 and 11.8.

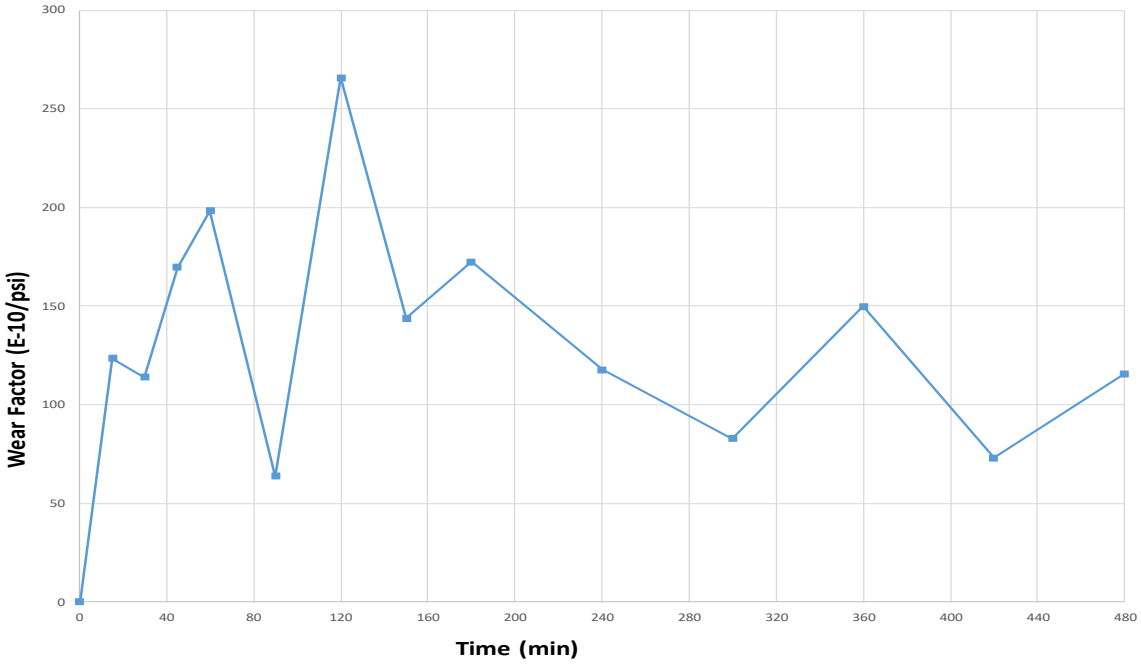

Figure 7. 9 - Wear factor values observed over time for Test No. 2

7.6. Wear tests results for steel casing with water-based mud as lubricant

The change of lubrication fluid was found to have a drastic impact on the wear intensity. In comparison to 1/3rd of removed wall thickness in presence of water, the total loss of WT on the steel casing in presence of drill mud was only 0.5 mm to 0.6 mm. All the other test parameters were observed to be the same as for the water tests. The recorded temperatures near the contact were also reduced to around 40°C.

The huge wear difference between water and drilling mud conditions for steel (by a factor of 8) suggests that the wear mechanism is highly influenced by the density and viscosity of the fluid. An explanation for this phenomenon is that this specific testing set-up creates a condition similar to a crankshaft bearing situation in which a “protective film” is formed between the shaft and

the bearing. This implies that the materials properties play a non-dominant role in a wear mechanism for this specific set-up, and that it is dominated by the hydrodynamic “bearing film-formation effect” for denser fluids like mud.

The wear test results for mud in all four tests were very comparable and only minor differences were observed. Once the contact area was worn enough to bring the setup in a “stable contact pressure region”, a very-low and steady wear rate was developed. This appeared to be the case also for the steel/water test where a stable but high wear rate was developed (Figure 7.7). Under mud conditions however, the wear rate decreased sharply to very low values and this supports the observation that a protective film is formed.

As with the water tests, the groove formation was formed over the entire specimen length. Some pictures of the worn groove from Test No. 7 (Fourth test with Steel Casing and Mud) are presented in Figure 7.10.

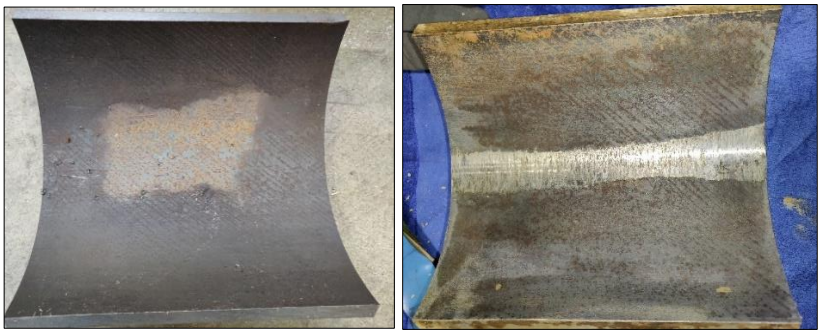

Figure 7. 10 - Casing specimen before (left) and after (right) Test No. 4

The presence of fluid layers and mud solids at the contact also shifted the wear mechanism from severe galling (adhesion) to particle (3-body) abrasion. This could also be observed in the micro-image for the specimen after the test.

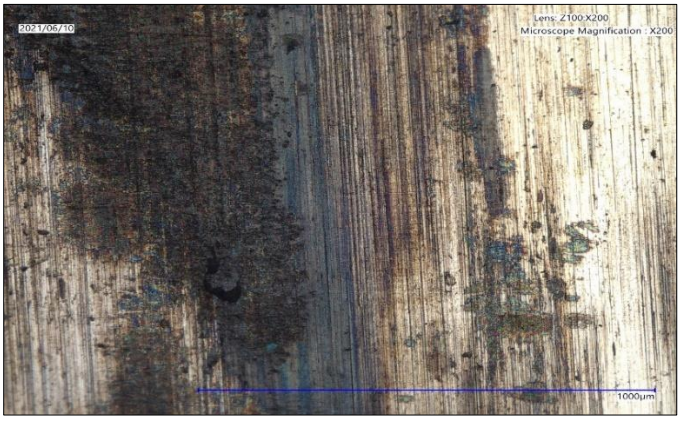

Figure 7. 11 - Wear pattern observed under a micro-imager (Test 4: 480 min at 200X Zoom)

The spots marked with mud solids and a lined abrasion pattern due to compression of particle while rotating can be observed in the above Figure.

A plot of wear depth with time for test shows a drastically reduced wear rate but the specimen did not reach contact pressure threshold in the 8 hours of contact.

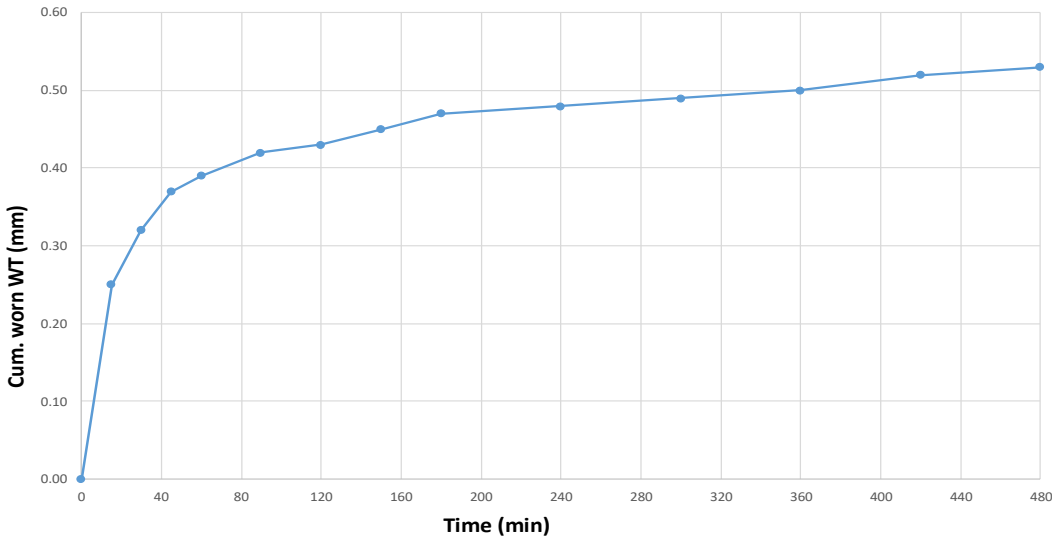

Figure 7. 12 - Cumulative worn WT observed over time for Test No. 7

The friction factor values observed over time were also lower in comparison to the wear test with water. Compared to values up to 0.3, wear contact with the mud film yield friction factor in range of 0.08 to 0.15 which corresponds to the values observed for greased and lubricated metal contacts. A plot of friction factor and wear factor for the test are shown in Figure 7.13.

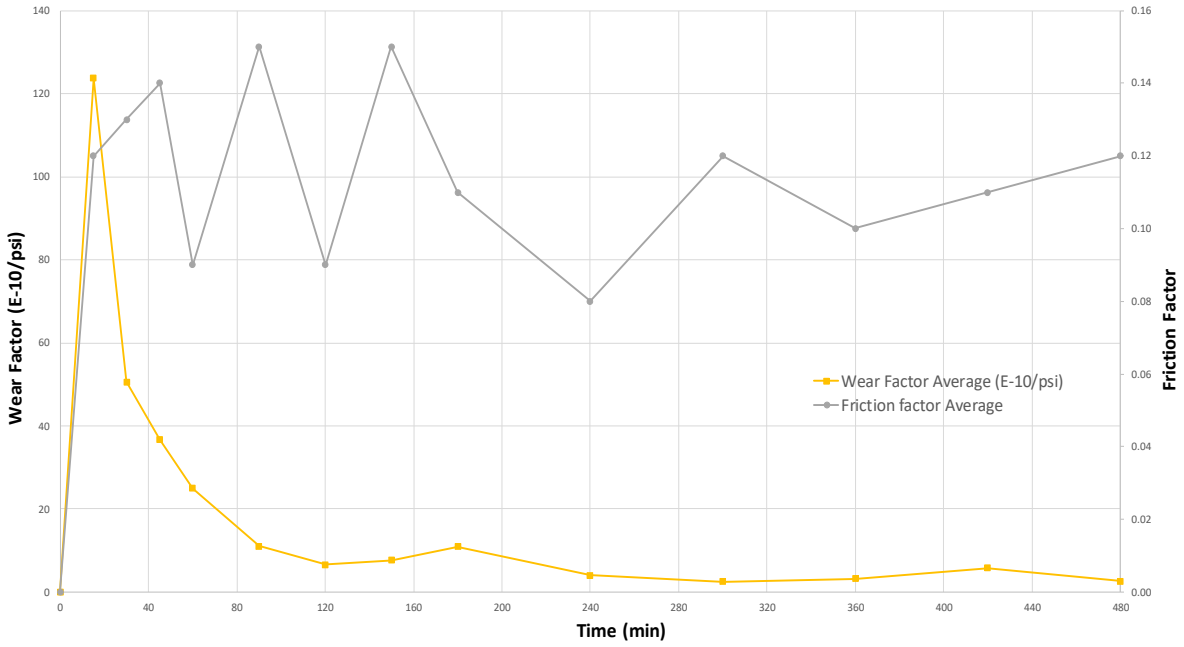

Figure 7. 13 - Friction factor and wear factor values observed over time for Test No. 7

A drastic reduction in wear rate is also depicted in the observed wear factor values. After the initial peak value, the wear factor declines significantly and lessens further at a slower rate. The protocol for the test is presented below.

Table 7. 6 - Test No. 7 protocol with measured and calculated parameters

Casing/TJ	Measured Side Force (kN)	Pressure on Cylinder (bar)	Arc length of Grove (mm)	Contact Area (m2)	Contact Pressure (MPa)	RPM	Time (min)	Mechanism	Worn WT (mm)	Cum. Worn WT (mm)	Cum. Wear Volume (xE^{-5}) (m^3/m)	Max Strain (µS)	Friction factor Average	Max Friction Stress (MPa)	Moment (N.m)	Cum. Frictional Work (J)	Cum. Frictional Work (x1E-7) (J)	Wear Factor Average (E-10/psi)
	0.00	0	0	0.00000	0	0	0	Rotating & Sliding	0.00	0.00	0	0	0.00	0	0	0	0.00	0
	6.73	3	29.88	0.00717	0.938	100	15	Rotating & Sliding	0.25	0.25	0.4975	11	0.12	0.413	70.6	665539	0.07	124
	6.73	3	33.77	0.00810	0.830	100	30	Rotating & Sliding	0.07	0.32	0.7192	12	0.13	0.451	77.1	1391581	0.14	51
	6.73	3	36.28	0.00871	0.773	100	45	Rotating & Sliding	0.05	0.37	0.8933	13	0.14	0.488	83.5	2178127	0.22	37
	6.73	3	37.24	0.00894	0.753	100	60	Rotating & Sliding	0.02	0.39	0.9663	8	0.09	0.301	51.4	2662155	0.27	25
Casing 95HC (244,5x11,95) mm- Stainless Steel TJ- Drilling Mud 9,4ppg, Viscosity 15cp	6.73	3	38.63	0.00927	0.726	100	90	Rotating & Sliding	0.03	0.42	1.0792	14	0.15	0.526	89.9	4356253	0.44	11
	6.73	3	39.08	0.00938	0.718	100	120	Rotating & Sliding	0.01	0.43	1.1179	8	0.09	0.301	51.4	5324309	0.53	7
	6.73	3	39.96	0.00959	0.702	100	150	Rotating & Sliding	0.02	0.45	1.1963	14	0.15	0.526	89.9	7018407	0.70	8
	6.73	3	40.83	0.00980	0.687	100	180	Rotating & Sliding	0.02	0.47	1.2763	10	0.11	0.376	64.2	8228478	0.82	11
	6.73	3	41.26	0.00990	0.680	100	240	Rotating & Sliding	0.01	0.48	1.3171	7	0.08	0.263	44.9	9922576	0.99	4
	6.73	3	41.68	0.01000	0.673	100	300	Rotating & Sliding	0.01	0.49	1.3579	11	0.12	0.413	70.6	12584731	1.26	3
	6.73	3	42.09	0.01010	0.666	100	360	Rotating & Sliding	0.01	0.50	1.3996	9	0.10	0.338	57.8	14762858	1.48	3
	6.73	3	42.91	0.01030	0.653	100	420	Rotating & Sliding	0.02	0.52	1.4838	10	0.11	0.376	64.2	17182999	1.72	6
	6.73	3	43.32	0.01040	0.647	100	480	Rotating & Sliding	0.01	0.53	1.5263	11	0.12	0.413	70.6	19845154	1.98	3

The same test procedure and calculations were performed for the other three tests for steel casing wear with water-based mud. The protocols for tests No. 4, 5 and 6 are presented in Appendices 11.9, 11.10 and 11.11 respectively.

7.7. Wear tests results for glass fiber casing with water-based mud as lubricant

Due to the low friction resin layer on the inner wall, the expected friction and wear behavior for glass fiber casing was expected to be similar to the behavior of the steel casing with drilling mud film at the contact.

To wear out the resin layer and the glass fiber material, the contact duration of test No. 10 (Third test with glass fiber casing and mud) was extended to 16 hours instead of 8 hours. This was the only test with an extended test period to observe the effects at- and beyond the resin protector film. The 16 hours of contact resulted in a total reduction of 0.67mm from the 5mm wall thickness at the contact. No significant heating of the specimen was observed and a temperature increase of only 6°C was observed (from 22°C to 28°C). The protective mud film, as observed for steel casing, was also observed for glass fiber casing. This implied that for such a localized wear situation, the material of the casing may not play as important of a role as the density of the drilling mud film in between the contacting bodies.

A view of the casing specimen before and after wear is presented in Figure 7.14.

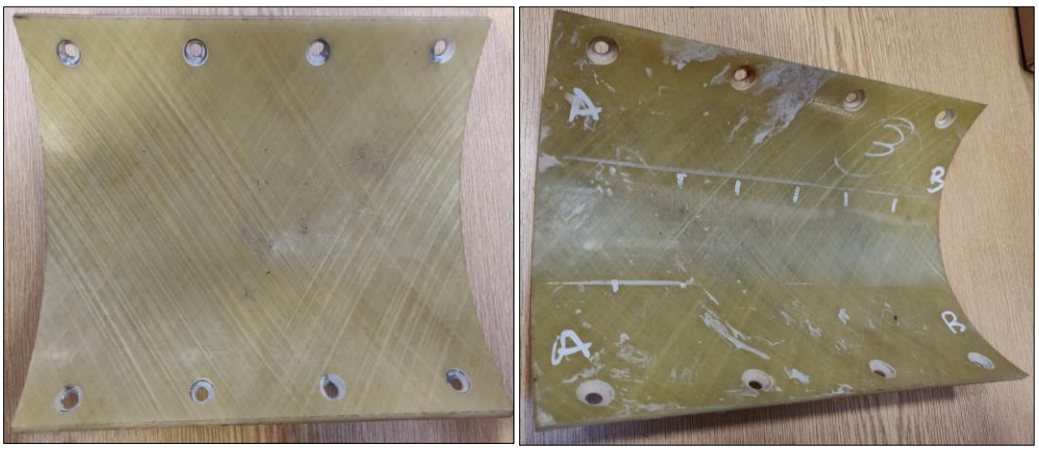

Figure 7. 14 - Glass fiber casing specimen before (left) and after (right) Test No. 10

The initial reduction in wear rate was similar to that of steel with drilling mud, and the contact pressure threshold was not achieved. However, since the resin layer (0.3mm) was abraded during the test and the tool joint had already reached the glass fiber layer beneath, it was expected that the wear would continue with a steady wear rate.

Very low friction factor values were observed for the contact between steel and glass fiber surfaces. The friction factor remained in the range of 0.03 to 0.06. This corresponds to the value of dynamic friction factor for smooth steel and glass surfaces from wear literature (reported to

be less than 0.1). The wear factor, similarly, reduced and lessened over time after the initial spike. The plots for worn thickness, friction factor and wear factor over time are presented in Figures 7.15 and 7.16.

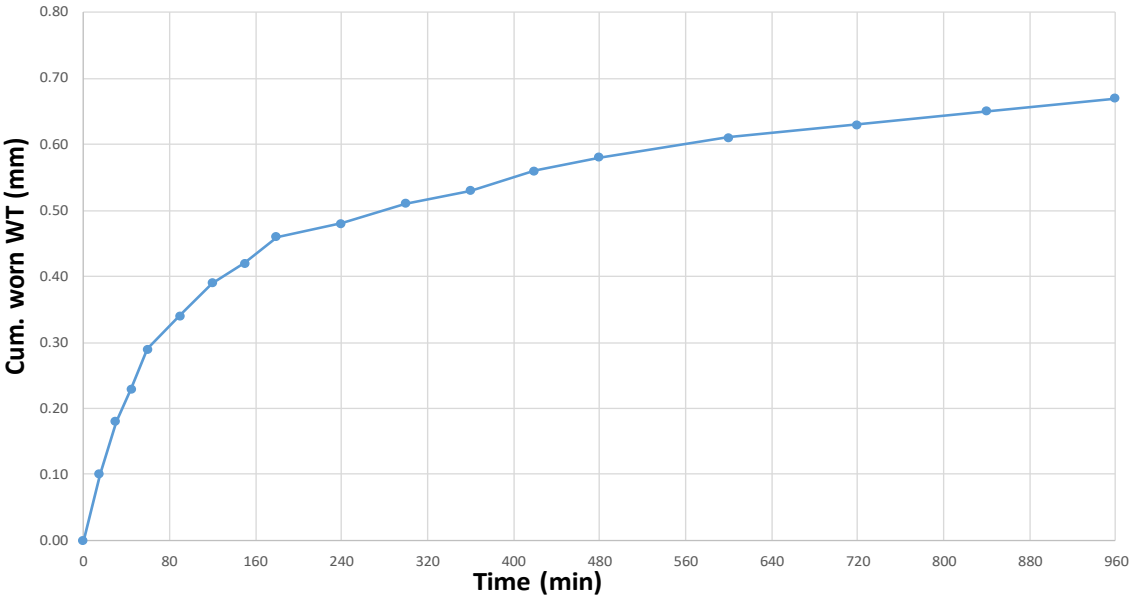

Figure 7. 15 - Cumulative worn WT observed over time for Test No. 10

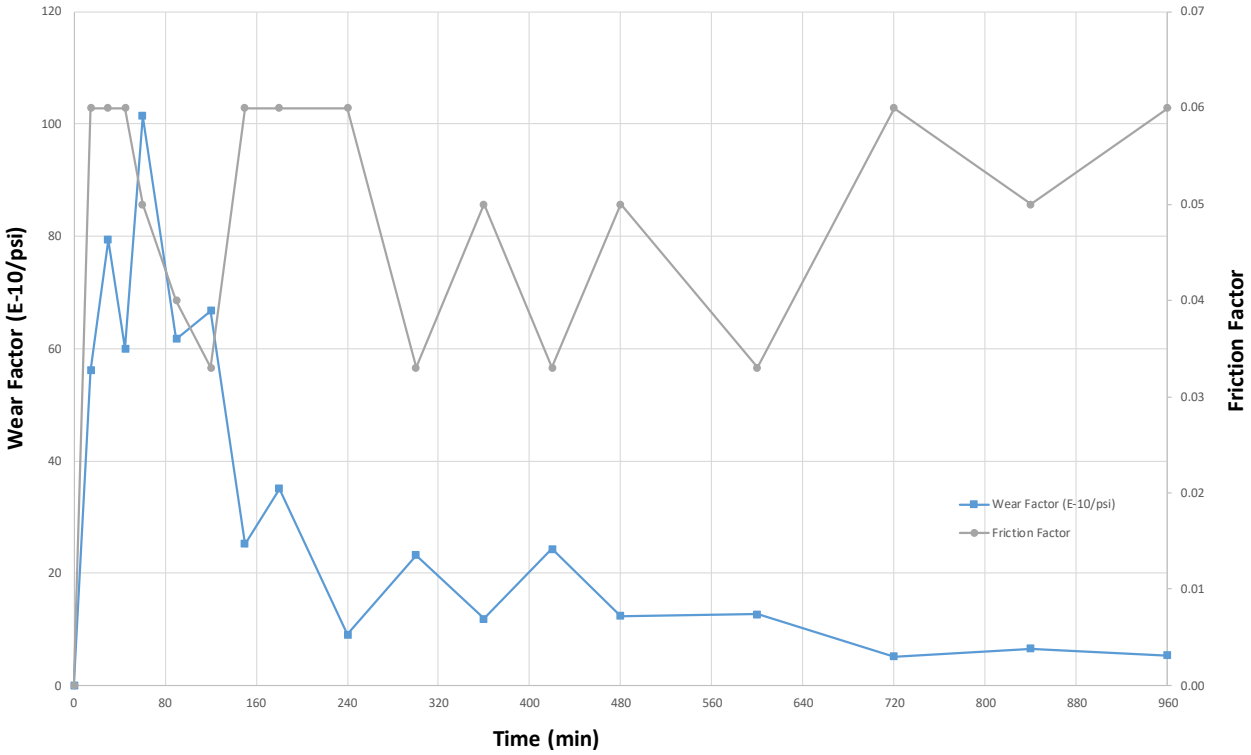

Figure 7. 16 - Friction factor and wear factor values observed over time for Test No. 10

A simplified protocol for the test is presented in the Table 7.7.

Table 7. 7 - Test No. 7 protocol with measured and calculated parameters

Casing/TJ	Measured Side Force (kN)	Pressure on Cylinder (bar)	Contact Area (m2)	Contact Pressure (MPa)	RPM	Time (min)	Mechanism	Worn WT (mm)	Cum. Worn WT (mm)	Cum. Wear Volume (xE5) (m^3/m)	Wear Volume (xE5) (m^3/m)	Max Strain (µS)	Friction factor	Max Friction Stress (MPa)	Moment (N.m)	Cum. Frictional Work (J)	Cum. Frictional Work (x1E-7) (J)	Wear Factor (E-10/psi)
	0.00	0	0.00000	0	0	0	Rotating & Sliding	0.00	0.00	0	0	0	0.00	0	0	0	0.00	0
	6.10	3	0.00369	1.652	100	15	Rotating & Sliding	0.10	0.10	0.1025	0.1025	5	0.06	0.187	32.1	302517	0.03	56
	6.10	3	0.00495	1.232	100	30	Rotating & Sliding	0.08	0.18	0.2475	0.145	5	0.06	0.187	32.1	605034	0.06	79
	6.10	3	0.00559	1.090	100	45	Rotating & Sliding	0.05	0.23	0.3571	0.1096	5	0.06	0.187	32.1	907551	0.09	60
	6.10	3	0.00628	0.972	100	60	Rotating & Sliding	0.06	0.29	0.5054	0.1483	4	0.05	0.15	25.7	1149565	0.11	101
	6.10	3	0.00680	0.897	100	90	Rotating & Sliding	0.05	0.34	0.6408	0.1354	3	0.04	0.113	19.3	1512586	0.15	62
	6.10	3	0.00728	0.838	100	120	Rotating & Sliding	0.05	0.39	0.7871	0.1463	3	0.03	0.105	17.9	1875607	0.19	67
Casing Glass Fiber (260,3x4,90) mm- Stainless Steel TJ- Drilling Mud 9,4ppg, Viscosity 14cp	6.10	3	0.00755	0.808	100	150	Rotating & Sliding	0.03	0.42	0.8792	0.0921	5	0.06	0.187	32.1	2480642	0.25	25
	6.10	3	0.00790	0.772	100	180	Rotating & Sliding	0.04	0.46	1.0071	0.1279	5	0.06	0.187	32.1	3085677	0.31	35
	6.10	3	0.00807	0.756	100	240	Rotating & Sliding	0.02	0.48	1.0733	0.0663	5	0.06	0.187	32.1	4295747	0.43	9
	6.10	3	0.00831	0.734	100	300	Rotating & Sliding	0.03	0.51	1.175	0.1017	3	0.03	0.109	18.6	5021789	0.50	23
	6.10	3	0.00847	0.720	100	360	Rotating & Sliding	0.02	0.53	1.2446	0.0696	4	0.05	0.15	25.7	5989845	0.60	12
	6.10	3	0.00870	0.702	100	420	Rotating & Sliding	0.03	0.56	1.3513	0.1067	3	0.03	0.12	20.6	6715887	0.67	24
	6.10	3	0.00886	0.688	100	480	Rotating & Sliding	0.02	0.58	1.4238	0.0725	4	0.05	0.15	25.7	7683943	0.77	12
	6.10	3	0.00908	0.672	101	600	Rotating & Sliding	0.03	0.61	1.535	0.1113	3	0.03	0.094	16.1	9136027	0.91	13
	6.10	3	0.00923	0.661	102	720	Rotating & Sliding	0.02	0.63	1.6108	0.0758	5	0.06	0.187	32.1	11556168	1.16	5
	6.10	3	0.00937	0.651	103	840	Rotating & Sliding	0.02	0.65	1.6879	0.0771	4	0.05	0.15	25.7	13492281	1.35	7
	6.10	3	0.00952	0.641	104	960	Rotating & Sliding	0.02	0.67	1.7658	0.0779	5	0.06	0.187	32.1	15912422	1.59	5

The micro images of the worn surface showed lined abrasive (3-body) patterns due to mud solids and glass fiber particles grinding between the contact bodies.

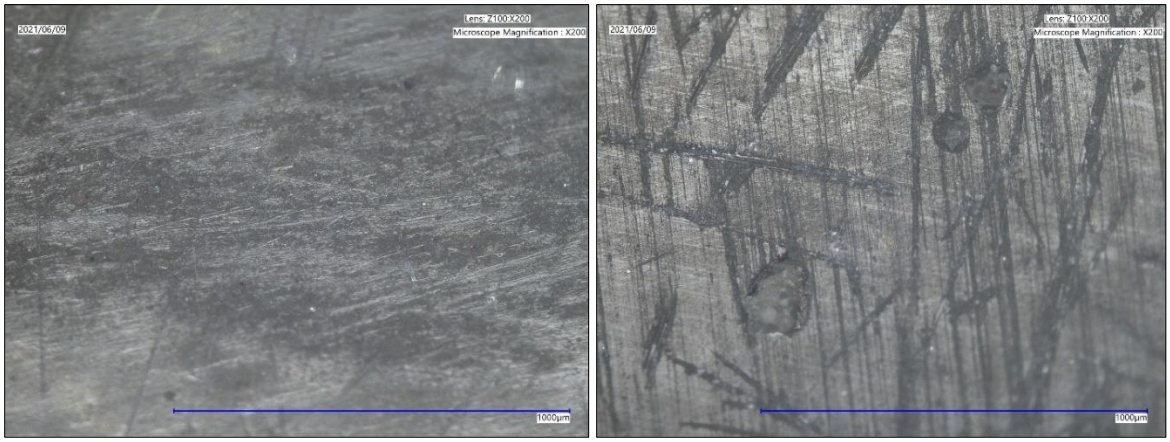

Figure 7. 17 - Wear patterns for glass casing before (left) and after (right) test 7 (960 min at 200X)

The protocols for the other two tests with glass fiber casing (tests No. 8 and 9) are presented in Appendix 11.12 and 11.13.

7.8. Wear tests results for glass fiber casing with water

The added wear test for glass fiber casing (Test No. 13) with water was carried out with the sole objective to compare the wear behavior of the material in presence of water instead of drill mud. The test was conducted for the prescribed 8 hours and, as expected, a slightly higher wear rate and friction factor was observed as compared to drill mud conditions. The specimen was worn with over 0.8mm of WT removed in 8 hours (compared to 0.67 in 16 hours with mud), which again validated the presence of the protective mud film.

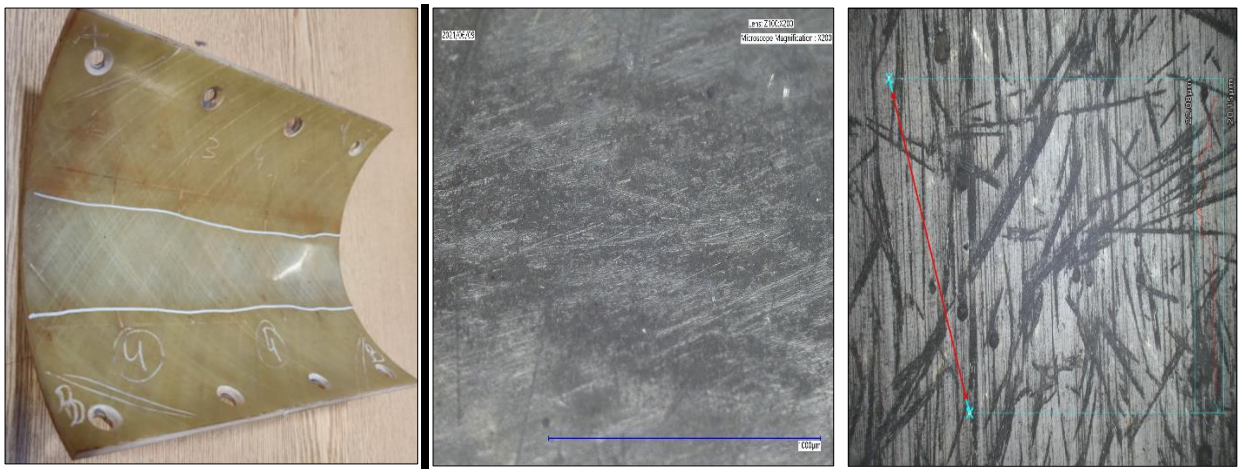

Figure 7. 18 - Worn specimen after 480 min (left) and its micro image at 200X before test (middle) and after test (right)

The friction factor was in the range of 0.07 to 0.12, with the wear factor being higher in the beginning and then dropping significantly after increase in wear area.

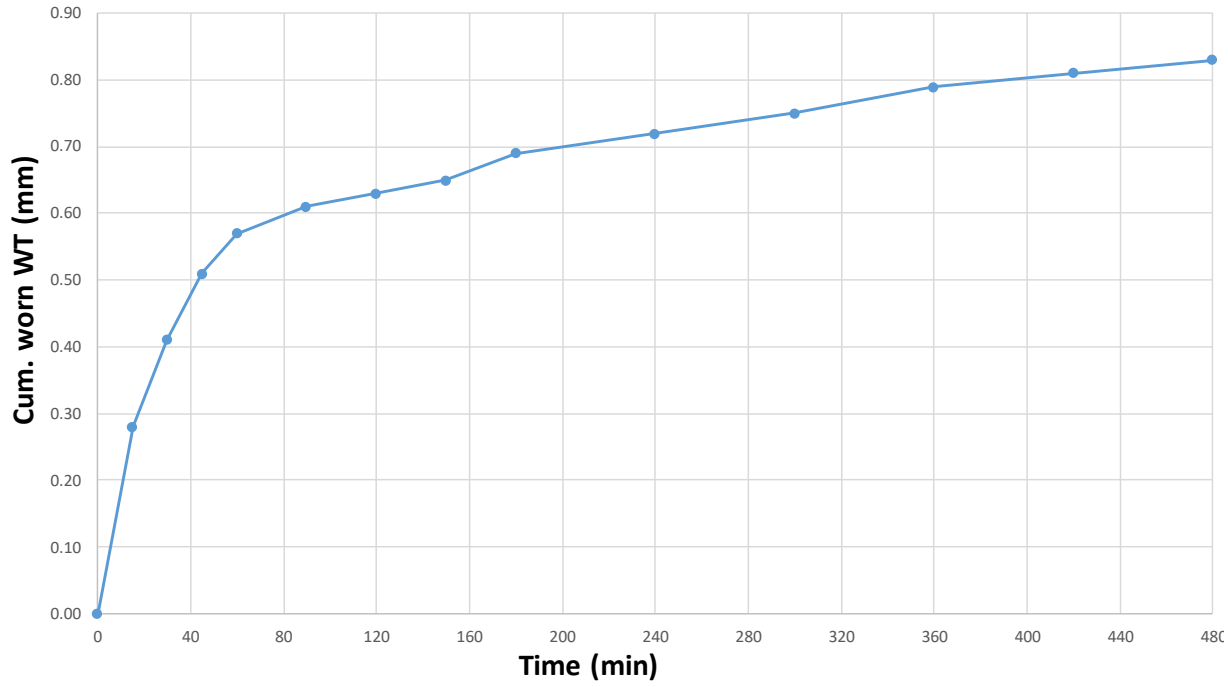

Figure 7. 19 - Cumulative worn WT observed over time for Test No. 13

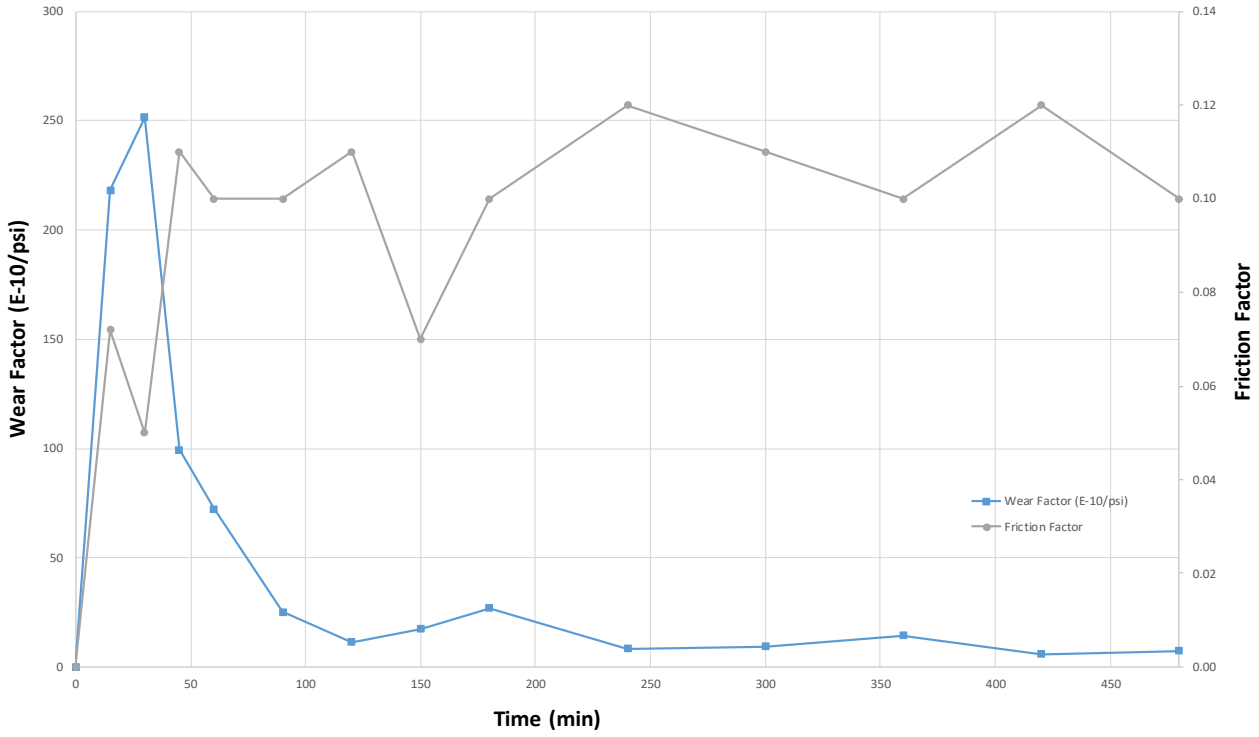

Figure 7. 20 - Friction factor and wear factor values observed over time for Test No. 13

A cumulative temperature change from 24°C to 43°C was recorded at the casing (water temperature up to 36°C from 25°C). Though a notable change, this is attributed to a more exact measurement in the presence of water (compared to drill mud) as it does not gel or accumulate around the contact area, which blocks the laser contact and creates inaccuracies in temperature measurements.

The protocol with measured and calculated parameters for test 13 is presented in Appendix 11.14.

7.9. Wear tests results for carbon fiber casing with water-based mud as lubricant

For carbon fiber casing, the material had no resin or inner protective layer so it was expected to have a steady, low wear rate. From wear literature for metal-epoxy resin contact, carbon resin layers generally have a wear resistance that is higher than glass and lower than steel. However, such wear conditions are normally for a fixed and dry contact area and both of these conditions are not met in the casing wear setup and also not expected under field conditions.

The worn specimen along with its micro image after the test is presented in Figure 7.21.

Figure 7. 21 - Worn specimen after 480 min (left) and its micro image at 200X before test (middle) and after test (right)

The test results showed a steady wear rate that was higher than both steel and glass fiber under mud conditions. A total of about 0.9mm was removed on average during the 8 hours of contact. Though the wear was not particularly higher, the behavior was unexpected and was attributed to the following reasons:

1. The inner diameter of the carbon fiber casing is the lowest of the three casings (approx. 205mm) due to added thickness (approx. 29mm). Though this results in a greater contact area from initial wear due to less difference in pipe ID and tool joint OD, it may restrict the flow of mud over the contact surface, causing slightly higher wear.

2. The carbon fiber material is softer and more ductile than glass fiber or steel (though thicker), and has a lower density. This results in ploughing due to greater hardness difference between the tool joint and the casing.
3. Another factor supporting the argument on added wear due to ploughing of the softer material is the lower friction factor (in the range of 0.05 to 0.08) along with a higher wear depth (wear factor higher than glass fiber). This can be visualized in Figure 7.22.

The micro image and roughness profile after the test showed a particle-abraded, but relatively smooth surface without much increase in roughness, which further validates presence of ploughing and deformation of material due to the side force itself.

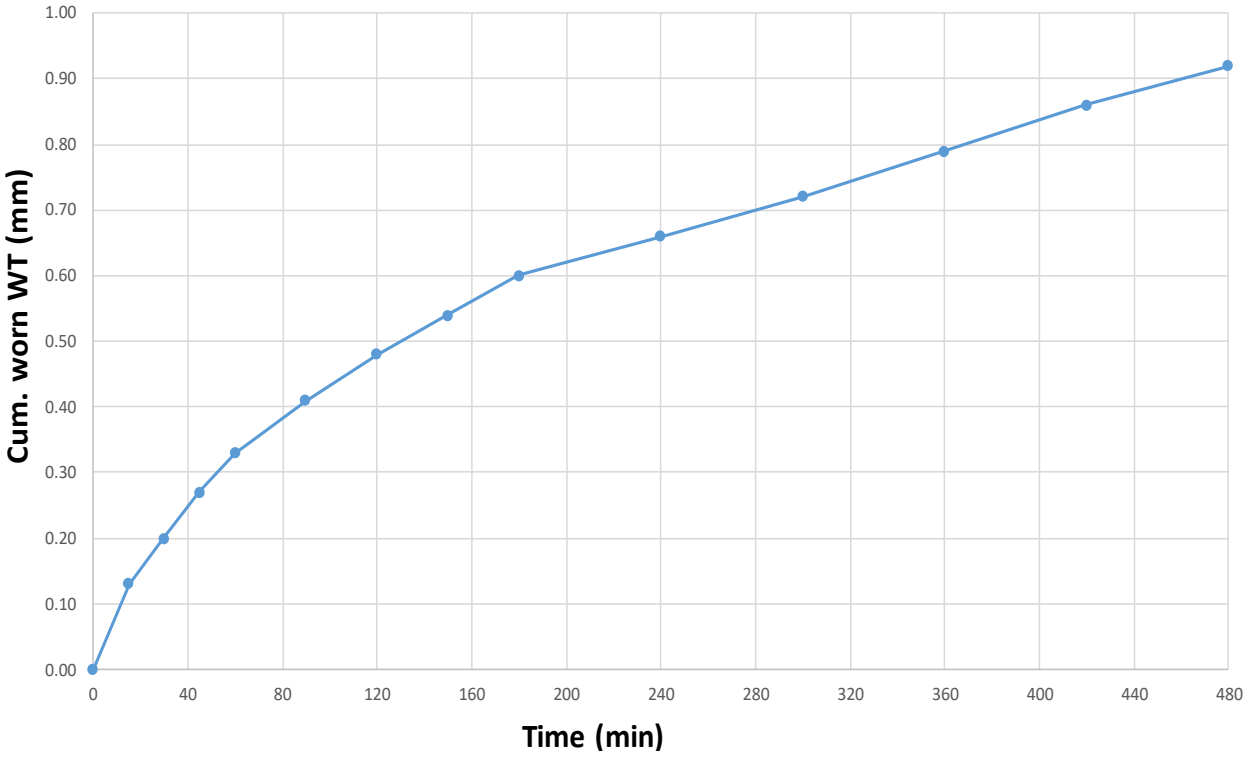

Figure 7. 22 - Cumulative worn WT observed over time for Test No. 12

The observed friction factor lies in the range of lubricated plastic on steel contact, having a dynamic friction factor of around 0.1. The temperature changed measured around the specimen was 11°C (from 25°C to 36°C) with the mud temperature increasing about 5°C.

The test protocol for tests 12 and 11 are presented in Appendix 11.15 and 11.16.

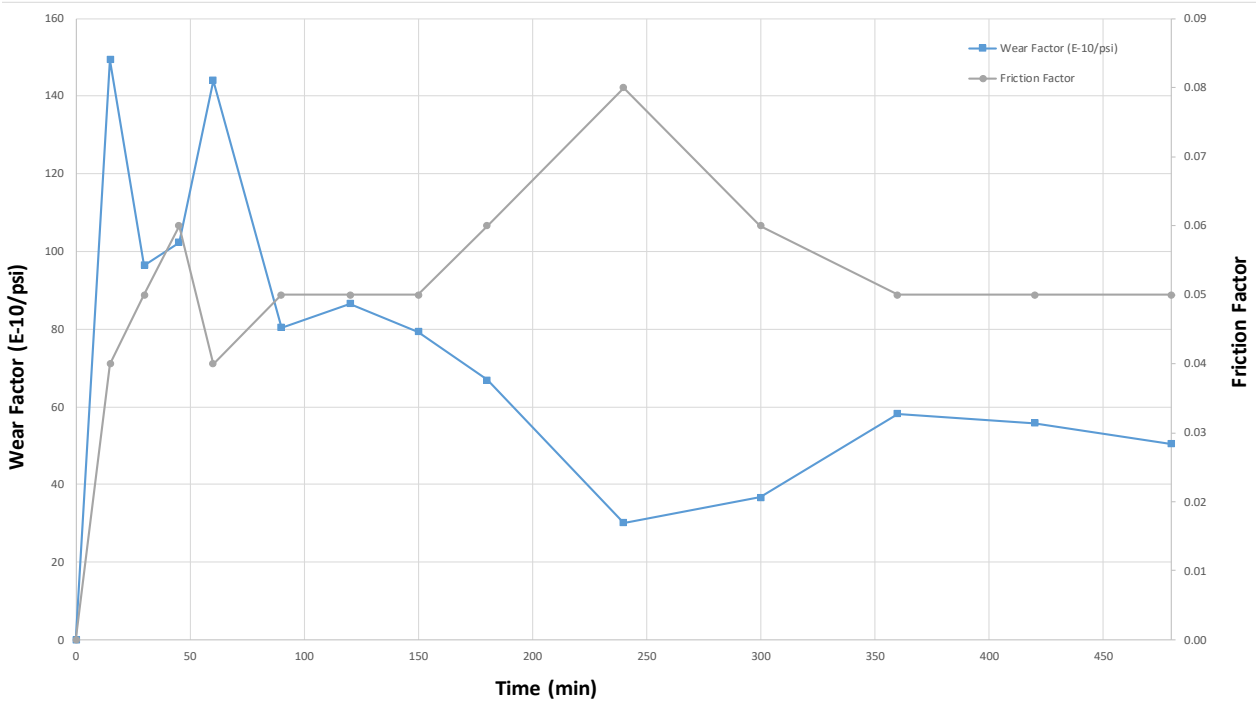

Figure 7. 23 - Friction factor and wear factor values observed over time for Test No. 12

7.10. Wear tests results for carbon fiber casing with water

Similar to the case with glass fiber casing, an added test was carried out to compare the wear behavior of carbon fiber casing in mud and water conditions. The wear test with water yielded a higher worn WT of 1.2mm over 8 hours. The wear rate was observed to be higher in the beginning due to the absence of the protective mud film, but was driven down with wear propagation to the values observed with the mud case. This, and the observed friction factor being similar to the mud case, again indicates that the wear occurring on the carbon fiber casing is a combined effect due to ploughing of the soft material, distortion by the side force, and abrasion due to its own particles.

No defining optical changes were detected in the wear groove texture for the casing compared to the mud case and similar micro images were obtained.

Furthermore, the temperature of the specimen increased to same range as observed with mud. Specimen temperature was increased from 24°C to 35°C. This is also consistent with the similar friction factors and implies that the drill mud may not have reached the contact throughout the entire contact interval due to lesser $ID_{casing}/OD_{tooljoint}$ ratio, and due to the distortion of soft carbon fiber-resin material with the harder steel tool joint.

The worn wall thickness over time for test 14 is presented in Figure 7.24.

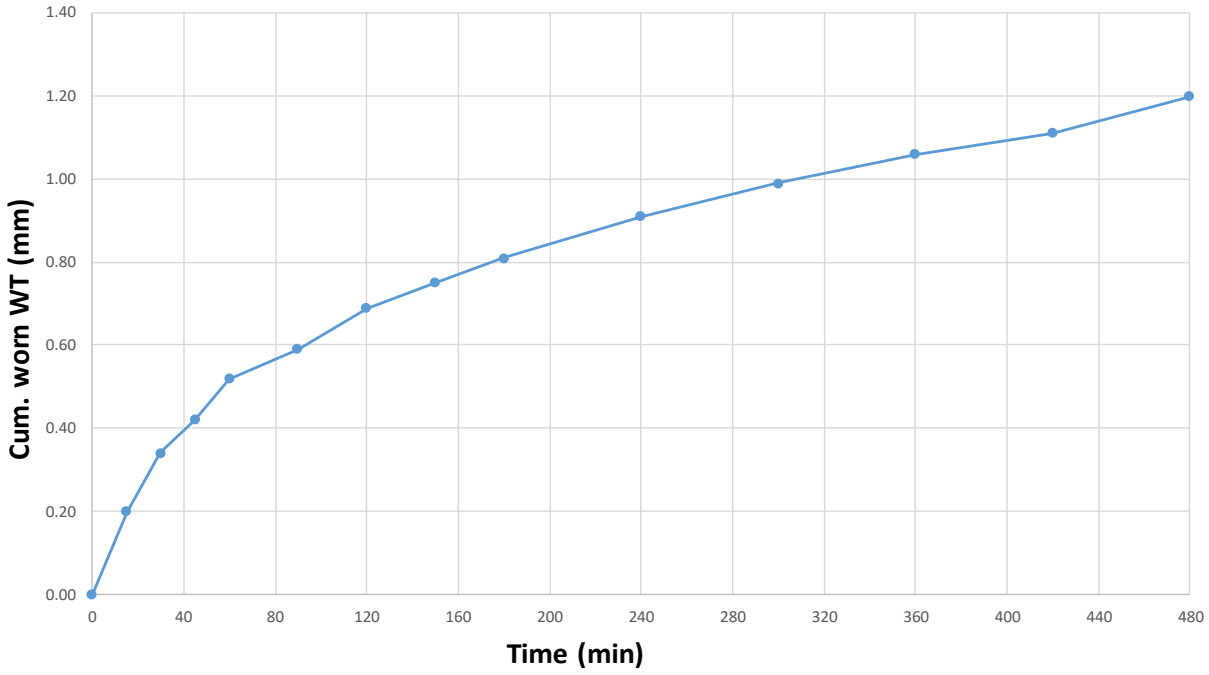

Figure 7. 24 - Cumulative worn WT observed over time for Test No. 14

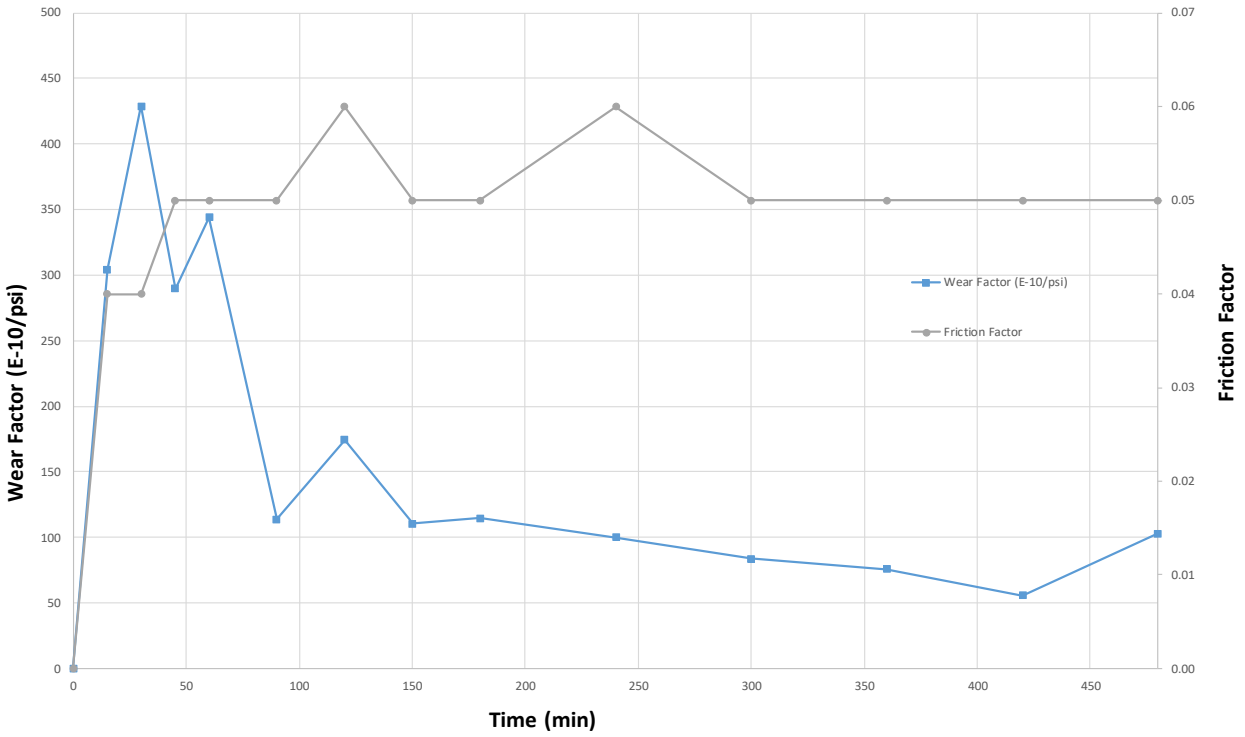

Figure 7. 25 - Friction factor and wear factor values observed over time for Test No. 14

The protocol of observed wear parameters for the test is presented in Appendix 11.17.

7.11. Comparison of wear test results

A comparison of averaged test measured and calculated wear parameters is presented in this section for casing materials under water and mud conditions.

The wear rate, as depicted by the worn wall thickness, was heavily influenced by the type of fluid and the hardness of the material. On average, the curves indicating the highest worn thicknesses are representing tests in water conditions. This strongly suggests that surfaces are covered and "caked" by a journal-bearing-like mud film which is reducing direct contact at fixed side force conditions.

A combination of different wear mechanisms was observed in the wear behavior of different materials:

1. For steel and water, severe adhesive galling, cutting and polishing patterns was observed. Some material welding was also present which is discussed further in Chapter 8.
2. For steel and mud, compressed abrasion and polishing were the primary wear patterns.
3. For glass fiber with water, low friction is observed due to contact with the epoxy resin layer. As the contact pressure reduces, wear is dominated chiefly by grain removal and 3-body abrasion.
4. For glass fiber with mud, the wear mechanisms remain the same as with water except for inclusion of mud solids and lower surface contact due to protective mud film.
5. For carbon fiber casing, the contact area is pressed and distorted by the TJ in both water and mud cases. Ploughing and 3-body abrasion are prime wear mechanisms in both cases.

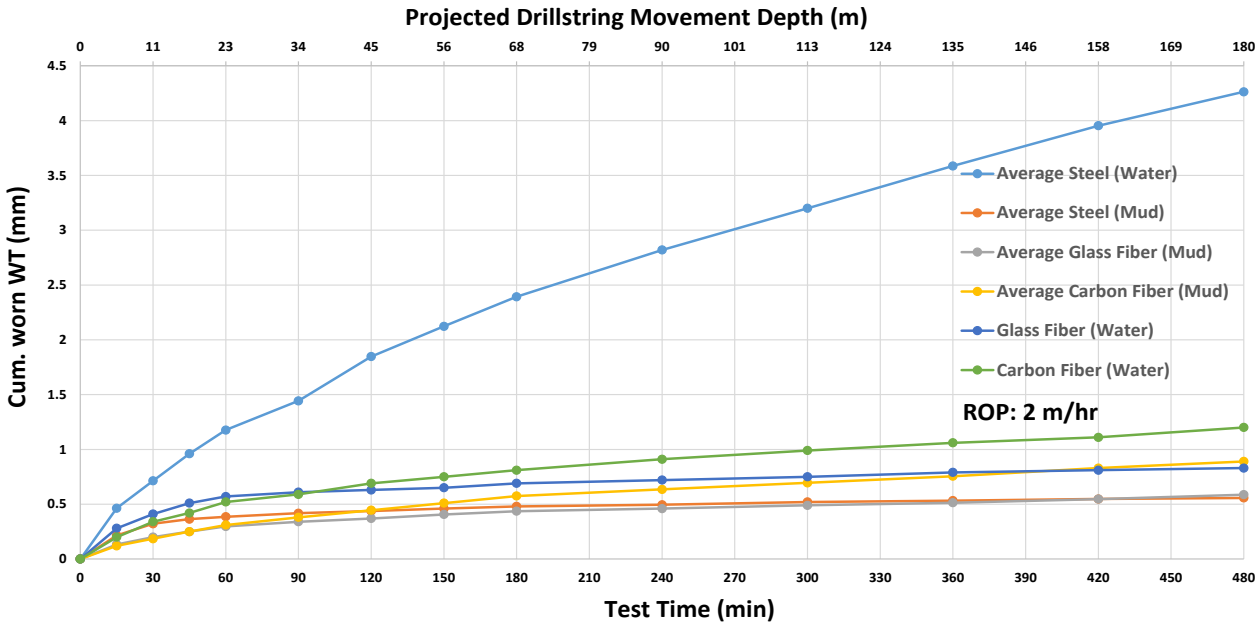

Figure 7. 26 - Averaged cumulative worn WT for materials under water and mud conditions

The friction coefficient for steel with water is attributed to a combined friction effect of dry adhesion and ploughing. For mud cases, galling did not take place as it can only occur after breaking through the mud film, which was continually renewed due to the constant flow. Density (Barite) plays a very important role here in terms of number of solids conveyed at the contact to hinder galling. Fluid viscosity is also relevant here as it increases the retention time of the fluid at the contact.

For glass fiber casing, the friction performance exceeded the benchmarks for steel casing, both with water and with mud. Due to the brittle nature of the material, however, a thin casing may not be able to directly withstand high contact forces without a back support. On a relative note, glass fiber casings generally also have a lower yield, burst and collapse rating as compared to steel.

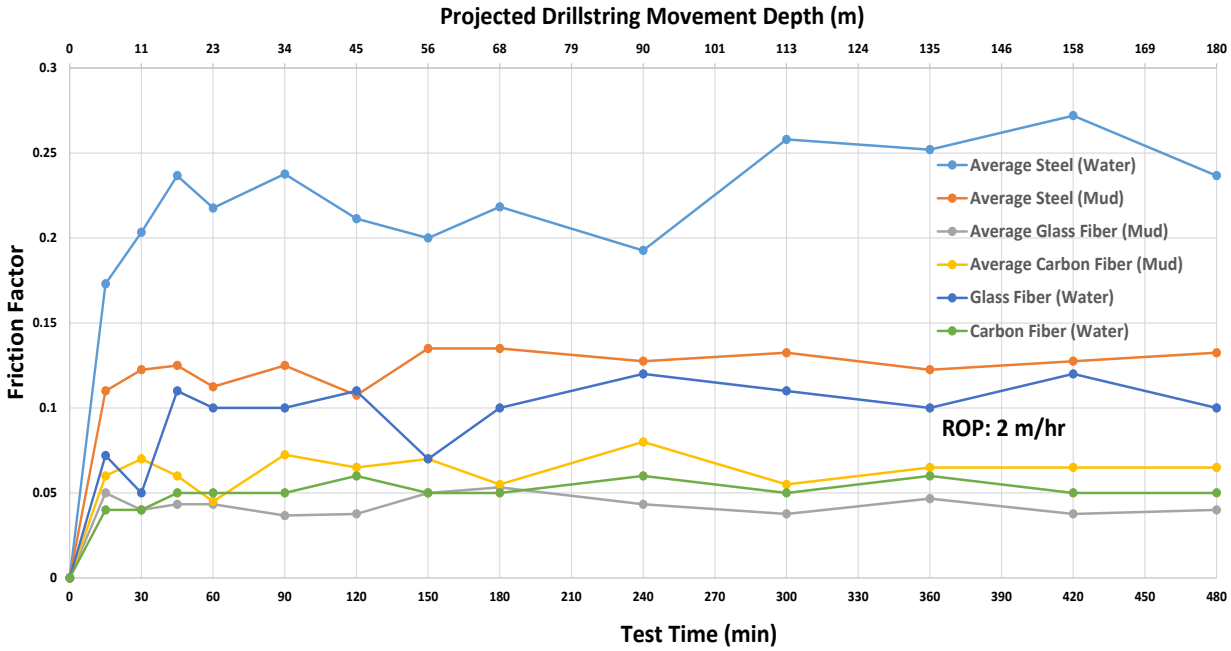

Figure 7. 27 - Averaged friction factors for casing contacts under water and mud conditions

Wear factor for casing-TJ contact, like its wear rate, is a non-linear factor. The initial peak value and then the sudden drop is very characteristic of field conditions and previous full scale test experimental studies. Plotting average wear factors for steel casing against its respective average worn WT values shows that the initial peak value is only for the first 0.4mm of worn WT for the water case (0.2mm for the mud case). Beyond that, it has a steadily declining pattern for the entire remaining worn WT (Figure 7.28). The steady wear rate is controlled by the consistency in the side force, rotation and the fluid parameters. The average of WF points in this steady range should provide a good estimate of wear over time also for field scenarios.

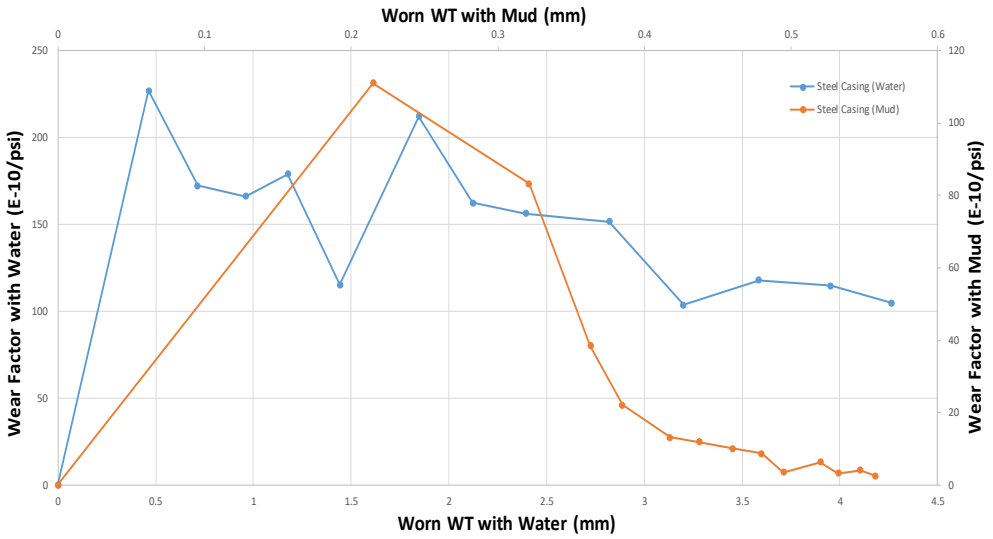

Figure 7. 28 - Wear factor variation with worn wall thickness for steel casing under water and mud conditions

A comparison of averaged wear factors for all the materials and conditions shows that wear factor peak was the highest for carbon fiber casing (due to material compression and ploughing) but the value drastically declined to below steel wear factor upon contact pressure reduction. For all materials, the steady downward range of values could provide an estimate of steady wear over time for a particular DS tension and RPM, particularly for scenarios such as drilling and rotation off-bottom.

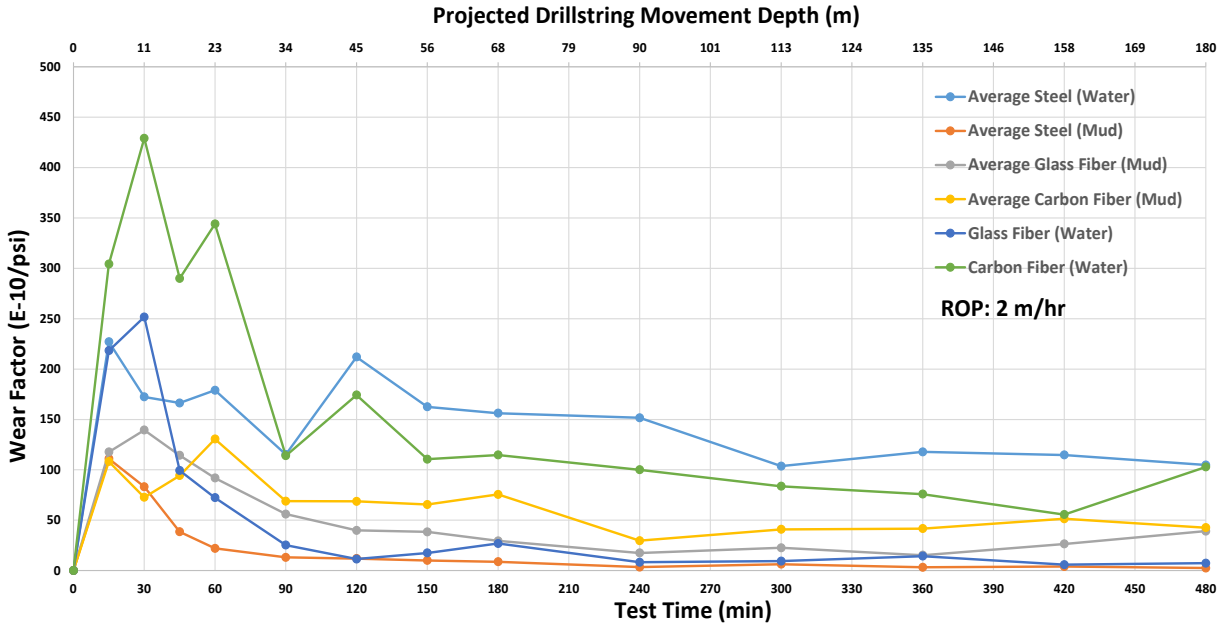

Figure 7. 29 - Averaged wear factors for casings under water and mud conditions

The projected drillstring movement depths are based on the tool joint length L_{TJ} of 29inch, a drill pipe body length L_{DP} of 28ft and an axial reciprocation speed ω_{Axial} of 2 m/hr. This implies casing-tooljoint contact every 8.53m of drillpipe in the use-case scenario.

The continual reduction in contact pressure is a controlling factor driving the wear factor down. As the comparison in Figure 7.30 shows, the decline is non-linear and directly derived from the continual increase in worn area. Similar amounts of worn volumes were excavated over different time intervals, suggesting that wear volume is more localized in the beginning and then distributed more evenly over the larger area.

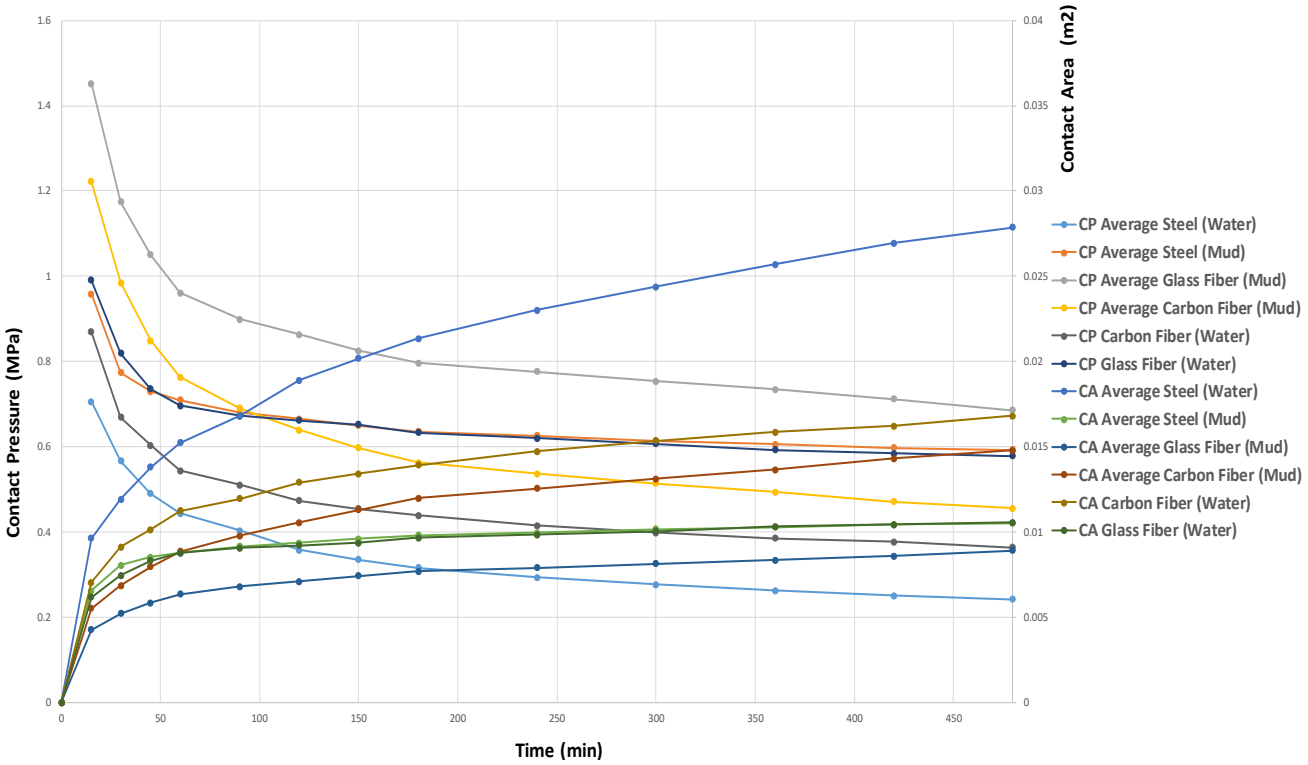

Figure 7. 30 - Averaged contact areas (CA) and contact pressures (CP) for different materials

The elevated temperatures during steel casing wear (up to 90°C were recorded in flow areas) are primarily attributed to the high particle grinding speed and the associated reduction in surface strength (friction heat alteration in material). The phenomenon, observed during all steel (water) tests, is explained further in Chapter 8.

With glass fiber and carbon fiber, no substantial increments in temperature were recorded to suggest any material alteration within the prescribed test hours. This is particularly attributed to the reduced hardness of the casings (compared to steel) and their lower heat conductivity. The low degree of adhesion compared to steel-steel contact hinders any strong heat buildup and the

accumulated heat remains near the contact region due to poor conductivity. The temperature is then further reduced by the fluid flow and heat loss into the surroundings.

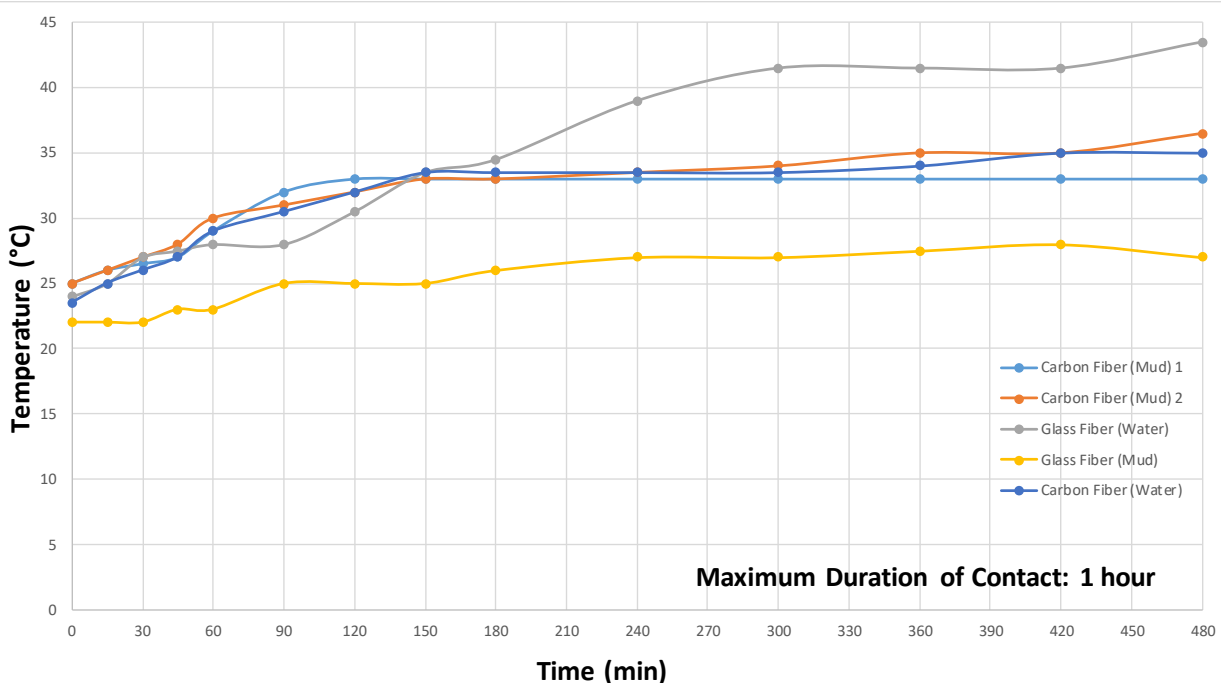

Figure 7. 31 - Recorded temperatures with time for glass fiber and carbon fiber materials

8. Discussion of test results and observations

In the scope of the experimental results in Chapter 7, different wear parameters were presented that were either measured or directly derived from measurements. The focus of discussion in this chapter is to utilize those measured parameters and observations to draw analytical inferences on wear behavior. Contact pressure threshold determination for limiting casing wear based on the test results will then summarize the experimental work and help derive conclusions of the study.

8.1. Analysis of calculated wear factors

Further to the comparison of wear factors and removed wall thicknesses, an analysis of the worn volumes as a function of infused frictional work in the casing specimen is carried out to determine the conventional (linear) wear factor and differential (non-linear) wear factor. The approach from R.W.Hall (presented in Section 2.2.7) has been used to determine expected contact pressure thresholds for the casing materials under the prevailing test conditions.

A plot of worn volume against applied frictional work for steel casing under mud conditions from test 7 is presented in Figure 8.1. The wear factor for linear behavior is ratio of the line joining the beginning and the end of the curve, whereas the differential wear factor for the actual non-linear behavior is the line tangent to the curve.

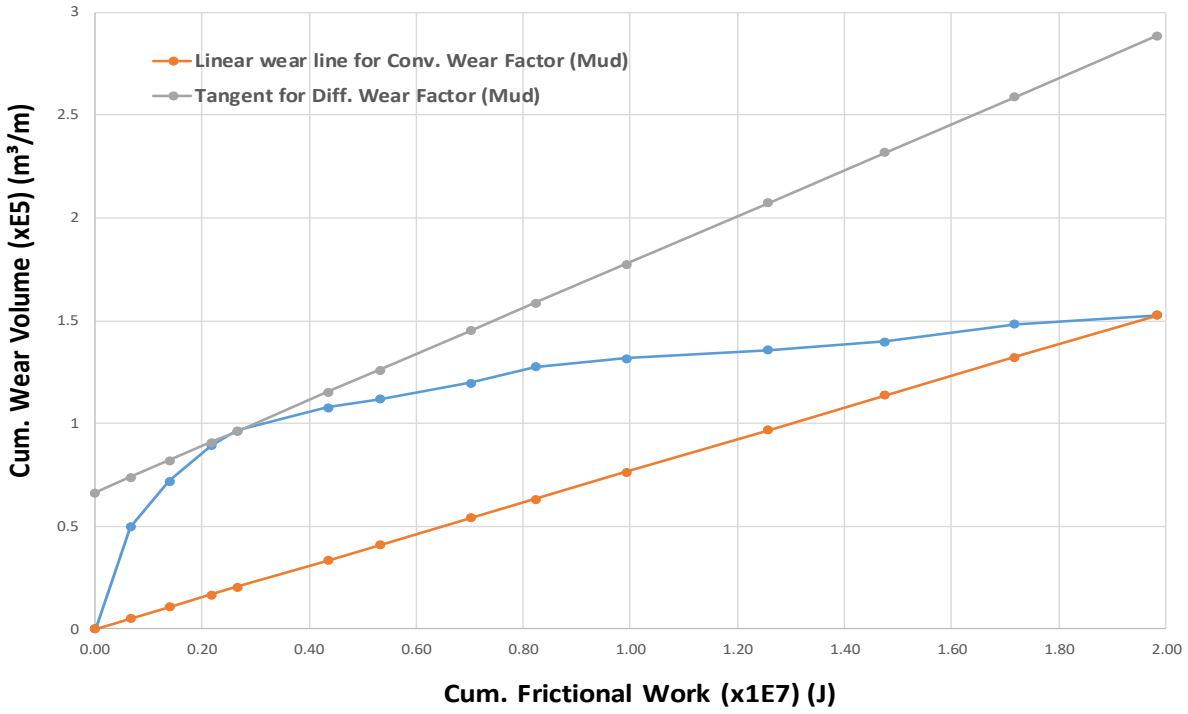

Figure 8. 1 - Cumulative wear volume vs. cumulative frictional work plot (for test 7) as the basis for defining conventional and differential wear factors

A similar plot is shown in Figure 8.2 for the steel casing under water conditions (for test 3). The obtained curve has a higher range due to significantly higher frictional work (approx. twofold friction factor) and higher worn volumes (approx. 24 times higher wear volume in comparison). Though also non-linear, the curve is steep due to the steady high wear rates and continual removal of large volumes under high friction.

For this reason, the similar lines for linear and non-linear wear factor on the curve run close to each other.

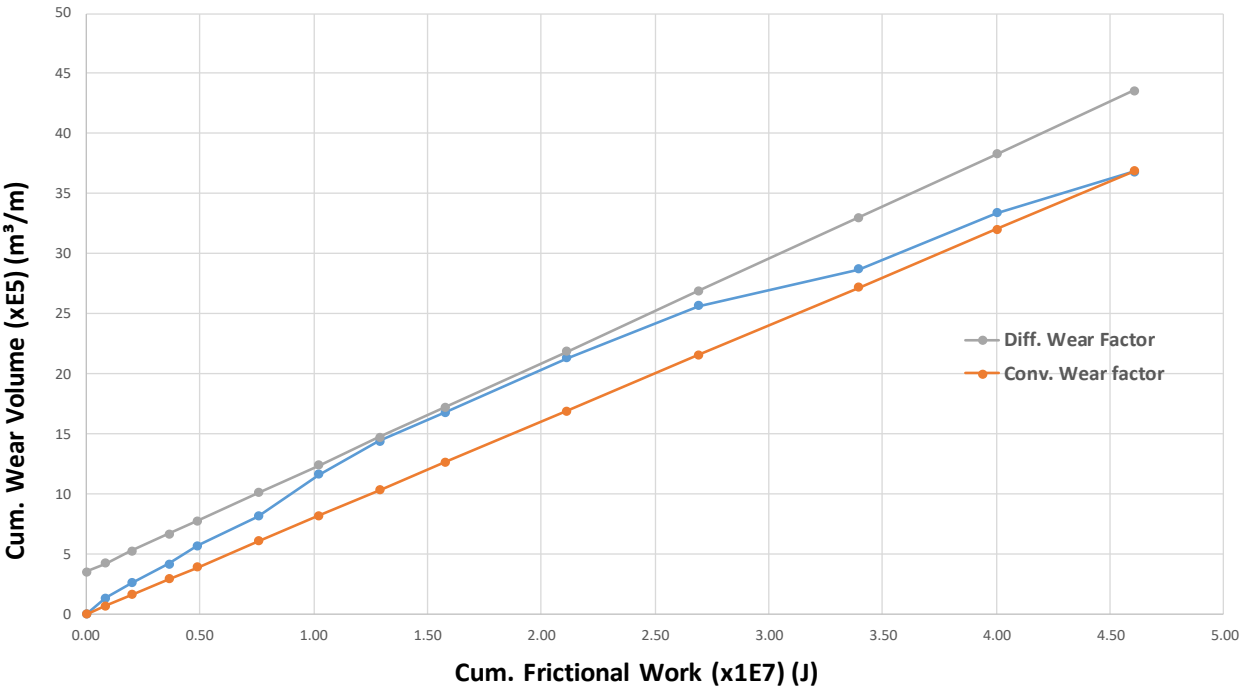

Figure 8. 2 - Cumulative wear volume vs. cumulative frictional work plot (for test 3)

8.2. Contact pressure thresholds (CPT) for casing materials

8.2.1. Steel casing

Plots like Figures 8.1 and 8.2 are then plotted for all other steel wear tests, yielding similar curves. The obtained data points for linear and differential wear factors are then plotted against measured contact pressure for their respective tests.

Both conventional and differential data points converge upon the abscissa (contact pressure axis) on the pressure values where least wear factors are observed. The pressure signifies the contact pressure limit (after continually reducing) that limits the wear volume and corresponds to the maximum depth of wear groove at existing test conditions. From the plot in Figure 8.3, the values of the CPT do not converge sharply to specific pressure values as considerable wear was still ongoing at the end of the test duration (only measured data points are included in the plot).

Assuming that the wear behavior remains constant for all steels tests, an extrapolation of the curves can provide a more exact approximation of the CPT. From the plots in Figure 8.3, steel casing specimens appear to have a CPT around 0.2MPa with water and about 0.6 MPa with mud at 6.7KN side force and 100RPM rotational speed.

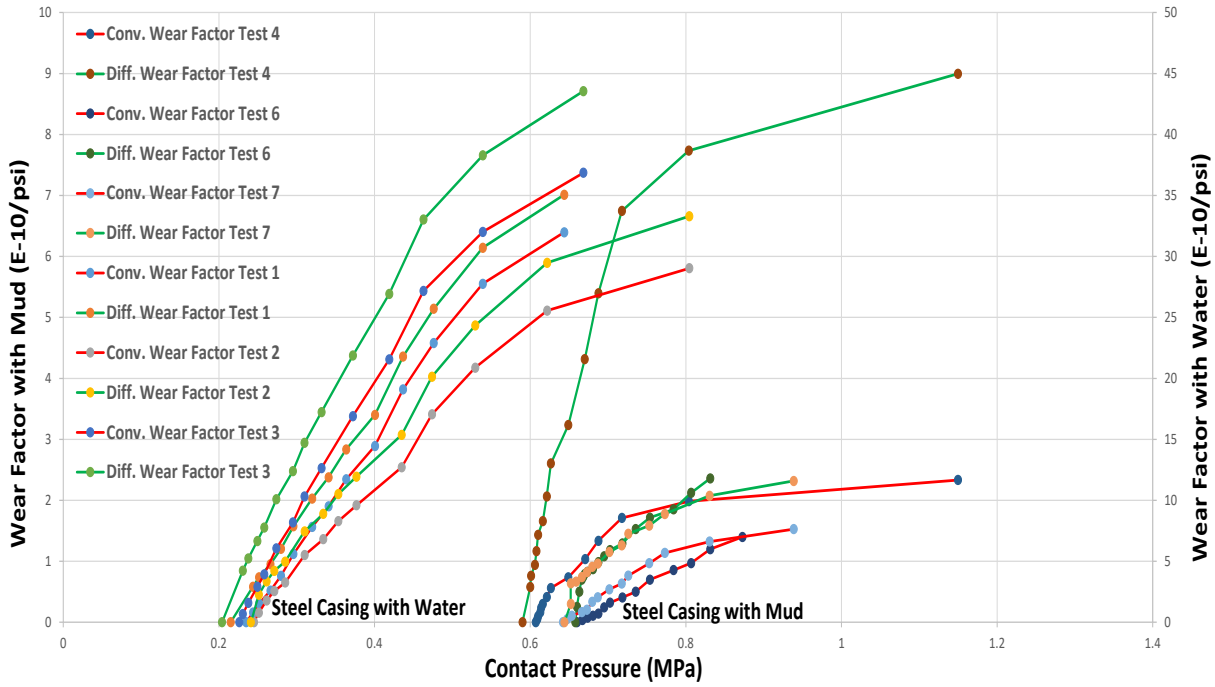

Figure 8. 3 - Linear and differential wear factor points plotted against contact pressure to obtain CPT for steel specimens

8.2.2. Glass fiber casing

The same approach is applied for tests with glass fiber casing where the wear rate was considerably reduced until the end of the prescribed test time. For this reason, the wear factors converge more sharply upon the contact pressure axis and more exact approximations of the CPT can be made. From the plot in Figure 8.4, glass fiber casing had a CPT of about 0.55MPa with water and 0.64MPa with mud under the prescribed test conditions. This implies that the wear behavior for glass fiber casing under water and mud conditions is relative similar, with a "no further wear" pressure limit close to each other (a difference of 0.11MPa or 13psi). This behavior is dissimilar to steel casings.

Another observation from the obtained CPT curves for glass fiber casing is the relative "S" shape of the curve, compared to the obtained curves for steel and carbon fiber casing. This is attributed to the presence of the resin layer at the inner wall of the casing that has a different frictional behavior than the underlying fibered glass layer. This method of determining CPT can be further

be refined to include casings with different layered materials by obtaining more data points (longer tests) specific to the glass layer only and eliminating the initial curl in the curve.

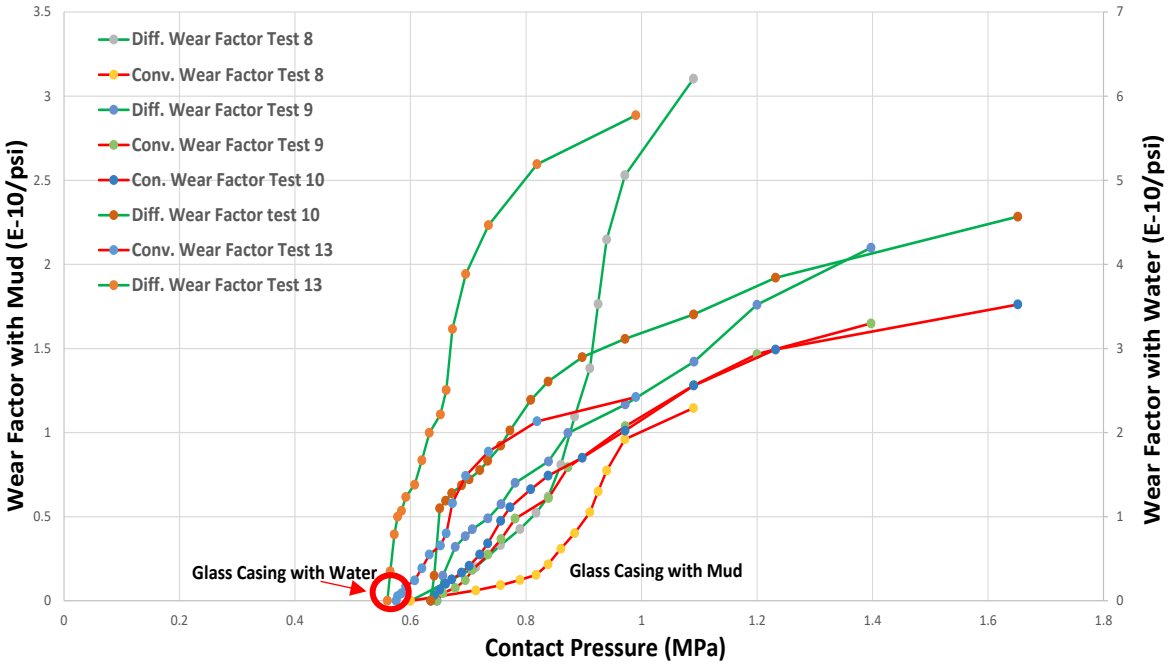

Figure 8. 4 - Linear and differential wear factor points plotted against contact pressure to obtain CPT for glass fiber casing specimens

8.2.3. Carbon fiber casing

The CPT curves for carbon fiber casings are similar to ones from steel in shape but with a lower range of wear factors. Figure 8.5 implies that the casing specimen has CPT of about 0.4MPa with water and about 0.44MPa with mud for the test plan.

It is important to differentiate here that the wear factor is a measure of the prevailing wear rate, and CPT is an indicator of limit wear where the wear factor becomes very little or zero. A confusion between the two sometimes makes routine operations difficult when a single wear factor (from the initial or later wear stages) is provided to operators for decision making on parameters such as top-drive speed or hook load. It is then assumed on the WF basis that the groove depth on casing will steadily increase. If the CPT for the casing TJ interaction is provided alongside and the value is high for the operating conditions, the operator can simply continue with the prescribed RPM and hook-load without worrying as the groove will remain shallow and not increase after CPT has been reached.

Like wear factor, CPT curves for casing materials are very specific to the wear conditions and can only be accurately determined experimentally. Companies involved in tool joint and hardband manufacturing (Tenaris, Vallourec, Arnco, Castolin etc.) are doing extensive experimental work

on wear-limiting hardbands and TJ dimensions for specific casing sizes. Considering both the experimentally determined averaged wear factors and CPTs as design objectives, non-productive time in terms of "lowering of surface parameters due to casing wear concerns" can be effectively reduced with such "self-wear-limiting" tool joints.

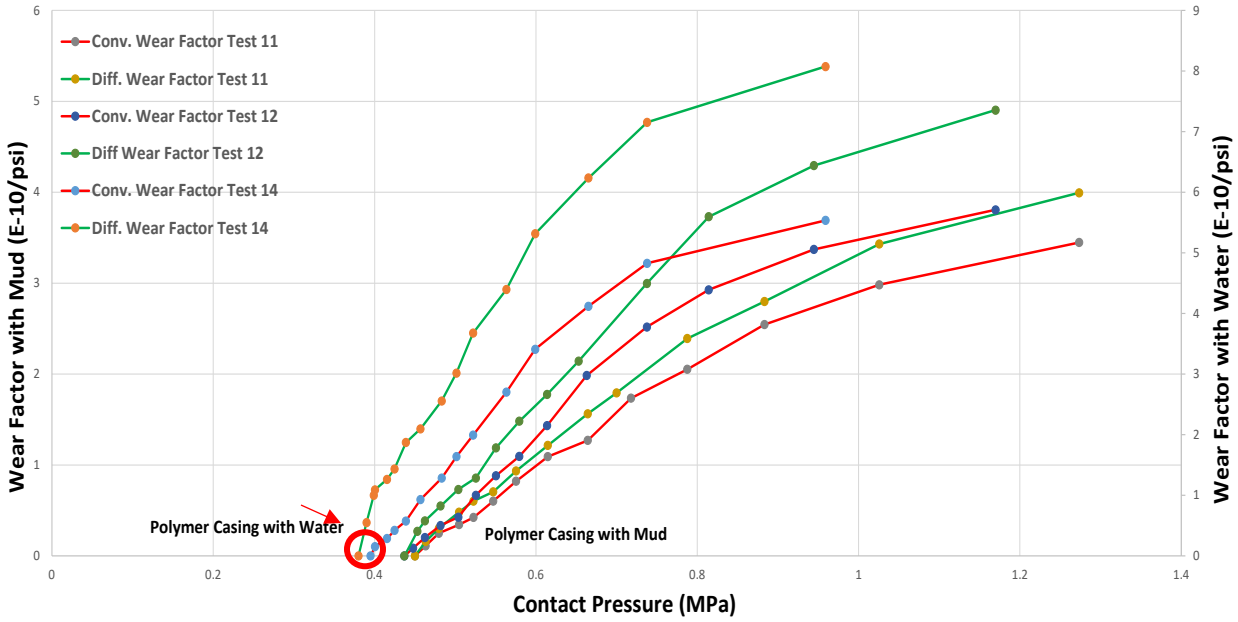

Figure 8. 5 - Linear and differential wear factors plotted against contact pressure to obtain CPT for carbon fiber casing specimens

8.3. Steady wear factor value for wear determination for long contact intervals

Due to the fluctuations in the initial stages in all wear factor plots, it has been proposed to use averaged steady wear factor values for wear volume projections for longer contact intervals (more than 8 hours). Though the specimens did not attain a constant wear factor (contact pressure threshold not reached within 8 hours), the values observed in the later stages of all the tests show a steady declining pattern without much fluctuation. For this purpose, the higher values obtained in the initial stages do not represent the wear propagation for longer wear durations.

In this regard, equation (34) can be modified to calculate wear volume under the test conditions.

$$V_W = W_{f_{St}} \times SF_{tj} \times \mu \times \pi \times D_{tj} \times RPM \times t \qquad (76)$$

Here,

$W_{f_{St}}$ is the steady wear factor value, E-10/psi

μ is the average measured friction factor

The determination of a steady wear factor involves selecting a range of at least 3 consecutive observed wear factors that fulfil the condition described in equation 78. The fluctuation of less than 20% is determined statistically and is expected to be improved with addition of more wear tests under similar conditions. The conditions for selection of steady wear factor is presented in equations 77 and 78.

$$W_{f_{avg}} = {\left(W_{f_1} + W_{f_2} + W_{f_3} + \cdots + W_{f_n}\right)}/{n} \quad , \; n \geq 3 \tag{77}$$

$$\left(\frac{|W_{f_{max}} - W_{f_{min}}|}{\overline{W_f}} \times 100\right) \leq 20\% \tag{78}$$

Here, $\overline{W_f}$ is the average of all 13 wear factor values, E-10/psi

If these conditions are met, the averaged value is adapted as the steady wear factor and can be used for wear prediction models.

$$W_{f_{avg}} = W_{f_{St}} \tag{79}$$

As an example, the wear volume for Test 5 projected over 29 hours using the above method is presented in Figure 8.6. The projected rate of wear is expected to be very low compared to the initial steep increase in wear volume.

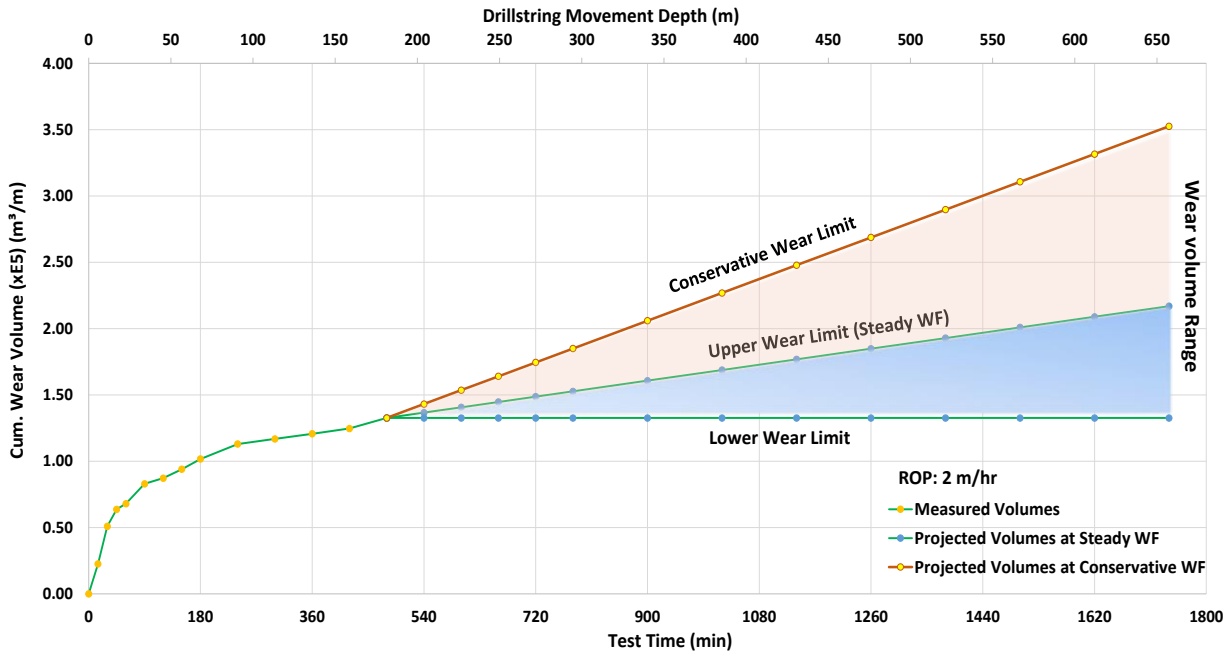

Figure 8. 6 - Projected wear volumes for Test 5 (Steel casing with mud) after 8 test hours

The presented approach is empirical and based on the observations of 14 wear tests. With inclusion of more test data, the method may be modified to obtain more exact representations of wear factor.

8.4. Analysis of the formation of protective film in mud tests

From the wear tests with mud, it was observed that for a functioning anti-galling film to exist, the mud must be:

1. dense to impart sufficient mud solids at the contact
2. viscous/adhering to the contact surfaces
3. chemically passive to the contact surface

The presence of barite particles in the mud tests was able to form a lubrication film that switched the wear mechanism from adhesive to abrasive wear. Furthermore, the added viscosity from bentonite made the fluid adhere to the surfaces and encouraged formation of the mud layer. Though no drilled solids were added during the wear test, it is anticipated that such addition will enhance the film effect for the test setup. Authors such as Bol [39] and Bradley & Fontenot [2] have expressed different experimental observations for wear reduction upon addition of mud solids. Based on the outcomes from the mud tests, this study tends to agree more with observations from Bradley and Fontenot [2]. Images showing the presence of the film between rotating TJ and casing during the test is presented in Figure 8.7.

An increase in the side force with the same RPM and mud situation increases the frictional shear at the contact and the metal surface can again replace the mud layer, causing reoccurrence of galling and increased wear rate. This is another reason why it is important to experimentally determine wear factor in terms of operational parameters. A steady wear factor is a non-linear resultant of the individual combination of the parameters and is not representative of field scenarios with significant deviations from test conditions

Figure 8. 7 - Hydrodynamic “bearing” formation between steel casing and TJ during wear tests

8.5. Discussion in friction heating and material alteration

During steel (water) wear tests, welded metal spots were observed on tool joint as it was friction-heated and immediately quenched thereafter by flowing water. This was particularly visible during longer test durations (1 hour) as big percentages of applied mechanical work done is converted into thermal energy. From literature, such sudden increase in temperature on the wear surface is usually accompanied by a rapid decrease in its yield strength. Image showing casing material degradation during steel tests are shown in Figure 8.8.

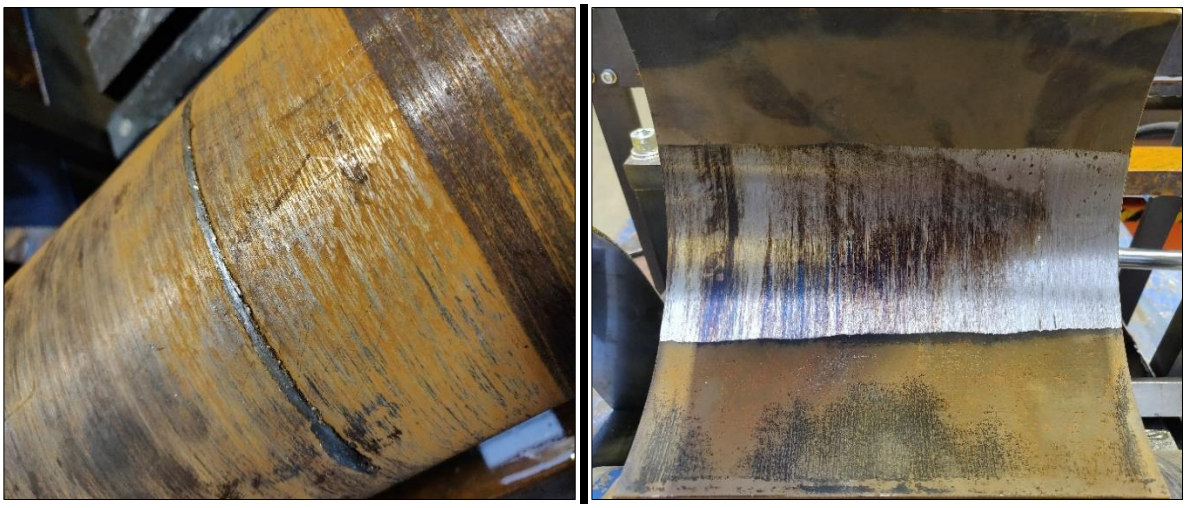

Figure 8. 8 - Material worn off steel casing and welded on to TJ during Test No. 2 (with water)

Heat checking, as the phenomenon is named by many authors, softens the material layer, accelerates the rate of galling, and keeps the wear rate steadily at high values and hinders it from reaching it contact pressure threshold. The extent of heating checking and resultant added loss of worn volume is individual to the casing material, side force, RPM and lubrication parameters and cannot be accurately calculated for general cases.

With mud case, no significant heat checking was observed as the bigger extent of contact area was cushioned and lubricated by mud solids.

8.6. Preliminary analysis of roughness profiles before and after tests

A preliminary analysis of the roughness profile of worn casing surfaces after wear tests was also carried out to obtain a better understanding of wear rate reduction in term of change in surface roughness. The roughness profile was determined using the profiling feature of a digital imaging microscope (Keyence VHX-970F). The profiling, however, was done at local spots with highest groove depth, and may not represent the entire surface roughness of the worn area.

For comparison, the arithmetic mean roughness profile ***(R_a)*** and peak-to-valley roughness profile ***(R_z)*** were taken as the roughness scale.

For steel casing wear with water, the measuring profile at all deep spots showed localized increase in the roughness profile compared to the unworn profile of the same specimen (not the same spot). As shown in Figure 8.9 on the spots, R_a and R_z were measured to be 1.51µm (from 0.4µm) and 10.71µm (from 2.54µm) respectively.

Figure 8. 9 - Roughness profile for steel casing (with water) pre-test vs after test

For mud tests for steel casing, an increase in roughness profile at most spots was observed, though clearly lesser than the worn profile for tests with water. From literature, such roughness profile (long scratches showing continuous wear lines as shown in Figure 7.11) is characteristic of three-body abraded surfaces when the moving surface is the harder (abrasive) surface.

Figure 8. 10 - Roughness profile for steel casing (with mud) pre-test vs after test

For glass fiber and carbon fiber casings, the majority of the spots yielded very comparable roughness profiles for pre- and post-wear. The surfaces appeared marginally rougher from touch and naked-eye inspection, and only minor increments in roughness were observed under the microscope (increase in 1µm - 2µm in R_a and 3µm - 4µm in R_z). Some images from the smooth worn surfaces after tests are presented in Figure 8.11.

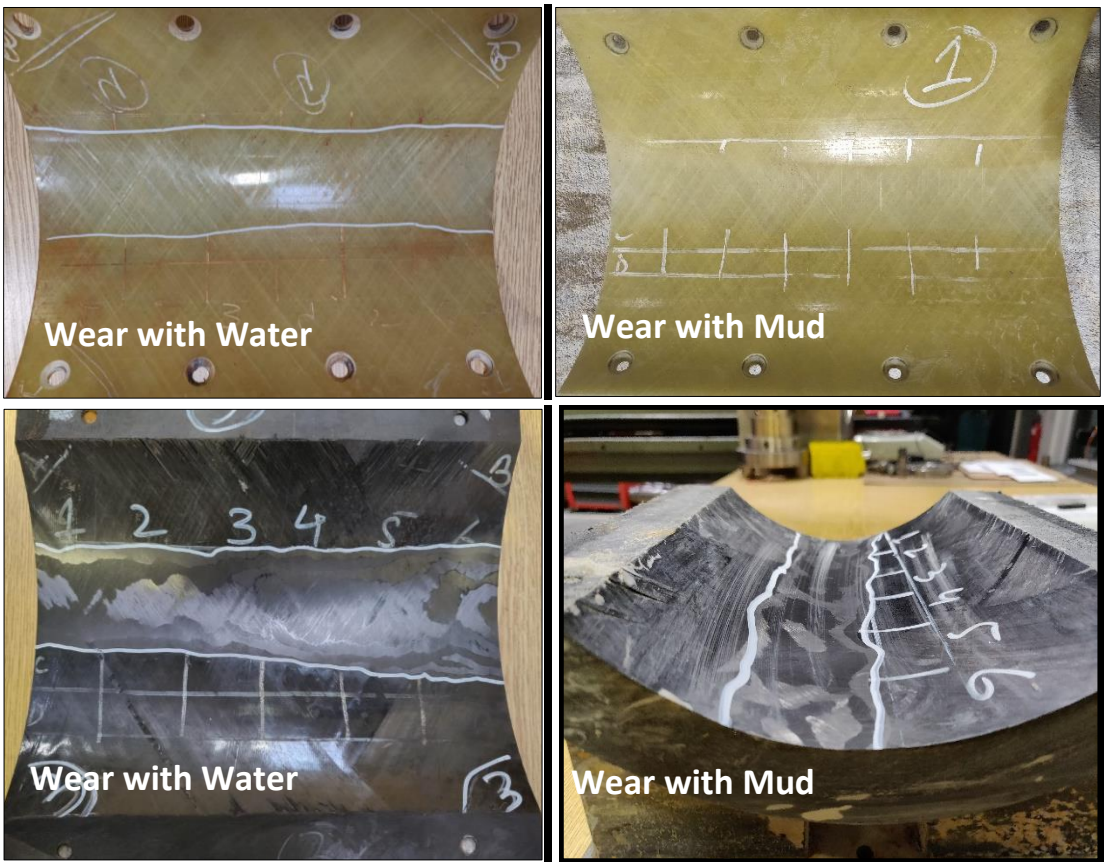

Figure 8. 11 - Smooth worn roughness profiles for glass fiber and carbon fiber casings with water and mud

8.7. Comparison to previous experimental setups

The number of design wear parameters included in the test setup, especially the inclusion of measured friction factors and wear factors over time, make it unique for carrying out a comprehensive wear analysis on different casing wear scenarios. No other recent experimental studies include measurements of friction factor over time under different pressures, materials and lubrications to the experimental wear analysis.

Experimental studies like Bol et al.[6] have reported the formation of a thin “hydrodynamic layer” for weighted muds. The effect of such protective layers upon friction factor and wear factor is observed and discussed in this study.

The measured friction factors for steel (with and without protective mud layer) in the experimental part are consistent with the results reported by White and Dawson et al. [3]. Furthermore, this study adds direct relation of the friction factors to wear factors and CPTs for 3 different casing materials.

In terms of wear factor analysis, a comparison can be made with the experimental work by Hall et al. and Mauer Engineering [6], which actually forms the basis of the API standard on casing

wear (API 7CW). Though different materials and wear conditions are prevalent in the available test data from Hall et al., the published results show similar wear plots and patterns compared to the results in this study.

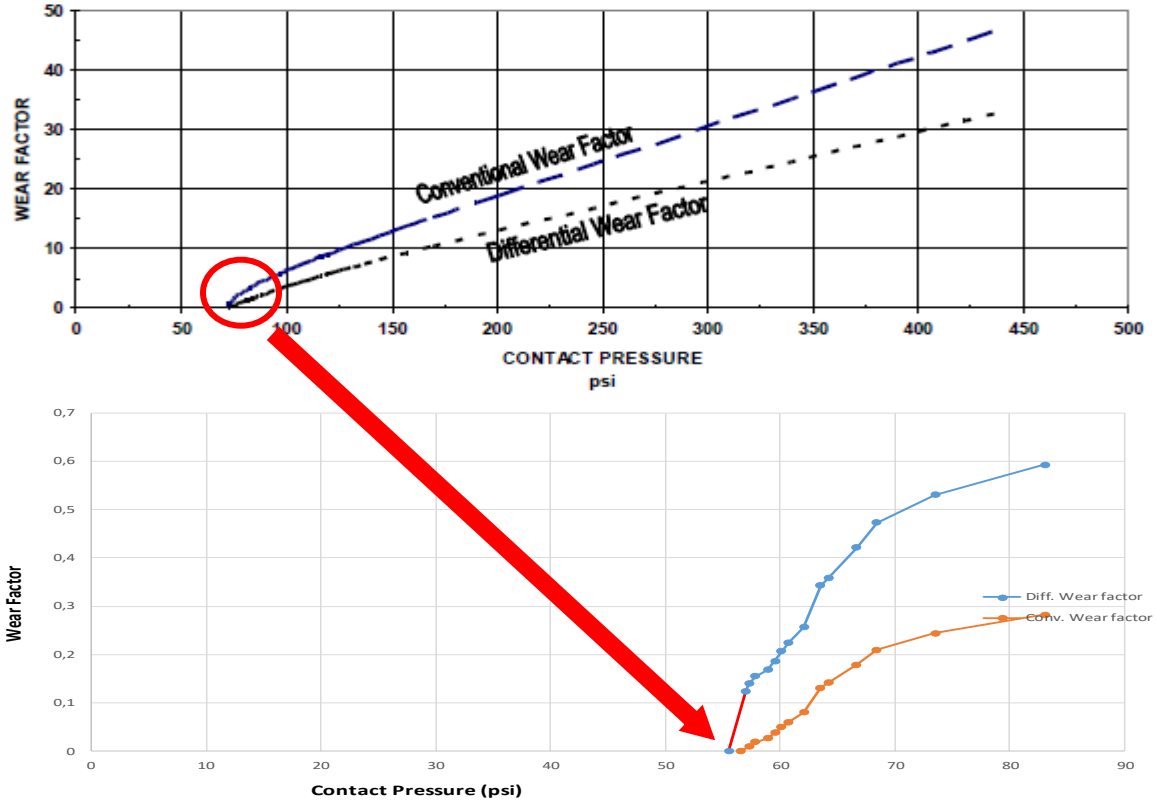

Figure 8. 12 - Comparison of CPT diagram from Hall et al. [6] with the one from test 7

The comparison and discussion on results have shown that repeated wear tests (for a database) can make casing wear predictable. Integration of the discussed parameters into industry casing wear solutions is a still an open topic. Attribution of specific wear factors or CPTs to certain field conditions via a wear test database, or its integration into a software solution, can fill gaps that can help reduce drilling and workover time extensively.

9. Conclusions and future investigations

Dynamic internal casing wear is a complex phenomenon due to the number of control variables influencing the wear behavior. Its recognition as a factor compromising well stability and drilling efficiency has been long overdue because of many reasons:

1. Abundance of simple, vertical wells until the end of the “easy oil” era
2. No software solutions available capable of accurately monitoring/predicting wear behavior
3. Inaccuracies in modeling casing wear without full-scale experimental investigations
4. Lack of published, experimental, and sorted data
5. Limited awareness about non-linear wear factors and Contact Pressure Threshold concepts

The aim of this thesis was to present an experimental approach highlighting critical wear parameters and their concurrent inter-relation upon the collective casing wear behavior. The wear behavior was initially discussed in terms of material wear mechanisms, simple mathematical models, wear measurement tools and mitigation techniques.

Conventional well planning software and existing mathematical models were then used to establish a wear test method in terms of side force, RPM, axial reciprocation speed, and type of fluid. This was used to design and configure a wear frame that allows simultaneous inclusion, monitoring and control of all these operational parameters and provides friction factor, wear volumes and wear factor as a measured output. The wear frame was also designed to be flexible to incorporate different casing materials and different fluid conditions.

The tests for specific materials and lubrication conditions were run together for ease, time-efficiency and comparison purposes. Comparing relevant test results with previous experimental studies is the best way to validate their reliability. In this regard, the test results were consistent and in line with the parameter ranges defined in previous studies. The test layout, experimental determination of friction factor (frictional work), wear volume and subsequent wear factor at different wear stages presents a unique analysis of wear factor variations over different wear stages. The novelty in this approach for determination of wear parameters lies in the comprehensiveness of determining surface parameters (side force, RPM, tubular diameters and mud settings) using specific software solutions, the flexibility to incorporate those parameters into an experimental setup for full-scale wear tests, and the determination of a time-based log of friction- and wear factors. Based on the test results, the obtained wear factors can then be applied to estimate wear under specific downhole sections.

Following the design and construction of the frame, a total of 14 tests could be carried out so far in the study time-frame for 3 different casing materials under water and mud conditions (excluding frame calibration and sensitivity runs). With the inclusion of more steel grades, diameters and new casing materials (aluminum, harder thermoset resins, glass or layered

composites), the wear frame can be used to develop a comprehensive record of wear factors under different field scenarios, and different wear phases for casing and TJ manufacturing industry. Representative multiple wear factors and CPTs can also be derived for an in-depth wear analysis on casing materials.

Wear factor for all materials was observed to have an initial peak value in the first hour of contact, and then decline drastically to steady ranges. These wear factor ranges, along with the material CPT value under test conditions, can provide a good input for field wear estimation and decision making on casing and tool joint selection. In terms of the peak, decline and steady regions observed in wear factor charts for 8-hour tests, the total period could be divided into initial, normalization, and steady wear stages. The observed wear factor ranges for the categories is presented in Table 9.1.

Table 9. 1 - Observed wear factors ranges and CPT for materials (same side force and RPM)

	Wear Factor			
	Initial Stage	Normalization Stage	Steady Stage	Contact Pressure Threshold
	E-10/psi	E-10/psi	E-10/psi	psi
Steel casing (Water)	200 to 225	90 to 151	90 and lower	29
Steel casing (Mud)	80 to 111	5 to 15	5 and lower	87
Glass fiber casing (Water)	80 to 200	25 to 70	25 and lower	80
Glass fiber casing (Mud)	90 to 140	20 to 55	20 and lower	93
Carbon fiber casing (Water)	170 to 340	60 to 170	60 and lower	58
Carbon fiber casing (Mud)	70 to 130	30 to 65	30 and lower	64

It is anticipated that under similar wear conditions, the most material specimens (steel, glass fiber or carbon fiber) will fail to acquire zero wear factor or ultimate wear depth within the 8-hour test duration. Wear tests can then be either extended to longer periods, or consistent wear data from repeated tests can be extrapolated using wear factors from the steady stage to have a good estimate on the CPT.

9.1. Further modifications to the wear frame

To improve accuracy of wear parameters, following modifications are underway for near future:

- Installation of sensors at the hydraulic axial reciprocation unit to identify frictional behavior specific to reciprocation. This will help further categorize the measured friction factor values into sliding and rotating friction factors.

- Installation of a more stable and smooth reciprocation platform for added stability against vibrations.
- Attachment of a sand feeder (Figure 9.1.) to introduce formation sand and cuttings at the contact

9.2. Future extensions of the study

A wide number of aspects are still open for further research to achieve the desired reduction in wear with operational flexibility. It is proposed to extend the scope of this research by means of experimental investigations using this wear frame in the following divisions:

1. **Effect of formation sand and cuttings on the stability of the protective mud film at the contact area:** The current wear tests were conducted with base mud solids of barite and bentonite. Added tests to include formation sands and drill cuttings can bring the test conditions a lot more representative of inclined borehole scenarios. Controlled precise amounts of sand and cuttings can be “poured” upon the contact using a “funnel weight feeder”. The vibrational conveyer is particularly feasible for exact continuous gravimetric feeding of sand and small cuttings in limited space installations.

Figure 9. 1 - Funnel weight feeder for inclusion of cuttings and sand at wear contact [60]

Some previous studies have indicated an improvement of wear resistance as cuttings are smeared upon the contact [2]. Its influence, however, in precise terms of friction and wear factors is a part that requires dedicated full-scale experimental work.

2. **Heat checking problems and thermal degradation of material:** Extreme heating and thermal quenching is expected to reduce casing yield strength in near-contact region. Though the phenomenon was observed multiple time during the experimental part of the study, a more precise representation of this strength reduction can be made by carrying out and comparing tensile test results for worn and unworn pieces from the same casing specimen.

3. **Inclusion of downhole temperatures:** Another research aspect similar to heat checking is the wear characteristics of a preheated casing specimen to account for bottomhole

temperatures. The sample can be heated using glued induction cable connections (owing to the small size of the casing) that can remain stable during TJ vibrations/casing reciprocations to keep the temperature steady. This test modification is particularly informative for determining depth limitations for resin-layered glass fiber casings as the strength of the resin layer deteriorates significantly at higher temperatures (above 90°C). For carbon fiber, test temperatures of around 162°C are required.

4. **Casing wear estimation based on tribological concepts of frictional energy density:** The estimation of material wear type based on frictional energy-density for dynamic contacts (Fleischer, 1997) takes a comprehensive tribological aspect into casing wear study. The concept is developed to determine wear and service life of moving machine elements in regular contact (such as roller or journal bearings) under direct- and lubricated-contact conditions [61].

   The approach is analogous to using frictional work and wear volume plots for wear behavior prediction used in this study (in Chapter 8). It however, takes a tribological context based on the principle that when energy/work is provided to the material at the contact, an amount is dissipated as heat energy and the remaining energy disrupts the micro-structure of the material in terms of elastic and plastic deformations. When this energy reaches a certain level, material wear starts to occur. The model categorizes the frictional workdone per worn volume as "apparent friction energy-density" (e_R) and a ratio of frictional shear stress to apparent friction energy density as "linear wear intensity" (I_h).

$$e_R = {}^{frictional\ workdone}/_{wear\ volume} \tag{80}$$

$$I_h = {}^{frictional\ shear\ stress}/_{e_R} \tag{81}$$

   A statistical distribution of e_R and I_h recognizes different wear regions in terms of wear intensity presented in Figure 9.2. As an example, putting measured frictional workdone, wear volume and friction shear stress from test 7 locates the wear type to category 3 for initial wear and category 2 for normalized wear.

   A quantitative analysis for wear type in terms of frictional workdone can help recommend range of operational parameters that can keep the wear intensity in tolerable ranges. However, the representation of wear in terms of energy density is based primarily on the micro-structure of the surfaces in contact and their contact geometry. It interprets the number of raised micro-contacts on the contact-surfaces by mathematical equations. A

representative roughness profile analysis of the casing/TJ microstructures of material surface types is necessary to accurately apply this method on casing wear.

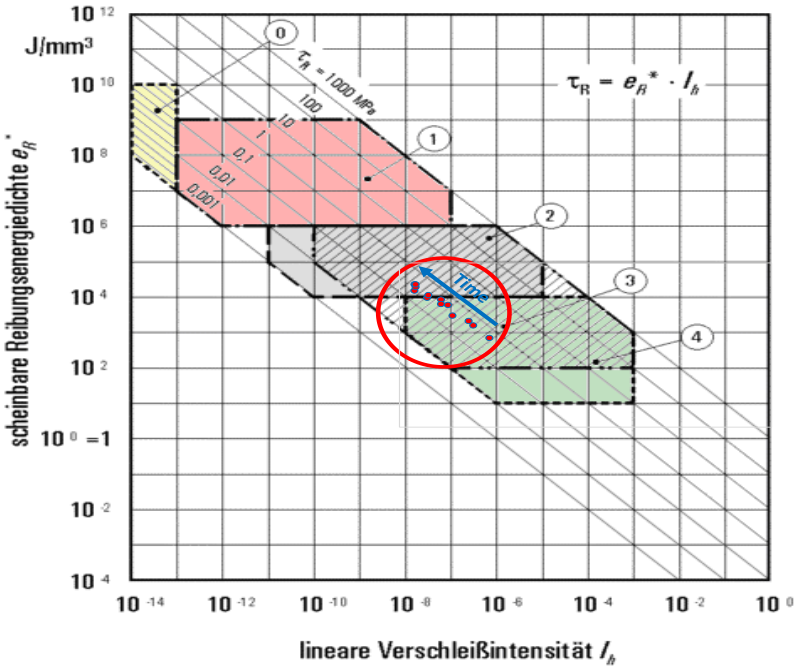

Color	Category	Wear type
	0	No Wear
	1	Micro-wear due to repeated elastic deformations
	2	Micro-wear due to repeated plastic deformations
	3	Increased-wear due to significant plastic deformation
	4	Intensive macro wear due to significant plastic deformation

Figure 9. 2 - Wear intensity based on frictional energy and frictional shear stress for test 7

5. **Inclusion of novel hard facings:** A casing-friendliness comparison of hard-faced tool joints (Arnco X150® and Duraband®) in specific weighted mud conditions is also planned for future experimental studies. The current wear tests were all carried out with steel tool joint on 95HC grade (carbon steel), glass fiber and carbon fiber casings. In addition, comparisons with important grades used in deeper sections such 110HC and 125HC or sour grades can benchmark wear performances for manufacturers and researchers.

Development of a statistical model and its algorithm to be fed into a software is the ultimate goal of this study. An extensive test program would be required for such a statistical study, and for the improvements on the accuracy of the obtained results.

10. Literature References

1. Tan, L., Gao, D., Zhou, J., Liu, Y., Wang, Z. January 2018. Casing wear prediction model based on drill string whirling motion in extended-reach drilling. King Fahd University of Petroleum and Minerals. Arabian Journal for Science and Engineering. DOI:10.1007/s13369-018-3074-9
2. Bradley, W.B., and Fontenot, J.E. February 1975. The prediction and control of casing wear. Journal of Petroleum Technology. Society of Petroleum Engineers. SPE-6399
3. White, J.P., and Dawson, R. March 1987. Casing wear: laboratory measurements and field predictions. SPE-14325.
4. Song, J.S., Bowen, J., and Klementich, F. 1992. The internal pressure capacity of crescent-shaped wear casing. SPE-23902-MS.
5. Hall, R.W., Garkasi, A., Deskins, G., Vozniak, J. 1994. Recent advances in casing wear technology. IADC/SPE Drilling Conference, Dallas, Texas. IADC/SPE 27532
6. Hall, R.W., Malloy, K.P. 2005. Contact pressure threshold: an important new aspect of casing wear. SPE Production Operations Symposium, Oklahoma City. SPE 94300
7. Gao, D.L., Sun, L.Z., Lian, J.H. 2010. Prediction of casing wear in extended-reach drilling. Pet. Sci. 7(4), 494–501.
8. Gao, D.L., Sun, L.Z. 2012. New method for predicting casing wear in horizontal drilling. Pet. Sci. Technol. 30(9), 883–892.
9. Sun, L.Z., Gao, D.L., Zhu, K.L. 2012. Models & tests of casing wear in drilling for oil and gas. J. Nat. Gas Sci. Eng. 4, 44–47.
10. Stachowiak, G.W., and Batchelor, A.W. 2014. Engineering Tribology. Department of mechanical and materials engineers; University of Western Australia. eBook ISBN: 9780080531038
11. Yu, H., Lian, Z., Lin, T., Liu, Y., and Xu, X. March 2016. Experimental and numerical study on casing wear in highly deviated drilling for oil and gas. Advances in mechanical engineering. Vol. 8(7) 1-15. DOI: 10.1177/1687814016656535
12. Mitchel, S., and Xiang, Y. 2012. Improving casing wear prediction and mitigation using statistically based model. Richardson, Texas. SPE 151448. DOI:10.2118/151448-MS
13. Shen, Z., and Beck, F.E. May 2012. Intermediate casing collapse induced by casing wear in high temperature and high pressure wells. SPE 155973. Richardson, Texas. SPE-155973-MS https://doi.org/10.2118/155973-MS
14. Wang, T., Yan X., and Wang, J. March 2013. Investigation of the ultimate residual strength of a worn casing by using the arc-length algorithm. Engineering Failure Analysis 28:1–15. DOI:10.1016/j.engfailanal.2012.09.008
15. Lin, Y., Deng, K., and Xing, Q. June 2015. A new crescent-shaped wear equation for calculating collapse strength of worn casing under uniform loading. J. pressure vessel technology 137(3). 031201. https://doi.org/10.1115/1.4029588

16. National Oil Varco: Well intervention and measurement tools. DOI: https://www.nov.com/Segments/Wellbore_Technologies/Downhole/Fishing_Tools/Milling_and_Cutting_Tools/Bowen_Ditch_Magnet.aspx
17. Sawaryn, S.J., Patillo, P.D., Brown, C., and Schoepf, V. June 2015. Assessing casing wear in absence of a baseline caliper log. SPE-173143-MS. London, U.K. https://doi.org/10.2118/173143-PA
18. Baker Hughes: Corrosion Evaluation- Magnetic Thickness Tool. DOI: https:// www.bhge.com/upstream/evaluation/wireline-products-and-equipment/wireline-logging-evaluation-equipment/corrosion-evaluation-magnetic
19. Schlumberger USI: Ultrasonic Imager Tool. August 2004. DOI: https://www.slb.com/drilling/drilling-fluids-and-well-cementing/well-cementing/cement-evaluation/usi-ultrasonic-imager
20. Williamson, J.S. December 1981. Casing wear: The effect of contact pressure. Journal of Petroleum Technology. https://doi.org/10.2118/10236-PA
21. Calhoun, B., Langdon, S., and Wu, J. October 2010. Casing Wear Prediction and Management in Deepwater Wells. SPE 137223-MS. Galveston, Texas. https://doi.org/10.2118/137223-MS
22. Hoffmann, K. 1990. An introduction to measurements using strain gauges. Hottinger Baldwin Messtechnik GmbH, Darmstadt, Germany. DOI: http://elektron.pol.lublin.pl/users/elekp/MNEQ_english/Hoffmann_An_Introduction_to_Measurements_using_Strain_Gages.pdf
23. Brillaud, L. February 2020. Field-proven approach to keep casing wear under control, methodology and case study. Drillscan Whitepaper. DOI: https://www.drillscan.com/casing_wear_monitoring/
24. Eaton, L.F. February 1993. Tool joint heat checking while predrilling for auger TLP project. IADC drilling conference, Amsterdam. SPE/IADC 25776
25. Hehn, L., Jellison, M., Chandler, R., and K. Wyble. February 2007. Catastrophic drillstring failures caused by downhole friction heating-an increasing trend. SPE/IADC Drilling conference, Amsterdam. SPE-105026-MS. https://doi.org/10.2118/105026-MS
26. Erguo, L., and Zifeng, L. November 2011. Computation Model for Collapse Strength of the Casing Wear. Advanced Materials Research Online. https://doi.org/10.4028/www.scientific.net/AMR.403-408.496
27. API Bulletin 5C3. October 1994. Bulletin on Formulas and Calculations for Casing, Tubing, Drill Pipe, and Line Pipe Properties, 6th Edition.
28. Anders, J., Cismoski, D., Daniel, R., Dube, A., Engel, H., Hughes, A., Norene, T., Hamilton, R., and Mohr, W. September 2008. Prudhoe Bay Well P2-15 Surface Casing Failure. SPE 116771. https://doi.org/10.2118/116771-MS
29. Best, B. 1986. Casing Wear Caused by Tooljoint Hardfacing. SPE Drill Eng 1 (01): 62–70. SPE-11992-PA. https://doi.org/10.2118/11992-PA
30. Kumar, A., and Samuel, R. March 2014. Modeling Method to Estimate the Casing Wear Caused by Vibrational Impacts of the Drillstring. SPE-167999-MS. DOI:10.2118/167999-MS

31. Samuel, R., Kumar, A., Gonzales, A., Marcou, S., and Rod, A. M. March 2016. Solving the Casing Wear Puzzle Using Stiff String Model. SPE-183386-MS. https:// doi.org/10.2118/178833-MS
32. HESP Nouvelles technologies: Multi finger imaging tool specifications. 2018. http://www.hesp.com/index.php/nouvelles-technologies/autres/multi-finger-imaging-tool-mit
33. Patitllo, P.D., Pruitt, R. D., Nakbi, A.I., Gent, L., Young, K., and Zhang, X. June 2003. Repair Intervention of worn production casing in the Sajaa field. SPE-81537, Bahrain. https://doi.org/10.2118/81537-MS
34. Wu, J., and Zhang, M. Casing Burst Strength after casing wear. SPE-94304. Oklahoma City. 2005.
35. Mitchell, S., and Xiang, Y., March 2012. Improving casing wear prediction and mitigation using a statistically based model. SPE 151448. San Diego. https://doi.org/10.2118/151448-MS
36. Samuel, R. September 2010. Friction factors: What are they for torque, drag, vibration, bottomhole assembly and transient surge/swab analyses?. IADC/SPE 128059. New Orleans. https://doi.org/10.1016/j.petrol.2010.07.007
37. Kumar, A., and Samuel, R. March 2015. Casing wear factors: How do they improve well integrity analyses?. IADC/SPE 173053-MS. London. https://doi.org/10.2118/173053-MS
38. Arnco 150XT™ hardbanding: Arnco field services. DOI: https://www.arncotech.com/wp-content/uploads/2020/07/Arnco-150XT-Data-Sheet_Rev.-1.pdf
39. Bol, G.M. October 1986. Effect of Mud Composition on Wear and Friction of Casing and Tool Joint. SPE-13457-PA. Shell E&P Laboratorium. https://doi.org/10.2118/13457-PA
40. Hood, J., Hovden, J., Heisig, G., and Knipper, A. February 2003. Real-Time BHA Bending Information Reduces Risk when Drilling Hard Interbedded Formations. SPE 79918. Amsterdam. https://doi.org/10.2118/79918-MS
41. Menand, S., Sellami, H., Akowanou, J., Simon, C., Macresy, L.P., Isambourg, P., and Durpuis, D.C. March 2008.How drill string rotation affects critical buckling load?. SPE-112571-MS. Orlando. https://doi.org/10.2118/112571-MS
42. Seitinger, P. June 2010. Casing wear analysis: An analysis of the parameters causing casing wear in Troll field and possible solutions. University of Leoben. DOI: https://pure.unileoben.ac.at/portal/en/publications/casing-wear-analysis-an-analysis-of-the-parameters-causing-casing-wear-in-troll-field-and-possible-solutions(84159fa4-d12e-40a4-8a4f-65bda49f3394).html
43. Moore, N.B., Mock, P.W., and Krüger, R.E. May 1996. Reduction of Drill String Torque and Casing Wear in Extended Reach Wells Using Non-Rotating Drill Pipe Protectors. SPE 35666. Alaska. https://doi.org/10.2118/35666-MS
44. Marx, C., Retelsdorf, H., and Knauf, P. 1991. Evaluation of new tool joint hardfacing material for extended connection life and minimum casing wear. SPE 22003. Amsterdam. ttps://doi.org/10.2118/22003-MS

45. Samuel, R., and Kumar, A. March 2018. Casing Wear Estimation: European Patent Specification: WO 2014/209282 (31.12.2014 Gazette 2014/53)
46. Pegasus Vertex Inc. 2018. White Paper: Casing Wear: Causes, Prediction and Prevention. DOI: https://issuu.com/pvisoftware/docs/casing-wear-causes-prediction-and-p
47. Zhang, Y., Samuel, R. September 2019. Engineers' Dilemma: When to use soft string and stiff string torque and drag models. SPE 196205-MS. Alberta, Canada. https://doi.org/10.2118/196205-MS
48. Rassenfoss, S. December 2015. Drilling wells ever faster may not be the measure of success. Journal of Petroleum Tech. DOI: https://jpt.spe.org/drilling-wells-ever-faster-may-not-be-measure-success
49. Altermann, J.A, and Smith, T.B. February 1992. Heat Checking/Quench Cracking Tool Joints. SPE 81537. New Orleans, Louisiana. https://doi.org/10.2118/23846-MS
50. Dai, W., Noel, B., Alvord, C., Njoku, J., Hopper, J., and Smith, L. September 2018. A practical approach to casing wear prediction, modeling and mitigation on challenging ERD wells. SPE-191495-PT. Dallas, Texas. https://doi.org/10.2118/191495-MS
51. Stephens, A.A., Akindipe, O., and Leong, C. March 2020. Downhole ultrasonic thickness measurements for inspection of casing. SPE-199806-MS. The Woodlands, Texas. https://doi.org/10.2118/199806-MS
52. WWT Non-rotating protectors. 2015. WWT Non-rotating protectors prevented additional casing wear. WWT Case History- North America-7869. DOI: https://www.wwtco.com/media/k2/attachments/WWT-NRP-Case-History-Horizontal-Casing-Wear-US-Land-7869.pdf
53. WWT Non-rotating protectors. 2020. Reduced Drill Pipe Wear with WWT Non-Rotating Protectors in Lateral Wells. WWT Case History- North America- 8009. DOI: https://www.wwtco.com/media/k2/attachments/WWT-NRP-Case-History-Directional-North-America-8009.pdf
54. WWT Non-rotating protectors. 2015. Latin American Operator Protects Casing in Low-ROP Drilling. WWT Case History- Latin America-7096. DOI: https://www.wwtco.com/media/k2/attachments/WWT-NRP-Case-History-Directional-Latin-America-7096.pdf
55. Medina, M., Bedino, H., Sierra, S., Scagliarini, S., Romero, D., Rocha, R., and Rosas, R. March 2014. Case history: Casing collapse during concentric drilling operation leads to new casing design approach for HP/HT wells with low reservoir pressure and/or N2 injection. IADC/SPE 167929. Texas. https://doi.org/10.2118/167929-MS
56. WWT Non-rotating protectors. 2015. Increased casing protection measurably reduces metal collected. WWT Case History- Latin America-7631. DOI: https://www.wwtco.com/media/k2/attachments/WWT-NRP-Case-History-Directional-Latin-America-7631.pdf
57. WWT Non-rotating protectors. 2014. Torque reduced by 20% as WWT NRPS moved through build section. WWT Case History- Permian-8923-2. DOI:

https://www.wwtco.com/media/k2/attachments/WWT-NRP-Case-History-Horizontal-Permian-8923-2.pdf
58. Griekspoor thermal coatings. Plasma Spraying highlights. DOI: https://www.griekspoorthermalcoatings.com/techniques.
59. API Bulletin 7CW. June 2015. Casing Wear Test, 1st Edition. American Petroleum Institute.
60. AViTEQ Vibrationstechnik GmbH. Technical Brochure. Neuentwicklung Differentialdosierwaagen. DOI: https: //aviteq.com/en/news/detail/article /neuentwicklung- differentialdosierwaagen/
61. Fleischer, G., and Bosse, H. 1982. Berechnung der Reibung auf energetischer Grundlage. In: Wissenschaftliche Zeitung der TU Magdeburg 26. Nr. 6, S. 17-27. DOI: http://www.hoogi.de/tribo/verschleiss.html

11. Appendices

11.1. Well parameters for horizontal well H1

Cased Sections

Section Type	Section Depth (m)	Section Length (m)	Shoe Depth (m)	ID (in)	OD (in)	Drift (in)	Eff. Hole Diameter (in)	Coefficient of Friction	Casing Weight
L-80 Casing	1893.47	1893.470	1893.47	8.681	9.625	8.625	12.250	0.25	47
C-95 Casing	2952.89	1059.420	2952.89	8.435	9.625	8.375	12.250	0.25	58.4
Open Hole	4340.00	1387.110		8.250			8.250	0.40	

Operation Sequence

Name	Type	Start MD (m)	End MD (m)	Fluid	String	Weight on Bit (kip)	Revolutions Per Minute (rpm)	On-Bottom Time (hr)	Default Wear Factor (E-10/psi)
Oper #1	Drilling	2952.89	3490	Mud #1	H1 BHA1	17.6	130	85.22	1.5
Oper #2	Drilling	3230	3517.27	Mud #1	H1 BHA 2	9.0	40	50.25	2
Oper #3	Drilling	3517.27	3735	Mud #1	H1 BHA3	9.0	35	105.00	5
Oper #4	Drilling	3735	3980	Mud #1	H1 BHA 4	17.6	40	64.30	10
Oper #5	Drilling	3980	4320	Mud #1	H1 BHA 5	14.0	50	111.87	30

Drilling Parameters

Operation	Weight on Bit (kip)	Revolutions Per Minute (rpm)	On-Bottom Time (hr)
Oper #1	17.6	130	85.22
Oper #2	9.0	40	50.25
Oper #3	9.0	35	105.00
Oper #4	17.6	40	64.30
Oper #5	14.0	50	111.87

Applied BHAs

BHA 1

Type	Length (m)	Depth (m)	Body		Stabilizer / Tool Joint				Weight (ppf)	Material	Grade
			OD (in)	ID (in)	Avg. Joint Length (m)	Length (m)	OD (in)	ID (in)			
Drill Pipe	3,344	2,494	5.5	4.67	9.66	0.457	7.5	3	28.87	CS_API 5D/7	S
Sub	1	2,494	5.4	2.76	0.54				59.71	CS_API 5D/7	4145H MOD
Drill Pipe	752	3,246	5	4	9.64	0.433	6.62	2.75	28.32	CS_API 5D/7	G

Type	Length (m)	Depth (m)	Body		Stabilizer / Tool Joint				Weight (ppf)	Material	Grade
			OD (in)	ID (in)	Avg. Joint Length (m)	Length (m)	OD (in)	ID (in)			
Heavy Weight	131	3,377	5	3	9.14	1.219	6.5	3.063	49.7	CS_1340 MOD	1340 MOD
Jar	10	3,387	6.75	2.5	9.9				104.76	SS_15-15LC	15-15LC MOD (1)
Drill Collar	91	3,478	6.5	3	9.14				88.86	CS_API 5D/7	4145H MOD
Stabilizer	2	3,480	6.25	2.813	1.64	0.305	8.12		83.27	CS_API 5D/7	4145H MOD
Drill Collar	9	3,489	6.5	3	9.14				87.95	SS_15-15LC	15-15LC MOD (1)
Sub	1	3,490	6.24	2.76	0.91				83.26	CS_API 5D/7	4145H MOD
Bit	0	3,490	8.25		0.25				140		

BHA 2

Type	Length (m)	Depth (m)	Body		Stabilizer / Tool Joint				Weight (ppf)	Material	Grade
			OD (in)	ID (in)	Avg. Joint Length (m)	Length (m)	OD (in)	ID (in)			
Drill Pipe	2,090	2,090	5.5	4.67	9.66	0.457	7.5	3	28.87	CS_API 5D/7	S
Sub	1	2,091	5.4	2.76	0.92				59.71	CS_API 5D/7	4145H MOD
Drill Pipe	1,322	3,413	5	4.27	9.64	0.433	6.62	3.25	21.92	CS_API 5D/7	G
Heavy Weight	28	3,441	5	3	9.38	1.219	6.5	3.06	49.7	CS_1340 MOD	1340 MOD
Jar	10	3,451	6.62	2.5	9.91				104.76	SS_15-15LC	15-15LC MOD (1)
Heavy Weight	28	3,479	5	3	9.34	1.219	6.5	3.06	49.7	CS_1340 MOD	1340 MOD

Type	Length (m)	Depth (m)	Body		Stabilizer / Tool Joint				Weight (ppf)	Material	Grade
			OD (in)	ID (in)	Avg. Joint Length (m)	Length (m)	OD (in)	ID (in)			
Drill Collar	18	3,497	6.75	3	9.14				96.71	SS_15-15LC	15-15LC MOD (1)
MWD	10	3,507	6.75	2.87	9.64				100.8	SS_15-15LC	15-15LC MOD (1)
Drill Collar	1	3,508	6.5	3	9.14				96.71	SS_15-15LC	15-15LC MOD (1)
Sub	1	3,508	6.5	2.76	0.61				83.26	CS_API 5D/7	4145H MOD
Mud Motor	9	3,517	6.75	3	8.67				79.41	SS_15-15LC	15-15LC MOD (1)
Bit	0	3,517	8.25		0.25				85		

BHA 3

Type	Length (m)	Depth (m)	Body		Stabilizer / Tool Joint				Weight (ppf)	Material	Grade
			OD (in)	ID (in)	Avg. Joint Length (m)	Length (m)	OD (in)	ID (in)			
Drill Pipe	2,073	2,073	5.5	4.67	9.66	0.457	7.5	3	28.87	CS_API 5D/7	S
Sub	1	2,074	5.4	2.76	0.92				59.71	CS_API 5D/7	4145H MOD
Drill Pipe	1,322	3,396	5	4.27	9.64	0.433	6.625	3.25	21.92	CS_API 5D/7	G
Heavy Weight	47	3,443	5	3	9.38	1.219	6.5	3.063	49.7	CS_1340 MOD	1340 MOD
Jar	10	3,453	6.62	2.5	9.91				104.76	SS_15-15LC	15-15LC MOD (1)
Heavy Weight	253	3,706	5	3	9.34	1.219	6.5	3.06	49.7	CS_1340 MOD	1340 MOD

Type	Length (m)	Depth (m)	Body		Stabilizer / Tool Joint				Weight (ppf)	Material	Grade
			OD (in)	ID (in)	Avg. Joint Length (m)	Length (m)	OD (in)	ID (in)			
Drill Collar	9	3,715	6.75	3	9.14				96.71	SS_15-15LC	15-15LC MOD (1)
MWD	10	3,725	6.75	2.87	9.64				100.8	SS_15-15LC	15-15LC MOD (1)
Drill Collar	1	3,725	6.5	3	9.14				96.71	SS_15-15LC	15-15LC MOD (1)
Sub	1	3,726	6.5	2.76	0.61				83.26	CS_API 5D/7	4145H MOD
Mud Motor	9	3,735	6.75	3	8.67				79.41	SS_15-15LC	15-15LC MOD (1)
Bit	0	3,735	8.25		0.25				85		

BHA 4

Type	Length (m)	Depth (m)	Body		Stabilizer / Tool Joint				Weight (ppf)	Material	Grade
			OD (in)	ID (in)	Avg. Joint Length (m)	Length (m)	OD (in)	ID (in)			
Drill Pipe	2,318	2,318	5.5	4.67	9.66	0.457	7.5	3	28.87	CS_API 5D/7	S
Sub	1	2,319	5.4	2.76	0.92				59.71	CS_API 5D/7	4145H MOD
Drill Pipe	1,322	3,641	5	4.276	9.64	0.433	6.62	3.25	21.92	CS_API 5D/7	G
Heavy Weight	47	3,688	5	3	9.38	1.219	6.5	3.06	49.7	CS_1340 MOD	1340 MOD
Jar	10	3,698	6.625	2.5	9.91				104.76	SS_15-15LC	15-15LC MOD (1)
Heavy Weight	253	3,951	5	3	9.34	1.219	6.5	3.06	49.7	CS_1340 MOD	1340 MOD

Type	Length (m)	Depth (m)	Body		Stabilizer / Tool Joint				Weight (ppf)	Material	Grade
			OD (in)	ID (in)	Avg. Joint Length (m)	Length (m)	OD (in)	ID (in)			
Drill Collar	9	3,960	6.75	3	9.14				96.71	SS_15-15LC	15-15LC MOD (1)
MWD	10	3,970	6.75	2.875	9.64				100.8	SS_15-15LC	15-15LC MOD (1)
Drill Collar	1	3,970	6.5	3	9.14				96.71	SS_15-15LC	15-15LC MOD (1)
Sub	1	3,971	6.5	2.76	0.61				83.26	CS_API 5D/7	4145H MOD
Mud Motor	9	3,980	6.75	3	8.67				79.41	SS_15-15LC	15-15LC MOD (1)
Bit	0	3,980	8.25		0.25				85		

BHA 5

Type	Length (m)	Depth (m)	Body		Stabilizer / Tool Joint				Weight (ppf)	Material	Grade
			OD (in)	ID (in)	Avg. Joint Length (m)	Length (m)	OD (in)	ID (in)			
Drill Pipe	2,686	2,686	5.5	4.67	9.66	0.457	7.5	3	28.87	CS_API 5D/7	S
Sub	1	2,686	5.4	2.76	0.91				59.71	CS_API 5D/7	4145H MOD
Drill Pipe	837	3,524	5	4.276					59.71	CS_API 5D/7	4145H MOD
Heavy Weight	47	3,570	5	3	9.14	1.219	6.5	3.063	49.7	CS_1340 MOD	1340 MOD
Jar	6	3,576	6.75	2.5	5.5				104.76	SS_15-15LC	15-15LC MOD (1)

Type	Length (m)	Depth (m)	Body		Stabilizer / Tool Joint				Weight (ppf)	Material	Grade
			OD (in)	ID (in)	Avg. Joint Length (m)	Length (m)	OD (in)	ID (in)			
Heavy Weight	206	3,782	5	3	9.38	1.219	6.5	3.063	49.7	CS_1340 MOD	1340 MOD
Drill Pipe	485	4,267	5	4.28	9.51	0.433	7	3.75	22.46	CS_API 5D/7	G
Heavy Weight	28	4,295	5	3	9.14	1.219	6.5	3.063	49.7	CS_1340 MOD	1340 MOD
MWD	14	4,309	6.75	2.875	14.22				100.8	SS_15-15LC	15-15LC MOD (1)
Sub	1	4,310	6.5	2.76	0.61				83.26	CS_API 5D/7	4145H MOD
Mud Motor	10	4,320	6.75	3	9.63				79.41	SS_15-15LC	15-15LC MOD (1)
Bit	0	4,320	8.25		0.33				85		

11.2. Well parameters for S-shaped well S1

Cased Sections

Section Type	Section Depth (m)	Section Length (m)	Shoe Depth (m)	ID (in)	OD (in)	Drift (in)	Eff. Hole Diameter (in)	Coefficient of Friction	Linear Capacity (bbl/ft)	Casing Weight
L-80 Casing	2681.00	2681.000	2681.00	8.535	9.625	8.500	12.250	0.25	0.0708	53.5
Open Hole	**3151.50**	**470.500**		**8.500**			**8.500**	**0.35**	**0.0702**	

Operation Sequence

Name	Type	Start MD (m)	End MD (m)	Fluid	String	Max Load Per Joint (lbf)	Max Load Per Protector (lbf)	Default Wear Factor (E-10/psi)
Oper #1	Drilling	2686	3151.5	Mud #1	S1 8.5 BHA	1000	1500	1.5
Oper #2	Rotating Off Bottom	3145	3145	Mud #1	B-2 8.5 BHA	1000	1500	3

Drilling Parameters

Operation	Weight on Bit (kip)	Revolutions Per Minute (rpm)	On-Bottom Time (hr)
Oper #1	27.0	135	31.50
Oper #2	-	140	2.0

Applied BHAs

Type	Length (m)	Depth (m)	Body		Stabilizer / Tool Joint				Weight (ppf)	Material	Grade
			OD (in)	ID (in)	Avg Joint Length (m)	Length (m)	OD (in)	ID (in)			
Drill Pipe	2,844	2,844	5	4.276	9.14	0.433	6.5	3	22.32	CS_API 5D/7	G
Sub	1	2,845	6.24	2.76	0.91				83.26	CS_API 5D/7	4145H MOD
Heavy Weight	84	2,929	5	3	9.14	1.219	6.5	3.063	49.7	CS_1340 MOD	1340 MOD
Jar	3	2,933	6.75	2.5	3.2				104.76	SS_15-15LC	15-15LC MOD (1)
Heavy Weight	141	3,073	5	3	9.14	1.219	6.5	3.063	49.7	CS_1340 MOD	1340 MOD
Drill Collar	54	3,127	6.5	3	9.14				88.86	CS_API 5D/7	4145H MOD
Sub	1	3,128	6.72	3	0.91				97.72	CS_API 5D/7	4145H MOD
Stabilizer	2	3,130	6.25	2.813	1.52	0.305	8.453		83.27	CS_API 5D/7	4145H MOD
Drill Collar	9	3,139	6.75	2.25	9.14				107.13	SS_15-15LC	15-15LC MOD (1)
MWD	8	3,147	6.75	2.875	8.39				100.8	SS_15-15LC	15-15LC MOD (1)
Rotary Steerable System	4	3,151	8.375	4.925	4.11				100.8		
Bit	0	3,152	8.5		0.3				90		

11.3. Well parameters for calculations in Chapter 3

Well vertical depth (m)	2000
BHA length (m)	120,42
DP length (m)	1879,6
Weight of BHA (MT)	15,61
Per meter weight of DP (Kg/m)	43,7
Weight of DP (MT)	82,1
DP Cross-sectional Area (mm^2)	3401

Side force calculation (Hall 1994)	$F = 2T \sin(\alpha/2)$
Doglegs (°/10m)	**Force (KN)**
0,5	3,56
0,75	5,33
1	7,11
1,5	10,67
2	14,23
2,5	17,78
3	21,34

11.4. Drilling parameters for calculations in Chapter 3

WF	5,50E-10	/psi
TJ OD	6,25	inches
Rotating time	1	hours
RPM	80	rev
L_dp	30	ft
L_tj	14	inches
ϕ	5000	lb/ft

11.5. Wellbore parameters for case study calculations for Sysdrill™ in Chapter 4

Casing Grades and Section Depths

Casing	Grade	Shoe MD[ft]	Shoe TVD[ft]	Weight (ppf)	ID (in)
18 5/8in Surface Casing	K55	820.21	820.21	96.5	17.5
13 3/8in Intermediate Casing	K55	4,488.19	4,487.96	68	12.25
10 3/4in Intermediate Casing	N80	9,740.81	9,184.29	79.2	9.13
9 5/8in Intermediate Liner	N80	12,119.42	10,341.17	47	8.52
8 1/2in Open hole					

Production Section Drillstring

Name	Type	Item Length (ft)	OD (in)	ID (in)	Weight (lb/ft)	Upper Tool Joint
8-1/2" PDC Bit	PDC bit	0.88	8 1/2		100.00	4-1/2 REG
Powerdrive X5 675	Rotary steerable system	13.50	6 3/4	3.0	126.11	NC50 (4-1/2 IF)
Stabiliser	Non-magnetic stabiliser	31.00	8 1/2	2 1/4	47.00	3-1/2 REG
MWD/LWD tool	MWD/LWD tool	60.01	6 3/4	2 1/4	99.99	NC38 (3-1/2 IF)
Stabiliser	Non-magnetic stabiliser	4.00	8 1/2	2 1/4	46.97	NC38 (3-1/2 IF)
Drill collar	Drill collar	31.00	5 1/2	2 1/4	57.00	NC38 (3-1/2 IF)
Cougar D6 Jar - 6 3/4"	Hydraulic / mechanical jar	18.00	6 3/4	2 5/8	72.22	NC50 (4-1/2 IF)
Drill collar	Drill collar	31.00	5 1/2	2 1/4	57.00	NC38 (3-1/2 IF)
HWDP	Heavy weight drill pipe	31.00	6 5/8	2 1/4	71.43	NC38 (3-1/2 IF)
5-1/2" 24.7# E-75 HT55 (Grant Prideco)	Drill pipe	31.00	5 1/2	4.670	27.85	HT55
6-5/8" 25.2# S-135 XT65 (Grant Prideco)	Drill pipe	31.00	6 5/8	5.965	29.18	XT65

Operation Parameters in the production section

Operating Mode	Mud weight (ppg)	Mud Type
Motor Drilling	13.32	KCl/Polymer
Rotating off bottom	13.32	KCl/Polymer
Reaming	13.32	KCl/Polymer
Tripping Into Hole	13.32	KCl/Polymer
Tripping Out Of Hole	13.32	KCl/Polymer

Operation Parameters for drilling horizontal section

Operation	MD Begin (ft)	MD End (ft)	MW (ppg)	Existing Wear	WOB (Kips)	Surface RPM	Time (hrs)
Drill 1	12119	13619	13,12	No	4	140	114,33
Circulate 1	13619	13619	13,12	Yes	0	60	25,00
Drill 2	13619	15519	13,12	Yes	4	60	144,82
Circulate 2	15519	15519	13,12	Yes	0	140	39,00
Drill 3	15519	16819	13,12	Yes	4	60	99,09
Circulate 3	16819	16819	13,12	Yes	0	140	15,00
Ream 1	16819	13819	13,12	Yes	0	60	25,00
Drill 4	16819	18119	13,12	Yes	5	60	108,33
Circulate 4	18119	18119	13,12	Yes	0	140	55,00
Drill 5	18119	19685	13,12	Yes	5	60	142,36
Circulate 5	19685	19685	13,12	Yes	0	140	84,00
Ream 2	19685	16185	13,12	Yes	0	140	22,00

Calculation of maximum horizontal stress

Depth (ft)	YVD 5" S135	YVD 6.625" S135	YS S135	Temperature
0	10,45727	7,73997		-195
3300	28,42179	24,91868	144,4447	-80
6600	46,38632	42,09738	140,3948	-30
9900	64,35085	59,27609	134,995	25
13200	82,31537	76,4548	128,2453	100
16500	100,2799	93,63351	122,8455	150
19800	118,2444	110,8122	117,4457	205
23100	136,209	127,9909	112,0459	260
26400	154,1735	145,1696	106,6461	315
29700	172,138	162,3483	99,8963	370

11.6. Diameter and Wall Thickness measurements for the base steel casing pipe

WALL THICKNESS (t) [mm]							Total average
measuring positions	"1"	"2"	"3"	"4"	"5"	"6"	
"A"	12.24	12.62	12.63	12.64	12.23	12.35	
"B"	12.32	12.59	12.44	12.33	12.24	12.36	
"C"	12.70	12.72	12.41	12.11	12.45	12.70	
"D"	12.70	12.44	12.40	12.37	12.65	12.73	
"E"	12.82	12.57	12.62	12.78	12.93	12.86	
"F"	12.79	12.74	12.65	12.99	12.82	12.69	
"G"	12.49	12.63	12.67	13.09	12.54	12.47	
"H"	12.45	12.62	12.69	12.90	12.37	12.40	
Average	***12.56***	***12.62***	***12.56***	***12.65***	***12.53***	***12.57***	***12.58***
e [%]	***4.62***	***2.38***	***2.31***	***7.75***	***5.59***	***4.06***	***4.45***

e [%] = (tmax-tmin)/tavg x 100 %

OUTER DIAMETER (OD) [mm]							Total average
Oval. Max	6.90	6.79	6.51	6.72	6.55	6.68	
Oval. Min	5.84	5.54	5.74	5.66	5.71	5.68	
PI Tape	***245.98***	***245.72***	***245.66***	***245.69***	***245.73***	***245.70***	***245.75***
Oval. [%]	***0.43***	***0.51***	***0.31***	***0.43***	***0.34***	***0.41***	***0.41***

Oval. [%] = (Oval. Max - Oval. Min)/PI Tape x 100 %

(Oval. = Ovalimeter)

11.7. Test protocol with measured and calculated parameters for wear test No. 1

Casing/TJ	Measured Side Force (kN)	Contact Area (m2)	Contact Pressure (MPa)	RPM	Time (min)	Mechanism	Worn WT (mm)	Cum. Worn WT (mm)	Cum. Wear Volume (xE5) (m³)	Wear Volume (xE5) (m³/m)	Max Strain (µS)	Friction factor	Max Friction Stress (MPa)	Moment (N.m)	Cum. Frictional Work (J)	Cum. Frictional Work (xE7) (J)	Wear Factor (E-10/psi)
Casing 95HC (244,5x11,95) mm- Stainless Steel TJ	0.00	0.00000	0	0	0	Rotating & Sliding	0.00	0.00	0	0	0	0.00	0	0	0	0.00	0
	6.73	0.01046	0.644	100	15	Rotating & Sliding	0.55	0.55	1.5933	1.5933	15	0.17	0.563	96.3	907552	0.09	291
	6.73	0.01249	0.539	100	30	Rotating & Sliding	0.24	0.79	2.7292	1.1358	14	0.15	0.525	89.9	1754601	0.18	222
	6.73	0.01414	0.476	100	45	Rotating & Sliding	0.23	1.02	3.9858	1.2567	20	0.22	0.751	128.4	2964671	0.30	172
	6.73	0.01542	0.437	100	60	Rotating & Sliding	0.20	1.22	5.1929	1.2071	23	0.25	0.864	147.7	4356252	0.44	144
	6.73	0.01681	0.400	100	90	Rotating & Sliding	0.24	1.46	6.7663	1.5733	17	0.19	0.638	109.2	6413372	0.64	127
	6.73	0.01852	0.363	100	120	Rotating & Sliding	0.33	1.79	9.1267	2.3604	21	0.23	0.788	134.8	8954520	0.90	154
	6.73	0.01975	0.341	100	150	Rotating & Sliding	0.26	2.05	11.13	2.0033	16	0.18	0.601	102.7	10890633	1.09	171
	6.73	0.02105	0.320	100	180	Rotating & Sliding	0.30	2.35	13.583	2.4529	21	0.23	0.788	134.8	13431781	1.34	160
	6.73	0.02276	0.296	100	240	Rotating & Sliding	0.43	2.78	17.336	3.7529	13	0.14	0.488	83.5	16577964	1.66	197
	6.73	0.02407	0.280	100	300	Rotating & Sliding	0.36	3.14	20.672	3.3358	22	0.24	0.826	141.3	21902274	2.19	104
	6.73	0.02529	0.266	100	360	Rotating & Sliding	0.36	3.50	24.167	3.4954	18	0.20	0.676	115.6	26258528	2.63	133
	6.73	0.02676	0.251	100	420	Rotating & Sliding	0.47	3.97	28.949	4.7817	23	0.25	0.864	147.7	31824853	3.18	142
	6.73	0.02762	0.244	100	480	Rotating & Sliding	0.29	4.26	32.012	3.0633	20	0.22	0.751	128.4	36665135	3.67	105

11.8. Test protocol with measured and calculated parameters for wear test No. 3

Casing/TJ	Measured Side Force (kN)	Contact Area (m2)	Contact Pressure (MPa)	RPM	Time (min)	Mechanism	Initial WT (mm)	Cum. Worn WT (mm)	Cum. Wear Volume (xE5) (m^3/m)	Max Strain (µS)	Friction factor	Max Friction Stress (MPa)	Moment (N.m)	Cum. Frictional Work (J)	Cum. Frictional Work (x1E-7) (J)	Wear Factor (E-10/psi)
Casing 95HC (244,5x11,95) mm- Stainless Steel TJ	0.00	0.00000	0	0	0	Rotating & Sliding	13.85	0.00	0	0	0.00	0	0	0	0.00	0
	6.73	0.01007	0.668	100	15	Rotating & Sliding	13.85	0.49	1.3671	14	0.15	0.525	89.9	847049	0.08	267
	6.73	0.01248	0.539	100	30	Rotating & Sliding	13.36	0.76	2.6258	19	0.21	0.713	122.0	1996616	0.20	181
	6.73	0.01454	0.463	100	45	Rotating & Sliding	13.09	1.04	4.1788	27	0.29	1.014	173.4	3630211	0.36	157
	6.73	0.01607	0.419	100	60	Rotating & Sliding	12.81	1.28	5.6771	21	0.23	0.788	134.8	4900785	0.49	195
	6.73	0.01809	0.372	100	90	Rotating & Sliding	12.57	1.64	8.1733	22	0.24	0.826	141.3	7562940	0.76	155
	6.73	0.02028	0.332	100	120	Rotating & Sliding	12.21	2.09	11.652	22	0.24	0.826	141.3	10225095	1.02	216
	6.73	0.02172	0.310	100	150	Rotating & Sliding	11.76	2.42	14.424	22	0.24	0.826	141.3	12887250	1.29	172
	6.73	0.02281	0.295	100	180	Rotating & Sliding	11.43	2.69	16.814	24	0.26	0.901	154.1	15791419	1.58	136
	6.73	0.02459	0.274	100	240	Rotating & Sliding	11.16	3.17	21.311	22	0.24	0.826	141.3	21115729	2.11	140
	6.73	0.02607	0.258	100	300	Rotating & Sliding	10.68	3.61	25.683	24	0.26	0.901	154.1	26924068	2.69	125
	6.73	0.02699	0.249	100	360	Rotating & Sliding	10.24	3.90	28.683	29	0.32	1.089	186.2	33942477	3.39	71
	6.73	0.02830	0.238	100	420	Rotating & Sliding	9.85	4.24	33.398	25	0.27	0.939	160.5	39992830	4.00	129
	6.73	0.02917	0.231	100	480	Rotating & Sliding	9.51	4.55	36.831	25	0.27	0.939	160.5	46043183	4.60	94

11.9. Test protocol with measured and calculated parameters for wear test No. 4

Casing/TJ	Measured Side Force (kN)	Pressure on Cylinder (bar)	Contact Area (m2)	Contact Pressure (MPa)	RPM	Time (min)	Mechanism	Worn WT (mm)	Cum. Worn WT (mm)	Cum. Wear Volume (xE5) (m^3/m)	Wear Volume (xE5) (m^3/m)	Max Strain (µS)	Friction factor	Max Friction Stress (MPa)	Moment (N.m)	Cum. Frictional Work (J)	Cum. Frictional Work (x1E-7) (J)	Wear Factor (E-10/psi)
Casing 95HC (244,5x11,95) mm- Stainless Steel TJ- Drilling Mud 9,4ppg, Viscosity 15cp	0.00	0	0.00000	0	0	0	Rotating & Sliding	0.00	0.00	0	0	0	0.00	0	0	0	0.00	0
	6.73	3	0.00585	1.150	100	15	Rotating & Sliding	0.17	0.17	0.2763	0.2763	8	0.09	0.3	51.4	484028.26	0.05	94
	6.73	3	0.00837	0.804	100	30	Rotating & Sliding	0.18	0.35	0.8129	0.5367	8	0.09	0.3	51.4	968056.52	0.10	184
	6.73	3	0.00938	0.718	100	45	Rotating & Sliding	0.09	0.44	1.1433	0.3304	10	0.11	0.375	64.2	1573091.5	0.16	90
	6.73	3	0.00979	0.688	100	60	Rotating & Sliding	0.04	0.48	1.3017	0.1583	12	0.13	0.45	77.1	2299133.5	0.23	36
	6.73	3	0.00989	0.681	100	90	Rotating & Sliding	0.01	0.49	1.3425	0.0408	5	0.05	0.187	32.1	2904168.5	0.29	11
	6.73	3	0.01037	0.649	100	120	Rotating & Sliding	0.05	0.54	1.5517	0.2092	9	0.10	0.338	57.8	3993231.5	0.40	32
	6.73	3	0.01074	0.626	100	150	Rotating & Sliding	0.04	0.58	1.7258	0.1742	12	0.13	0.45	77.1	5445315.5	0.54	20
	6.73	3	0.01083	0.621	100	180	Rotating & Sliding	0.01	0.59	1.77	0.0442	14	0.15	0.525	89.9	7139413.5	0.71	4
	6.73	3	0.01092	0.616	100	240	Rotating & Sliding	0.01	0.60	1.815	0.045	12	0.13	0.45	77.1	10043583	1.00	3
	6.73	3	0.01153	0.584	100	300	Rotating & Sliding	0.07	0.67	2.1388	0.3238	12	0.13	0.45	77.1	12947752	1.29	18
	6.73	3	0.01170	0.575	100	360	Rotating & Sliding	0.02	0.69	2.2342	0.0954	15	0.16	0.563	96.3	16577963	1.66	4
	6.73	3	0.01186	0.567	100	420	Rotating & Sliding	0.02	0.71	2.3313	0.0971	11	0.12	0.413	70.6	19240118	1.92	6
	6.73	3	0.01186	0.567	100	480	Rotating & Sliding	0.00	0.71	2.3313	0	14	0.15	0.525	89.9	22628315	2.26	0

11.10. Test protocol with measured and calculated parameters for wear test No. 5

Casing/TJ	Measured Side Force (kN)	Pressure on Cylinder (bar)	Contact Area (m2)	Contact Pressure (MPa)	RPM	Time (min)	Mechanism	Worn WT (mm)	Cum. Worn WT (mm)	Cum. Wear Volume (xE5) (m^3/m)	Wear Volume (xE5) (m^3/m)	Max Strain (µS)	Friction factor	Max Friction Stress (MPa)	Moment (N.m)	Cum. Frictional Work (J)	Cum. Frictional Work (x1E-7) (J)	Wear Factor (E-10/psi)
	0.00	0	0.00000	0	0	0	Rotating & Sliding	0.00	0.00	0	0	0	0.00	0	0	0	0.00	0
	6.73	3	0.00543	0.874	100	15	Rotating & Sliding	0.15	0.15	0.2263	0.2263	11	0.12	0.413	70.6	665538	0.07	56
	6.73	3	0.00754	0.630	100	30	Rotating & Sliding	0.14	0.29	0.6067	0.3804	14	0.15	0.525	89.9	1512587	0.15	74
	6.73	3	0.00767	0.620	100	45	Rotating & Sliding	0.01	0.30	0.6379	0.0313	14	0.15	0.525	89.9	2359636	0.24	6
	6.73	3	0.00779	0.610	100	60	Rotating & Sliding	0.01	0.31	0.67	0.0321	11	0.12	0.413	70.6	3025174	0.30	8
Casing 95HC (244,5x11,95) mm- Stainless Steel TJ- Drilling Mud 9,4ppg. Viscosity 15cp	6.73	3	0.00851	0.558	100	90	Rotating & Sliding	0.06	0.37	0.8725	0.2025	14	0.15	0.525	89.9	4719272	0.47	20
	6.73	3	0.00851	0.558	100	120	Rotating & Sliding	0.00	0.37	0.8725	0	11	0.12	0.413	70.6	6050349	0.61	0
	6.73	3	0.00862	0.551	100	150	Rotating & Sliding	0.01	0.38	0.9088	0.0363	12	0.13	0.45	77.1	7502433	0.75	4
	6.73	3	0.00895	0.531	100	180	Rotating & Sliding	0.03	0.41	1.0171	0.1083	13	0.14	0.488	83.5	9075524	0.91	11
	6.73	3	0.00927	0.513	100	240	Rotating & Sliding	0.03	0.44	1.13	0.1129	14	0.15	0.525	89.9	12463721	1.25	6
	6.73	3	0.00937	0.507	100	300	Rotating & Sliding	0.01	0.45	1.1688	0.0388	15	0.16	0.563	96.3	16093932	1.61	2
	6.73	3	0.00947	0.502	100	360	Rotating & Sliding	0.01	0.46	1.2075	0.0388	13	0.14	0.488	83.5	19240115	1.92	2
	6.73	3	0.00957	0.496	100	420	Rotating & Sliding	0.01	0.47	1.2471	0.0396	10	0.11	0.375	64.2	21660256	2.17	3
	6.73	3	0.00977	0.486	100	480	Rotating & Sliding	0.02	0.49	1.3267	0.0796	10	0.11	0.375	64.2	24080397	2.41	5

11.11. Test protocol with measured and calculated parameters for wear test No. 6

Casing/TJ	Measured Side Force (kN)	Pressure on Cylinder (bar)	Contact Area (m2)	Contact Pressure (MPa)	RPM	Time (min)	Mechanism	Worn WT (mm)	Cum. Worn WT (mm)	Cum. Wear Volume (xE5) (m^3/m)	Wear Volume (xE5) (m^3/m)	Max Strain (µS)	Friction factor Average	Max Friction Stress (MPa)	Moment (N.m)	Cum. Frictional Work (J)	Cum. Frictional Work (x1E7) (J)	Wear Factor Average (E-10/psi)
Casing 95HC (244,5x11,95) mm- Stainless Steel TJ- Drilling Mud 9,4ppg, Viscosity 15cp	0.00	0	0.00000	0	0	0	Rotating & Sliding	0.00	0.00	0	0	0	0.00	0	0	0	0.00	0
	6.73	3	0.00771	0.873	100	15	Rotating & Sliding	0.29	0.29	0.62	0.62	10	0.11	0.376	64.2	605035	0.06	170
	6.73	3	0.00810	0.831	100	30	Rotating & Sliding	0.04	0.32	0.7183	0.0983	11	0.12	0.413	70.6	1270574	0.13	24
	6.73	3	0.00834	0.807	100	45	Rotating & Sliding	0.02	0.34	0.7867	0.0683	9	0.10	0.338	57.8	1815106	0.18	21
	6.73	3	0.00858	0.784	100	60	Rotating & Sliding	0.02	0.36	0.8567	0.07	10	0.11	0.376	64.2	2420141	0.24	19
	6.73	3	0.00893	0.754	100	90	Rotating & Sliding	0.03	0.39	0.9654	0.1088	14	0.15	0.526	89.9	4114240	0.41	11
	6.73	3	0.00915	0.735	100	120	Rotating & Sliding	0.02	0.41	1.04	0.0746	11	0.12	0.413	70.6	5445318	0.54	9
	6.73	3	0.00937	0.718	100	150	Rotating & Sliding	0.02	0.43	1.1167	0.0767	12	0.13	0.451	77.1	6897403	0.69	9
	6.73	3	0.00958	0.702	100	180	Rotating & Sliding	0.02	0.45	1.195	0.0783	13	0.14	0.488	83.5	8470495	0.85	8
	6.73	3	0.00968	0.695	100	240	Rotating & Sliding	0.01	0.46	1.2346	0.0396	14	0.15	0.526	89.9	11858693	1.19	2
	6.73	3	0.00979	0.688	100	300	Rotating & Sliding	0.01	0.47	1.275	0.0404	11	0.12	0.413	70.6	14520848	1.45	3
	6.73	3	0.00989	0.680	100	360	Rotating & Sliding	0.01	0.48	1.3154	0.0404	8	0.09	0.301	51.4	16456961	1.65	3
	6.73	3	0.00999	0.674	100	420	Rotating & Sliding	0.01	0.49	1.3567	0.0413	16	0.17	0.601	102.7	20329187	2.03	2
	6.73	3	0.01009	0.667	100	480	Rotating & Sliding	0.01	0.50	1.3979	0.0413	14	0.15	0.526	89.9	23717385	2.37	2

11.12. Test protocol with measured and calculated parameters for wear test No. 8

Casing/TJ	Measured Side Force (kN)	Pressure on Cylinder (bar)	Contact Area (m2)	Contact Pressure (MPa)	RPM	Time (min)	Mechanism	Worn WT (mm)	Cum. Worn WT (mm)	Cum. Wear Volume (xE5) (m^3/m)	Wear Volume (xE5) (m^3/m)	Max Strain (µS)	Friction factor	Max Friction Stress (MPa)	Moment (N.m)	Cum. Frictional Work (J)	Cum. Frictional Work (xE-7) (J)	Wear Factor (E-10/psi)
Casing Glass Fiber (260,3x4,90) mm- Stainless Steel TJ- Drilling Mud 9,4ppg, Viscosity 14cp	0.00	0	0.00000	0	0	0	Rotating & Sliding	0.00	0.00	0	0	0	0.00	0	0	0	0.00	0
	6.10	3	0.00467	1.306	100	15	Rotating & Sliding	0.16	0.16	0.2075	0.2075	4	0.05	0.15	25.7	242014	0.02	142
	6.10	3	0.00560	1.090	100	30	Rotating & Sliding	0.07	0.23	0.3571	0.1496	2	0.03	0.075	12.8	363021	0.04	205
	6.10	3	0.00628	0.971	100	45	Rotating & Sliding	0.06	0.29	0.505	0.1479	2	0.03	0.075	12.8	484028	0.05	202
	6.10	3	0.00649	0.940	100	60	Rotating & Sliding	0.02	0.31	0.5583	0.0533	2	0.03	0.075	12.8	605035	0.06	73
	6.10	3	0.00660	0.925	100	90	Rotating & Sliding	0.01	0.32	0.5854	0.0271	2	0.03	0.075	12.8	847049	0.08	19
	6.10	3	0.00670	0.911	100	120	Rotating & Sliding	0.01	0.33	0.6129	0.0275	3	0.04	0.112	19.3	1210070	0.12	13
	6.10	3	0.00690	0.884	100	150	Rotating & Sliding	0.02	0.35	0.6696	0.0567	3	0.04	0.112	19.3	1573091	0.16	26
	6.10	3	0.00709	0.860	100	180	Rotating & Sliding	0.02	0.37	0.7275	0.0579	4	0.05	0.15	25.7	2057119	0.21	20
	6.10	3	0.00728	0.838	100	240	Rotating & Sliding	0.02	0.39	0.7871	0.0596	2	0.03	0.075	12.8	2541147	0.25	20
	6.10	3	0.00746	0.818	100	300	Rotating & Sliding	0.02	0.41	0.8479	0.0608	2	0.03	0.075	12.8	3025175	0.30	21
	6.10	3	0.00773	0.790	100	360	Rotating & Sliding	0.03	0.44	0.9425	0.0946	3	0.04	0.112	19.3	3751217	0.38	22
	6.10	3	0.00807	0.756	100	420	Rotating & Sliding	0.04	0.48	1.0733	0.1308	3	0.04	0.112	19.3	4477259	0.45	30
	6.10	3	0.00855	0.713	100	480	Rotating & Sliding	0.06	0.54	1.28	0.2067	2	0.03	0.075	12.8	4961287	0.50	71

11.13. Test protocol with measured and calculated parameters for wear test No. 9

Casing/TJ	Measured Side Force (kN)	Pressure on Cylinder (bar)	Contact Area (m2)	Contact Pressure (MPa)	RPM	Time (min)	Mechanism	Worn WT (mm)	Cum. Worn WT (mm)	Cum. Wear Volume (xE5) (m^3/m)	Wear Volume (xE5) (m^3/m)	Max Strain (µS)	Friction factor	Max Friction Stress (MPa)	Moment (N.m)	Cum. Frictional Work (J)	Cum. Frictional Work (x1E-7) (J)	Wear Factor (E-10/psi)
Casing Glass Fiber (260,3x4,90) mm- Stainless Steel TJ- Drilling Mud 9,4ppg, Viscosity 14cp	0.00	0	0.00000	0	0	0	Rotating & Sliding	0.00	0.00	0	0	0	0.00	0	0	0	0.00	0
	6.10	3	0.00437	1.397	100	15	Rotating & Sliding	0.14	0.14	0.17	0.17	3	0.04	0.112	19.3	181510	0.02	155
	6.10	3	0.00508	1.200	100	30	Rotating & Sliding	0.05	0.19	0.2683	0.0983	2	0.03	0.075	12.8	302517	0.03	135
	6.10	3	0.00559	1.091	100	45	Rotating & Sliding	0.04	0.23	0.3571	0.0888	3	0.04	0.112	19.3	484027	0.05	81
	6.10	3	0.00628	0.972	100	60	Rotating & Sliding	0.06	0.29	0.505	0.1479	4	0.05	0.15	25.7	726041	0.07	101
	6.10	3	0.00699	0.873	100	90	Rotating & Sliding	0.07	0.36	0.6979	0.1929	3	0.04	0.112	19.3	1089062	0.11	88
	6.10	3	0.00727	0.839	100	120	Rotating & Sliding	0.03	0.39	0.7867	0.0888	3	0.04	0.112	19.3	1452083	0.15	40
	6.10	3	0.00781	0.781	100	150	Rotating & Sliding	0.06	0.45	0.9742	0.1875	4	0.05	0.15	25.7	1936111	0.19	64
	6.10	3	0.00806	0.757	100	180	Rotating & Sliding	0.03	0.48	1.0729	0.0988	4	0.05	0.15	25.7	2420139	0.24	34
	6.10	3	0.00831	0.734	100	240	Rotating & Sliding	0.03	0.51	1.1746	0.1017	3	0.04	0.112	19.3	3146181	0.31	23
	6.10	3	0.00863	0.707	100	300	Rotating & Sliding	0.04	0.55	1.3146	0.14	4	0.05	0.15	25.7	4114237	0.41	24
	6.10	3	0.00878	0.695	100	360	Rotating & Sliding	0.02	0.57	1.3867	0.0721	4	0.05	0.15	25.7	5082293	0.51	12
	6.10	3	0.00900	0.677	100	420	Rotating & Sliding	0.03	0.60	1.4971	0.1104	3	0.04	0.112	19.3	5808335	0.58	25
	6.10	3	0.00930	0.656	100	480	Rotating & Sliding	0.04	0.64	1.6483	0.1513	3	0.04	0.112	19.3	6534377	0.65	34

11.14. Test protocol with measured and calculated parameters for wear test No. 13

Casing/TJ	Measured Side Force (kN)	Pressure on Cylinder (bar)	Contact Area (m2)	Contact Pressure (MPa)	RPM	Time (min)	Mechanism	Worn WT (mm)	Cum. Worn WT (mm)	Cum. Wear Volume (xE5) (m^3/m)	Wear Volume (xE5) (m^3/m)	Max Strain (µS)	Friction factor	Max Friction Stress (MPa)	Moment (N.m)	Cum. Frictional Work (J)	Cum. Frictional Work (x1E-7) (J)	Wear Factor (E-10/psi)
	0.00	0	0.00000	0	0	0	Rotating & Sliding	0.00	0.00	0	0	0	0.00	0	0	0	0.00	0
	6.10	3	0.00616	0.990	100	15	Rotating & Sliding	0.28	0.28	0.4788	0.4788	6	0.07	0.22	38.5	363021	0.04	218
	6.10	3	0.00745	0.819	100	30	Rotating & Sliding	0.13	0.41	0.8467	0.3679	4	0.05	0.15	25.7	605035	0.06	252
	6.10	3	0.00830	0.735	100	45	Rotating & Sliding	0.10	0.51	1.1733	0.3267	9	0.11	0.34	57.8	1149567	0.11	99
	6.10	3	0.00877	0.696	100	60	Rotating & Sliding	0.06	0.57	1.385	0.2117	8	0.10	0.3	51.4	1633595	0.16	72
	6.10	3	0.00907	0.673	100	90	Rotating & Sliding	0.04	0.61	1.5329	0.1479	8	0.10	0.3	51.4	2601651	0.26	25
Casing Glass Fiber (260,3x4,90) mm-Stainless Steel TJ-Water	6.10	3	0.00922	0.662	100	120	Rotating & Sliding	0.02	0.63	1.6083	0.0754	9	0.11	0.34	57.8	3690715	0.37	11
	6.10	3	0.00936	0.652	100	150	Rotating & Sliding	0.02	0.65	1.685	0.0767	6	0.07	0.22	38.5	4416757	0.44	17
	6.10	3	0.00964	0.633	100	180	Rotating & Sliding	0.04	0.69	1.8421	0.1571	8	0.10	0.3	51.4	5384813	0.54	27
	6.10	3	0.00984	0.620	100	240	Rotating & Sliding	0.03	0.72	1.9629	0.1208	10	0.12	0.38	64.2	7804954	0.78	8
	6.10	3	0.01005	0.607	100	300	Rotating & Sliding	0.03	0.75	2.0863	0.1233	9	0.11	0.34	57.8	9983081	1.00	9
	6.10	3	0.01031	0.592	100	360	Rotating & Sliding	0.04	0.79	2.2542	0.1679	8	0.10	0.3	51.4	11919194	1.19	14
	6.10	3	0.01044	0.585	100	420	Rotating & Sliding	0.02	0.81	2.3396	0.0854	10	0.12	0.38	64.2	14339335	1.43	6
	6.10	3	0.01056	0.578	100	480	Rotating & Sliding	0.02	0.83	2.4263	0.0867	8	0.10	0.3	51.4	16275448	1.63	7

11.15. Test protocol with measured and calculated parameters for wear test No. 12

Casing/TJ	Measured Side Force (kN)	Pressure on Cylinder (bar)	Contact Area (m2)	Contact Pressure (MPa)	RPM	Time (min)	Mechanism	Worn WT (mm)	Cum. Worn WT (mm)	Cum. Wear Volume (xE5) (m^3/m)	Wear Volume (xE5) (m^3/m)	Max Strain (µS)	Friction factor	Max Friction Stress (MPa)	Moment (N.m)	Cum. Frictional Work (J)	Cum. Frictional Work (x1E-7) (J)	Wear Factor (E-10/psi)
	0.00	0	0.00000	0	0	0	Rotating & Sliding	0.00	0.00	0	0	0	0.00	0	0	0	0.00	0
	6.73	3	0.00575	1.170	100	15	Rotating & Sliding	0.13	0.13	0.2075	0.2075	4	0.04	0.143	24.4	229913	0.02	149
	6.73	3	0.00713	0.945	100	30	Rotating & Sliding	0.07	0.20	0.3954	0.1879	5	0.05	0.199	34.2	552397	0.06	96
	6.73	3	0.00826	0.814	100	45	Rotating & Sliding	0.07	0.27	0.6188	0.2233	6	0.06	0.224	38.3	913603	0.09	102
	6.73	3	0.00912	0.738	100	60	Rotating & Sliding	0.06	0.33	0.8346	0.2158	4	0.04	0.154	26.3	1161667	0.12	144
Casing Carbon Fiber (257,8x25)mm- Stainless Steel TJ- Drilling Mud 9,4ppg. Viscosity 15cp	6.73	3	0.01015	0.663	100	90	Rotating & Sliding	0.08	0.41	1.1533	0.3188	5	0.05	0.204	34.8	1817525	0.18	80
	6.73	3	0.01096	0.614	100	120	Rotating & Sliding	0.07	0.48	1.4579	0.3046	5	0.05	0.18	30.9	2399569	0.24	87
	6.73	3	0.01162	0.579	100	150	Rotating & Sliding	0.06	0.54	1.7371	0.2792	5	0.05	0.18	30.9	2981613	0.30	79
	6.73	3	0.01223	0.550	100	180	Rotating & Sliding	0.06	0.60	2.0308	0.2938	6	0.06	0.225	38.5	3707655	0.37	67
	6.73	3	0.01281	0.526	100	240	Rotating & Sliding	0.06	0.66	2.3388	0.3079	7	0.08	0.263	44.9	5401754	0.54	30
	6.73	3	0.01336	0.504	100	300	Rotating & Sliding	0.06	0.72	2.6604	0.3217	6	0.06	0.225	38.5	6853839	0.69	37
	6.73	3	0.01397	0.482	100	360	Rotating & Sliding	0.07	0.79	3.0517	0.3913	5	0.05	0.173	29.5	7967104	0.80	58
	6.73	3	0.01455	0.462	100	420	Rotating & Sliding	0.07	0.86	3.4596	0.4079	5	0.05	0.188	32.1	9177175	0.92	56
	6.73	3	0.01503	0.448	100	480	Rotating & Sliding	0.06	0.92	3.8213	0.3617	5	0.05	0.184	31.5	10363044	1.04	50

11.16. Test protocol with measured and calculated parameters for wear test No. 11

Casing/TJ	Measured Side Force (kN)	Pressure on Cylinder (bar)	Contact Area (m2)	Contact Pressure (MPa)	RPM	Time (min)	Mechanism	Worn WT (mm)	Cum. Worn WT (mm)	Cum. Wear Volume (xE5) (m^3/m)	Wear Volume (xE5) (m^3/m)	Max Strain (µS)	Friction factor	Max Friction Stress (MPa)	Cum. Moment (N.m)	Cum. Frictional Work (J)	Cum. Frictional Work (xE-7) (J)	Wear Factor (E-10/psi)
Casing Carbon Fiber (257,8x25)mm- Stainless Steel TJ- Drilling Mud 9,4ppg, Viscosity 15cp	0.00	0	0.00000	0	0	0	Rotating & Sliding	0.00	0.00	0	0	0	0.00	0	0	0	0.00	0
	6.73	3	0.00528	1.274	100	15	Rotating & Sliding	0.11	0.11	0.1617	0.1617	7	0.08	0.248	42.4	399323	0.04	67
	6.73	3	0.00656	1.026	100	30	Rotating & Sliding	0.06	0.17	0.3096	0.1479	8	0.09	0.31	53.0	899082	0.09	49
	6.73	3	0.00762	0.883	100	45	Rotating & Sliding	0.06	0.23	0.4863	0.1767	6	0.06	0.21	36.0	1237902	0.12	86
	6.73	3	0.00854	0.788	100	60	Rotating & Sliding	0.06	0.29	0.6875	0.2013	5	0.05	0.176	30.2	1522269	0.15	117
	6.73	3	0.00937	0.718	100	90	Rotating & Sliding	0.06	0.35	0.9096	0.2221	5	0.10	0.199	34.0	2163606	0.22	57
	6.73	3	0.01013	0.664	100	120	Rotating & Sliding	0.06	0.41	1.1513	0.2417	7	0.08	0.244	41.7	2950152	0.30	51
	6.73	3	0.01095	0.615	100	150	Rotating & Sliding	0.07	0.48	1.4554	0.3042	8	0.09	0.302	51.6	3921839	0.39	52
	6.73	3	0.01170	0.575	100	180	Rotating & Sliding	0.07	0.55	1.7817	0.3263	5	0.05	0.199	34.0	4563176	0.46	84
	6.73	3	0.01230	0.547	100	240	Rotating & Sliding	0.06	0.61	2.0775	0.2958	7	0.08	0.259	44.3	6233074	0.62	29
	6.73	3	0.01288	0.523	100	300	Rotating & Sliding	0.06	0.67	2.3875	0.31	5	0.05	0.176	30.2	7370540	0.74	45
	6.73	3	0.01333	0.505	100	360	Rotating & Sliding	0.05	0.72	2.6558	0.2683	7	0.08	0.247	46.9	9137243	0.91	25
	6.73	3	0.01403	0.480	100	420	Rotating & Sliding	0.08	0.80	3.1033	0.4475	7	0.08	0.244	41.7	10710335	1.07	47
	6.73	3	0.01453	0.463	100	480	Rotating & Sliding	0.06	0.86	3.4533	0.35	7	0.08	0.259	44.3	12380233	1.24	35

11.17. Test protocol with measured and calculated parameters for wear test No. 14

Casing/TJ	Measured Side Force (kN)	Pressure on Cylinder (bar)	Contact Area (m2)	Contact Pressure (MPa)	RPM	Time (min)	Mechanism	Worn WT (mm)	Cum. Worn WT (mm)	Cum. Wear Volume (xE5) (m^3/m)	Wear Volume (xE5) (m^3/m)	Max Strain (µS)	Friction factor	Max Friction Stress (MPa)	Moment (N.m)	Cum. Frictional Work (J)	Cum. Frictional Work (xE-7) (J)	Wear Factor (E-10/psi)
	0.00	0	0.00000	0	0	0	Rotating & Sliding	0.00	0.00	0	0	0	0.00	0	0	0	0.00	0
	6.73	3	0.00702	0.959	100	15	Rotating & Sliding	0.20	0.20	0.3892	0.3892	4	0.04	0.131	22.5	211762	0.02	304
	6.73	3	0.00912	0.738	100	30	Rotating & Sliding	0.14	0.34	0.8596	0.4704	3	0.04	0.113	19.3	393272	0.04	429
	6.73	3	0.01012	0.665	100	45	Rotating & Sliding	0.08	0.42	1.1775	0.3179	3	0.05	0.113	19.3	574782	0.06	290
	6.73	3	0.01123	0.599	100	60	Rotating & Sliding	0.10	0.52	1.6175	0.44	4	0.05	0.113	22.5	786544	0.08	344
	6.73	3	0.01195	0.563	100	90	Rotating & Sliding	0.07	0.59	1.9508	0.3333	4	0.05	0.15	25.7	1270572	0.13	114
Casing Carbon Fiber (257,8x25)m m-Stainless Steel TJ-Water	6.73	3	0.01289	0.522	100	120	Rotating & Sliding	0.10	0.69	2.4604	0.5096	5	0.06	0.15	25.7	1754600	0.18	174
	6.73	3	0.01342	0.501	100	150	Rotating & Sliding	0.06	0.75	2.7838	0.3233	4	0.05	0.15	25.7	2238628	0.22	111
	6.73	3	0.01393	0.483	100	180	Rotating & Sliding	0.06	0.81	3.1192	0.3354	4	0.05	0.15	25.7	2722656	0.27	115
	6.73	3	0.01473	0.457	100	240	Rotating & Sliding	0.10	0.91	3.7042	0.585	5	0.06	0.15	25.7	3690712	0.37	100
	6.73	3	0.01534	0.439	100	300	Rotating & Sliding	0.08	0.99	4.1938	0.4896	4	0.05	0.15	25.7	4658768	0.47	84
	6.73	3	0.01584	0.425	100	360	Rotating & Sliding	0.07	1.06	4.6375	0.4438	4	0.05	0.15	25.7	5626824	0.56	76
	6.73	3	0.01620	0.416	100	420	Rotating & Sliding	0.05	1.11	4.9625	0.325	4	0.05	0.15	25.7	6594880	0.66	56
	6.73	3	0.01681	0.400	100	480	Rotating & Sliding	0.09	1.20	5.5642	0.6017	4	0.05	0.15	25.7	7562936	0.76	103

11.18. Wear frame pictures under test conditions